UNLV University Libraries
University of Nevada, Las Vegas

UNLV Theses, Dissertations, Professional Papers, and Capstones

12-1-2014

High Strength Steel Fiber Reinforced Flow-Able or SCC Concrete with Variable Fiber by Volume Fractions for Thin Plate and Shell Structures

Abebe Berhe
University of Nevada, Las Vegas, berhea@unlv.nevada.edu

Follow this and additional works at: https://digitalscholarship.unlv.edu/thesesdissertations

 Part of the Civil Engineering Commons, Mechanics of Materials Commons, and the Structural Materials Commons

Repository Citation

Berhe, Abebe, "High Strength Steel Fiber Reinforced Flow-Able or SCC Concrete with Variable Fiber by Volume Fractions for Thin Plate and Shell Structures" (2014). *UNLV Theses, Dissertations, Professional Papers, and Capstones*. 2244.
https://digitalscholarship.unlv.edu/thesesdissertations/2244

This Dissertation is protected by copyright and/or related rights. It has been brought to you by Digital Scholarship@UNLV with permission from the rights-holder(s). You are free to use this Dissertation in any way that is permitted by the copyright and related rights legislation that applies to your use. For other uses you need to obtain permission from the rights-holder(s) directly, unless additional rights are indicated by a Creative Commons license in the record and/or on the work itself.

This Dissertation has been accepted for inclusion in UNLV Theses, Dissertations, Professional Papers, and Capstones by an authorized administrator of Digital Scholarship@UNLV. For more information, please contact digitalscholarship@unlv.edu.

www.manaraa.com

HIGH STRENGTH STEEL FIBER REINFORCED FLOW-ABLE OR SCC CONCRETE WITH VARIABLE FIBER BY VOLUME FRACTIONS FOR THIN PLATE AND SHELL STRUCTURES

by

Abebe Tadesse Berhe

Bachelor of Science in Civil Engineering
Addis Ababa University, Ethiopia
1990

Master of Engineering
McGill University, Canada
1994

A dissertation submitted in partial fulfillment of
the requirements for the

Doctor of Philosophy in Civil and Environmental Engineering

Department of Civil and Environmental Engineering
Howard R. Hughes College of Engineering
The Graduate College

University of Nevada, Las Vegas
December 2014

www.manaraa.com

Copyright Abebe Tadesse Berhe 2014
All right Reserved

www.manaraa.com

UNLV | GRADUATE COLLEGE

We recommend the dissertation prepared under our supervision by

Abebe Tadesse Berhe

entitled

High Strength Steel Fiber Reinforced Flow-Able or SCC Concrete with Variable Fiber by Volume Fractions for Thin Plate and Shell Structures

is approved in partial fulfillment of the requirements for the degree of

Doctor of Philosophy in Engineering - Civil and Environmental Engineering

Department of Civil and Environmental Engineering and Construction

Samaan G. Ladkany, Ph.D., Committee Chair

Nadar Ghafoori, Ph.D., Committee Member

Mohamed Kaseko, Ph.D., Committee Member

Ying Tian, Ph.D., Committee Member

Brendan O'Toole, Ph.D., Graduate College Representative

Kathryn Hausbeck Korgan, Ph.D., Interim Dean of the Graduate College

December 2014

المنارة للاستشارات
www.manaraa.com

ABSTRACT

High Strength Steel Fiber Reinforced Flow-Able or SCC Concrete with Variable Fiber by Volume Fractions for Thin Plate and Shell Structures

by

Abebe Tadesse Berhe

Dr. Samaan G. Ladkany, Examination Committee Chair
Professor of Civil and Environmental Department
University of Nevada, Las Vegas

The purpose of this study is to incorporate discrete, short, mechanically deformed, small diameter steel fibers into high strength concrete with f'_c > 70 MPa (10 ksi) in an attempt to reduce and partially eliminate the need for steel rebar in concrete construction. By introducing steel fibers to high strength concrete mixture, the overall tensile, compressive and shear strength of the mixture can be improved immensely thus, replacing portions or major parts of the longitudinal, temperature and shrinkage reinforcements. The reduction or elimination of longitudinal and transverse reinforcements in the construction of structural or non-structural members can result in savings in manual labor time for the placement of longitudinal and transverse reinforcements and facilitating concrete pour without the need for vibration.

The research presents a two-phase study:

1. In the first phase, the fresh properties and behavior of high strength steel fiber reinforced flow-able concrete / self-consolidating concrete (HSSFRC) mixtures with different dosages of steel fibers, ranging from zero-to-4% by volume in 1%

www.manaraa.com

increments with variable high range water reducer (HRWR) are studied. The fresh properties of HSSFRC such as, flow-ability (spread diameter), pass-ability (J-Ring and U-Box test) and fill-ability (V-Funnel test) are presented for various steel by volume fractions. The effect of high range water reducing agent (HRWR) and viscosity modifying agent (VMA) on the fresh properties of HSSFRC are also studied. The research shows as well the effect of coarse-to-fine aggregate and water-to-cementitious ratios on the fresh and hardened properties of the HSSFRC mixtures.

In this phase, the mechanical properties and hardened behavior of high strength steel fiber reinforced concrete are also studied. The mechanical properties studied include: compressive strength, splitting tensile strength, modulus of elasticity for compression and beam modulus of rupture.

2. In the second phase, the unidirectional and bi-axial flexural properties, shear property, mode of failure and ductility of 0%, 1% and 2% high strength steel fiber reinforced concrete (HSSFRC) thin, $\leq$ 32 mm (1.25 in), plate and shell structures are studied. The structures in phase two have the same concrete constituents, including HRWR, with the exception of steel fiber by volume fractions.

The structures studied include:

1. Square plates simply supported at all sides and subjected to a concentrated center load.
2. Square plates supported at two corners and subjected to opposite corner loads.
3. Long and short span rectangular plates under center line loads.

www.manaraa.com

4. Circular plates supported at three discreet points and under a concentrated center load.
5. Circular cylindrical shells under concentrated center loads (pinching load).
6. Hyperbolic paraboloid shells simply supported at all sides and subjected to a uniformly distributed load.

The study in phase 1 shows that:

1. The addition of steel fibers to the concrete mixture results in the reduction of flow-ability, pass-ability, fill-ability and workability, which was mitigated through the adjustment of HRWR and VMA dosage.
2. Mixture with low coarse-to-fine aggregate ratio provided that other constituents of the mixture are kept the same, yielded more flow-able and workable mixtures.
3. A decrease in the water-to-cementitious materials ratio results in a loss of fresh mixture workability and increase in HRWR and at times VMA dosage in order to achieve SCC standards.
4. Substantial increase in the compression and tensile strength along with the modulus of elasticity of high strength steel fiber reinforced concrete.

The study in phase 2 shows that:

1. The ductility and capacity of plates and shells improved with the increase in steel fiber by volume fractions.
2. Flexural, shear and torsional capacity of plates and shells enhanced with the increase in steel fiber by volume fractions.
3. Effect of HRWR on the Poisson's ratio, modulus of elasticity, compressive and splitting tensile strength.

The research presents test results, comparisons and conclusion.

www.manaraa.com

ACKNOWLEDGMENTS

I express my sincere gratitude to my advisor and committee chair, Dr. Samaan G. Ladkany, for his support throughout the course of my study. I would also like to extend my sincere gratitude to my research advisory committee members: Dr. Nader Ghafoori, Dr. Brendan O'Toole, Dr. Mohamed Kaseko, Dr. Ying Tian and Dr. Aly Said.

I would like to equally express my gratitude to the civil and environmental engineering department and graduate college for supporting my study through graduate teaching assistantship, grants and scholarship. I would like to thank the Nevada Department of Transportation (NDOT) for the professional summer internship, employment and support throughout my study.

I greatly appreciate the support and cooperation I have gotten from the civil and mechanical engineering administration and laboratory personnel, friends and fellow graduate students throughout my graduate study.

Last but not least, I would like to thank and show my deepest gratitude to my parents, Tadesse Berhe, Yemar G/Medhin and Tarekech Teferi, siblings, family members and friends for the sacrifices and commitments they have made throughout my higher education.

www.manaraa.com

Table of Contents

www.manaraa.com

www.manaraa.com

www.manaraa.com

www.manaraa.com

www.manaraa.com

www.manaraa.com

www.manaraa.com

www.manaraa.com

www.manaraa.com

www.manaraa.com

www.manaraa.com

www.manaraa.com

www.manaraa.com

LIST OF TABLES

www.manaraa.com

www.manaraa.com

www.manaraa.com

www.manaraa.com

www.manaraa.com

LIST OF FIGURES

www.manaraa.com

www.manaraa.com

www.manaraa.com

www.manaraa.com

www.manaraa.com

www.manaraa.com

www.manaraa.com

www.manaraa.com

www.manaraa.com

www.manaraa.com

www.manaraa.com

www.manaraa.com

CHAPTER 1

INTRODUCTION AND LITERATURE REVIEW

The interest to minimize the use of longitudinal and transverse steel reinforcement in the construction of reinforced concrete structures and to reduce the structural weight has triggered the launch of this particular research. In areas such as beam-column joint, two way slab-column joints and heavily loaded columns, where considerable amount of transverse and longitudinal reinforcing steel are normally present, the required quantity of longitudinal reinforcing steel can be reduced greatly and in some cases eliminated if steel-fiber reinforcements coupled with high concrete strength are used. The desirability of high strength concrete is in the overall reduction of the weight of structures, the volume of concrete used in the construction, and the resulting beneficial environmental effects associated with reduction in weight and materials.

1.1 Purpose of the research

The purpose of this research is the investigation of mechanical properties of ultra-thin (1.25 in., 32 mm) steel fiber reinforced concrete shell and plate structures and the selection of a suitable high strength, high steel fiber by volume fraction (1.5% - 4%) and SCC/flow-able concrete mixtures. The suitability of the mixture is determined by its ease of placement for thin plates and shells construction, strength requirements in tension, compression, shear and having most practical and effective steel fiber by volume fraction in the mixture that satisfy the stated requirements.

www.manaraa.com

Self-Consolidating Concrete (SCC) characteristics for normal fiber-less concrete has been established by ASTM and the European Guidelines for Self-Compacting Concrete standards (European Project Group 2005). However, the literature does not show a set of similar standards for steel fiber concrete. Similarly, there are no standards set for a flow-able concrete other than its ability to flow easily in all directions without specific fiber orientation, its ability to pass confined areas and to fill forms once it is poured in place. The flow-able mixture, of course, should be stable; it should not exhibit fiber and aggregate separation, clumping or balling of steel fibers, and bleeding.

Extensive literature review of fiber concrete is summarized in Table 1.1. It shows a large number of papers with low fiber by volume fraction, $V_f \leq 0.5\%$, of normal concrete and very few papers with attempted mixtures of normal concrete with 1% and 1.5% of steel fiber by volume fractions but no paper with high strength $\geq$ 69 MPa (10 ksi) SCC/flow-able concrete and high steel fiber by volume fraction $\geq$ 2%, which is one of the two purposes of this research, the other being the application of HSSFRC to thin plates and shells.

www.manaraa.com

Table 1.1: Summary of literature review of fiber reinforced concrete

	Database	Keyword (Number of publications)			
1	Scopus		SFRC (10,491)	and HSC (4,361)	and SCC (0)
2	Scopus		SFRC (10,491)	and HSC (4,361)	and FAC (10)
3	Engineering Village	FRC	or SFC	or FAC (5,288)	and HSC/SCC (0)
4	Science Direct		Rheology of SFC	and Fiber	and C, FC (18)
5	Science Direct			SCC	and SFC (30)
6	ACI			SFRC (59)	And HSFRC (31)

The keywords used in Table 1.1 are:

SFRC: Steel Fiber Reinforced Concrete HSC: High Strength Concrete

SCC: Self-Consolidating Concrete FAC: Flow-Able Concrete

SFR: Steel Fiber Concrete FRC: Fiber Reinforced Concrete

HS: High Strength C/FC: Concrete/Fiber Concrete

HSFRC: High Strength Fiber Reinforced Concrete

www.manaraa.com

The study will establish the most effective and practical percentage (%) of steel fiber in high strength concrete that could satisfy the flow-able concrete characteristics required for placement in thin layers of high strength, high steel fiber by volume fraction concrete. This study will refer to this type of concrete mixture as flow-able concrete (refer to Section 1.3 for specifics). The aim is to design an easy to manufacture and place flow-able concrete with characteristics somewhat similar to SCC that could be easily used in the construction of plate and shell structures using minimum longitudinal reinforcement.

1.2 Phases of the research

The research is performed in two phases:

- Phase 1 - the selection of a high strength, high steel fiber by volume fraction and SCC/flow-able concrete mixture from various experimental mixtures to be used in the construction of plate and shell structures. In this phase, the fresh (Phase 1a) and mechanical (Phase 1b) properties of five mixtures with variable steel by volume fractions (0%, 1%, 2%, 3% and 4%) and variable HRWR are investigated. Phases (1a) and (1b) of the research are presented in Chapters 1 through 7.
- Phase 2 - the construction and testing of ultra thin (1.5 in., 38 mm) models of plates and shells and the investigation of their structural strength, behavior and failure modes under different loading and support conditions. In this phase, the behavior of plate and shell structures with variable steel by volume fractions (0%, 1%, and 2%) but constant HRWR are studied. Phase (2) of the research is presented in Chapters 8 through 13.

www.manaraa.com

The literature contains very few research items on concrete that combines high strength with high steel fiber (2%, 3%, and 4%) and that is SCC/flow-able concrete. Therefore, it was determined that investigations should first be conducted to select an appropriate SCC/flow-able mixture that satisfies the requirements of the ultra thin concrete plates and shells which are the subject of this study.

It is important to note that, *this research does not seek to compare the fresh or rheological properties of HSSFRC mixtures such as slump flow diameter, flow rate…etc for various fiber volume fractions*. However, the study will conduct experiments to determine SCC/flow-able and stable high strength concrete mixtures for various levels of steel fiber by volume fractions that are suitable for the production of ultra thin high strength concrete structures.

1.3 Scope of the dissertation

The scope of this research is to study the behavior of thin steel fiber reinforced high strength concrete (HSSFRC) structures with various amount of steel fiber by volume fractions (1 - 4%). The research is conducted in two phases. In phase (1a), the fresh properties and behavior of high strength steel fiber reinforced concrete (HSSFRC) /self-consolidating (SFRSCC) mixtures with different dosages of steel fibers, ranging from zero-to-4% by volume in 1% increments are studied. The fresh properties of HSSFR concrete such as, flow-ability (spread diameter), pass-ability (J-Ring and U-Box test) and fill-ability (V-Funnel test) are presented for various steel by volume fractions. The effect of high range water reducing agent (HRWR) and viscosity modifying agent (VMA) on the fresh properties of SFRC/SCC are also studied. The research shows as well the effect

www.manaraa.com

of coarse-to-fine aggregate and water-to-cementitious ratios on the fresh and hardened properties of HSSFRC mixtures

In the phase (1b), the mechanical (hardened) properties and behavior of high strength steel fiber reinforced concrete (HSSFRC) are studied. The mechanical properties studied include: compressive strength, splitting tensile strength, and young's modulus of elasticity for compression and modulus of rupture for flexure.

In the phase (2), the shear and flexural properties of high strength steel fiber reinforced concrete of thin, $\leq$ 32 mm (1.25 in.), plates and shells are studied.

Previous SFRC studies concentrated on adding steel fibers to a concrete mixture, mainly, to enhance the ultimate strength and energy absorbing capacity of the concrete and to control cracking of the FRC (Johnston 2001). Studies, (Nawy 2001), have shown an increase in: ultimate compression, tensile and shear strength, durability, and energy dissipation capability of concrete by adding steel fibers to a regular concrete matrix. In this research, the intent of adding steel fibers to a well proportioned high strength, 70 MPa (10 ksi), concrete mixture will be to either partially or fully replace flexural and shear reinforcements in a thin concrete structures such as plates and shells.

The thin structures under consideration in the second phase of the research are 25 – 38 mm (1 – 1.5 in.) thick, with nominal maximum aggregate size of 9.5 mm (3/8 in.). The nominal maximum sizes of aggregates are chosen per the recommendation of ACI 318-05, Section 3.3.2(b).

The goal of the research is to investigate:

(a) The limitations of fiber reinforced concrete (FRC) as a self-consolidating concrete (SCC) material with two major constraints:

www.manaraa.com

- Steel fiber percentage varying from 1% to 4% by volume fraction
- Maintaining high compressive strength of > 70 MPa (10 ksi)

(b) The effect of introduction of steel fibers on the overall compressive, tensile, and shear strength and young's modulus on high strength concrete mixtures.

(c) The flexural and shear properties of thin high strength concrete plates and shells with varying steel fiber by volume fractions.

Thus, due to the above constraints, the standard SCC requirements for slump flow, pass ability, and fill ability without vibration may be achievable for lower steel fiber by volume fraction mixtures. For higher percentages of steel fiber by volume fraction mixtures however, some of the above standards may not be attainable. Therefore, such mixtures presented in this research shall be referred as a *flow-able concrete*.

1.4 Historical development of steel fiber reinforced concrete (FRC)

Fiber reinforced concrete (FRC) is a composite material made of hydraulic cements, water, Fine and coarse aggregate, and dispersion of discontinuous fibers. In general, fiber length and diameter varies from 6.35 to 63.5 mm and 0.51 to 1.2 mm (0.25 to 2.5 in. and 0.02 to 0.04 in.), respectively and has a specific gravity of 7.85 (ACI 2008).

The addition of fibers affects the plastic and hardened properties of mortar and concrete. Depending on the fiber material, length and diameter, deformation geometry, and the addition rate, many properties are improved, notably plastic shrinkage cracking, impact resistance, and toughness or ductility (ACI 2008).

www.manaraa.com

1.5 Literature survey

After conducting an extensive research of the databases on steel fiber concrete, it was concluded that there are few studies in the literature under the topic of high-strength steel fiber- reinforced concrete (HSSFRC/SCC), whether SCC or highly flow-able concrete mixtures. While the literature contains large numbers of papers on various types of normal fiber concrete with low fiber by volume fraction of 0.5%, it contains very few papers in the area of high strength fiber concrete whether normal, flow-able or SCC, as shown in Table 1.1.

1.5.1 Self-consolidating concrete (SCC)

SCC has been extensively used in Japan since the early 1980's (ACI 237R-07 2008). The use of SCC concrete has also grown in many part of the world such as, Canada, Switzerland and USA. The estimated use of SCC in precast concrete manufacturing in the United States has grown by more than 12 fold from 2000 to 2003 (ACI 237R-07 2008).

The fresh properties of self-consolidating concrete; slump flow size, flow rate, and visual index with respect to different dosage of HRWRA and VMA were studied. In addition to passing and filling abilities, dynamic and static stabilities of SCC mixtures, the influence of hauling time and temperature on fresh properties of SCC mixtures were also investigated by Diawara (Diawara 2008).

1.5.2 Steel fiber self-consolidating concrete (SFSCC)

Various types of studies have been conducted in regard to self-consolidating concrete reinforced with steel fibers (FRSCC). Most of the studies are focused on the lower range,

www.manaraa.com

0 – 1.5%, of steel fiber reinforcement by volume fraction, notably by Destree (Destree 2004).

The effect of mechanical properties and mesostructural properties (type, distribution and orientation) of fiber reinforced self-compacting concrete (FRSCC), with 0.46% steel fiber by volume fraction, on placement of FRC were studied by Torrijos (Torrijos 2010). In this paper two types of steel fiber reinforced SCC mixtures with the same constituents, except for steel fibers aspect ratios (length of fiber/ fiber diameter), 50 (50 mm long and 1 mm in diameter) and 79 (30 mm long and 0.38 mm in diameter), were studied. Hooked steel fibers were used in both investigations. The mixtures exhibited: slump flow diameter of 540 mm (21.3 in) and 590 mm (23.2 in), slump flow time of 2.6 seconds and 3.2 seconds, V-funnel flow time of 9.7 seconds and 19.5 seconds, and J-ring diameter of 505 mm (19.9 in) and 535 mm (21.1 in) for steel fiber aspect ratios of 50 and 70, respectively. In this study twelve beams with the size of 6 x 6 x 12 in. (150 x 150 x 600 mm) were prepared in three different concrete placing/pouring conditions. The first four beams were placed by pouring the concrete at the center (C) of the mould. The second four beams were cast, via 16.4 ft (5 m) long and 6 in (150 mm) diameter tube (T) inclined at 20° slope, by pouring concrete from one end of the mould. The final four were cast in a vertical position (V) poured from the top end. In the case of (T) and (V) beams, the pour end were labeled “A” and the opposite ends were labeled “B”. After beam flexural tests were completed, fiber orientation and distribution were studied by cutting the beam in three orthogonal planes. The study established the following conclusions: (a) the preferential orientation of steel fibers is mainly in the horizontal plane, which is similar to *vibrated* FRC, (b) SFRC poured by method of tube (T) with longer steel fibers and

www.manaraa.com

smaller aspect ratio showed high post-peak response than the other two (C and V) methods. However, for SFRC with shorter steel fibers and higher aspect ratio, the beams cast from the center (C), showed higher post-peak response than the (T) and (V) methods and (c) beams casted vertically and tested horizontally were less effective in their post-peak response.

Shear behavior of SCC with and without steel fibers was studied by Greenough et al. (Greenough 2008). SFRSCC slender beams with 1% steel fibers by volume fraction were constructed and tested to failure. The SFRSCC exhibited 128% shear capacity over similar plain SCC slender beams. In addition, it was concluded that, if an adequate amount of steel fiber is used, it is possible to employ steel fibers as minimum shear reinforcements, replacing minimum transverse shear reinforcement.

The fresh properties (slump flow, funnel flow time and J-ring) of plain SCC and steel fiber reinforced SCC were investigated by Grunewald and Walraven (Grunewald 2001). Four types of steel fibers were used with different aspect ratios and shape (hooked and deformed). The steel fiber content used ranges from 0.26% to 1.56% at an increase of 0.26% by volume fraction. The authors concluded that the addition of steel fibers along with maximum aggregate size affect the workability of SCC. The passing ability is also affected by the ratio of coarse to fine aggregate, maximum size of the coarse aggregate, size of bar spacing and segregation resistance of the mixture.

A series of full scale axial compression column tests were conducted on normal strength reinforced concrete and steel fiber reinforced self-consolidating concrete (SCC) columns by Aoude et al. (Aoude 2009). The average compressive strength of 46 MPa (6.7 ksi) was used. The study used hooked end steel fibers with aspect ratio of 55 (30

www.manaraa.com

mm/0.55 mm) with a tensile strength of 1,100 MPa (160 ksi). The steel fiber contents under consideration were: 0%, 1%, 1.5% and 2% by volume fractions. A prepackaged SCC mixture, which includes HRWR, VMA and air-entraining admixture, was used per the manufacturer's guide with a water-cement ratio (w/c) of 0.42. Slump flow, V-funnel and L-Box tests were conducted to verify the workability of the SCC. The slump flow diameters were 690 mm (27.1in), 585 mm (23.0 in), 500 mm (19.7 in), 360 mm (14.2 in) for 0%, 1%, 1.5% and 2% steel fiber by volume fractions, respectively which shows a rapid decrease in the slump flow diameter with increase in fiber content. Results for V-funnel test flow time were 2.7 seconds, 3.9 seconds, and 11.9 seconds for 0%, 1% and 1.5% steel fiber by volume fraction, respectively. The authors were not successful in obtaining the flow time for 2% (V_f). The L-Box tests for 1%, 1.5% and 2% steel fiber by volume fractions were not successful. The average modulus of rupture for 0%, 1%, 1.5% and 2% steel fiber fractions were: 7.7 MPa (1.1 ksi), 8.0 MPa (1.2 ksi), 8.5 MPa (1.23 ksi) and 8.8 MPa (1.3 ksi), respectively. The above SFRSCC mixtures were used to investigate the behavior of columns with four types of transverse reinforcement arrangements. They concluded that: (a) the limiting fiber content is 1.5% for their study, (b) the addition of steel fibers can increase peak load-carrying capacity and response of columns, (c) the steel fibers can partially substitute for the transverse reinforcement in RC columns, which is a very important conclusion and (d) gradual and improved cover spalling resulting from steel fiber.

The effect of coarse to fine aggregate ratio, silica fume, fly ash and high range water reducer (HRWR) on the compressive strength of fiber reinforced self-consolidating concrete with 0.33% fiber volume fraction were investigated by Doli and Ladkany (Doli

www.manaraa.com

2004). The study was able to show that by using proper combinations of the above mentioned constituents, high strength, 76 MPa (11 ksi), fiber reinforced self-consolidating concrete with 0.33% steel fiber content can be obtained.

1.5.3 Fiber reinforced concrete (FRC)

The correlation among mechanical properties of fiber reinforced concrete was studied by Xu and Shi (Xu 2009). The study was able to find strong correlation between compressive and splitting strength, and between splitting tensile and flexural strength of steel fiber reinforced concrete with water – binder ratio of 0.25-0.5, steel fiber aspect ratio and volume fraction ranging from 55-80, and 0.5-2.0%, respectively. On the other hand, empirical relations developed for normal concrete, polypropylene and glass-reinforced concrete in previous studies were not applicable to steel fiber reinforced concrete.

The effects of aspect ratio (L/d) and steel fiber by volume fraction (v_f) on the fracture energy (G_F) and characteristic length (l_{ch}) were investigated by Bayramov et al. (Bayramov 2004). The study investigated 9 types of FRC mixtures with the same constituents except HRWR, steel fiber aspect ratios (55, 65 and 80) and steel by volume fractions ranging from 0.26% to 0.64%. The compressive strength, flexural strength, splitting tensile strength, modulus of elasticity, fracture energy and characteristic length of the nine mixtures ranged between: 46.1 MPa (6.69 ksi) to 74.4 MPa (10.8 ksi), 6.04 MPa (0.88 ksi) to 12.1 MPa (1.76 ksi), 5.6 MPa (0.81 ksi) to 7.55 MPa (1.1 ksi), 44.6 GPa (6,469 ksi) to 51.7 GPa (7,499 ksi), 957 N/m (65.6l lbf/ft) to 4,371 N/m (300 lbf/ft) and 1,599 mm (63 in.) to 4,845 mm (191 in.), respectively. The study was able to show:

www.manaraa.com

(a) splitting tensile strength, flexural strength and fracture energy increased with the increase in steel by volume fractions and (b) flexural and energy strength increased with the increase in steel fiber aspect ratio.

The influences of matrix and steel fiber tensile strength on the fracture energy of normal to high strength FRC were studied by Sahin and Koksal (Sahin 2011). The study investigated three independent variables: (a) three types of water/cement ratios - 0.35, 0.45 and 0.45, with an average strength of 48.6 MPa (7.05 ksi), 59.2 MPa (8.58 ksi) and 72.3 MPa (10.5 ksi), respectively, (b) two types of steel tensile strengths – 160 ksi (1100 MPa) and 290 ksi (2000 MPa) and (c) three types of steel volume fractions – 0.33%, 0.67% and 1%. Compressive strength, modulus of elasticity, splitting tensile strength and beam flexural strength tests were conducted. The study was able to conclude the following: (a) steel fiber volume fraction and steel fiber strength have little effect on compressive strength and modulus of elasticity, (b) splitting tensile strength increased on average by 22% for w/c ratio of 0.35, 9.7% for w/c ratio of 0.45 and 9.4% for w/c ratio of 0.55 for steel fiber volume fractions 0.33%, 0.67% and 1%, respectively, (c) flexural strength increased on average by 63% for w/c ratio of 0.35, 93% for w/c ratio of 0.45 and 105% for w/c ratio of 0.55 for steel fiber volume fractions 0.33%, 0.67% and 1%, respectively, (d) the ductility, the ability of the specimens to deform excessively without rupture, of the FRC increased with the increase of steel fiber volume fraction, (e) the fracture energy of FRC increased with the increase in tensile strength steel fibers by an average of 444% for w/c ratio of 0.35, 272% for w/c ratio of 0.45 and 64% for w/c ratio of 0.55 for steel fiber volume fractions of 0.33%, 0.67% and 1%, respectively.

www.manaraa.com

Recent trends of high strength steel fiber reinforced concrete were presented by Shah and Ribakov (Shah 2011). This study presents the most current experimental results, applications and testing methods in the field of FRC. Refer to Section 1.5.5 for summary of the current applications of FRC.

The pull out response of straight steel fibers distributed randomly in the cement matrices was studied by Laranjeira et al. (Laranjeira 2010). Mechanical behavior of SCC with hybrid fiber reinforcement (steel and polymeric synthetic) was studied by Pons et al. (Pons 2007). They were able to show that self-compacting concrete exhibited better fiber-matrix bond than vibrated normal concrete with similar mechanical properties. The effect of high temperatures on mechanical properties of steel fiber reinforced concrete was investigated by Colombo et al. (Colombo 2010). The research shows the decay of peak and post-cracking strength as the temperature increases for uniaxial compression, uniaxial tension and bending.

Casanova and Rossi conducted experiments on steel fiber reinforced beams, with compressive strength of 27.5 MPa (4 ksi), under flexural stress and on cylinders subjected to uniaxial tension stress (Casanova 1996). They investigated two beam sizes and two types of steel fibers: (a) 0.54% volume fraction, hooked end with aspect ratio (l/d) of 75 and (b) 0.67% volume fraction, two-headed nail with aspect ratio (l/d) of 54. The study proposed a model to analyze SFRC beams subjected to bending. The model takes into account, after the onset of a macrocrack, a beam section acts like a plastic hinge. The hinge is modeled into parts; the macrocrack - as a uniaxial tension and the uncracked section is modeled by non-linear behavior of concrete. Comparison of the model and experimental results from: compressive strain vs crack opening, curvature vs

www.manaraa.com

crack opening and moment vs curvature diagrams demonstrated the modeling results in agreement with the experimental results.

The effect of steel fibers on bond strength performance of normal-strength steel fiber reinforced concrete (SFRC) through a series of pullout tests was conducted by Garcia-Taengua (Garcia-Taengua 2011). The study was conducted for three types of fiber volume fractions 0%, 0.54% and 0.95%; and for two types of steel fiber aspect ratio (l/d), 65 and 80. The average compressive strength of the concrete was 30 MPa (4.35 ksi). The flexural stresses at the limit of proportionality were: 4.13 MPa (0.6 ksi) for 0% fiber, 3.51 MPa (0.51 ksi) for V_f = 0.54% (l/d = 65), 3.47 MPa (0.50 ksi) for V_f = 0.54% (l/d = 80), 3.72 MPa (0.54 ksi) for V_f = 0.95% (l/d = 65), 3.52 MPa (0.51 ksi) for V_f = 0.95% (l/d = 80). The effects of: fiber volume fraction, fiber type and concrete cover were investigated. The study was able to conclude that: (a) fiber type (aspect ratio) affects the bond capacity and the slip corresponding to the peak bond stress and (b) fiber content affect the bond stress positively and hence bond performance.

The mechanical properties of normal to high strength steel fiber reinforced concrete, 3.6, 7.2 and 10.0 ksi (25, 50 and 69 MPa, respectively), with fiber content ranging from 0 to 1.5% by volume were studied by Khaloo and Kim (Khaloo 1996).

The influence silica fume on the mechanical properties such as impact resistance, surface abrasion and splitting tensile strength were studied for hooked-end steel fibers with three different aspect ratios- 60, 75 and 83 by Eren et al. (Eren 1999). Steel fiber contents of 0.5%, 1.0% and 2.0% by volume of concrete were considered. Their resulted showed, the inclusion of steel fibers improved impact resistance, surface abrasion and splitting tensile strength.

www.manaraa.com

The effect of steel fibers on the flexural and shear behavior of rectangular normal concrete strength beams, f'_c of 24 MPa (3.5 ksi), with1% steel fiber volume fraction was investigated by Ahmed and S.G. Ladkany (Ahmed, 2001). The study showed an increase of 11.3% on average tensile strength of FRC beams when compared to their counterpart plain concrete beams. Whereas, the average flexural strength of the FRC beams was 23.5% higher compared to plain concrete beams.

1.5.4 Steel fiber reinforced thin plates and shallow shells

Behavior of thin planar and curved concrete plates reinforced conventionally and with steel fibers was studied by Kearns and McConnell (Kearns 1989). Three types of specimen, 20 mm (0.8 in.) thick and with two-way plan dimension of 500 mm (19.7 in.), were studied: Type 1, 1.5% steel fiber by volume fraction; Type 2, 0.5% galvanized steel wires by volume fraction; and Type 3, both 0.5% steel fiber and 0.5% galvanized steel wire by volume fraction. A total of 21 specimens, 7 of each type, were tested for transverse loading. Three specimens were flat and the remaining four were doubly curved plates with a rise of 100 mm (3.94 in.) between supports. All specimens were 500 mm (20 in.) long, 500 mm (20 in.) wide and 20 mm (0.8 in.) thick. The studies which included a uniform type loading showed that: (1) curved plates behaved better than flat plates in: first crack strength in the case of type 2 and 3, maximum strength and toughness, (2) Type 1 specimen (1.5% steel fibers) possess the most strength at the proportionality limit, the most elastic stiffness, ductility, comparable toughness and maximum strength than Type 2 and 3 specimens.

www.manaraa.com

Full scale free suspended elevated fiber reinforced circular slabs with a slab diameter of 1.5 m (4.92 ft) and 2.0 m (6.56 ft), and a thickness of 150 mm (5.91 in.) and 200 mm (7.87 in.), respectively were studied for flexural behavior under center point loading by Destree (Destree 2004). The study investigated the behavior of FRC slab with steel fiber dosage ranging from 45 kg/m^3 (2.81 lb/ft^3) to 120 kg/m^3 (7.49 lb/ft^3), equivalent to 0.57% to 1.53% by volume fraction, and steel fiber aspect ratios of 40 and 60. Full scale rectangular slabs, 6 m (19.7 ft) by 6 m (19.7 ft) and 0.2 m (0.7 ft) thick, were also constructed using 100 kg/m^3 (6.24 lb/ft^3), equivalent to 1.28% by volume fraction, of deformed steel fibers and subjected to a full scale test. The study was able to conclude that replacement of the traditional rebar reinforcement in suspended slabs is possible with steel fiber-only reinforced slabs for spans ranging from 3 m (9.84 ft) to 5 m (16.4 ft) with span to depth ratios of 12 to 25.

1.5.5 Applications of SFRC

The application of SFRC as a bridge overlay was investigated by Meda and Rosalt (Meda 2003). The use of FRC in precast tunnel lining construction is gaining ground because of the advantages in performance, durability and manufacturing. Test of Precast tunnel segments subjected to local critical forces were conducted to compare performance with other materials such as, plain concrete and concrete reinforced with rebars. Tests show SFRC's efficiency compared to the traditional reinforcement (Riaz 2008). A 2.42 mi (3.9 km) long heating tunnel from the island of Amager to the center of Copenhagen is lined with SFRC without any conventional steel reinforcement (Kasper 2007). SFRC can be implemented in beam-column joints to improve the ductility and

www.manaraa.com

stiffness degradation of the joint (Ganesan 2007). Traditional mesh reinforcement with #3 bars spaced at 152 mm (6 in.) on center was used in conjunction with 0.67% steel fibers by volume fraction, for the construction of shell roof on the submarine restaurant at the oceanographic park in Valencia, Spain (Serna 2009) with the concrete dry sprayed from the lowest to the highest point. An infrastructure in West Beach, Benidorm (Spain) built 13 ft (4m) high and 4,265 ft (1,300 m) long wall with merely steel fibers (V_f = 0.67%) without utilization of traditional reinforcement (Serna 2009). Steel fibers were used in place of traditional reinforcement because the nature of the wall surface was not regular. Fiber reinforced concrete can be used for strengthening, retrofitting and rehabilitation purposes. High strength fiber reinforced concrete (HSSFRC) provides an excellent option for design of seismic resistant structures. By using HSSFRC, which is a ductile material that has adequate seismic response, rigorous seismic detailing can be eliminated in the design thus, incurring great savings in time and labor (Serna 2009). The use of steel fibers as a sole minimum shear reinforcement in beams is allowed by ACI 544.3R-08, provided the conditions stated in ACI 318-08, Section 11.4.6.1 (f) are met. Section 11.4.6 (f) states that "a minimum area of shear reinforcement shall be provided in all reinforced concrete flexural members where V_u exceeds $0.5\phi V_c$ except, beams constructed of steel fiber reinforced, normal weight concrete with f'_c not exceeding 6000 psi, h not greater than 24 in., and V_u not greater than $\phi 2\sqrt{f'_c} b_w d$ ".

www.manaraa.com

CHAPTER 2

HIGH STRENGTH STEEL FIBER REINFORCED CONCRETE (HSSFRC)

2.1 Aggregates for high strength steel fiber reinforced concrete

Aggregates, in addition to their use as economical fillers, generally occupy 70 to 80% of the volume of concrete and therefore are expected to have an important influence on its properties (Mindess 2003), since the ultimate strength of concrete is limited by the strength of its coarse aggregates.

Aggregates must conform to certain standards for optimum engineering use: they must be clean, hard, strong, durable particles free of absorbed chemicals, coatings of clay, and other fine materials in amounts that could affect hydration and bond of the cement paste (Steven H. Kosmatka 2002)

Normal-weight aggregates should meet the standards set forth by ASTM C 33. ASTM C 33 standard gives directions as to: the limit of deleterious substances, grading, soundness and method of sampling and testing of aggregates.

To resist the stress of repeated loads and to avoid aggregate degradation, base-course aggregates must exhibit strength and toughness to serve their intended purpose. Of equal importance to base-course material other than strength is particle shape and toughness (Derucher 1998). Angular and tough aggregates are preferred as a base-course material. Angularity enhances aggregate interlock and a rough surface inhibits movement of one particle over another.

www.manaraa.com

2.1.1 Coarse aggregates

Coarse and fine aggregates were obtained, for this research, from a local quarry in Las Vegas, Nevada. Since the application of the concrete mixtures were ultimately to be used for thin plates and shells about 32 mm (1.25 in.) thick, the size of the coarse aggregate was limited to nominal sizes of 9.53 mm (3/8 in.) and #4 sieve size. The oven-dry specific gravity and absorption of the coarse aggregate (ASTM C 128-07a) were 2.777 and 0.60%, respectively. Deleterious substances were substantially below the maximum allowable limits for both coarse and fine aggregates.

2.1.2 Fine aggregates

Fine aggregates with minimum and maximum fineness modulus of 2.70 and 3.10, which is the sum of cumulative % retained in sieve numbers 4 to 100 divided by 100, met the requirements of ASTM C33 grading limitations, refer to Table 2.1. The oven-dry specific gravity and absorption of the fine aggregate (ASTM C 128-07a) were 2.785 and 0.64%, respectively.

Sieve analysis results for coarse and fine aggregates are presented in Table 2.1 and Figure 2.1.

www.manaraa.com

2.1.3 Sieve analysis of coarse and fine aggregates

Table 2.1: Sieve analysis of fine aggregate, mass in percent, and a fineness modulus of 3.04

Sieve number	Percent passing	Fine aggregate (ASTM C 33)	
	(%)	Min (%)	Max (%)
4	100	95	100
8	90	80	100
16	55	50	85
30	30	25	60
50	15	5	30
100	6	0	10

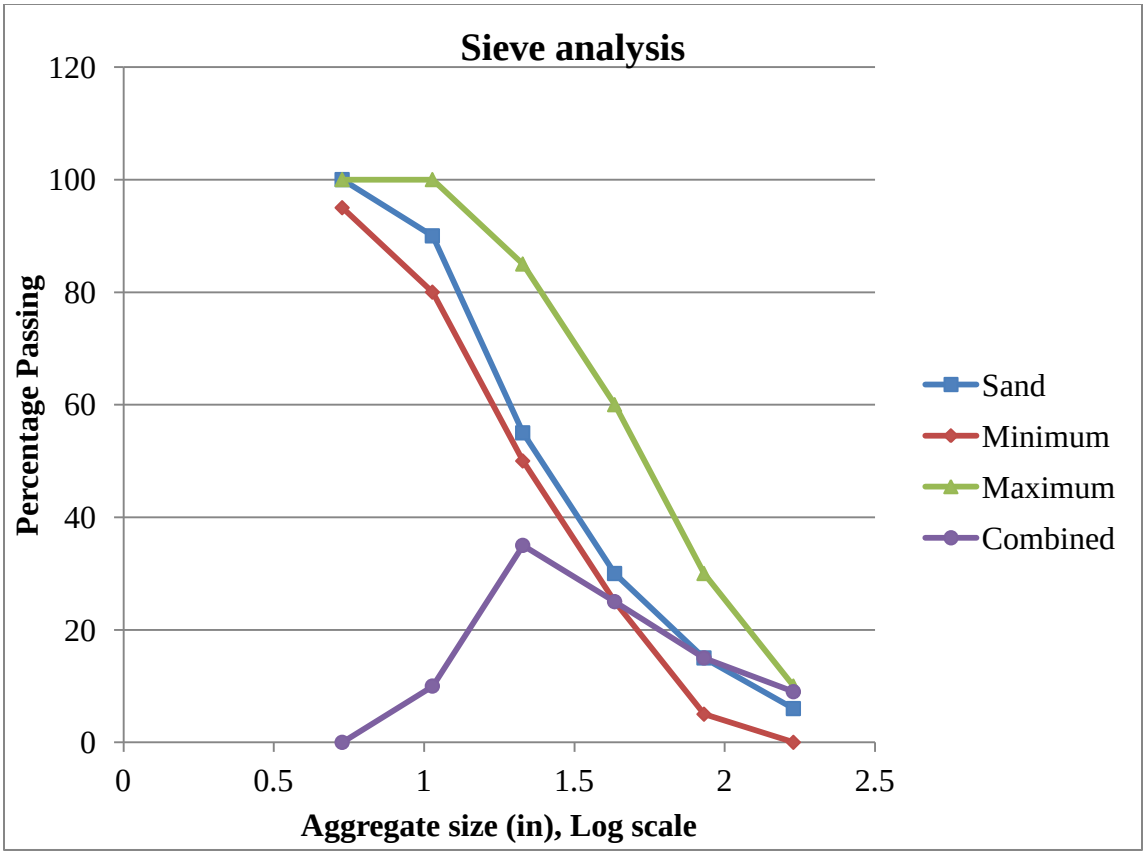

Figure 2.1: Sieve analysis of fine and coarse aggregates

www.manaraa.com

2.2 Cement

ASTM C 150 Type V Portland cement with a dosage of 404 kg/m^3 (25.2 lb/ft^3) was used to prepare the concrete mixtures. Portland cement is defined by ASTM C 150 as "hydraulic cement produced by pulverizing clinker consisting essentially of hydraulic calcium silicates, usually containing one or more of the forms of calcium sulfate as an interground addition". Type V Portland cement is widely used in the local area due to its resistance to sulfate. Use of Type V Portland cement should be accompanied by the use of low water to cementitious ratio and low permeability for the concrete to resist sulfate exposure (Steven H. Kosmatka 2002).

2.3 Chemical admixtures

2.3.1 High-range water reducing agent (HRWR)

Water reducing admixtures are used to lower the water-to-cement ratio in order to produce high strength concrete. They also increase workability, slump and are ideal for placing concrete by way of pumping. High-range water reducing admixtures, superplasticizer, can reduce the water demand by 12% to 30% (Steven H. Kosmatka 2002). In this study, ADVA Cast 540 type HRWR admixture was used which reduced the water demand by 35%. ADVA Cast 540 is a high efficiency polycarboxylate-based superplasticizer. ADVA Cast 540 complies with ASTM C494 as a Type A and F, and ASTM C1017 Type I admixture. The addition rate recommended by the manufacturer ranges between 325 to 1300 mL/100 kg (5 to 20 fl oz/100 lbs) of cementitious material.

www.manaraa.com

2.3.2 Viscosity-modifying agent (VMA)

Viscosity-modifying agent is used to modify the rheology of concrete mixtures. VMA increases the viscosity of the concrete mixture, while it still enabling the mixture to flow and be cohesive. It also enhances the dynamic stability of flow-able/SCC concrete mixtures. V-MAR 3 type VMA was used. The addition rate of 309 to 1,550 mL/m^3 (10 to 40 fl oz/yd^3) is recommended by the manufacturer.

2.4 Mineral admixtures

Fly ash, silica fume, slag and natural pozzolans, which are also referred as supplementary cementitious materials, contribute to the hardened properties of concrete. They are also used to enhance a specific concrete property, such as high strength. Supplementary cementitious materials can be used in addition to or as a partial replacement of Portland cement in concrete mixtures (Steven H. Kosmatka 2002). Depending on the anticipated concrete properties, one or a combination of two or more of supplementary cementitious materials may be used.

2.4.1 Silica fume

Silica fume or Microsilica is defined by ASTM C 1240 as "very fine pozzolonic material, composed mostly of amorphous silica produced by electric arc furnace as a byproduct of the production of elemental silicon or ferrosilicon alloys". Silica fume has a surface area of about 20,000 m^2/kg (97,649 ft^2/lb), and a relative density of 2.20 to 2.50 (Steven H. Kosmatka 2002). Silica fume should conform to the physical properties and chemical composition requirements set forth by ASTM C 1240 standard. The amount of

www.manaraa.com

silica fume used is usually between 5% and 10% of the total cementitious material. In this study, silica fume used was about 5% to the total mass of cementitious material.

2.4.2 Fly ash

Fly ash is widely used supplementary cementitious material and defined by ASTM C 618 as, "the finely divided residue that results from the combustion of ground or powdered coal and that is transported by flue gasses". Fly ash should conform to the physical properties and chemical composition requirements set forth by ASTM C 618 standard. The specific gravity and surface area of fly ash varies between 1.9 and 2.8 and 300 to 500 m^2/kg (1,464 to 2,441 ft^2/lb), respectively (Steven H. Kosmatka 2002). Fly ash is gray or tan in color and looks like Portland cement. Fly ash is classified into three classes: Class C, Class F and Class N depending on their chemical composition. Class F type fly ash was used in this study because of its availability. The dosage of Class F fly ash is typically between 15% to 25% of the total mass of the cementitious material (Steven H. Kosmatka 2002). The percentage of fly ash used in this research was a little higher than the upper bound indicated above at 28.5% to the total mass of cementitious material.

2.5 Steel fibers

Fiber reinforced concrete (FRC) is a composite material constituted of: water, hydraulic cement, coarse and fine aggregates, admixtures (if necessary) and discontinuous and dispersed fibers. Fibers can be: steel, glass, cellulose, polymers or woven fabrics.

www.manaraa.com

Steel fibers that are intended to be used in fiber reinforced concrete shall comply with ASTM specifications. ASTM A 820, specifies there are five types of Steel fibers: cold-drawn wire, cut sheet, melt-extracted fibers, mill cut or modified cold-drawn wire steel fibers (ASTM A 820 2006).

Fibers can be added to the concrete matrix as monofilaments (single filaments) or multi-filament strands. Multi-filament strands are temporarily or permanently bonded individual strands. Temporarily bonded multi-filament strands are intended to disperse to individual filaments during the concrete mixing process (Johnston 2001).

The commonly used steel fiber lengths are in the range of 12.7 to 63.5 mm (0.5 to 2.5 inches) with aspect ratio varying from 30 to 100 in/in. Aspect ratio is defined as fiber length divided by equivalent fiber diameter. Where, the equivalent fiber diameter is defined as the diameter of a circle having the same cross-sectional area as the fiber (Mindess 2003).

Steel fibers are short, discrete lengths of steel with an aspect ratio (ratio of length to diameter) from about 20 to 100 (Steven H. Kosmatka 2002). The cross section of a steel fiber can be: oval, round, polygonal or crescent in shapes, depending on the process of manufacturing and raw materials used (ACI 2008).

In this case, ASTM 820-90 Type II Deformed cut sheet carbon steel fibers with equivalent diameter of 0.584 mm (0.023 in.) and aspect ratio, l/D, of 47:1 were used. The steel fibers, as shown in Figure 2.2, have rectangular cross section of 0.406 x 0.838 x 19.05 mm (0.016 x 0.033 x 0.75 in.) and specific gravity of 7.85. The tensile strength of steel-fibers ranges between 379 to 763 MPa (55,000 to 111,000 psi).

www.manaraa.com

Figure 2.2: Mechanically deformed steel fibers

www.manaraa.com

CHAPTER 3

MIXTURE PROPORTIONING

3.1 Proportioning methods

In many cases, no changes are necessary to conventional concrete mixture proportions when adding fibers at low to moderate dosages. Adding fibers at less than approximately 0.25% by volume will typically not require adjustment to conventional mixtures as for as cementitious content and fine and course aggregate ratios are concerned (ACI 2008).

The tendency for wet steel fibers to ball during mixing increases with increases in the maximum size aggregate, the coarse-to-fine aggregate ratio, the fiber aspect ratio, and the amount and the rate of addition of fibers to the mixer (Tatnall 1984). It also depends on the method of addition of fibers to the mixer, geometry of the fiber, and whether or not they are collated (ACI 2008).

Depending on the fiber type and amount it may be required to adjust the water content, or preferably to add or increase water-reducing admixture quantities, to maintain workability, slump, and water-cement ratio (ACI 2008).

3.2 Mixing procedures

Preparation of concrete ingredients and procedure of mixing concrete were conducted per ASTM C 192. The concrete ingredients were stored in dry, clean and temperature controlled environment (67 – 74 °F) before they were mixed to comply with the requirements of ASTM C 192.

www.manaraa.com

The mixer and other tools that came into contact with the concrete were dampened to prevent mixing water fluctuation. Coarse aggregates were mixed for two minutes with 1/3 of the mixing water and steel fibers. Fine aggregates were added to the mixer and mixed for two minutes with 1/3 of mixing water and steel fibers. Lastly, the silica fume, fly ash and cement were added and mixed for two more minutes with the remaining 1/3 of mixing water and steel fibers. The admixtures, HRWRA and VMA, were added and the content mixed for three minutes followed by three minutes of rest and two more minutes of mixing, for a net mixing time of 14 minutes.

The mixer was stopped while the ingredients were loaded into it, with the exception of water and steel fibers. Two types of adding steel fibers to a concrete mixture have been described in ACI 544.3R-08. The first method is adding fibers as the last ingredient directly to the mixer while the mixer is operating at normal charging speed. The second method involves mixing fibers with aggregates first. If this is not possible, add fibers into the mixer right after the aggregates. The steel fiber adding procedure, in this study, falls to the latter procedure. In which, one third of the steel fibers were added by spreading them manually, a pitch at a time, right after coarse aggregate, fine aggregate, and cementitious materials, respectively. Steel fibers should not be allowed to form clumps or balling at any stage of the mixing process.

3.3 Balling of fibers

As per ACI 544.3R, most of balling occur before the fibers get into the mixture. Once the fibers get into the mixture ball-free, they generally stay ball-free. Fibers should not be allowed to pile up or slide down the vanes of partially filled drums. Fibers should not be

www.manaraa.com

added too fast. Fibers also should be added into the mixture, and the mixer should carry them away into the mixture as fast as they are added.

Other possible explanations for balling are due to adding high dosage of fibers to a mixture (more than 2% by volume or even 1% of a fiber with high aspect ratio). Adding fibers to the mixer first will also cause the fibers to ball because there is nothing to keep them apart. The most common causes of wet fiber balling is over-mixing and using a mixture with coarse aggregate more than 55% of the total combined aggregate by absolute volume (ACI 2008).

In this research, 1% and 2 % steel fibers by volume fractions were hardly noticeable both during mixing and placement of concrete mixtures. As the steel fiber by volume fraction increased to 3% and 4%, the steel fibers were very visible and abundant, but balling was not observed due to the fact that: (a) steel fibers were added gradually into the mixer after each constituent was charged, and (b) the presence of larger amount of fine to coarse aggregate ratio facilitates the mixing of steel fibers with the rest of the constituents easily.

www.manaraa.com

CHAPTER 4

SPECIMEN PREPARATIONS AND TESTING PROCEDURES

4.1 Specimen preparations for standard fiber reinforced concrete

Procedures outlined in ASTM C192 should be followed when making and curing concrete test specimens, and ASTM C 1018 when flexural toughness and first-crack strength are being considered.

According to the procedure stated in ACI 544.2R, the following steps should be followed while preparing FRC specimens:

1. Specimens should be prepared using external vibrators when possible.
2. Internal vibration is not preferable. Rodding should be avoided, since both procedures affect the distribution of fibers in the concrete mix.
3. The method, time, frequency and amplitude of vibration ought to be recorded.
4. If the depth of the specimen is 75 mm (3 in.) or less, single layer should be used to cast the specimen.
5. If the depth of the specimen is greater than 75 mm (3 in.), two layers should be used to cast the specimen; each layer should be vibrated as required.
6. The smallest specimen dimension should be at least three times the larger of the fiber length or the maximum aggregate size, whichever is greater.

Specimens for flexural toughness should be prepared and selected according the recommendations of ASTM 1018:

1. Test specimens length should be at least 50 mm (2 in.) greater than three times the depth, and must not be less than 350 mm (14 in.).

www.manaraa.com

2. Test specimens width should be at least three times the maximum fiber length.
3. The depth and size of test specimens shall conform to either:
    - *Thick Section* - The depth of test specimens shall be at least three times the maximum fiber length, the preferred size is 350 by 100 by 100 mm (14 by 4 by 4 in.).
    - *Thin Section* – When the requirements of *Thick Section* are not met, specimen's depth equal to the actual section thickness to be used shall be tested.
4. Compaction shall be made by external vibration. The time of vibration shall be adequate enough to provide sufficient consolidation.
5. Avoid fiber discontinuity by allowing uniform placement of successive layers.
6. At least three specimens from each sample of fresh or hardened concrete shall be prepared for testing.

4.2 Specimen preparations for self-consolidating concrete (SCC)

Self-consolidating concrete specimen preparations should follow the same procedures as Section 4.1 with the exception that, SCC specimens should not be vibrated. The inherent property of SCC is, its ability to consolidate on its own weight without the help of vibration or other form of consolidation techniques.

www.manaraa.com

4.3 Test procedures for fresh properties of high strength steel fiber reinforced concrete [Phase (1a)]

Phase (1a) focuses on the search for a suitable mixture of high strength flow-able/SCC concrete with varying steel fiber by volume fractions. During this phase, the research concentrates on the selection of suitable flow-able/SCC concrete that would be easy to use in the testing and manufacturing of ultra thin (< 1.5 in., 38 mm thick) structures. Note that, this research *does not attempt* to create varying fiber concrete mixtures having different fiber by volume fractions with the same rheological properties. FRC with variable steel fiber by volume fractions were mixed and undergone tests to see if they could satisfy self-consolidating concrete (SCC) criteria, especially so when the steel content is equal to or exceeds 1% by volume fraction . The concrete batches have the same constituents in each mixture except for steel fiber by volume fraction and high-range water reducing agent (HWRW), which helps make the mixture flow-able. Bear in mind that, the *fresh (rheological) properties*, such as slump flow diameter, fiber orientations, V-funnel flow rate and J-ring flow diameter of mixtures with different steel by volume fractions, are *not* compared to one another. The tests are conducted merely to check whether the mixtures can be classified as SCC or flow-able FRC and to monitor their ability to flow uniformly when placed in the plate and shell forms.

Since the ultimate goal of the research is to have very thin high strength, high fiber by volume fraction ($\geq$ 1.5%) structural members, it will be valuable to have the mixtures behave in somewhat similar manner to SCC to ease and speed up their placement. Hence, extensive trial mixtures numbering 125 were conducted to achieve desirable fresh

www.manaraa.com

properties of the various mixtures under consideration. Test results are shown in the main body of the proposal.

4.3.1 Flow ability: slump flow (spread diameter) and flow rate tests

The unconfined workability of SCC was measured using slump flow. In the procedure, a standard slump cone (upright or inverted) is filled with concrete and the cone is lifted vertically with no lateral or torsional motion to let the mixture flow. Slump flow is measured by taking the average of two perpendicular diameters of the flow (Figure 4.1). If the diameters differ by more than 50 mm (2 in.), the test is invalid and need to be repeated (ASTM C 1611 2009).

The time elapsed for flow to reach 508 mm (20 in.) diameter from the initial time of test cone lift is defined as the rate of flow (ASTM C 1611 2009). Target flow rate for standard SCC is 5 seconds or less (ASTM C09.47 2009). For summary of slump flow and flow rate test results, refer to Section 5.1.

www.manaraa.com

Figure 4.1: Typical SCC slump flow (spread diameter)

4.3.2 Pass ability: J-Ring Test

A similar set up as slump flow test except a J-Ring, circular ring with 16 #5 deformed bars shown in Figure 4.2, is placed around the perimeter of the test cone before the lift. The J-Ring flow diameter is the average of the two perpendicular diameters measured. The difference between the slump flow and J-Ring flow determines the passing ability of the concrete mixture. A difference of 25 mm (1 in.) shows good passing ability and a

www.manaraa.com

difference of more than 50 mm (2 in.) shows poor passing ability for standard SCC (ASTM C1621 2009). For summary of J-Ring test results, refer to Section 5.1.

Figure 4.2: Typical J-Ring test apparatus

4.3.3 Fill ability: V-Funnel Test

A V- shaped funnel, Figure 4.3, is filled with concrete mixture, the bottom door is opened and the time passed for the content to clear the apparatus is recorded as V-Funnel flow time (t_v). V-Funnel flow time of 10 seconds or less shows good filling ability for standard SCC concrete mixtures (ASTM C09.47 2009). Summary of V-Funnel test results are present in Section 5.1.

www.manaraa.com

Figure 4.3: Typical V-Funnel test apparatus

4.3.4 Fill and pass ability: U-Box Test

A U-shaped box equipped with 3 #4 bars placed in the vertical position at the bottom center of the box and a sliding door, (Figures 4.4 and 4.5), is filled with the concrete mixture. The sliding door is lifted and the height of the mixture in the two chambers is measured. The difference in height, U-Box filling height, of 304.8 mm (12 in.) or less indicates the mixture has good filling and passing ability for standard SCC (ASTM C09.47 2009). For summary of U-Box test results, refer to Section 5.1.

www.manaraa.com

Figure 4.4: Typical U-Box test apparatus

www.manaraa.com

Figure 4.5: Rebar set-up in U-Box test apparatus

4.3.5 Slump test

In general, the slump for standard FRC determined from ASTM C143 should be at least 25.4 mm (1 in.), but not greater than 177.8 mm (7 in.). Factors that influence the measured slump include the fiber type, length, aspect ratio, amount, cement content, fine aggregate content, aggregate shape, and grading (ACI 2008).

Slump for FRSCC is measured from the top of the test cone's initial position to the top of the spread, with a slump equal or larger than 230 mm (9 in.) is required for flow-able and SCC.

www.manaraa.com

4.3.6 Visual stability index test

The visual stability index (VSI) test is a visual inspection of a slump flow in a slump flow spread test to determine or establish the stability of SCC mixture. VSI test is conducted to see whether the SCC mixture is showing signs of bleeding, segregation, aggregate piling, rough spread perimeter and an overall characteristic of the mixture to flow in a cohesive manner. There are four visual stability index ratings of SCC mixtures per ACI 237R-07:

i. VSI = 0, No evidence of segregation in slump flow
ii. VSI = 1, No mortar halo or aggregate pile in the slump flow spread
iii. VSI = 2, A slight mortar halo (< 10 mm [0.375 in.]) or aggregate pile, or both, in the slump flow spread
iv. VSI = 3, Clearly segregating (mortar halo > 10 mm [0.375 in.]) or a large aggregate pile in the center of the spread, or both.

In this research all acceptable mixtures satisfy VSI 0 and 1.

4.4 Test procedures for hardened properties of high strength steel fiber reinforced concrete specimens [Phase (1b)]

Once the desirable fresh properties of HSSFRC mixtures were obtained in phase (1a) for each steel fiber by volume fraction (0% - 4%), tests were conducted to determine the mechanical properties such as compressive, splitting tension and beam flexural strength. The main reason for having the same constituents in the various mixtures, except for steel fiber by volume fraction and HRWR dosage, was primarily to be able to compare the mechanical properties such as, tension, compression, modulus of elasticity, modulus of

www.manaraa.com

rupture and flexural strength of the various HSSFRC specimens under different loading conditions.

Splitting tension, compression and flexure test results were conducted for 0% - 4% high strength steel fiber reinforced concrete specimens. All results reflect un-vibrated HSSFRC specimens.

4.4.1 Compressive strength test

Compression tests were conducted per requirements set forth by ASTM C 39 for cylindrical concrete specimens. Four specimens from each batch of concrete mixtures were collected for testing purposes. The specimens were standard size of 101 mm (4 in.) diameter by 203 mm (8 in.) in length. *Soiltest* compression machine was used to test all concrete cylinders (Figure 4.6). The testing machine meets the requirements of ASTM C 39 standard and is fully calibrated every 12 month interval. Load was applied to the specimens within the range of 0.15 to 0.35 MPa/s (20 to 50 psi/s) as suggested by the standard.

www.manaraa.com

Figure 4.6: Compression strength test machine

Test procedures (ASTM C 39 2001):

1. Specimens were removed from the curing room.
2. Specimens were wiped dry thoroughly.
3. Two diameters of the specimen perpendicular to each other were measured.
4. Two lengths of the specimen directly opposite to each other were measured.
5. Compressometer was attached and tightened to the middle section of the specimen, for 28 and 56 day tests only (Refer to Section 4.4.2).

www.manaraa.com

6. End caps were fitted on the top and bottom sides of the specimen. End caps were equipped with urethane pads.
7. Specimen was placed in the compression machine so that it was in the center of the top bearing block.
8. Load was applied to the specimen at a rate of 0.15 to 0.35 MPa/s (20 to 50 psi/s).
9. The peak load was recorded.
10. The maximum compressive stress was calculated by dividing the peak load with the average area (from average diameter). No correction was needed as the length to diameter ratio was greater than 1.75.

For summary of compressive strength test results, refer to Section 5.2.1.

4.4.2 Static modulus of elasticity test for concrete in compression

This test method establishes a stress to strain ratio value for hardened concrete at 28 and 56 days curing stage. The tests were conducted to conform to ASTM C 469 standard. The loading rate and test machine type (Figure 4.7) are similar to the one stated in Section 4.4.1. A Compressometer device sensitive to 0.00254 mm (0.0001 in.) is used to measure the longitudinal deflection of the concrete specimens.

www.manaraa.com

Figure 4.7: Static modulus of elasticity test

The total longitudinal deformation is given as - the gage reading divided by two. The effective gage length, which is the distance between the gage support points, of the Compressometer is measured to be 136.5 mm (5.375 in.). A steady amount of load was applied at a rate of 0.15 to 0.35 MPa/s (20 to 50 psi/s). The applied load and the corresponding longitudinal deformation were recorded every 8,896N (2,000 lb) intervals without interruption. The longitudinal strain is defined as the total longitudinal deformation divided by the effective gage length.

www.manaraa.com

The modulus of elasticity is given as (ASTM C 469 1994):

$$E = (S_2 - S_1) / (\varepsilon_2 - \varepsilon_1) \quad (4.1)$$

Where:

E = modulus of elasticity

S_2 = stress corresponding to 40% of ultimate load

S_1 = stress corresponding to a longitudinal strain, ε_1, of 50 millionths

ε_2 = longitudinal strain produced by stress S_2.

For summary of static modulus of elasticity strength results at 28- day, refer to Section 5.2.1.

4.4.3 Poisson's ratio for concrete in compression

Test method for Poisson's ratios of molded cylinders under longitudinal compressive stress was conducted per ASTM C 469-94 standard. Test procedures described in Section 4.3 of ASTM C 469 were followed to determine Poisson's ratio of the cylinders. A device with a combined Compressometer and Extensometer was used to measure the longitudinal and transverse deformation of the cylinders. The Compressometer measures the longitudinal deformation of the cylinder and follows the same procedures stated in Section 4.4.2. In addition to Compressometer, the test set up includes an Extensometer that measures the deformation of the cylinder in the transverse direction. The Extensometer is equipped with a yoke, hinged at pivot points midway between top and bottom Compressometer's yokes, a pivot rod and a dial gage. The pivot rod and the dial gage are at the opposite ends of the yoke. The dial gage should be capable of measuring to the nearest 1.27 μm (50 μin.).

www.manaraa.com

The transverse deformation of the specimen diameter is given as (ASTM C 469 1994):

$$d' = g' \, e'_h / (e'_h + e'_g) \qquad (4.2)$$

Where:

d' = transverse deformation of the specimen diameter, μm (μin.)

g' = transverse gage reading , μm (μin.)

e'_h = the perpendicular distance from the hinge to the vertical plane passing through the support points of the middle yoke, mm (in.)

e'_g = the perpendicular distance from the gage to the vertical plane passing through the support points of the middle yoke, mm (in.).

In this case, dimensions obtained from the Extensometer used in the experiments show that e'_h = 76.2 mm (3 in.) and e'_g = 101.6 mm (4 in.).

4.4.4 Splitting tensile strength test of cylindrical concrete specimens

ASTM C 496 standards were followed to conduct the test method and procedures. The test method as described in Section 3 of ASTM C 496 - "consists of a diametral compressive force along the length of a cylindrical concrete specimen at a rate that is within a prescribed range until failure occurs". The loading rate and test machine type are similar to the one stated in Section 4.4.1. The two main reasons for performing splitting tensile strength test are: (i) it is simpler to determine than direct tensile strength and, (ii) it is used to determine the shear resistance provided by concrete members. Shear strength is also computed as a function of tensile splitting strength (Nawy 2001).

www.manaraa.com

Figure 4.8: Cylinder splitting tensile test

Test procedures (ASTM C 496 1996):

1. Remove concrete specimens from the curing room.
2. Mark diametrical line on each end of the specimen and ensure the lines are in the same plane.
3. Measure the diameter of the test specimen along the plane indicated in step 2 in three locations, at the ends and the middle section of the test specimen. Determine the average of the three measurements.
4. Take length measurements along the plane indicated in step 2. Determine the average of the two measurements.

www.manaraa.com

5. Place bearing plywood strip at the bottom and top of the specimen. Plywood strip should be 3.2 mm (0.125 in.) thick, approximately 25 mm (1 in.) wide and a length equal to or slightly longer than the specimen.
6. Place supplementary bearing plate on the top of the bearing strip and ensure the stripes, specimen and the bearing plate are aligned to the center of the thrust of the bearing block. The supplementary plate complies with the dimensional requirements of the standard.
7. Apply the load continuously at a rate of 689 to 1,380 kPa/min (100 to 200 psi/min) until failure of the test specimen.
8. Record the maximum applied load.

The splitting tensile strength is given as (ASTM C 469 1994):

$$T = 2P/\pi ld \qquad (4.3)$$

Where:

T = splitting tensile strength, kPa (psi)

P = maximum applied load indicated by the testing machine, kN (lb)

l = length, m (in.)

d = diameter, m (in.).

For summary of splitting tensile strength results, refer to Section 5.2.2.

4.4.5 Flexural strength test using simple beam with third-point loading

The test method and procedures were conducted to conform to ASTM C 78. Tinius-Olsen testing machine was used to test the flexural strength of the concrete beam specimens, as shown in Figure 4.9. The machine is equipped to apply a steady and

www.manaraa.com

controlled load; it was also connected to a computerized data acquisition system to measure and record load, strain and deflection data of the test specimens at predetermined time interval. The size of test specimens conforms to the dimension requirement of Section 5 of ASTM C 78; that is, the length of the beam specimen be 3 times its depth, 102 x 102 x 305 mm (4 x 4 x 12 in.).

Figure 4.9: Third-point beam test set up

www.manaraa.com

Test procedures (ASTM C 78 2000):

1. Take beam specimen out of the curing room and mark midpoint, support and third point locations on the beam.
2. Place the beam specimen on the steel channel, bottom plate, equipped with steel balls for end supports. The steel balls have a diameter of 50 mm (2 in.), a length of 152 mm (6 in.) and are located 305 mm (12 in.) apart. The channel has a width of 152 mm (6 in.) and a depth of 54.8 mm (2.2 in.).
3. Place steel plate with two steel balls at 102 mm (4 in.) apart on the top of the beam. The steel plate is 19 mm (0.75 in.) thick, 76 mm (3 in.) wide, and 203 mm (8 in.) long. The steel balls are 25 mm (1 in.) in diameter and about 152 mm (6 in.) in length. Make sure the centers of the steel balls are resting on the previously marked third points.
4. Attach deflection gage at the mid span of the beam specimen.
5. Apply the load on the top steel plate at the rate between 0.025 – 0.051 mm/minute (0.001 – 0.002 in./minute).
6. Record applied load and corresponding mid span deflection.
7. Record peak load.
8. Indicate where the initial fracture (crack) occurred.

The modulus of rupture is given as (ASTM C 78 2000):

A. If fracture initiated in the tension surface within the middle third of the span length,

$$R = PL / bd^2 \qquad (4.4)$$

Where: R = modulus of rupture, psi or MPa

www.manaraa.com

P = maximum applied load indicated by the testing machine, lb or N

L = span length, mm or in

b = average width of specimen at the fracture, mm or in.

d = average depth of specimen at the fracture, mm or in.

B. If the fracture occurs in the tension surface outside of the middle third of the span length by not more than 5% of the span length,

$R = 3Pa/bd^2$ (4.5)

Where: a = average distance between line of fracture and the nearest support measured on the tension surface of the beam, mm or in.

Beam flexural strength test results and summary are presented in Section 6.5.2.

4.4.6 Strain gage installations for concrete structures

The strain gages were installed on the concrete structures per the manufacturer's, Micro-Measurements, recommendations. The strain gages and all other accessories such as conditioner, neutralizer, degreaser, epoxy, etc. were supplied by Micro-Measurements and applied according to the instruction provided by the manufacturer. Installation of strain gages on the concrete surface is a two step process: Step 1, concrete surface preparation and Step 2, installation of the strain gages on the prepared area.

The following measures were taken to ensure proper surface preparation (Step 1):

- Irregularities on concrete surfaces, if present, were removed with the help of wire brush, disc sander or grit.
- Any loose materials or dirt on the surface were rinsed off with brush and mild detergent or just water.

www.manaraa.com

- CSM-2 degreaser was applied to remove greasy or oily substances.
- M-Prep Conditioner A were applied to the surface around the gage area and scrubbed with brush. The conditioner was blotted with gauze sponges. The area was rinsed with water.
- The area was scrubbed with M-Prep Neutralizer 5A to reduce the acidity and blotted with gauze and rinsed with water thoroughly.
- To seal the voids on the surface, M-Bond AE-10 type adhesive material was used. The adhesive was applied smoothly on the surface to fill the voids up and was allowed to cure. After the adhesive was cured, it was abraded with 320-grit abrasive paper till the surface was exposed.
- An outline of the strain gages were laid out on the gage area.

The following steps were taken for proper installation of strain gages on prepared concrete surfaces (Step 2):

- Scrub the installation area with Conditioner A and cotton applicator. Wipe dry using gauze sponges repeatedly till the surface is clean.
- Scrub the installation area with Neutralizer 5A and cotton applicator. Wipe dry using gauze sponges. Effort should be made to thoroughly neutralize all Condition A used in the previous steps. Install strain gage within 30 minutes.

www.manaraa.com

Strain gage installation procedure:

- Once the gage area is dry, apply slow curing adhesive M-Bond AE-10 on the installation area and the strain gage (curing time of the adhesive compound depends on the room the temperature).
- Install the strain gage within the outlined location.
- Apply a release film on the strain gage followed by pressure pad and plate.
- Finally, a pressure must be applied on the strain gage using heavy items or clamping hardware.
- Once the adhesive is cured, lead wires can be soldered.

www.manaraa.com

CHAPTER 5

HIGH STRENGTH STEEL FIBER RIENFORCED CONCRETE TEST RESULTS

5.1 Fresh properties results and concrete mixture proportioning

The whole purpose of the study is to achieve two properties of steel fiber reinforced concrete at the same time - high strength and self-consolidation (SCC). High concrete strength implies low water-to-cementitious ratio, while self-consolidating concrete requires more water or water reducing agents to make the mixture flow-able and workable. Hence, it can be seen from the start that the two properties, fresh and hardened properties, demand opposite constituent proportioning. Fresh property requires more water while the hardened property is obtained with less water. Therefore, the constituents of the initial mixtures were proportioned or designed with an intention to accommodate both the above requirements with different levels of steel fiber by volume fractions.

As a starting platform to our experimental studies, it was decided to use a concrete mixture that was obtained in previous studies by Doli (Doli 2004). The concrete mixture had yielded high compressive strength exceeding 70 MPa (10 ksi) and it has admixtures such as, superplasticizer (HRWR), fly ash and silica fume. The constituents of the original concrete mixture are given in Table 5.1.

There are at least three and potentially four variables to address while determining the optimum mixture, for a given percent of steel fiber by volume fraction. These are: water-to-cementitious ratio, coarse-to-fine aggregate ratio, superplasticizer (HRWR) and/or viscosity modifying admixture (VMA).

www.manaraa.com

Table 5.1: Constituents of the original concrete mixture

Mixture components	kg/m^3	
	(lb/ft^3)	(lb/yd^3)
3/8" Coarse aggregate	414.9	
	(25.9)	(700)
#4 Coarse aggregate	504.6	
	(31.5)	(850)
Fine aggregate, (Sand)	724	
	(45.2)	(1219)
Water	150.6	
	(9.4)	(255)
Cement Type V	400	
	(25)	(677)
Silica Fume	30.4	
	(1.9)	(50)
Fly Ash	171.4	
	(10.7)	(290)
Total cementitious	602.3	
	(37.6)	(1015)
Entrained Air	-	-

www.manaraa.com

In general, for comparison purpose, for a given steel fiber by volume fraction, most of the ingredients such as, coarse and fine aggregates, fly ash, silica fume, and cement were kept constant while water, superplasticizer and/or VMA were adjusted to meet the SCC requirements. If it was determined that the preliminary SCC requirements, such as slump flow and stability were not able to be met, the coarse-to-fine aggregate ratio were adjusted and the experiment proceeded by adjusting water, superplasticizer and/or VMA until a suitable mixture was achieved or further adjustment to the coarse-to-fine aggregate ratio was made. Once the mixture satisfied the preliminary requirements, namely: slump flow, rate of flow, J-ring, bleeding and aggregate piling (dynamic stability) for 0% steel fiber (control mixture), all the ingredients including water and coarse-to-fine aggregate ratio were kept constant while HRWR and/or VMA were adjusted to see if the mixture would satisfy the SCC requirements for 1% steel fiber by volume fraction. Adjust water if needed and once the desired mixture was achieved, the process would move on to the next steel fiber by volume fraction until 4% steel by volume fraction was reached. At this point, for 4% steel by volume fraction, the water-to-cement ratio along with other ingredients was fixed except HRWR and VMA; and work the way down to satisfy 3%, 2%, 1% and 0% for the new water-to-cement ratio standard set by the 4% steel by volume fraction. At this stage all mixtures will have the same amount of ingredients except HRWR and VMA (if used). All mixtures, 0%, 1%, 2%, 3% and 4% steel fiber by volume fractions (SFVF), that did satisfy the preliminary requirements were subjected to further fresh properties tests such as, fill ability (V-funnel test), and pass ability (J-Ring and U-Box test). If the mixture did not pass the preliminary requirements though, water-

www.manaraa.com

to-cement ratio and/or coarse-to-fine ratio will be adjusted and the process will be repeated all over again.

Other crucial factors affecting fresh properties of fiber reinforced mixtures are: temperature and humidity of the mixing environment, and moisture content of the aggregates. The step that was taken to limit or eliminate effects of temperature and humidity on the mixture was to mix the concrete in doors under relatively controlled laboratory settings. The effect of moisture content was addressed by oven drying both coarse and fine aggregates prior to using them.

Overall, about 125 concrete mixture experiments were conducted and their fresh properties studied.

1. Experiments #1 through #29 (0% SFVF)

29 experiments were conducted to establish a basic control mixture for the research experiments with 0% SFVF,. For convenience, fine aggregates were not used. Size #67 (ASTM C 33, Table 2) coarse aggregate with other ingredients described in Table 5.1 were used instead. HRWR, VMA and water-to-cementitious ratio were adjusted to get the best possible mixture. The best slump flow (spread) that could be achieved without the mixture losing its stability, as shown in Table 5.2 for experiment #13, was 432 mm (17 in.), below the minimum spread diameter of 508 mm (20 in.) required. Therefore, it was concluded that the coarse and fine aggregate composition had to be adjusted.

2. Experiments #30 through #42 (0%, 1%, and 4% SFVF)

In Experiments 30 through 42, 56% coarse to 44% fine aggregate ratio in conjunction with the rest of the ingredients shown in Table 5.1 were used. The coarse aggregate that is referred from here on words is composed of 50% of 9.9 mm (3/8 in.) and 50% of sieve

www.manaraa.com

#4 aggregate material. HRWR, VMA and water-to-cementitious ratio were adjusted to get the best possible mixture. The best possible mixture, as shown in Table 5.3 for experiment #41, met the minimum slump flow requirement but failed flow rate, and used higher than the maximum amount of HRWR allowed by the manufacturer. Hence, the coarse-to-fine aggregate ratio was adjusted once more to obtain suitable mixture.

Table 5.2: Fresh property results for experiment #13, kg/m^3 (lb/ft^3)

Mix	HRWR kg (lb)	VMA kg (lb)	Water to cement (cementitious) ratio	Steel fiber (%) (lb)	Slump flow mm (in)	Halo mm (in)	Slump mm (in)	T_{50} sec.
13	6.023 (0.376)	0.0 (0.0)	0.39 (0.25)	0% (0)	432 (17)	0 (0)	209.6 (8.25)	N/A

Table 5.3: Fresh property results for experiment #41, kg/m^3 (lb/ft^3)

Mix	HRWR kg (lb)	VMA kg (lb)	Water to cement (cementitious) ratio	Steel fiber (%) (lb)	Slump flow mm (in)	Halo mm (in)	Slump mm (in)	T_{50} sec.
41	8.938 (0.558)	0.005 (0.01)	0.424 (0.282)	2% (10)	578 (22.75)	0 (0)	241.3 (9.5)	15

www.manaraa.com

3. Experiments #43 through #125 (except experiment #46) (0%, 1%, 2% and 4% SFVF)

These series of experiments were conducted with 44 % coarse to 56% fine aggregate ratio in conjunction with the rest of the ingredients shown in Table 5.1. HRWR and water-to-cementitious ratio were adjusted to get the best possible mixtures. VMA was not used. In these experiments, a number of satisfactory mixtures for 0%, 1% and 2% SFVF were obtained. The results are show in Tables 5.4, 5.5 and 5.6.

Table 5.4: Fresh property results for experiments #91, #95, #99, #102 and # 124, kg/m^3 (lb/ft^3)

Mix	HRWR kg (lb)	VMA kg (lb)	Water to cement (cementitious) ratio	Steel fiber (%) (lb)	Slump flow mm (in.)	Halo mm (in.)	Slump mm (in.)	T_{50} sec
91	6.279 (0.392)	0	0.438 (0.291)	0% (0)	759.4 (29.9)	None	276.4 (11.0)	5
95	6.023 (0.376)	0	0.438 (0.291)	1% (5.00)	689.1 (27.13)	None	273.1 (10.75)	5
99	6.664 (0.416)	0	0.438 (0.291)	2% (10.00)	673.1 (26.5)	None	270.0 (10.63)	12
102	6.920 (0.432)	0	0.438 (0.291)	3% (15.00)	616.0 (24.25)	None	254 (10.00)	30
124	7.561 (0.472)	0	0.438 (0.291)	4% (20.00)	577.9 (22.75)	None	244.5 (9.63)	60

www.manaraa.com

In Table 5.5, the effects of HRWR and steel fibers on the fresh properties of HSSFRC mixtures are presented.

Table 5.5: Effect of HRWR and steel fibers on fresh properties of HSSFRC mixtures, kg/m^3 (lb/ft^3)

Mix. #	HRWR kg (lb)	VMA kg (lb)	Steel fiber % (lb)	Slump flow mm (in.)	Halo mm (in.)	Slump mm (in.)	T_{50} sec.
91	6.279 (0.392)	0	0% (0)	759.4 (29.9)	None	279.4 (11)	5
93	6.920 (0.432)	0	1% (5.00)	793.75 (31.25)	$\leq$ 38.1 (1.5)	279.4 (11)	5
94	6.407 (0.400)	0	1% (5.00)	762 (30)	$\leq$ 25.4 (1.0)	279.4 (11)	4
95	6.023 (0.376)	0	1% (5.00)	689.1 (27.13)	None	273.05 (10.75)	5
96	6.151 (0.384)	0	2% (10.00)	641.35 (25.25)	None	266.7 (10.5)	10
97	6.407 (0.400)	0	2% (10.00)	641.35 (25.25)	None	270.0 (10.63)	12
99	6.664 (0.416)	0	2% (10.00)	673.1 (26.5)	None	270.0 (10.63)	12

www.manaraa.com

In Table 5.6, fresh property results: J-Ring, V-Funnel and U-Box for successful experiments, #91, #95 and #99, are presented.

Table 5.6: J-Ring, V-Funnel and U-Box test results for experiments #91, #95, #99, #102 and #124, kg/m^3 (lb/ft^3)

Mix #	HRWR kg (lb)	VMA Kg (lb)	Steel-fiber (%) (lb)	J-Ring flow diameter mm (in.)	Slump flow diameter mm (in.)	V – Funnel sec.	U - Box H_1 - H_2 mm (in.)
91	6.279 (0.392)	0	0% (0)	768.4 (30.25)	759.4 (29.9)	8	1.52 (0.06)
95	6.023 (0.376)	0	1% (5.0)	666.8 (26.25)	689.1 (27.13)	18	25.4 (1.00)
99	6.664 (0.416)	0	2% (10.0)	628.7 (24.75)	673.1 (26.5)	31	495.3 19.50
102	6.920 (0.432)	0	3% (15.0)	616.0 (24.25)	759.4 (30.0)	N/A	N/A
124	7.561 (0.472)	0	4% (20.0)	577.9 (22.75)	689.1 (27.13)	N/A	N/A

www.manaraa.com

5.2 Hardened properties results

5.2.1 Compressive strength test results for HSSFRC cylinders

5.2.1.1 Compressive strength test results for HSSFRC cylinders

The 7, 28 and 56-day average compressive strength results for HSSFRC cylinders with variable SFVF are given in Table 5.7. The results show that the compressive strength of HSSFRC cylinders increased as the curing time increased.

Table 5.7: Comparison of 7, 28, and 56-day average compressive strength results for HSSFRC cylinders with various steel fiber by volume fractions

Cylinder	Compressive strength			percent increase 28-day to 7-day strength	percent % increase 56-day to 28-day strength
	7-day MPa (ksi)	28-day MPa (ksi)	56-day MPa (ksi)		
0%	50.28 (7.29)	67.98 (9.86)	78.58 (11.40)	35.21%	15.59%
1%	60.13 (8.72)	75.31 (10.92)	77.70 (11.27)	25.25%	3.17%
2%	61.2 (8.88)	80.72 (11.71)	86.75 (12.58)	31.90%	7.47%
3%	N/A	85.80 (12.44)	N/A	N/A	N/A
4%	61.4 (8.91)	73.18 (10.61)	82.14 (11.91)	19.19%	12.24%

www.manaraa.com

Average 28-day compressive strength test results for HSSFRC cylinders with variable steel fiber by volume fractions are given in Table 5.8 and Figure 5.1, while the modulus of elasticity is presented in Figure 5.2 and the stress versus strain curves are shown in Figure 5.3.

Table 5.8: Comparison of 28-day average compressive strength results for HSSFRC cylinders with various steel fiber by volume fractions

Cylinder	28-day compressive stress MPa (ksi)	Percentage increase over 0% steel fiber
0%	67.98 (9.86)	0%
1%	75.31 (10.92)	11%
2%	80.72 (11.71)	19%
3%	85.80 (12.44)	26%
4%	73.18 (10.61)	8%

www.manaraa.com

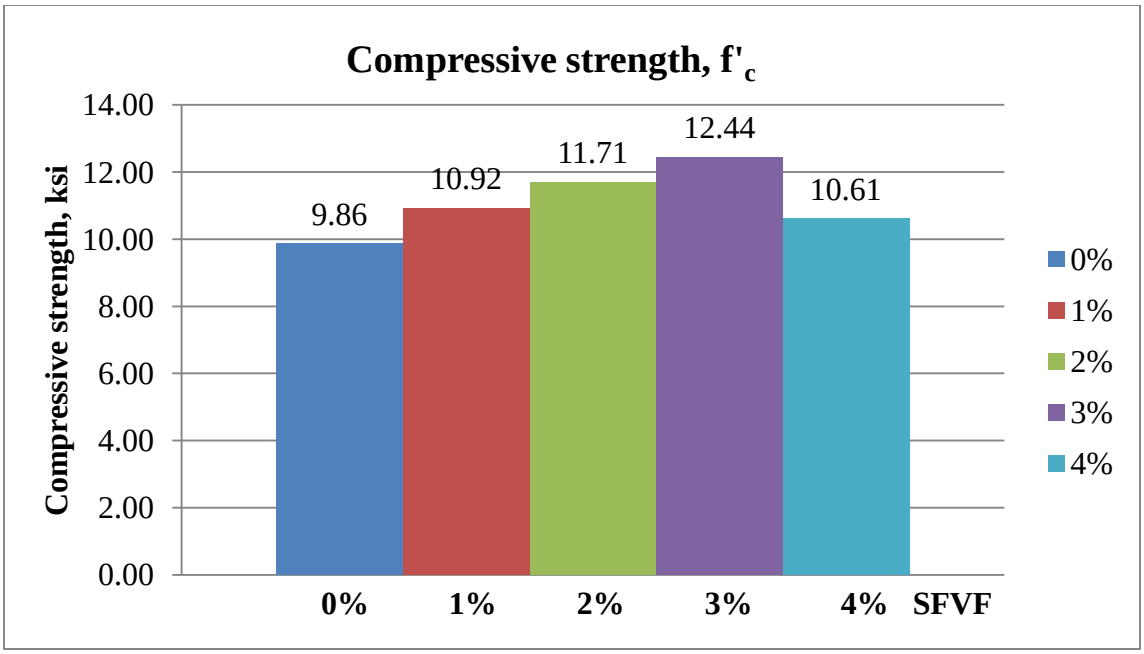

Figure 5.1: 28-day compressive strength results for HSSFRC cylinders with various steel fiber by volume fractions

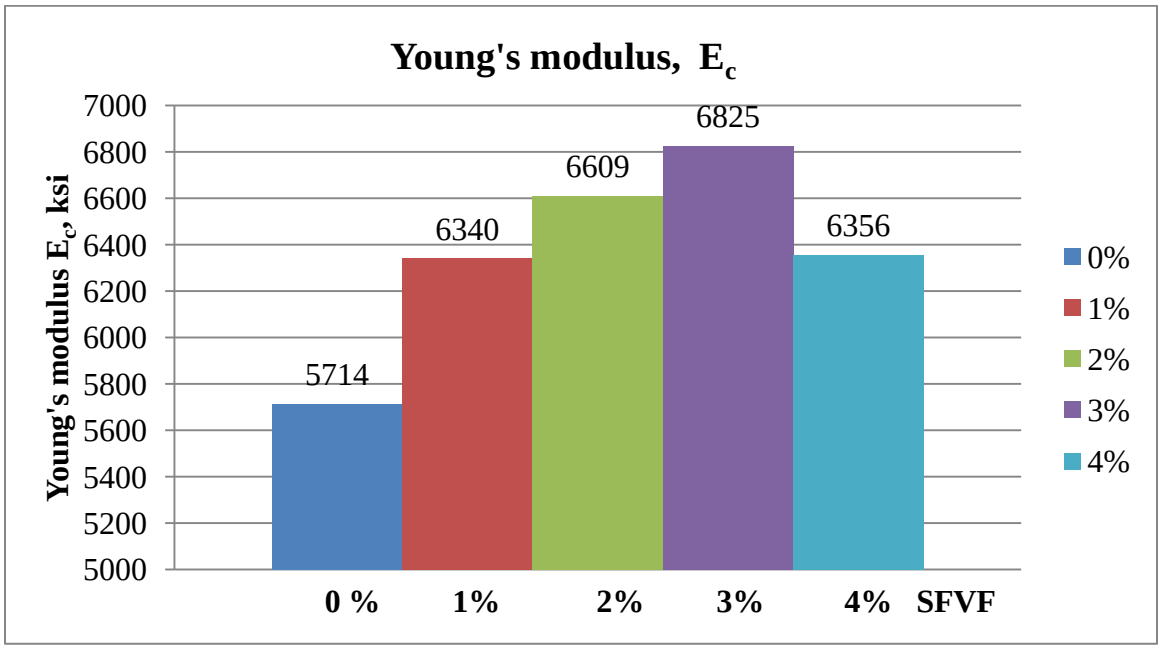

Figure 5.2: 28-day young's modulus results for HSSFRC cylinders in compression with various steel fiber by volume fractions

www.manaraa.com

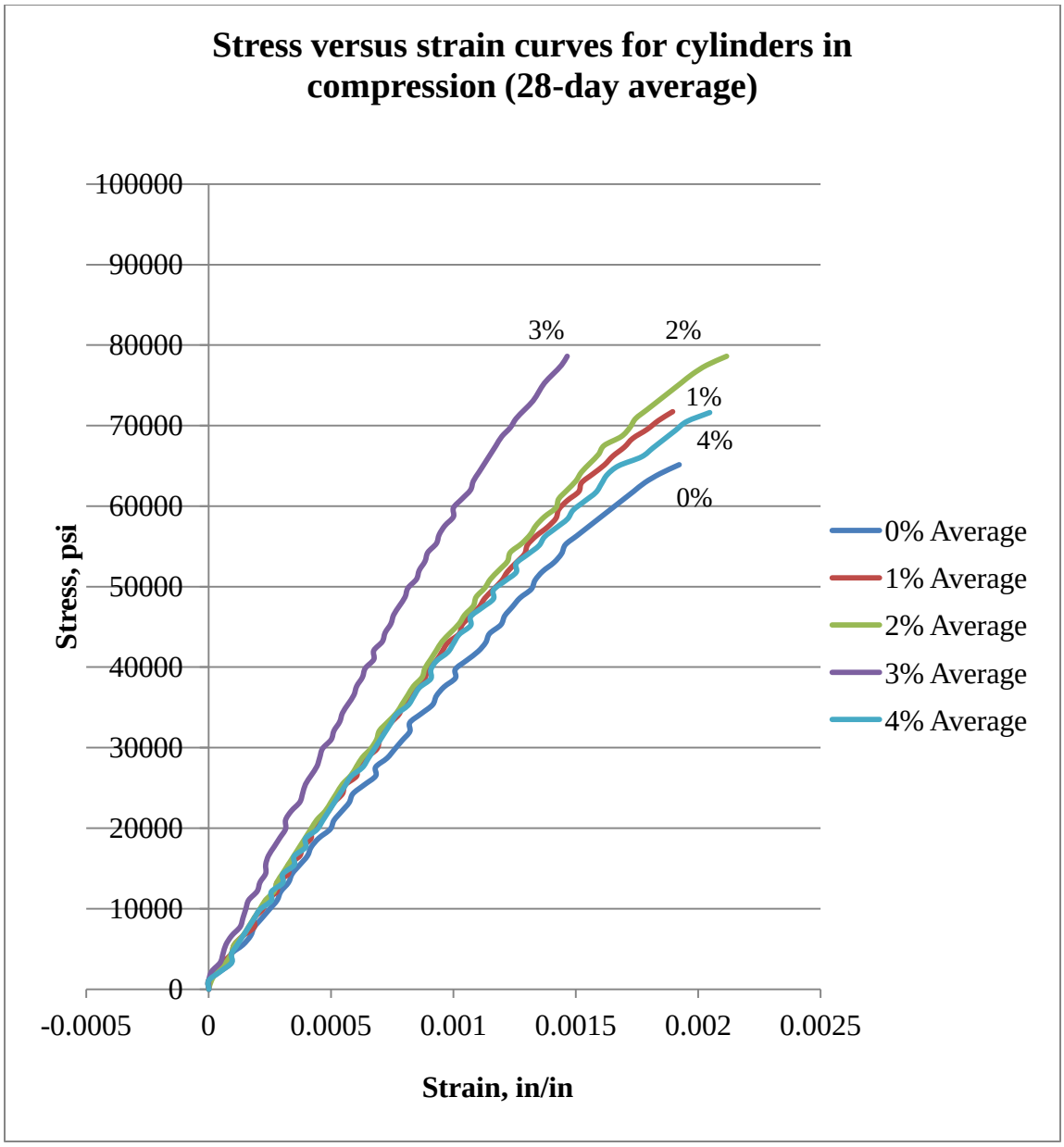

Figure 5.3: Stress versus strain curves for 0%, 1%, 2%, 3% and 4% HSSFRC cylinders

www.manaraa.com

5.2.1.2 Failure modes for HSSFRC cylinders under compression

The failure modes described in Table 5.9 were observed while testing 0%, 1%, 2% and 3% HSSFRC cylinders under compressive force. Refer to Figures 5.4, 5.5 and 5.6 for failure modes of 0%, 1% and 2% HSSFRC cylinders, respectively. The results show that the ductile form of failure of HSSFRC cylinders under compression increased as the steel fiber by volume fraction increased.

Table 5.9: Failure modes for HSSFRC cylinders under compression

Cylinder	Failure modes			
	Sound	Speed	Damage	Fracture type
0%	Very loud	Fast, Abrupt	Complete pulverization	Cone
1%	Loud	Fast	Less damage than 0%, Portion of the specimen damaged	Shear and Cone
2%	Mute mostly	Slow	Little damage, Specimen shape maintained	Shear
3%	Mute	Slow	Very little damage	Shear

www.manaraa.com

Figure 5.4: Failure mode for 0% HSSFRC cylinders under compression

www.manaraa.com

Figure 5.5: Failure mode for 1% HSSFRC cylinders under compression

www.manaraa.com

Figure 5.6: Failure mode for 2% HSSFRC cylinders under compression

www.manaraa.com

5.2.2 Cylinder splitting tensile strength test results

5.2.2.1 Splitting tensile strength test results for HSSFRC cylinders

A table comparing the average splitting tensile strength of HSSFRC cylinders at different stages of curing, 7, 28 and 56-day, with variable SFVF are given in Table 5.10. The results show that the splitting tensile strength of HSSFRC cylinders increased as the curing time increased.

Table 5.10: Comparison of 7, 28, and 56-day average splitting tensile strength results for HSSFRC cylinders with various steel fiber by volume fractions

Cylinder	Tensile strength 7-day MPa (ksi)	Tensile strength 28-day MPa (ksi)	Tensile strength 56-day MPa (ksi)	Percentage increase at 28-day over 7-day	Percentage increase at 56-day over 28-day
0%	5.34 (0.78)	6.63 (0.96)	7.46 (1.08)	24.16%	12.52%
1%	7.64 (1.11)	8.88 (1.29)	9.81 (1.42)	16.23%	10.47%
2%	8.08 (1.17)	10.33 (1.50)	11.71 (1.70)	27.85%	13.36%
3%	9.76 (1.42)	12.44 (1.80)	N/A	27.46%	N/A
4%	8.91 (1.29)	12.70 (1.84)	13.17 (1.91)	42.54%	3.70%

www.manaraa.com

Average 28-day splitting tensile strength test results for HSSFRC cylinders with variable steel fiber by volume fractions are given in Table 5.11 and Figure 5.7. The results show that the splitting tensile strength of HSSFRC cylinders increased as the steel fiber volume fraction increased.

Table 5.11: Comparison of 28-day average splitting tensile strength results for HSSFRC cylinders with various steel fiber by volume fractions

Cylinder	28-day tensile strength, MPa (ksi)	28-day strength increase over 28-day 0% steel fiber
0%	6.63 (0.96)	0%
1%	8.88 (1.29)	34%
2%	10.33 (1.50)	56%
3%	12.44 (1.80)	88%
4%	12.7 (1.84)	91%

www.manaraa.com

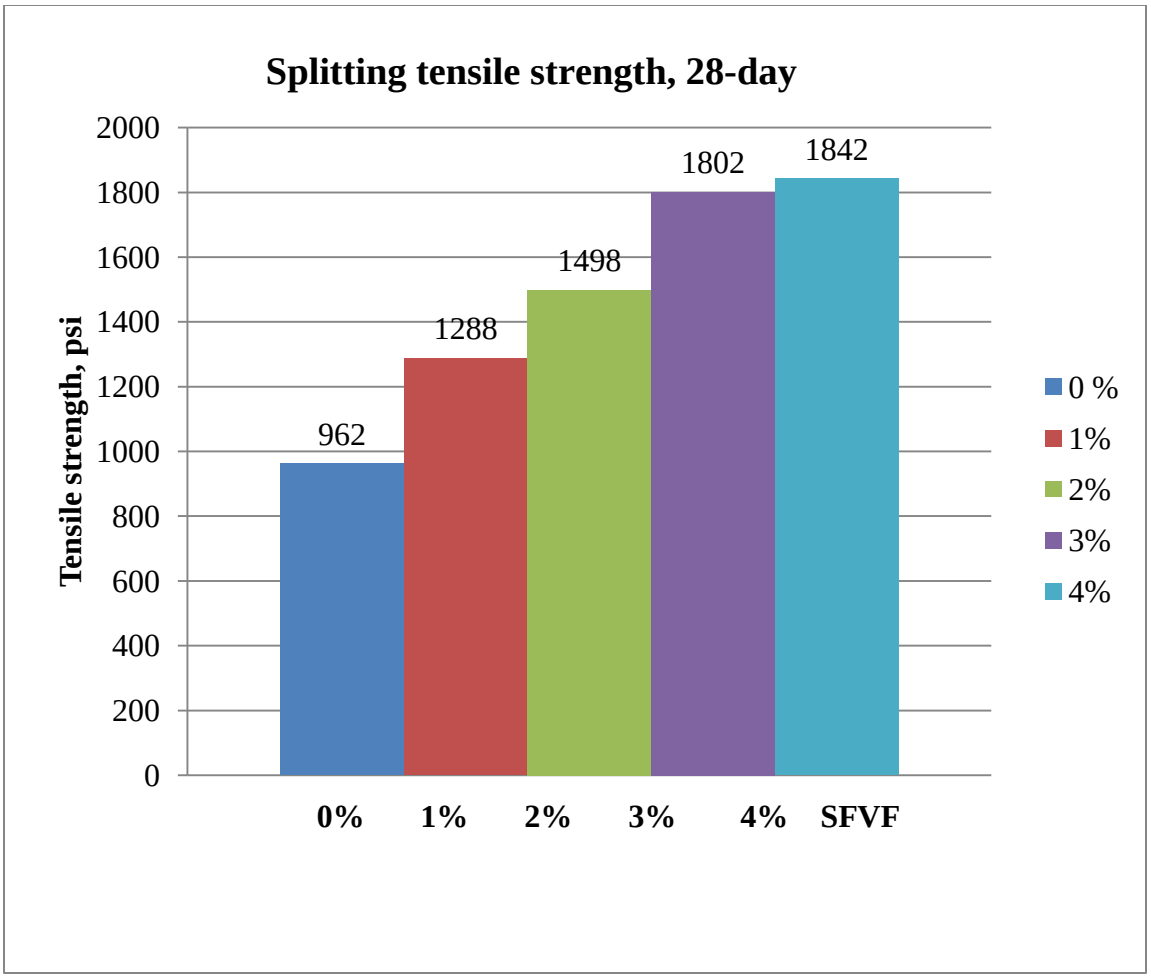

Figure 5.7: 28- day average splitting tensile strength for HSSFRC cylinders with various steel fiber by volume fractions

www.manaraa.com

Tensile to compressive strength ratios of high strength steel fiber reinforced concrete cylinders for 28 and 56-day test results are given in Table 5.12.

Table 5.12: 28 and 56-day splitting tensile to compressive strength ratios for high strength steel fiber reinforced cylinders

Steel fiber %	Compress. strength 28-day MPa (ksi)	Tensile strength 28-day MPa (ksi)	28-day ratio of tensile to compress. strength	Compress. strength 56-day MPa (ksi)	Tensile strength 56-day MPa (ksi)	56-day ratio of tensile to compress. strength
0%	67.98 (9.86)	6.63 (0.96)	9.7%	78.58 (11.4)	7.46 (1.08)	9.47%
1%	75.31 (10.92)	8.88 (1.29)	11.8%	77.7 (11.27)	9.81 (1.42)	12.6%
2%	80.72 (11.72)	10.33 (1.50)	12.8%	86.75 (12.58)	11.71 (1.70)	13.5%
3%	85.8 (12.44)	12.44 (1.80)	14.5%	N/A	N/A	N/A
4%	73.18 (10.61)	12.7 (1.84)	17.3%	82.14 (11.91)	13.17 (1.91)	16%

www.manaraa.com

5.2.2.2 Failure modes for HSSFRC cylinders under splitting tension

The failure modes described in Table 5.13 and shown in Figures 5.8, 5.9, 5.10 and 5.11 were observed while testing 0%, 1%, 2% and 3% HSSFRC cylinders under splitting tensile force. The results show that the ductile form of failure of HSSFRC cylinders under splitting tension increased as the steel fiber by volume fraction increased.

Table 5.13: Failure modes of HSSFRC cylinders under splitting tensile force

Steel fiber	Failure modes		
	Sound	Speed	Damage
0%	Loud	Fast, Abrupt	Complete destruction of specimen
1%	Mute	Slow	Less damage than 0%, Lots of cracks on the specimen
2%	Mute	Slow	Little damage, Minor cracks
3%	Mute	Slow	Very little damage

www.manaraa.com

Figure 5.8: Failure mode for 0% HSSFRC cylinders under splitting tensile force

www.manaraa.com

Figure 5.9: Failure mode for 1% HSSFRC cylinders under splitting tensile force

www.manaraa.com

Figure 5.10: Failure mode for 1% HSSFRC cylinders under splitting tensile force

www.manaraa.com

Figure 5.11: Failure mode for 2% HSSFRC cylinders under splitting tensile force

www.manaraa.com

CHAPTER 6

FLEXURAL STRENGTH TEST OF HIGH STRENGTH STEEL FIBER REINFORCED CONCRETE SIMPLE BEAM WITH THIRD-POINT LOADING

6.1 Introduction

This experiment was conducted to determine the flexural strength of high strength steel fiber reinforced concrete (HSSFRC) beams. Beams with the following dimensions: 305 mm (12 in.) long, 102 mm (4 in.) wide, and 102 mm (4 in.) deep, length three times the width and depth, were subjected to third-point loading per ASTM C 78 (ASTM C 78 2000), as shown in Figure 6.1. The significance of the experiment is to determine the modulus of rupture, which is one of the most important mechanical properties of flexural members such as beams.

6.2 Preparation of test specimens - beams

Four beam specimens with dimensions of 305 mm (12 in.) long, 102 mm (4 in.) wide and 102 mm (4 in.) deep were formed for each steel fiber by volume fraction, 0%, 1%, 2%, 3% and 4%. SCC/Flow-able HSSFRC mixtures, prepared per Section 3.2, were used to cast the beams. The ingredients for each concrete mixture are given in Table 6.1. Once the concrete mixture was prepared, it was emptied into buckets and allowed to rest for 1 minute before it was poured in one sweeping motion into the middle of the beam formwork from one end of the form to the other along the length.

www.manaraa.com

Figure 6.1: HSSFRC simple beam (4 in. x 4 in. x 12 in.) subjected to a third-point loading

www.manaraa.com

Table 6.1: Concrete mixture constituents for 0%, 1%, 2%, 3% and 4% HSSFRC beams

Mixture Components	**0%**	**1%**	**2%**	**3%**	**4%**
Batch Volume	**0.3 ft^3**	**0.3 ft^3**	**0.3 ft^3**	**0.3 ft^3**	**0.3 ft^3**
3/8" Coarse Aggregate (lb)	6.84	6.84	6.84	6.84	6.84
#4 Coarse Aggregate (lb)	6.72	6.72	6.72	6.72	6.72
Fine Aggregate, FA3* (lb)	17.28	17.28	17.28	17.28	17.28
Water (lb)	3.48	3.48	3.48	3.48	3.48
Cement Type V (lb)	7.5	7.5	7.5	7.5	7.5
Silica Fume (lb)	0.57	0.57	0.57	0.57	0.57
Fly Ash (lb)	3.21	3.21	3.21	3.21	3.21
Total Cementitious (lb)	11.28	11.28	11.28	11.28	11.28
Water to Cement Ratio	0.46	0.46	0.46	0.46	0.46
Water / Cementitious Ratio	0.31	0.31	0.31	0.31	0.31
Gravel : Sand Ratio	.44:.56	.44:.56	.44:.56	.44 : .56	.44 : .56
HRWR ADVA540 (lb)	0.118 *	0.113 *	0.126 *	0.130 *	0.142 *
Steel Fiber by Volume %	0%	1%	2%	3%	4%
Steel Fiber by weight (lb)	0	1.5	3	4.5	6.0
Concrete total Weight (lb)	45.72	47.21	48.73	50.23	51.74
Concrete Unit weight (pcf)	152.4	157.4	162.4	167.4	172.4

* HRWR volume varies with the steel fiber by volume fraction under consideration

** Fineness modulus of 2.05

www.manaraa.com

The concrete matrix was then allowed to travel sideways and fill up the form without any external vibration or agitation. The top of the form was then leveled with metal bar repeatedly to get a flat and smooth beam top. The method and position of pouring steel fiber reinforced (SFR) concrete are among the most important factors that affect the mechanical properties of the SFR concrete as explained in Section 1.5.2. Hence, the way SFR concrete was poured and the pour position of the specimen were kept consistent for all test specimens to avoid or minimize discrepancies related to the mechanical properties of the specimens. In this case, the beam formwork was placed flat in a horizontal position (width and length flat on a hard and level surface) and concrete was poured to fill up the thickness of the specimen.

Once the beam specimens were cast, they were covered with a plastic sheet or tarp to reduce evaporation of mixing water from the structures and were left in temperature controlled laboratory for 24 hours after which the beams were de-molded and placed in a curing room for 28-days.

6.3 Test apparatus and procedures for beams

Test apparatus and procedures for beam specimens were conducted per Section 4.4.5, except the load was applied at much slower rate than the one indicated on Step 5 of Section 4.4.5. All contact surfaces were checked for any kind of rocking or gap (lack of contact) between the test specimen, supports and load bar. All the gaps were shimmed to ensure full contact and uniform load transfer between units. Finally, the load cell was lowered slowly just to make contact with the loading bar and to engage the test specimen.

www.manaraa.com

Thereafter, the load was applied at a steady rate of 0.03 – 0.08 mm/minute (0.001 – 0.002 in./minute).

6.4 Flexural strength test using simple beam with third-point loading

The testing procedures of simple beam with third-point loading and the corresponding governing equations for modulus of rupture are presented in Section 4.4.5.

6.5 Experiment results for beams under third-point load

6.5.1 Load capacity

Table 6.2, presents the average load capacity of HSSFRC beams with 0%, 1%, 2%, 3% and 4% SFVF.

www.manaraa.com

Table 6.2: Average load capacity of HSSFRC beams (4 x 4 x 12 in.) under third-point loading

Beam	P_{Max} N (lb)	Percentage increase in load
0%	30,154 (6,779)	0%
1%	32,529 (7,313)	8%
2%	35,475 (7,975)	18%
3%	38,662 (8,692)	28%
4%	37,036 (8,326)	23%

www.manaraa.com

6.5.2 Modulus of rupture

Modulus of rupture for HSSFRC beams were computed per Equation 4.4 in Section 4.4.5. The average modulus of rupture results for 0% through 4% HSSFRC beams are presented in Table 6.3 and Figure 6.4. The moduli of rupture test results are representative of 28-day curing period.

Table 6.3: Average modulus of rupture values for 0%, 1%, 2%, 3% and 4% HSSFRC beams (4 x 4 x 12 in.) under third-point loading

Beam	Modulus of rupture MPa (psi)	Percentage increase in modulus of rupture
0%	8.76	
	(1,271)	0%
1%	9.45	
	(1,371)	8%
2%	10.30	
	(1,495)	18%
3%	11.23	
	(1,630)	28%
4%	10.77	
	(1,561)	23%

www.manaraa.com

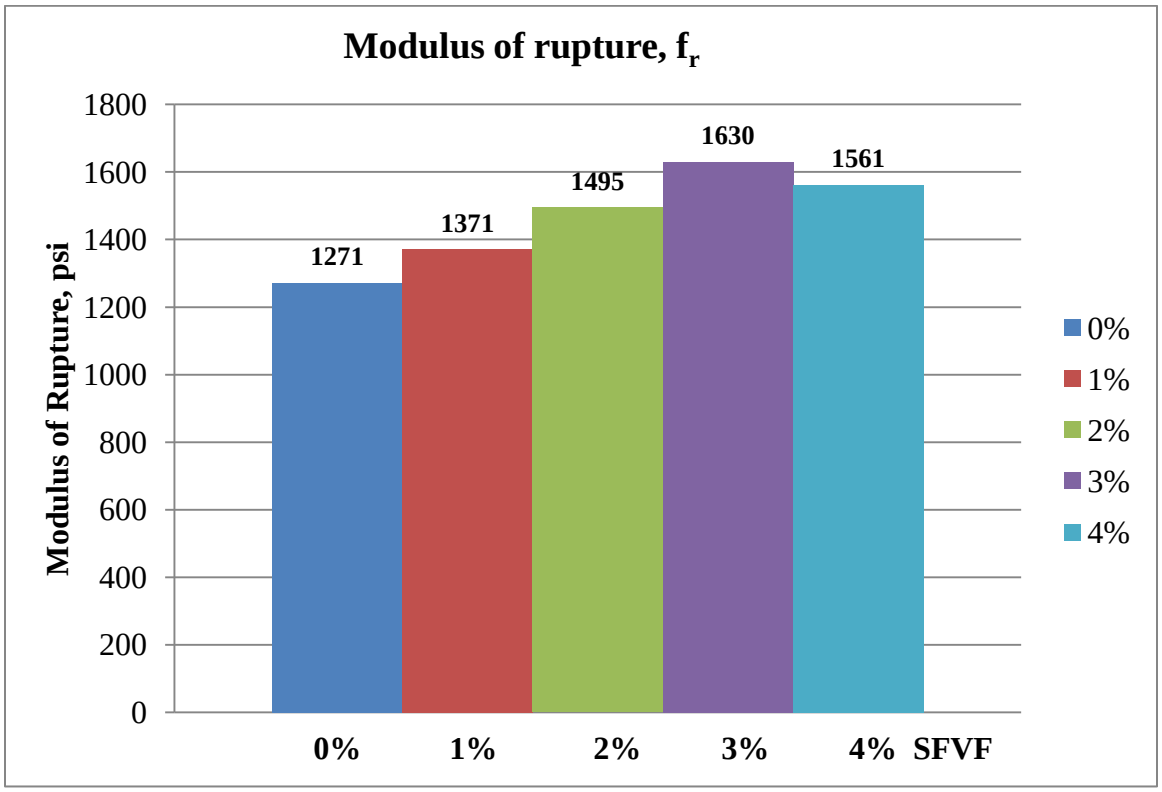

Figure 6.2: Modulus of rupture for 0%, 1%, 2% 3% and 4% HSSFRC beams (4 x 4 x 12 in.) under third-point loading

6.5.3 Cylinder compressive strength test results

Compressive strength and modulus of elasticity of HSSFRC cylinders were computed according to the procedures described in Sections 4.4.1 and 4.4.2, respectively. 7, 28 and 56-day average compressive strength test results for 0% through 4% high strength steel fiber reinforced concrete cylinders are presented in Section 5.2.1. Modulus of elasticity and stress versus strain curves for 0% through 4% HSSFRC cylinders in compression are presented in Section 5.2.1 in Figures 5.2 and 5.3, respectively.

www.manaraa.com

6.5.4 Cylinder splitting tensile strength results

The splitting tensile strength of HSSFRC cylinders were computed according to the procedure described in Section 4.4.4. 7, 28 and 56-day average splitting tensile strength test results for 0% through 4% steel fiber reinforced concrete cylinders are presented in Section 5.2.2 in Figure 5.4.

Comparisons between 28-day splitting tensile strength and modulus of rupture results are presented in Table 6.4. When comparing modulus of rupture and splitting tensile strength results, in Table 6.4, keep in mind that the two types of specimens were not made from the same concrete batch and were made with fine aggregates with different values of fineness modulus.

www.manaraa.com

Table 6.4: Comparisons between modulus of rupture of beams and splitting tensile strength of cylinders for 0%, 1%, 2%, 3% and 4% SFVF

Steel fiber %	Modulus of rupture MPa (psi)	Splitting tensile strength MPa (psi)	Modulus of rupture to Splitting tensile strength ratio
0%	8.76	6.63	1.32
	(1,271)	(960)	
1%	9.45	8.88	1.06
	(1,371)	(1,290)	
2%	10.30	10.33	1.00
	(1,495)	(1,500)	
3%	11.23	12.44	0.90
	(1,630)	(1,800)	
4%	10.77	12.70	0.85
	(1,561)	(1,840)	

www.manaraa.com

6.6 Discussion and beam failure mode

6.6.1 Load capacity

The flexural capacity of beams under third-point loading increased as the steel fiber by volume fraction (SFVF) increased from 0% through 4%. The flexural capacity of beams increased by 8%, 18%, 28% and 23% for 1%, 2%, 3% and 4% SFVF compared to 0% (plain) HSSFRC beams, respectively.

Maximum deflection of HSSFRC beams generally increased as the SFVF increased from 0% through 4%.

6.6.2 Modulus of rupture

The modulus of rupture (MOR) of HSSFRC beams increased by 8%, 18%, 28% and 23% for 1%, 2%, 3% and 4% SFVF, respectively from 0% (plain) HSSFRC beams. The introduction of steel fibers to the high strength flow-able concrete indeed increased the flexural capacity of beams.

www.manaraa.com

CHAPTER 7

DISCUSSION OF FRESH AND HARDENED PROPERTIES OF HIGH STRENGHT STEEL FIBER REINFORCED CONCRETE

7.1 Fresh properties of high strength steel fiber reinforced concrete (HSSFRC)

7.1.1 Effects of high range water reducer (HRWR) on HSSFRC mixture

High range water reducing agent is used in this study to reduce the amount of mixing water and hence achieve high concrete compressive strength and to get a self-consolidating or flow-able concrete mixture as well. The addition of HRWR to the steel fiber concrete mixture increases the slump flow (spread) diameter, slump and the chance of bleeding. The amount of HRWR needed also increases with the increase of steel fiber content, for similar spread diameter of the mixture.

7.1.2 Effects of viscosity modifying agent (VMA) on HSSFRC mixture

VMA enhances the deformability and uniformity of a mixture. VMA can be used to minimize aggregate piling, segregation and bleeding as the amount of water and/or HRWR in the mixture increases to obtain optimum mixture properties. The main drawback generally is that, VMA slows down the flow of the mixture hence, increasing the time of the flow rate (T_{50}).

Tests were conducted to determine the influence of VMA on the steel fiber mixtures. An amount of 0.385 kg/m^3 (0.024 lb/ft^3), minimum manufacturer's recommendation, was added to the successful mixtures #91, #95 and #99, having 0%, 1% and 2% SFVF,

www.manaraa.com

respectively. Results showed that, VMA shrinks the flow diameter by 15.2 mm (0.6 in.) for 0%, 88.9 mm (3.5 in.) for 1% and an increase of 10.2 mm (0.4 in.) for 2% SFVF. The flow rate (T_{50}) of the mixtures increased by 0, 8 and 5 seconds for 0%, 1%, and 2% SFVF, respectively. However, bleeding of 12.7 mm (0.5 in.) and 15.9 mm (0.625 in.) were observed in 0% and 2% steel by volume fraction (SFVF) mixtures, which explains the increase in spread diameter and flow rate of the mixtures.

7.1.3 Effects of steel fibers on HSSFRC mixture

It has been shown that, the addition of 1% steel fibers by volume fraction to SCC/Flow-able mixture had very little effect on the fresh properties of HSSFRC mixture. The steel fibers were not even noticeable during the mixing and casting process. However, the introduction of steel fibers to the concrete mixture reduced the work-ability, pass-ability, fill-ability and flow-ability progressively as the fiber content increased to 2%, 3% and 4% SFVF. With the increase in steel fiber by volume fraction in the concrete mixture, the workability and slump flow decreased.

7.1.4 J-Ring test results for HSSFRC mixture

Test results for J-Ring experiments #91, #95 and #99 showed decrease in spread diameter and slump flow. The J-Ring spread diameter decreased by 22.4 mm (0.88 in.) and 44.5 mm (1.75 in.) for 1% and 2% SFVF, respectively which is within the acceptable range [less than 50 mm (2 in.)]. For 0% HSSFRC mixture, the presence of ring barrier made no difference. In this case, all three mixtures, 0%, 1% and 2% SFVF, satisfied J-

www.manaraa.com

Ring standard SCC test requirements. In general, the introduction of steel fibers to the concrete mixtures reduced the J-Ring spread diameter of the HHSFRC mixtures.

7.1.5 V-Funnel test results for HSSFRC mixture

V-Funnel test results showed that, the time needed for a mixture to clear the funnel increased from 8 seconds for 0% to 18 seconds for 1% and 31 seconds for 2% SFVF concrete mixtures. Therefore, the increase in steel fiber by volume fraction in the concrete mixture decreased its fill-ability. Even though, 1% and 2% steel fiber by volume fractions did not meet the standard SCC requirements for filling ability of concrete mixtures, as discussed earlier, it had been clearly and consistently observed during the experimental procedures that the concrete mixtures were able to fill the cylinder and beam specimens easily without any vibration. When the cylinder and beam specimens were de-molded, they showed no sign of honeycombing or serious voids.

In case of 3% steel fiber by volume fraction, 1 out of 4 cylinder and beam specimens prepared exhibited a sign of honeycombing for mixtures with fine aggregate having higher fineness modulus (3.04).

In case of 4% steel fiber by volume fraction, 2 out of 4 cylinder and beam specimens prepared exhibited a sign of honeycombing for mixtures with fine aggregate having higher fineness modulus (3.04).

However, all specimens including 3% and 4% SFVF did not show any sign of honeycombing effect when prepared with concrete mixtures with fine aggregate having lower fineness modulus, 2.05 or less.

www.manaraa.com

7.1.6 U-Box test results for HSSFRC mixture

The experiment results showed that, the U-Box test requirements for standard SCC mixture were met for 0% and 1% SFVF concrete mixtures only. However, 2% SFVF concrete mixture exhibited 63% higher than the maximum allowable U-Box filling height requirement. For SFVF of 2% and higher, U-Box requirements were not met.

7.2 Hardened properties of high strength steel fiber reinforced concrete

7.2.1 Compressive strength of HSSFRC cylinders

Even though steel fibers were added to the high strength concrete mixture initially to increase its tensile and shear capacity, a steady and considerable increase in compressive strength had been observed. The percentage increase in 28-day compressive strength of HSSFRC cylinders with 1%, 2% 3% and 4% SFVF relative to 0% SFVF (plain high strength concrete) were 11%, 19%, 26% and 8%, respectively. The compressive strength of HSSFRC cylinders increased also from 7 to 28 and 56-day in all SFVF cases. The comparison between 28 and 56-day compressive strength for 0%, 1%, 2% and 4% HSSFRC cylinders indicated an increase of 15.6%, 3.2%, 7.5% and 12.2%, respectively. The above results were consistent for concrete mixtures with variable HRWR. While the compressive strength for 0%, 1% and 2% HSSFRC cylinders prepared with constant HRWR suitable for 0% HSSFRC were basically flat as shown in Chapters 8 through 13.

The mode of failure for cylinders under compressive force improved from brittle to a ductile type of failure as the SFVF increased from 0% to 4%.

www.manaraa.com

7.2.2 Splitting tensile strength of HSSFRC cylinders

The splitting tensile strength, as expected, exhibited large increase as the steel fibers in the concrete mixture increased. For the 28-day splitting tensile strength, an increase of 34%, 56%, 88% and 91% were observed over the 0% (plain) for 1%, 2%, 3% and 4% SFVF, respectively. The splitting tensile strength for HSSFRC cylinders increased from 7 to 28 and 56-day in all SFVF cases. The splitting tensile strength for 0%, 1%, 2% and 4% HSSFRC cylinders increased from 28 to 56-day by an amount of 12.5%, 10.5%, 13.4% and 3.7%, respectively.

Utilization of steel fibers beyond 3% SFVF may not be recommended as far as mechanical properties are concerned; since very little improvement has been observed between 3% and 4% SFVF.

The mode of failure for cylinders under splitting tensile force improved from brittle to a ductile type of failure as the SFVF increased from 0% to 4%.

www.manaraa.com

CHAPTER 8

SIMPLY SUPPORTED HIGH STRENGTH STEEL FIRBER REINFORCED CONCRETE RECTANGULAR PLATES UNLDER CENTRAL LINE LOADS

8.1 HSSFRC rectangular plates with two short edges simply supported and the other two free under central line load in the short direction

8.1.1 Introduction

In Section 1 of Chapter 8, flexural properties of long span high strength steel fiber reinforced concrete (HSSFRC) thin rectangular plates with 0%, 1% and 2% steel fiber by volume fraction are presented. The plates are predominantly subjected to unidirectional flexural stress due to the plate dimension, length to width ratio of 4:1, and the mid-span location of the transverse line load.

All constituents for the three types of concrete mixtures (0%, 1% and 2% SFVF), used for the making of plates and cylinders, are the same except for the content of steel fibers. The thin rectangular plates have dimensions of 1,219 mm (48 in.) long by 305 mm (12 in.) wide and 32 mm (1.25 in.) thick, with length to width ratio of 4:1 (long span). The plates are simply supported at the short ends and subjected to a line load at mid span along the short direction, as shown in Figure 8.1.1.

.

www.manaraa.com

Figure 8.1.1: HSSFRC rectangular plate (48 in. x 12 in.) subjected to a transverse line load at mid span

Two strain gages, perpendicular to one another, for each type of steel fiber by volume fraction mixture, are placed at the center bottom surface of the plate to measure the strain activities at the extreme fiber of the plate relative to the applied load. One rosette strain gage, for each steel fiber by volume fraction mixture, is placed on the side of the plate right at the support to measure the shear strain activities at the plate support.

The chapter presents HSSFRC specimen preparation, testing procedures and experiment results such as load versus deflection, stress versus flexural and shear strains and mode of failure of rectangular plates. The chapter discusses the influence of steel

www.manaraa.com

fibers on: flexural and shear capacity, mode of failure and ductility of thin rectangular plates; and modulus of elasticity, compression and splitting tensile strength of cylinders prepared from the same mixtures used for the plates.

Comparisons between long span rectangular plates with various steel fiber by volume fraction with respect to the mechanical properties such as flexural capacity, deflection, ductility, and mode of failure are made. The elastic analysis results corresponding to the first crack load such as stress, strain and deflection are presented. Test results are discussed and conclusions drown.

8.1.2 Theoretical background of rectangular plates

Rectangular plates are typically classified according to the type of support system provided. Rectangular plates can be simply supported, fixed or built-in, continuous or on elastic foundation, or a combination of one or more of the above support conditions. For a plate with symmetrical loading and simple support condition along two opposite edges, acting like a beam, the governing plate equation is:

$$\nabla^4 w = p/D \qquad (8.1)$$

Where:

$$D = \frac{Et^3}{12(1-\nu^2)} \quad \text{(Flexural rigidity)} \qquad (8.2)$$

p = uniformly distributed load

t = thickness of plate

ν = Poisson's ratio

E = modulus of elasticity.

www.manaraa.com

In case of three-dimensional state of stress, for homogeneous material, stress and strain are related by the generalized Hooke's law as follows:

$$\sigma_x = \frac{E}{(1-\nu^2)}(\varepsilon_x + \nu\varepsilon_y) \quad (8.3)$$

$$\sigma_y = \frac{E}{(1-\nu^2)}(\varepsilon_y + \nu\varepsilon_x) \quad (8.4)$$

$$\tau_{xy} = G\gamma_{xy} \quad (8.5)$$

Where: G = shear modulus, E/2(1+ν) (8.6)

γ_{xy} = shear strain

ε_x = strain in the x-direction

ε_y = strain in the y-direction.

8.1.3 Preparation of test specimens - cylinders and rectangular plates

Two types of test specimens, rectangular plates and cylinders, were prepared for each test (0%, 1% and 2% SFVF) from the same concrete batch:

- Three rectangular thin plates for each SFVF with dimensions of 305 mm (12 in.) wide by 1,270 mm (50 in.) long and 32 mm (1.25 in.) thick. Therefore, a total of nine plate specimens were prepared.
- Six 102 mm (4 in.) diameter by 203 mm (8 in.) long cylinders for each SFVF. Three cylinders each were used for compressive and splitting tensile strength tests, respectively. Therefore, a total of eighteen cylinders were prepared.

www.manaraa.com

To form the rectangular plates, a crate with dimensions of approximately 1,270 mm (50 in.) long and 305 mm (12 in.) wide was made by nailing 32 mm (1.25 in.) thick plywood strip around the perimeter of base board.

SCC/SFR Flow-able concrete mixtures, prepared per Section 3.2, were used to cast the rectangular plates and cylinders. It is important to mention that, both plates and cylinders were made from the same concrete batch. The ingredients for all concrete mixtures were kept the same except for the amount of steel fibers used by volume fraction in each concrete mixture type. The ingredients for 0%, 1% and 2% steel fiber concrete mixtures are given in Table 8.1.1.

Since the mechanical properties such as compressive strength, splitting tensile strength and modulus of elasticity will be required to perform structural analysis on the plate structures; it was imperative to cast both the plate and cylinder specimens from the same concrete batch for each concrete mixture type.

Once the concrete mixture was prepared, it was emptied into buckets and allowed to rest for 1 minute before it was poured in one sweeping motion into the middle of the plate formwork from one end of the form to the other along the length. The plate formwork was placed flat in a horizontal position (width and length flat on a hard and level surface). The concrete matrix was then allowed to travel sideways and fill up the form thickness without any external vibration or agitation. The top of the form was leveled with

www.manaraa.com

Table 8.1.1: Concrete batch constituents for 0%, 1% and 2% HSSFRC rectangular plates (48 in. x 12in.) and cylinders

Mixture Components			**0%**	**1%**	**2%**
Batch Volume			**2 ft^3**	**2 ft^3**	**2 ft^3**
3/8" Coarse Aggregate	(lb)		45.6	45.6	45.6
#4 Coarse Aggregate	(lb)		44.8	44.8	44.8
Fine Aggregate, FA3*	(lb)		115.2	115.2	115.2
Water	(lb)		23.2	23.2	23.2
Cement Type V	(lb)		50.0	50.0	50.0
Silica Fume	(lb)		3.8	3.8	3.8
Fly Ash	(lb)		21.4	21.4	21.4
Total Cementitious	(lb)		75.2	75.2	75.2
Water to Cement Ratio			0.46	0.46	0.46
Water / Cementitious Ratio			0.31	0.31	0.31
Gravel : Sand Ratio			0.44 : 0.56	0.44 : 0.56	0.44 : 0.56
HRWR ADVA540	(lb)		0.784	0.784	0.784
Steel Fiber by Volume	%		0%	1%	2%
Steel Fiber by weight	(lb)		0	10	20
Concrete Total Weight	(lb)		304.78	314.78	324.78
Concrete Unit Weight	(pcf)		152.4	157.4	162.4

*Fine aggregate with fineness modulus of 2.05

www.manaraa.com

metal bar repeatedly to get a flat and smooth plate top. The method and position of pouring steel fiber reinforced concrete are one of the most important factors that affect the mechanical properties of the steel fiber reinforced (SFR) concrete as explained in Section 1.5.2. Hence, the way SFR concrete was poured and the pour position of the specimen were kept consistent for all test specimens to avoid or minimize discrepancies related to the mechanical properties of the specimens.

HSSFRC cylinder specimens were prepared per Section 4.1. HSSFRC matrix was poured into the cylinders, which were positioned vertically, in one motion, without any vibration.

Once the plates and cylinders were cast, they were covered with a plastic sheet or tarp to reduce the evaporation of mixing water from the structures and were left in a temperature controlled laboratory for 24 hours after which the plates and cylinders were de-molded and placed in a curing room for 28-days.

8.1.4 Types of strain gages used

The size and type of strain gages depend on the maximum aggregate size. Two types of strain gages, which were recommended by the manufacturer, were used:

1. N2A-06-10CBE-350/E – is an individual strain gage, used to measure strain in a single direction. It can be installed as shown in Figure 8.1.2 individually or in group to measure strain in one or multiple directions, respectively. In this case, for plate type #2, two strain gages were installed perpendicular to one another to measure flexural strains in two orthogonal, longitudinal and transverse, directions.

www.manaraa.com

Refer to Section 8.1.5 for strain gage locations. The overall size of the strain gage used has a matrix length of 34.5 mm (1.36 in.) and width of 8.4 mm (0.33 in.).

2. CEA-06-250UR-120 – is a rosette, group, type strain gage with three grids oriented 45° apart, angularly, from each other. Refer to Figures 8.1.3 and 8.1.4 for strain gage rosette orientation. It measures strain in three different directions/orientations: vertical, horizontal and at 45° from horizontal or vertical grids. In our case, the strain in horizontal, 45° and vertical grids were labeled as ξ_1, ξ_2 and ξ_3, respectively. The strain measured by each grid can be used to calculate principal stresses and shear strain as indicated in Equations 8.7 through 8.12. The size of the rosette used has a matrix length of 20.3 mm (0.80 in.) and width of 16.5 mm (0.65 in.).

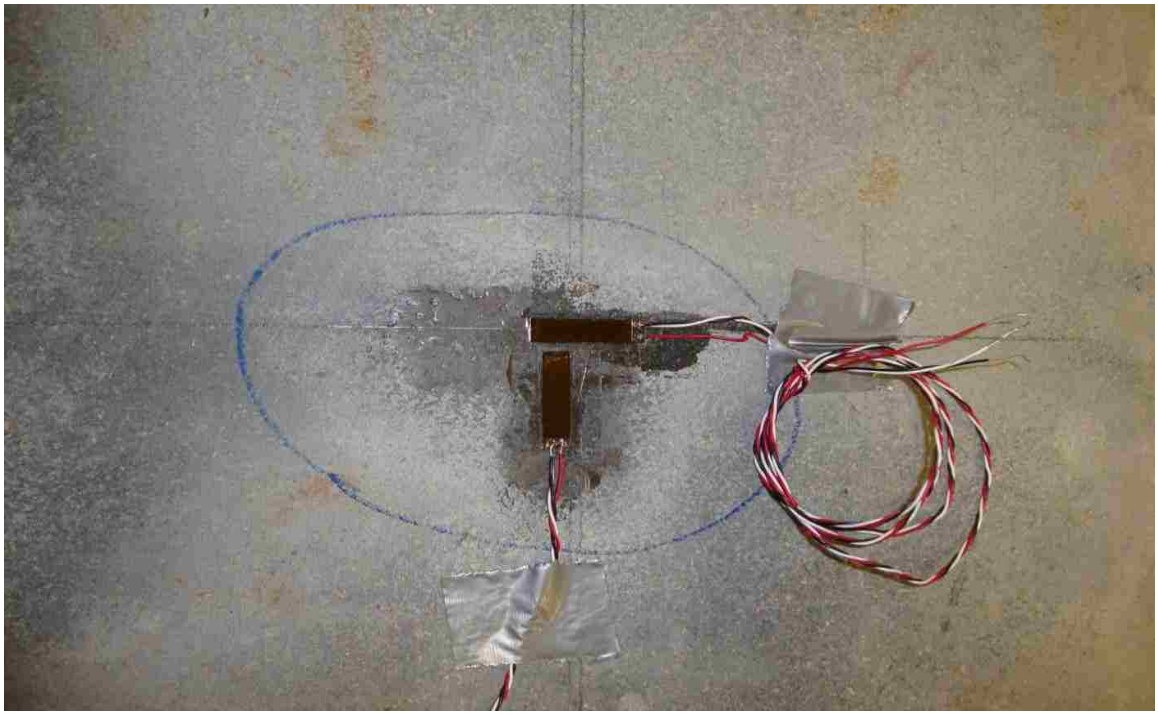

Figure 8.1.2: Strain gages located at mid span of HSSFRC rectangular plates (48 in. x 12 in.)

www.manaraa.com

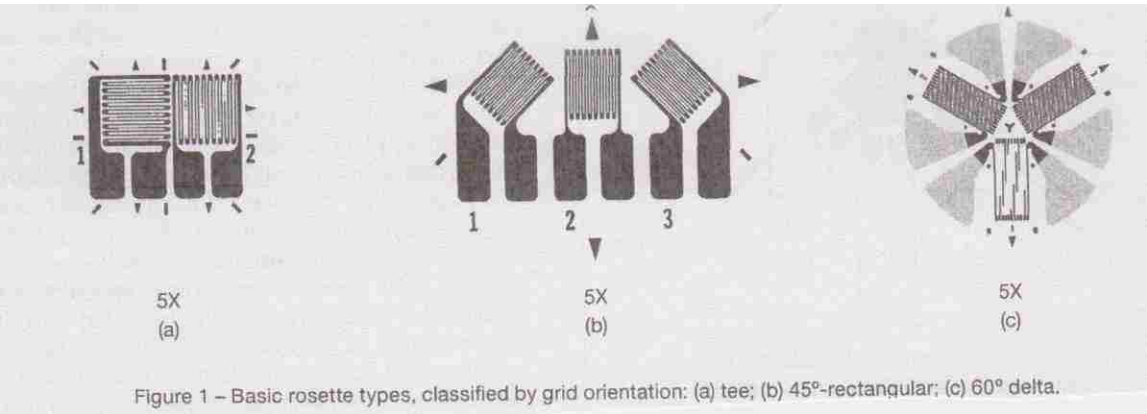

Figure 8.1.3: Types of rosette strain gages (Micro-Measurements 2010)

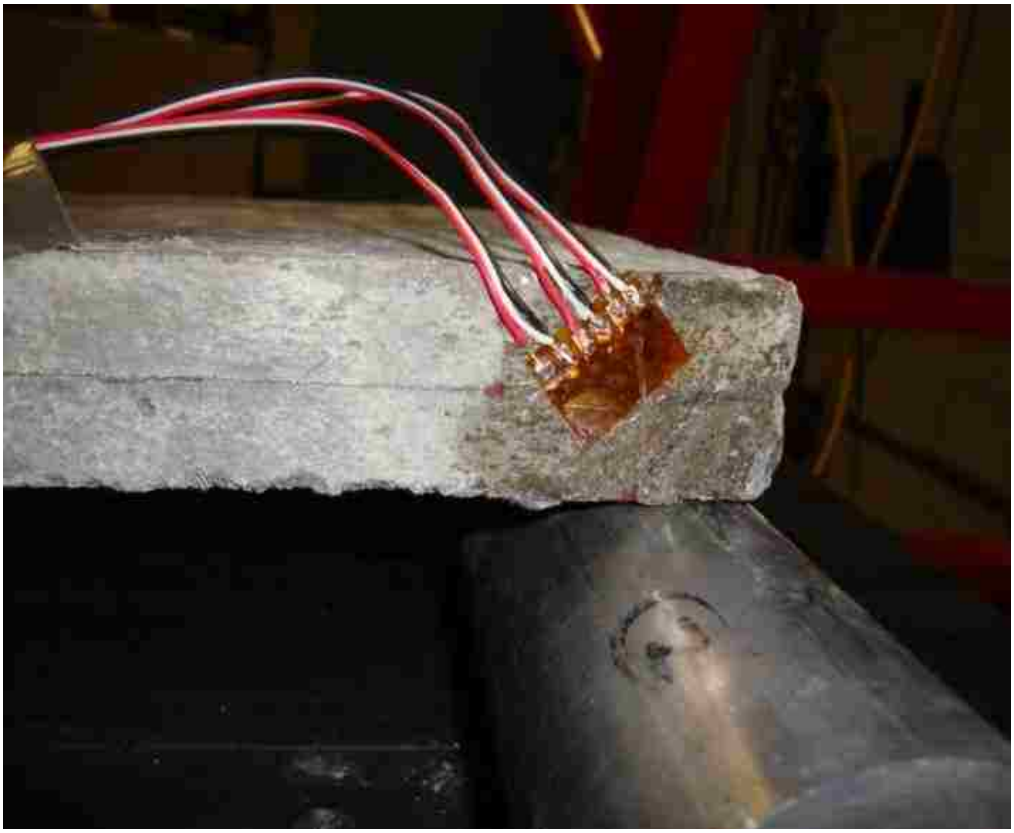

Figure 8.1.4: 45°- rectangular rosette at the support of HSSFRC rectangular plates (48 in. x 12 in.)

www.manaraa.com

The strain sensed by each grid can be expressed as follows (Micro-Measurements 2010):

$$\xi_1 = \frac{\xi p + \xi q}{2} + \frac{(\xi p - \xi q)}{2}\cos 2\theta \quad (8.7)$$

$$\xi 2 = \frac{\xi p + \xi q}{2} + \frac{(\xi p - \xi q)}{2}\cos 2(\theta + 45°) \quad (8.8)$$

$$\xi 3 = \frac{\xi p + \xi q}{2} + \frac{(\xi p - \xi q)}{2}\cos 2(\theta + 90°) \quad (8.9)$$

$$\xi p,q = \frac{\xi 1 + \xi 3}{2} \pm \frac{1}{\sqrt{2}}\sqrt{(\xi 1 - \xi 2)^2 + (\xi 2 - \xi 3)^2} \quad (8.10)$$

$$\theta = \frac{1}{2}\tan^{-1}\left(\frac{\xi 1 - 2\xi 2 + \xi 3}{\xi 1 - \xi 3}\right) \quad (8.11)$$

$$\Upsilon max = (\xi p - \xi q) \quad (8.12)$$

Where:

ξp, ξq = principal strains

Θ = angle measured from the principal axis to the Grid 1

ξ_1, ξ_2 and ξ_3 = Strains measured in Grid 1, Grid 2 and Grid 3, respectively

Υ_{max} = maximum shear strain.

8.1.5 Location and orientation of strain gages on the test specimens, (48 in. x 12 in.)

The strain gage arrangements for every test plate were determined by the capability of the data acquisition system to accommodate rosette and strain gage output, deflection measurements and load input combined.

At the end of the 28-day, both plate and cylinder specimens were pulled out of the curing room. Plate specimens were prepared as follows:

www.manaraa.com

1) Plate #1 had no strain gages attached to it. Plate #1 was used strictly to measure load versus deflection behavior of long span rectangular plates using an extensometer and load cell (Tinus-Olsun). The load and vertical deflection readings were electronically linked.
2) Plate #2 was furnished with two independent and orthogonally placed strain gages at the center bottom surface of the plate. See Figures 8.1.2 and 8.1.5 for strain gage locations. Plate #2, in addition to measuring load versus deflection, it also measured the elongation of the bottom surface of the plate both in the longitudinal and transverse directions.
3) Plate #3 was equipped with one 45°- rectangular rosette with three grids spaced at 45° interval. Refer to Section 8.1.4 for the properties, size and arrangement of rosette strain gages. The rosette was place on the side of the plate #3 directly above the support location. The center of the strain gage was aligned with the same vertical plane as the center of the support. It was designed to measure the shear strain of the plate at the support. For plate #3, a vertical dial gage was used to measure the deflection of the plate at mid span. For the arrangement of the rosette strain gage on the plate refer to Figures 8.1.4 and 8.1.6.

www.manaraa.com

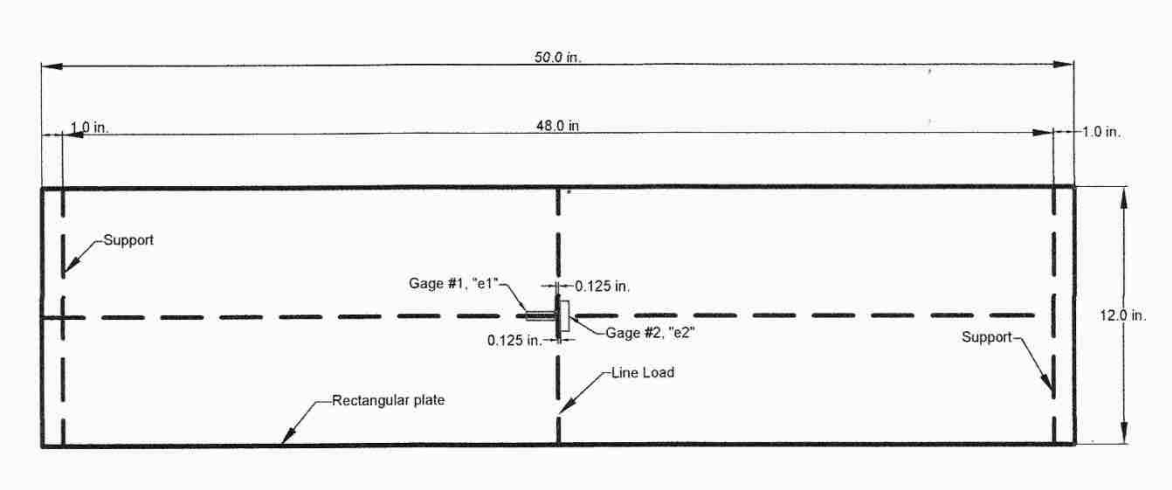

Figure 8.1.5: Location of strain gages at the bottom surface of HSSFRC rectangular plate (48 in. x 12 in.)

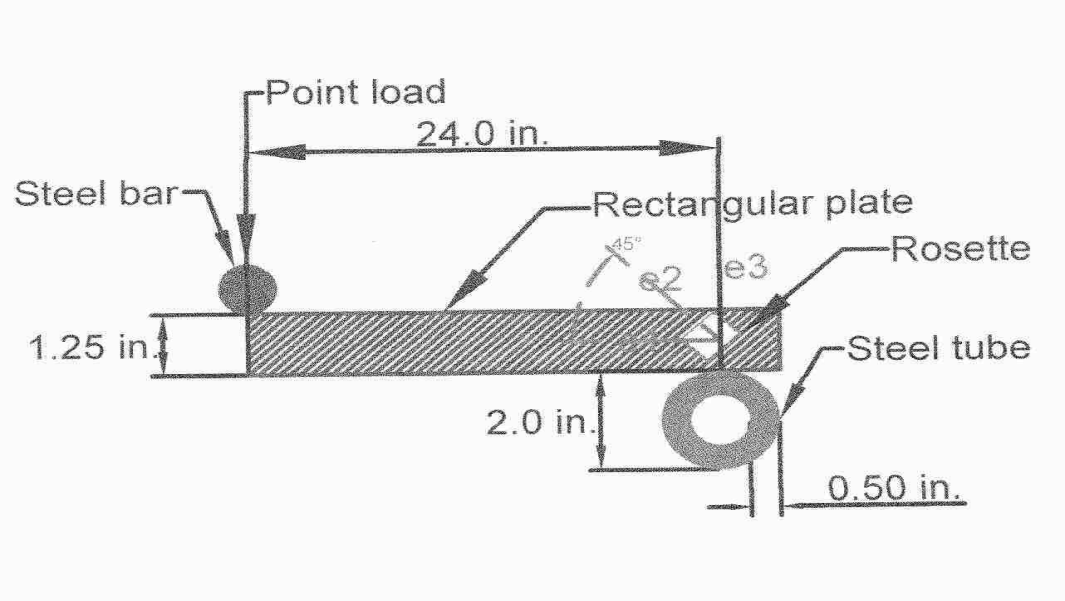

Figure 8.1.6: Location of rosette strain gage on the side of HSSFRC rectangular plate (48 in. x 12 in.)

www.manaraa.com

8.1.6 Test apparatus and procedures for long rectangular plates

Once the specimens were fitted with strain gages, they were ready for testing. The strain gages and rosettes were installed per manufacturer's recommendation as stated in Section 4.4.6. The apparatus involved were:

1. Tinus-Olsun testing machine (50,000 lb maximum capacity).
2. Extensometer to measure deflection of plate specimens.
3. Dial gage to measure deflection of plate specimens.
4. Steel base/platform as shown in Figure 8.1.7.
5. Two 13 mm (0.5 in.) thick steel support tubes.
6. Solid metal bar, part of the load assembly. Support system and load assembly sizes and dimensions are presented in Section 8.1.5.

The test set up for long span rectangular plates was assembled as follows:

1. First, the steel platform was placed flat on a very strong testing base.
2. Two support tubes were pinned parallel but 1,219 mm (48 in.) apart on the steel platform.
3. The specimen was laid flat on the top spanning between the two supports.
4. 51 mm (2 in.) diameter solid steel bar was placed on the specimen at midpoint between the supports. The thick steel support tubes and the steel bar were 305 mm (12 in.) long, which is equal to the width of the test specimens.
5. The entire test set up and all contact surfaces were checked for any kind of rocking or gap (lack of contact) between the test specimen, supports and load bar.

www.manaraa.com

All gaps were shimmed to ensure full contact and uniform load transfer between units.

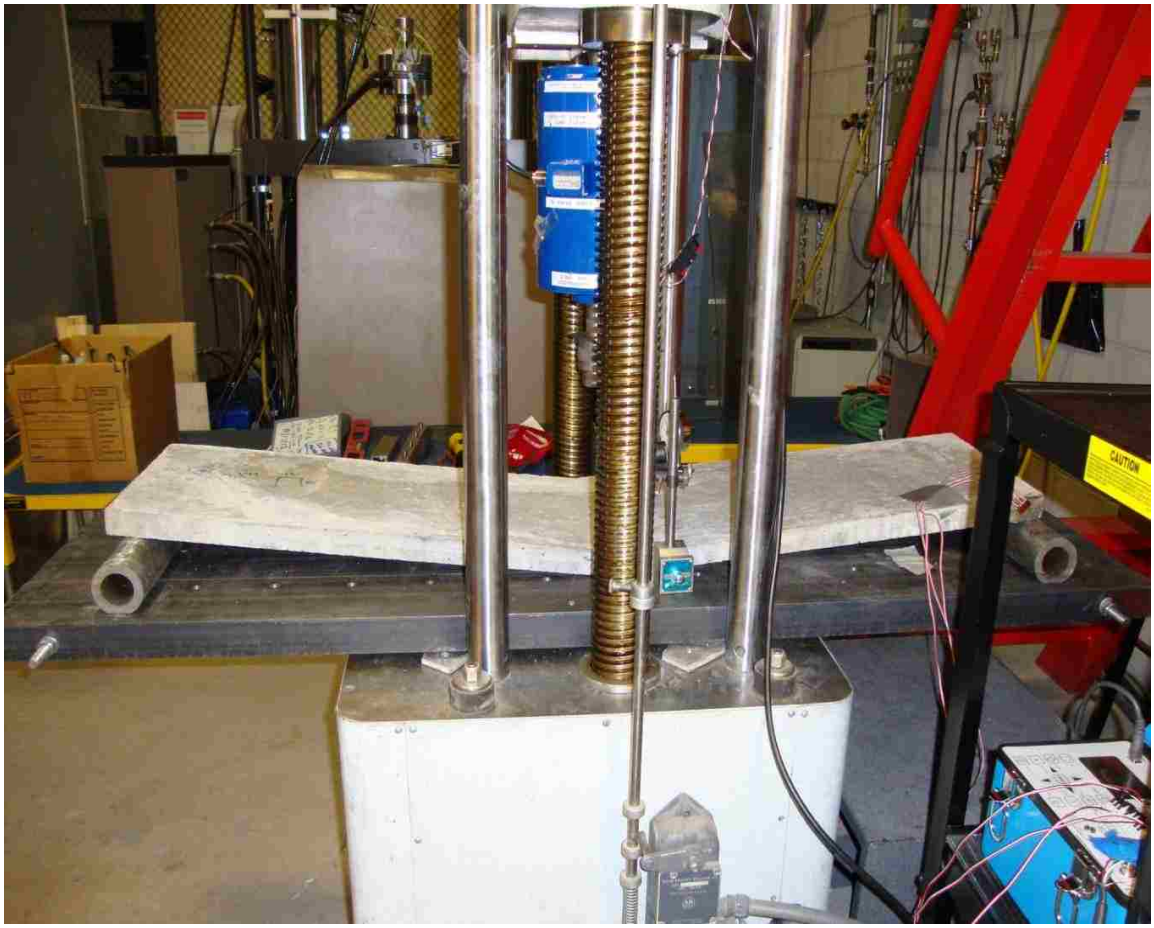

Figure 8.1.7: Support platform for HSSFRC rectangular test specimens, (48 in. x 12 in.)

6. Finally, the load cell was lowered slowly just to make contact with the steel bar and thereafter the load was applied at a steady rate of 0.025 – 0.051 mm/minute (0.001 – 0.002 in./minute) till the first major failure or crack occurred and

www.manaraa.com

increased to 0.102 – 0.203 mm/minute (0.004 – 0.008 in./minute) up to the complete failure of the specimen.

The HSSFRC cylinders, which were cast from the same concrete mixture used for plates, were tested for compressive and splitting tensile strength according to the test procedures that are presented in Sections 4.4.1 and 4.4.4, respectively. During the testing process for cylinders and plates: load, deflection and strain data were collected; failure and failure modes were noted.

8.1.7 Experiment results for rectangular plates (48 in. x 12 in.) supported along short edges under central line load

8.1.7.1 Load versus deflection results

Load versus deflection data were collected for long span HSSFRC rectangular plates, with 0% to 2% steel fiber by volume fractions (SFVF), under transverse central line load. Deflection of plates was measured at plate center. Average load versus deflection curves for 0%, 1% and 2% long span HSSFRC rectangular plates (48 in. x 12 in.) are presented in Figure 8.1.8. Each load versus deflection curve represents an average result of three HSSFRC rectangular plate specimens for each SFVF, a total of nine specimens for 0% and 2% SFVF. Table 8.1.2 presents the peak load, deflection of the plate at the peak load and maximum deflection of the plate at complete failure for 0%, 1% and 2% SFVF. Values in Table 8.1.2 were obtained from load versus deflection curves in Figure 8.1.8.

www.manaraa.com

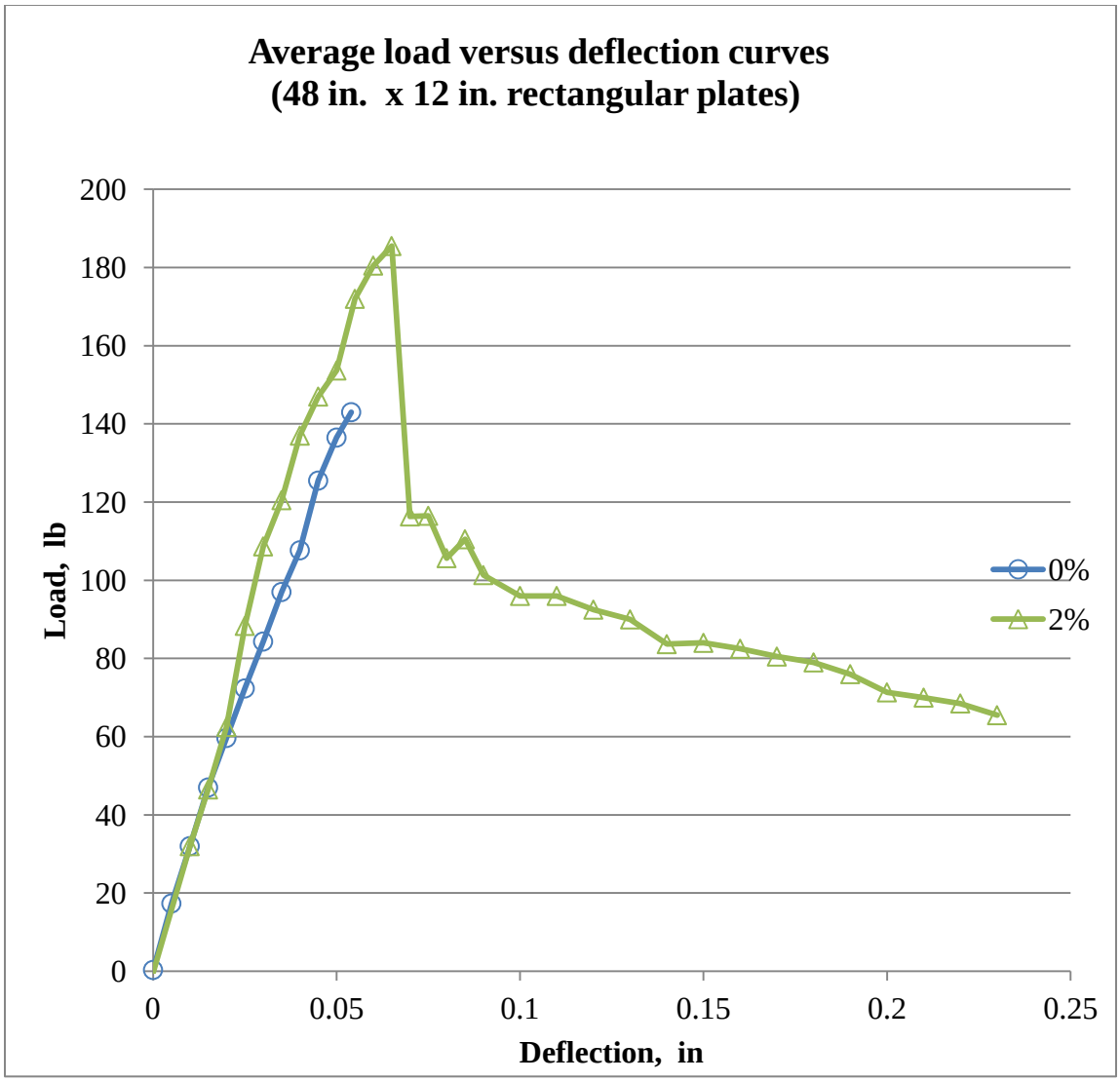

Figure 8.1.8: Average load versus deflection curves for 0% and 2% HSSFRC rectangular plates (48 in. x 12 in.) under transverse line load

www.manaraa.com

Table 8.1.2: Maximum load, deflection and ductility results for 0%, 1% and 2% HSSFRC rectangular plates (48 in. x 12 in.) under transverse line load

Plate	P_{Max} N (lb)	Percentage increase in load	Δ at P_{Max} mm (in.)	$\Delta_{failure}$ mm (in.)	Percentage increase in deflection	$\Delta_{failure}/\Delta$
0%	663 (149)	0%	1.50 (0.059)	1.50 (0.059)	0%	1.0
1%	712 (160)	7%	2.21 (0.087)	12.09 (0.476)	707%	5.47
2%	827 (186)	25%	1.52 (0.060)	14.83 (0.584)	890%	9.73

Where: P_{Max} = peak load, N (lb.)

Δ = plate deflection corresponding to the peak load, mm (in.)

$\Delta_{failure}$ = maximum deflection of the plate at complete failure, mm (in.).

8.1.7.2 Test results for strain gages located at mid span

For strain gages located at mid span, the longitudinal and transverse strain curves for HSSFRC long span rectangular plates (48 in. x 12 in.) with 0%, 1% and 2% steel fiber by volume fractions loaded in transverse direction are presented in Figure 8.1.9. The curves in Figure 8.1.9 show strains and stresses up to the first crack. The strains were measure at center bottom surface of the rectangular plates. The negative and positive strain values show the effect of Poisson's ratio. The 2% SFVF specimen exhibited larger elastic range compared to 0% and 1% HSSFRC specimen.

www.manaraa.com

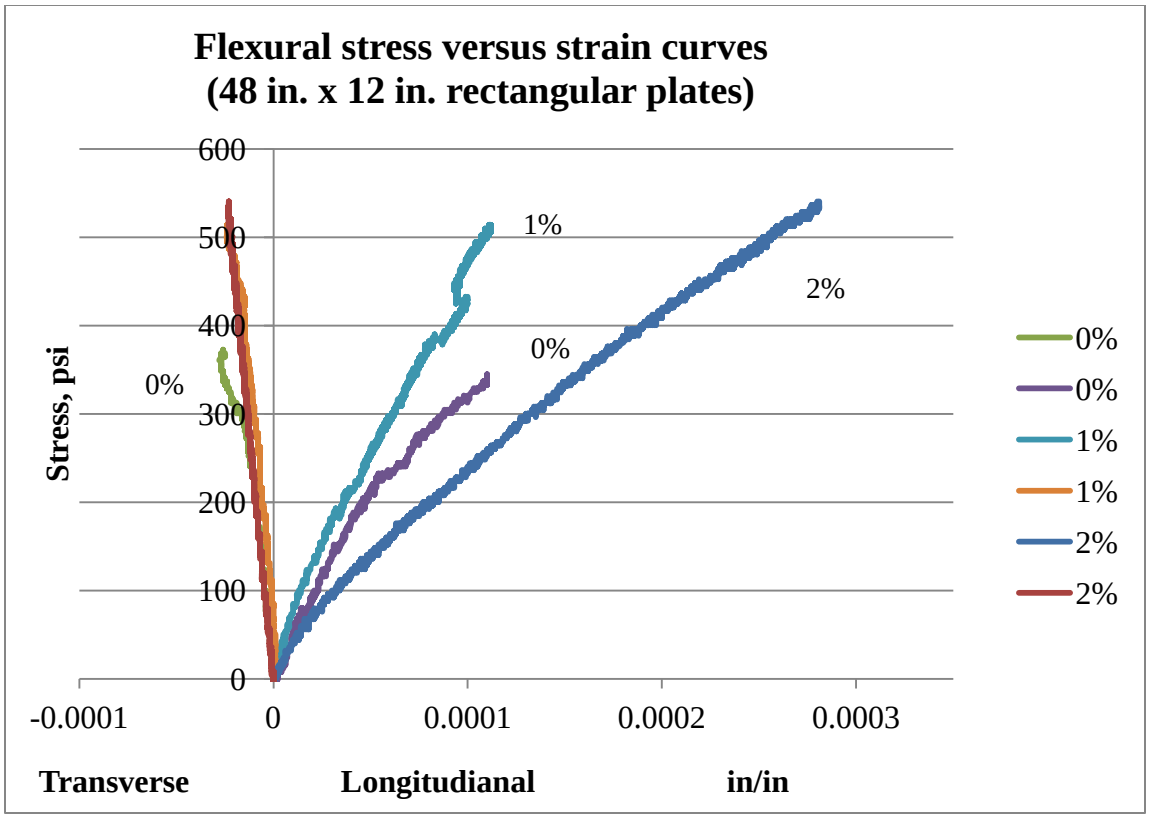

Figure 8.1.9: Flexural stress versus longitudinal and transverse strain curves for 0%, 1% and 2% HSSFRC rectangular plates (48 in. x 12 in.) loaded in transverse direction

8.1.7.3 Test results for rosette strain gages at the support

The shear strains recorded for HSSFRC rectangular plates (48 in. x 12 in.) with 0%, 1% and 2% SFVF loaded in the transverse direction were very small in magnitude. Therefore, shear strain results are not shown.

8.1.7.4 Cylinder compressive strength test results

As indicated before, the concrete cylinder specimens that were used for compressive strength tests were taken from the same batch of concrete the corresponding plates were made. The cylinders were tested, for compressive strength, within 24 hours of testing the

www.manaraa.com

corresponding plates. During the testing process both applied compression load and the corresponding longitudinal strain of cylinders were obtained.

The average compressive stress versus longitudinal strain curves for 0%, 1% and 2% steel fiber reinforced concrete cylinders are presented in Figure 8.1.10.

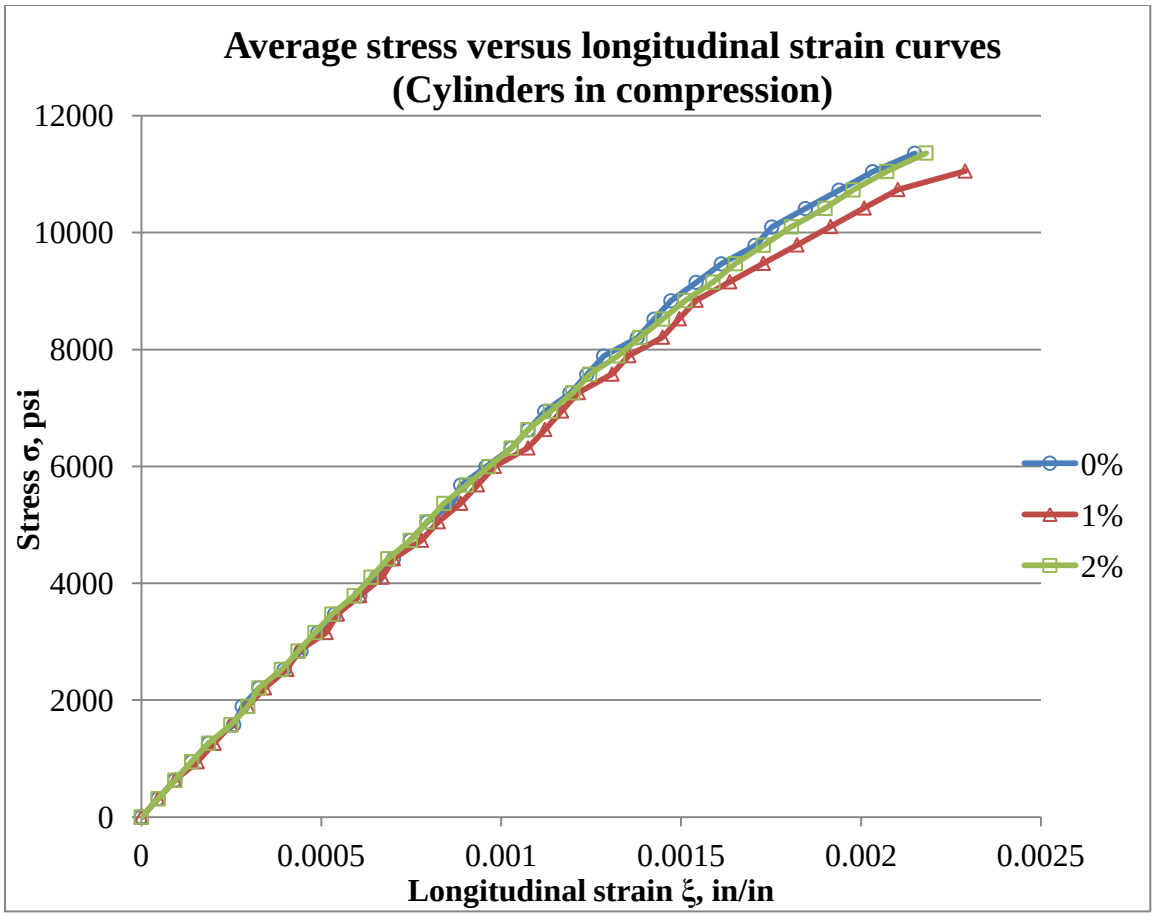

Figure 8.1.10: Average compressive stress versus strain curves for 0%, 1% and 2% HSSFRC cylinders (4 in. x 8 in.) casted with rectangular plates (48 in. x 12 in.)

The average compressive strength and modulus of elasticity test results for 0%, 1% and 2% high strength steel fiber reinforced cylinders under compression load are

www.manaraa.com

presented in Table 8.1.3. The compressive strength and modulus of elasticity results were calculated using procedures in Sections 4.4.1 and 4.4.2, respectively.

Table 8.1.3: Average compressive strength and modulus of elasticity results for 0%, 1% and 2% HSSFRC cylinders (4 in. x 8 in.) casted with rectangular plates (48 in. x 12 in.)

Cylinder	Compressive strength MPa (psi)	Percentage increase from 0% steel fiber	Modulus of elasticity MPa (ksi)	Percentage increase from 0% steel fiber
0%	79		44,416	
	(11,514)	0%	(6,442)	0%
1%	83		43,065	
	(12,035)	5%	(6,246)	-3.0%
2%	84		43,368	
	(12,115)	5%	(6,290)	-2.4%

8.1.7.5 Cylinder splitting tensile strength results

The average splitting tensile strength test results for 0%, 1% and 2% high strength steel fiber reinforced concrete cylinders are presented in Table 8.1.4, while the splitting tensile figures are presented in Figure 8.1.11. Splitting tensile strength results were computed using Equation 4.3.

www.manaraa.com

Table 8.1.4: Average splitting tensile strength results for 0%, 1% and 2% HSSFRC cylinders (4 in. x 8 in.) casted with rectangular plates (48 in. x 12 in.)

Cylinder	Splitting tensile Strength MPa (psi)	Percentage increase from 0% steel fiber	Splitting tensile to compression strength ratio
0%	6.27		
	(909)	0%	0.08
1%	7.52		
	(1,090)	20%	0.09
2%	13.01		
	(1,885)	107%	0.10

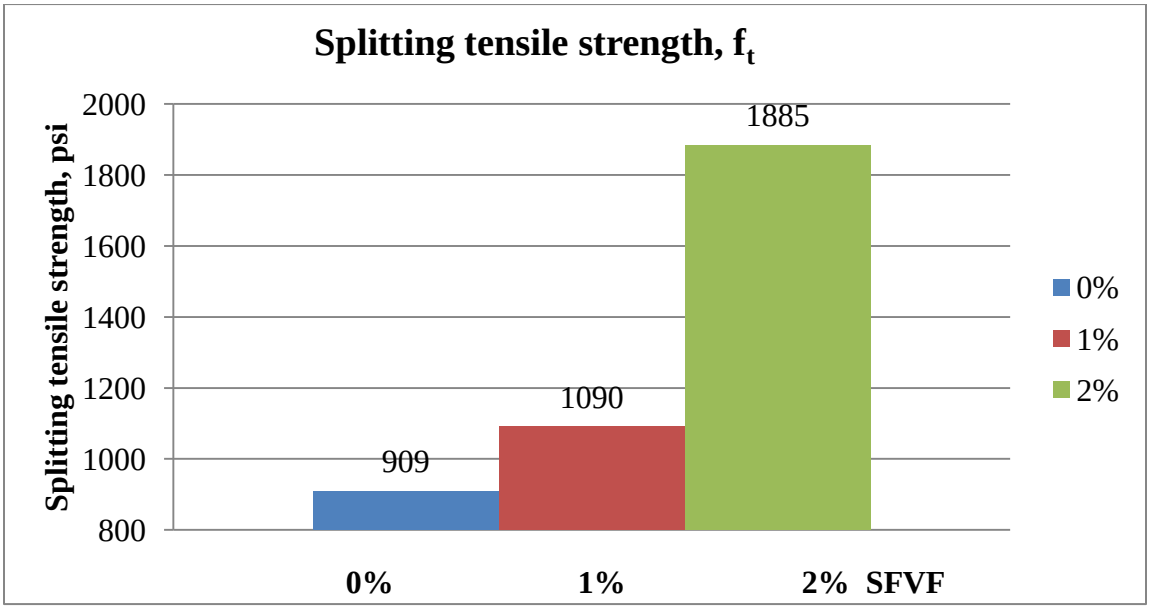

Figure 8.1.11: Average splitting tensile strength results for 0%, 1% and 2% HSSFRC cylinders (4 in. x 8 in.) casted with rectangular plates (48 in. x 12 in.)

www.manaraa.com

8.1.7.6 Stress-strain analysis and test results

Longitudinal and transverse strains at first noticeable crack and calculated stress results for 0%, 1% and 2% HSSFRC rectangular plates (48 in. x 12 in.) are presented in Table 8.1.5. The stress results for the rectangular plates were calculated using Equation 8.3 in Section 8.1.2 and modulus of elasticity values from cylinders in compression. The flexural stresses at first noticeable crack, as shown in Table 8.1.5, are comparable to the spitting tensile stress results of HSSFRC cylinders.

Table 8.1.5: Stress – strain results for 0%, 1% and 2% HSSFRC rectangular plates (48 in. x 12 in.) at first crack under transverse line load

Plate	Load N (lb)	f_t MPa (psi)	Strain (Measured) ε_x (10^{-6})	Strain (Measured) ε_y (10^{-6})	Stress, σ_x (Calculated) MPa (psi)
0%	712 (160)	6.27 (909)	136	-28	6.13 (889)
1%	934 (210)	7.52 (1,090)	147	-29	6.4 (928)
2%	964 (217)	13.01 (1,885)	281	-23	12.59 (1,824)

Where: P = applied transverse load at first noticeable crack, lb

f_t = splitting tensile strength of HSSFRC cylinders (from Table 8.1.4), psi

ε_x, ε_y = measured longitudinal and transverse strains of the rectangular plates, in/in

www.manaraa.com

σ_x = calculated stress along the span of the rectangular plates, psi.

8.1.7.7 Failure modes

The load versus deflection curves show that the HSSFRC rectangular plates under line load responded elastically till they reached their first crack load. Once the plates reached their initial crack load, 0% plates lost resistance abruptly while 1% and 2% SFVF rectangular plates lost resistance gradually.

Cracks for all SFVF rectangular plates subjected to line loads were consistently right at the middle of the plates close to the line load. For 0% plates, the crack planes or surfaces were straight and relatively smooth. The crack planes or surfaces for 1% and 2% plates on the other hand were rough and ragged.

The 0% HSSFRC rectangular plates exhibited the following behaviors:

- Sudden failure.
- Crack planes straight and 90 degrees with the bottom and top surfaces.
- A single plane failure.
- Plates broke into two separate pieces. Refer to Figure 8.1.12.
- The test duration for 0% HSSFRC rectangular plates was a lot shorter than for 1% and 2% SFVF specimens.

www.manaraa.com

Figure 8.1.12: Failure patterns for long span 0% HSSFRC rectangular plates under transverse line load

The 1% and 2% HSSFRC rectangular plates showed the following behaviors:

- Both types of plates showed more ductile failure behavior than 0% SFVF by demonstrating to undergo large deflections without complete failure and slow loss of resistance.

- The plates did not break into pieces at the end of the test; they stayed in one piece till the end of testing process.

www.manaraa.com

- Slow failure, plates had time to create visible plastic hinges, large cracks and deflections.

- The cracks did penetrate the whole depth of the plates at failure, which indicates the failure was slow and resistance to the applied load continued till the whole thickness of the plates was exhausted. This indicated the energy needed to break the plate increased from 0% to 1% and 2% SFVF drastically. Refer to Figures 8.1.13 and 8.1.14.

- The failure planes were not straight and perpendicular to the top and bottom surfaces. Cracks were ragged.

- Crushing of concrete was not observed at any time during testing process, neither at the supports nor at the area of load application for all SFVF.

www.manaraa.com

Figure 8.1.13: Failure patterns for long span 1% HSSFRC rectangular plates under transverse line load

www.manaraa.com

Figure 8.1.14: Failure patterns for long span 2% HSSFRC rectangular plates under transverse line load

8.1.7.8 Energy absorption (toughness)

The energy absorption (toughness), the area under the load versus deflection curves, for 0%, 1% and 2% HSSFRC long span rectangular plates were calculated as 7.2, 31.0 and 34.4 in-lb, respectively. The load versus deflection curves are shown in Figure 8.1.8. The energy absorption of HSSFRC long span rectangular plates increased as the steel fiber content increased: 331% and 378% for 1% and 2% SFVF plates, respectively over the 0% SFVF plates.

www.manaraa.com

8.1.7.9 Discussion of test results

Load-carrying capacity of long span HSSFRC rectangular plates under transverse central line load increased as the steel fiber by volume fraction (SFVF) increased from 0% to 1% and 2%. The capacity of long span HSSFRC rectangular plates increased by 7% and 25% for 1% and 2% SFVF, respectively compared to 0% (plain) HSSFRC rectangular plates.

The deflection of long span HSSFRC rectangular plates increased as the SFVF increased from 0% to 1% and 2%. Even though, the deflection at which all SFVF plates initially cracked is very comparable, the ultimate deflection at which the plates failed completely varied by a large margin. The higher value of deflection was exhibited by the higher SFVF, 2%. The total deflection at complete failure for long span rectangular plates at mid span increased by 707% and 890% for 1% and 2% SFVF, respectively compared to 0% (plain) rectangular plates.

The ductility of long span HSSFRC rectangular plates increased as the SFVF increased from 0% to 1% and 2%. The ratio of deflection at complete failure to the deflection at first crack increased from 1.0 for 0% to 5.47 and 9.73 for 1% and 2% SFVF, respectively. This shows greatly enhanced ductility and toughness capacities.

The splitting tensile strength results for HSSFRC cylinders exhibited an increase of 20% and 107% for 1% and 2% SFVF, respectively compared to 0% (plain) HSSFRC cylinders.

The young's modulus results for 0%, 1% and 2% HSSFRC cylinders remained roughly the same for all three SFVF at ±3.0%. The compressive strength results for all three SFVF are within ±5.0%. Therefore, the increase in young's modulus and

www.manaraa.com

compressive strength due to the addition of steel fibers is very small, almost flat. It can be concluded that, the addition of steel fibers to the plain mixture did not affect the behavior with respect to young's modulus and compressive strength in this case. It should be stressed that the same amount of High Range Water Reducer (HRWR) that is suitable for 0% mixture was used to prepare all 0%, 1% and 2% concrete mixtures. The effect of HRWR on young's modulus and compressive strength are shown in Phase (1b) of the research.

The stress versus strain diagram for cylinders in compression showed curves for all three SFVF samples being nearly identical, which is consistent with modulus of elasticity results.

Longitudinal strain gages were continuously in tension while the transverse strain gages were continuously subjected to compression during the entire testing process which was due to Poisson's effect. Longitudinal strains were observed to be larger in magnitude than the transverse strains.

The experimental tensile stress results for long span 0%, 1% and 2% HSSFRC rectangular plates at the first crack load correspond to the splitting tensile strength of 0%, 1% and 2% HSSFRC cylinders.

The theoretical elastic deflection results, for all three steel fiber by volume fractions, were consistently smaller than experimental values, even though the results seem to coincide within the 30% to 40% of the peak load. Theoretical deflection formulas tend to overestimate the stiffness of the plates.

www.manaraa.com

The area under the load versus deflection curves for HSSFRC rectangular plates with higher steel fiber by volume fractions exhibited higher energy absorption capacity (toughness) than the lower SFVF plates.

www.manaraa.com

8.2 HSSFRC rectangular plates with two long edges simply supported and the other two free under central line load in the long direction

8.2.1 Introduction

In Section 2 of Chapter 8, flexural properties of short span high strength steel fiber reinforced concrete (HSSFRC) thin rectangular plates with 0%, 1% and 2% steel fiber by volume fractions are presented. The plates are predominantly subjected to unidirectional flexural stress due to the mid-span location of the longitudinal line load.

All constituents for the three types of concrete mixtures (0%, 1% and 2% SFVF), used for the making of plates and cylinders, are the same except for the content of steel fibers. The thin rectangular plates have dimensions of 305 mm (12 in.) long by 1,219 mm (48 in.) wide and 32 mm (1.25 in.) thick, with length to width ratio of 1:4 (short span). The plates are simply supported at the long ends and subjected to a longitudinal line load at mid span along the long direction, as shown in Figure 8.2.1.

Two strain gages, perpendicular to one another, for each type of steel fiber by volume fraction mixture, are placed at the center bottom surface of the plate to measure the strain activities at the extreme fiber of the plate relative to the applied load. One rosette strain gage, for each steel fiber by volume fraction mixture, is placed on the side of the plate right at the support to measure the shear strain activity at the plate support.

www.manaraa.com

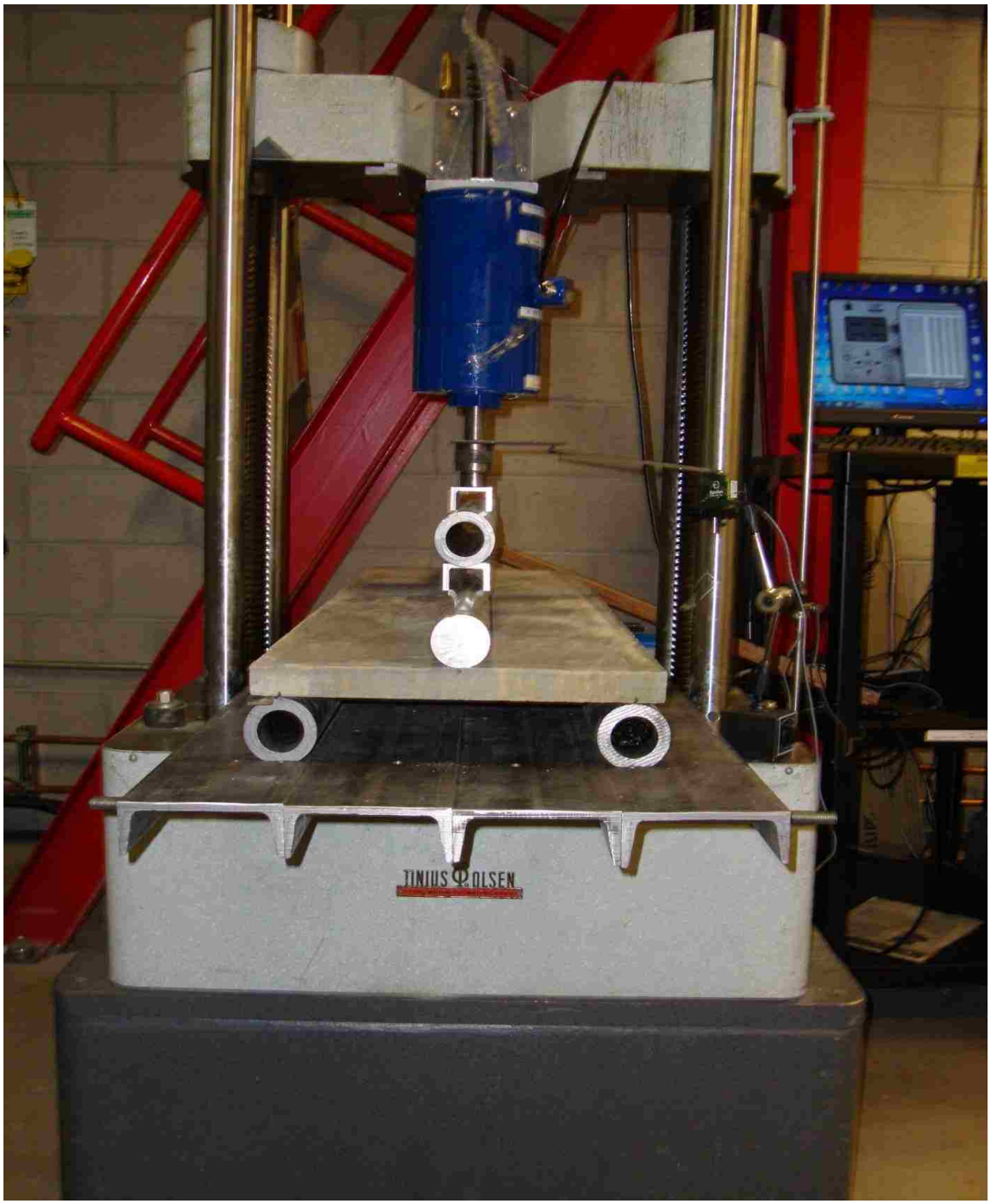

Figure 8.2.1: HSSFRC rectangular plate (12 in. x 48 in.) subjected to longitudinal line load at mid span

The chapter presents HSSFRC specimen preparation, testing procedures and experiment results such as load versus deflection, stress versus flexural and shear strains

www.manaraa.com

and mode of failure of rectangular plates. The chapter discusses the influence of steel fibers on: flexural and shear capacity, mode of failure and ductility of thin rectangular plates; and modulus of elasticity, compression and splitting tensile strength of cylinders prepared from the same mixtures used for the making of plates.

Comparisons are made between short span rectangular plates with various steel fiber by volume fraction with respect to the mechanical properties such as flexural capacity, deflection, ductility, and mode of failure. The elastic analysis results corresponding to the first crack load such as stress, strain and deflection are presented. Test results are discussed and conclusions drown.

8.2.2 Theoretical analysis of rectangular plates

Theoretical background and governing equations of rectangular plates are presented in Section 8.1.2.

8.2.3 Preparation of test specimens - cylinders and plates

The ingredients for the 0%, 1% and 2% steel fiber concrete mixtures are given in Table 8.1.1.

Two types of test specimens, rectangular plates and cylinders, were prepared for each test (0%, 1% and 2% SFVF) from the same concrete batch:

- Three rectangular thin plates for each SFVF with dimensions of 356 mm (14 in.) long by 1,219 mm (48 in.) wide and 32 mm (1.25 in.) thick. Therefore, a total of nine plate specimens were prepared.

www.manaraa.com

- Six 102 mm (4 in.) diameter by 203 mm (8 in.) long cylinders for each SFVF. Three cylinders each were used for compressive and splitting tensile strength tests, respectively. Therefore, a total of eighteen cylinders were prepared.

To form the rectangular plates, a crate with dimensions of approximately 1,219 mm (48 in.) wide and 356 mm (14 in.) long was made by nailing 32 mm (1.25 in.) thick plywood strip around the perimeter of base board. Refer to Section 8.1.3 for concrete and specimen preparations.

8.2.4 Types of strain gages used

The size and type of strain gages depend on the maximum aggregate size. Two types of strain gages, which were recommended by the manufacturer, were used:

1. N2A-06-10CBE-350/E – is an individual strain gage, used to measure strain in a single direction.
2. CEA-06-250UR-120 – is a rosette with three grids oriented 45° apart, angularly, from each other.

Refer to Section 8.1.4 for full description of both types of strain gages.

8.2.5 Location and orientation of strain gages on the test specimens, (12 in. x 48 in.)

Refer to Section 8.1.5 for strain gage locations and arrangements, since short span rectangular plates have similar number of strain gages and arrangements as long span rectangular plates.

www.manaraa.com

8.2.6 Test apparatus and procedures for short span rectangular plates

Once the specimens were fitted with strain gages, they were ready for testing. The strain gages and rosettes were installed per manufacturer's recommendation as stated in Section 4.4.6. The apparatus involved are discussed in Section 8.1.6.

The test set up for short span rectangular plates was assembled as follows:

1. First, the steel platform was placed flat on a very strong testing base.
2. Two support tubes were pinned parallel but 305 mm (12 in.) apart on the steel platform.
3. The specimen was laid flat on the top spanning between the two supports.
4. The steel bar is placed on the specimen at midpoint between the supports. The thick steel support tubes and the steel bar were 1,219 mm (48 in.) long, which is equal to the width of the test specimens.
5. The entire test set up and all contact surfaces were checked for any kind of rocking or gap (lack of contact) between the test specimen, supports and steel bar. All gaps were shimmed to ensure full contact and uniform load transfer between units.
6. Finally, the load cell was lowered slowly just to make contact with the steel bar and thereafter the load was applied at a steady rate of 0.025 – 0.051 mm/minute (0.001 – 0.002 in./minute) till the first major failure or crack occurred and increased to 0.102 – 0.203 mm/minute (0.004 – 0.008 in./minute) up to the complete failure of the specimen.

The HSSFRC cylinders, which were cast from the same concrete mixture used for plates, were tested for compressive and splitting tensile strength according to the test

www.manaraa.com

procedures that are presented in Sections 4.4.1 and 4.4.4, respectively. During the testing process for cylinders and plates: load, deflection and strain data were collected; failure and failure modes were noted.

8.2.7 Experiment results for rectangular plates (12 in. x 48 in.) supported along long edges under line load

8.2.7.1 Load versus deflection results

Load versus deflection data were collected for HSSFRC short span rectangular plates, with 0% to 2% steel fiber by volume fraction (SFVF), under central line load. Deflection was measured at plate center. Average load versus deflection curves of 0%, 1% and 2% short span HSSFRC rectangular plates (12 in. x 48 in.) are presented in Figure 8.2.2. Each load versus deflection curve represents an average result of three HSSFRC rectangular plate specimens for each SFVF, a total of nine specimens for 0%, 1% and 2% SFVF. Table 8.2.1 presents the peak load, deflection of the plate at the peak load and maximum deflection of the plate at complete failure for 0%, 1% and 2% SFVF. Values in Table 8.2.1 were obtained from average load versus deflection curves in Figure 8.2.2.

www.manaraa.com

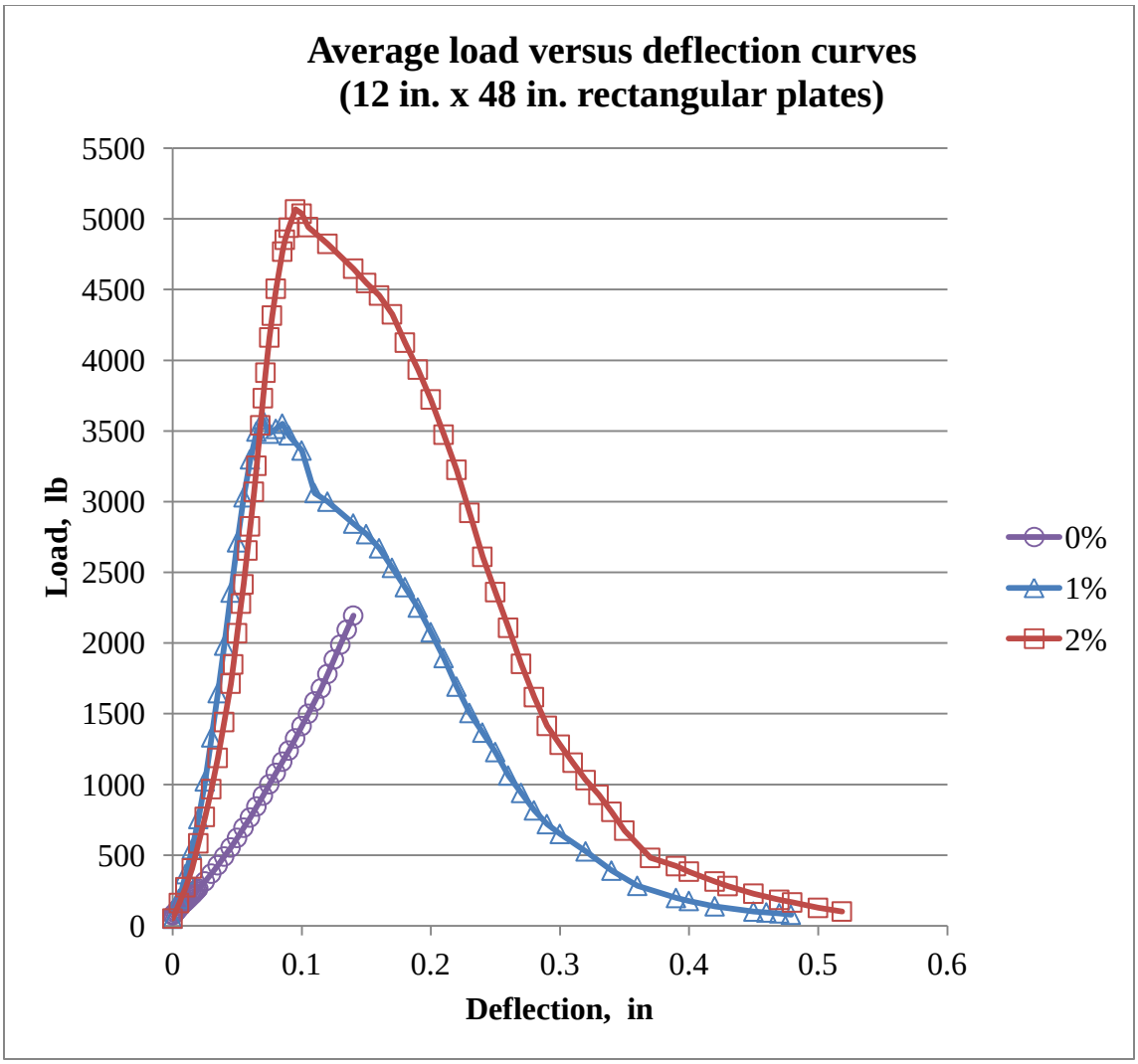

Figure 8.2.2: Average load versus deflection curves for 0%, 1% and 2% HSSFRC rectangular plates (12 in. x 48 in.) under longitudinal line load

www.manaraa.com

Table 8.2.1: Maximum load and deflection results for 0%, 1% and 2% HSSFRC rectangular plates (12 in. x 48 in.) under longitudinal line load

Plate	P_{Max} N (lb)	Percentage increase in load	Δ at P_{Max} mm (in.)	$\Delta_{failure}$ mm (in.)	Percentage increase in deflection	$\Delta_{failure}/\Delta$
0%	10,075 (2,265)	0%	3.66 (0.144)	3.66 (0.144)	0%	1.00
1%	15,746 (3, 540)	56%	1.65 (0.068)	12.14 (0.478)	232%	7.03
2%	22,833 (5,135)	127%	2.41 (0.095)	16.59 (0.653)	353%	6.87

Where: P_{Max} = peak load, N (lb.)

Δ = plate deflection corresponding to the peak load, mm (in.)

$\Delta_{failure}$ = maximum deflection of the plate at complete failure, mm (in.).

8.2.7.2 Test results for strain gages located at mid span

For strain gages located at mid span, the longitudinal and transverse strains for the short span HSSFRC rectangular plates (12 in. x 48 in.), with 0% and 2% SFVF, loaded in longitudinal direction are presented in Figures 8.2.3 and 8.2.4, respectively. Both figures show 2% SFVF specimen exhibited larger elastic range, ductile response and re-distribution of stress after the initial crack, about mid way. The negative strains in Figure 8.2.4 show the effect of Poisson's on the plates. The strains were measure at center bottom surface of the rectangular plates.

www.manaraa.com

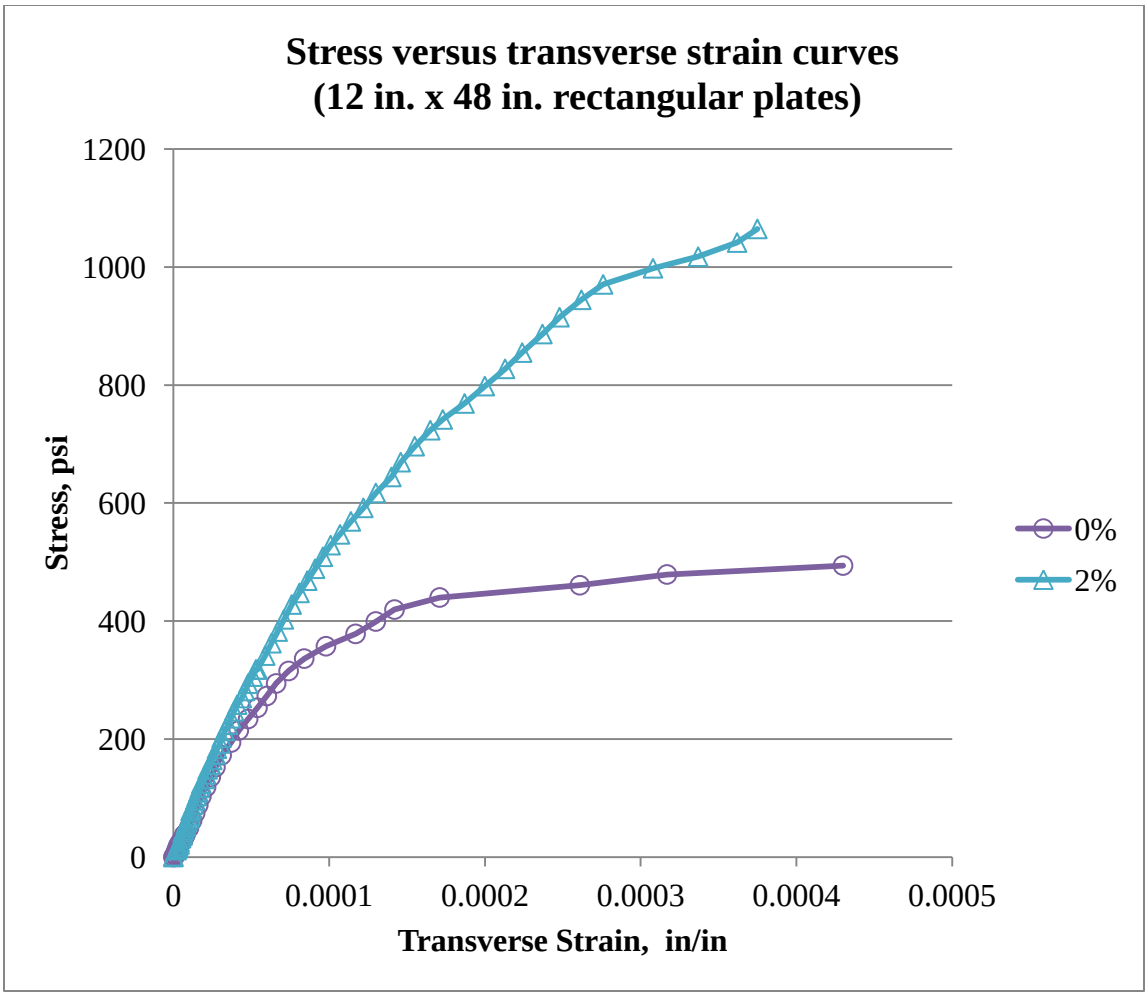

Figure 8.2.3: Stress versus transverse strain curves for 0% and 2% HSSFRC rectangular plates (12 in. x 48 in.) under longitudinal line load

www.manaraa.com

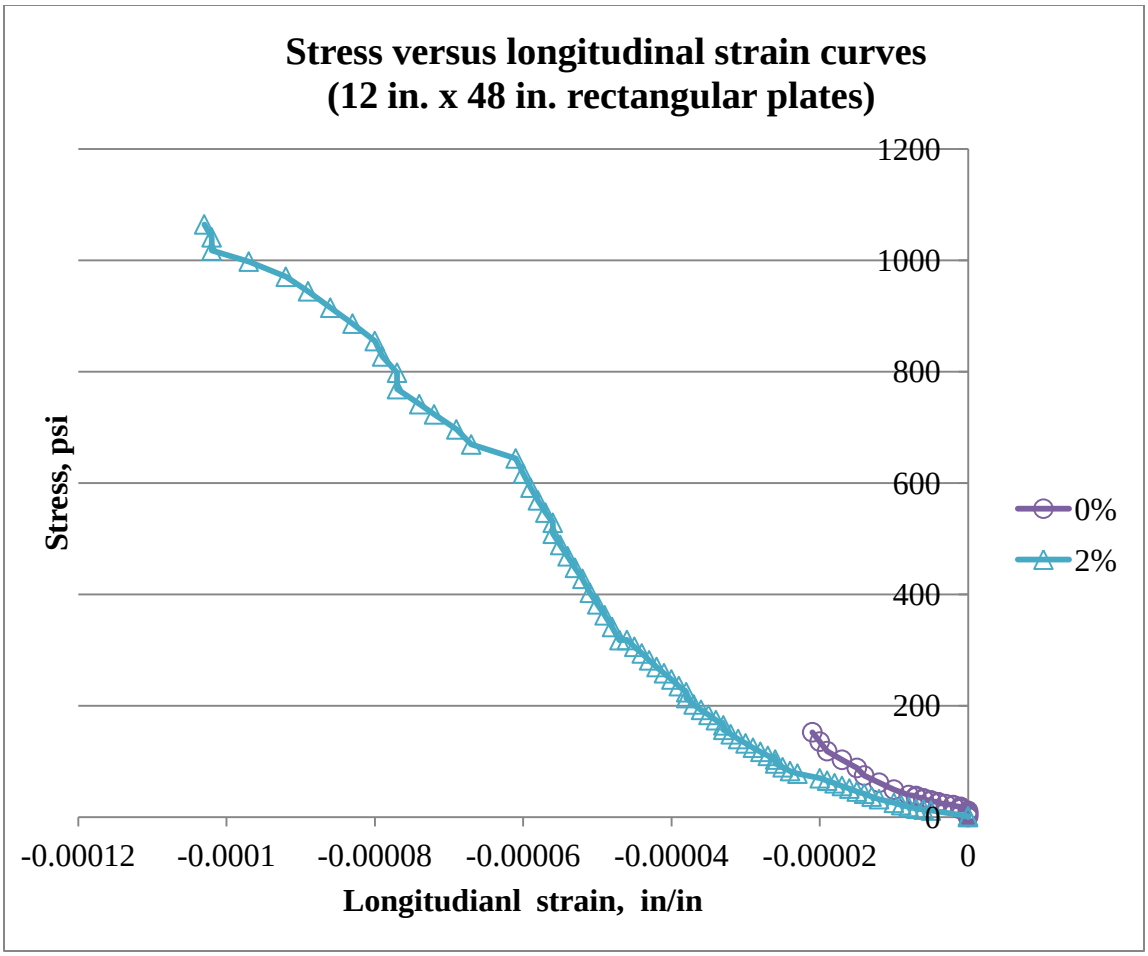

Figure 8.2.4: Stress versus longitudinal strain curves for 0%, 1% and 2% HSSFRC rectangular plates (12 in. x 48 in.) under longitudinal line load

8.2.7.3 Test results for rosette strain gages at the support

Stress versus vertical, horizontal and 45° rosette strain curves for short span HSSFRC rectangular plates (12 in. x 48 in.) with 2% SFVF are presented in Figure 8.2.5. The strains were measured at the support on the plane coinciding with the depth and length of the rectangular plate (12 in. x 48 in.). Rosette strain results for 0% and 1% were similar to 2% and are not shown.

www.manaraa.com

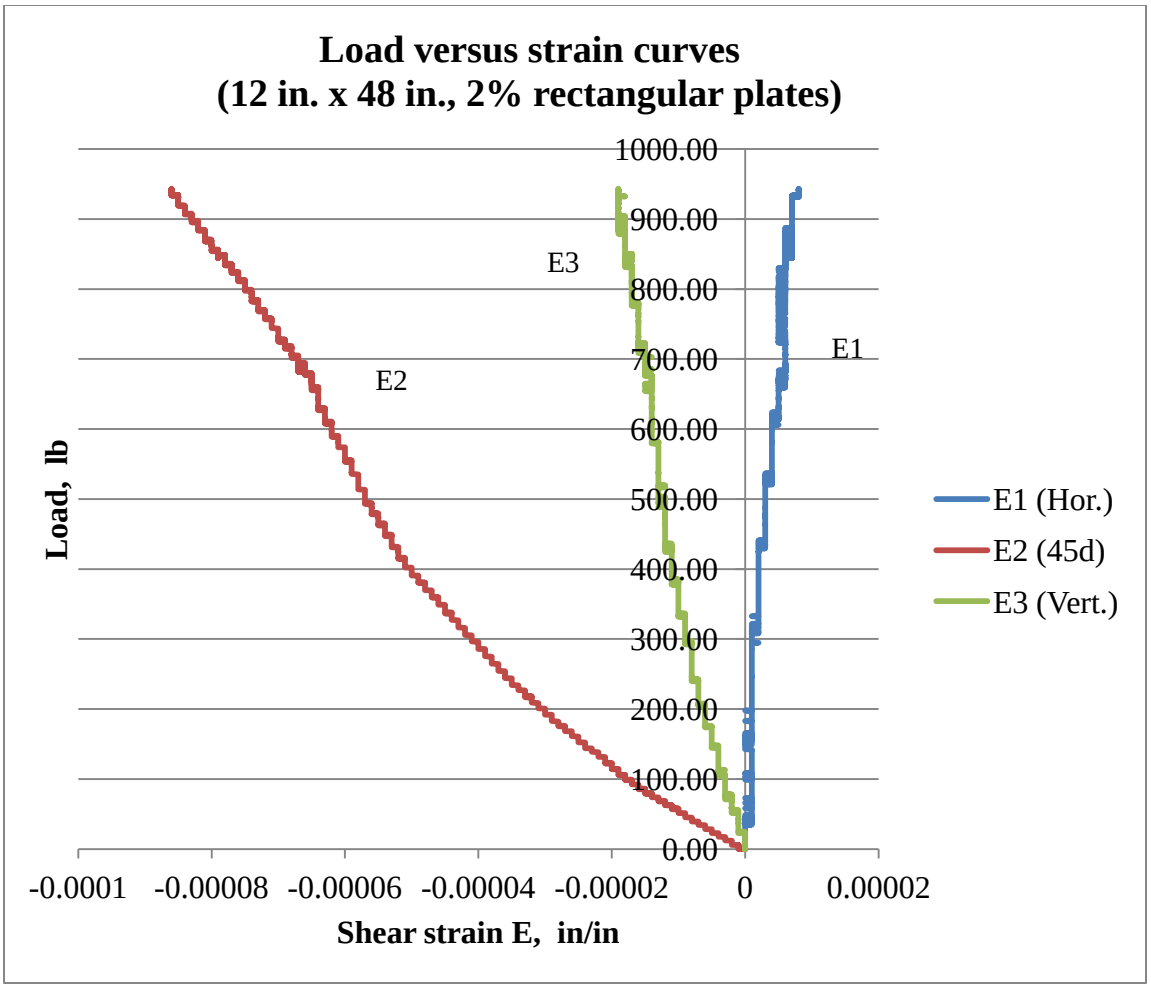

Figure 8.2.5: Stress versus rosette shear strain curves for 2% HSSFRC rectangular plates (12 in. x 48 in.) under longitudinal line load

Shear stress versus maximum shear strain curve for short span HSSFRC rectangular plate (12 in. x 48 in.) with 2% SFVF are presented in Figure 8.2.6. Maximum shear strains were calculated using Equation 8.12 in Section 8.1.4 with strain values from Figure 8.2.5. The shape of the shear stress versus maximum strain curve is dominated by the response of grid, strain, at 45 degrees from neutral axis (E2).

www.manaraa.com

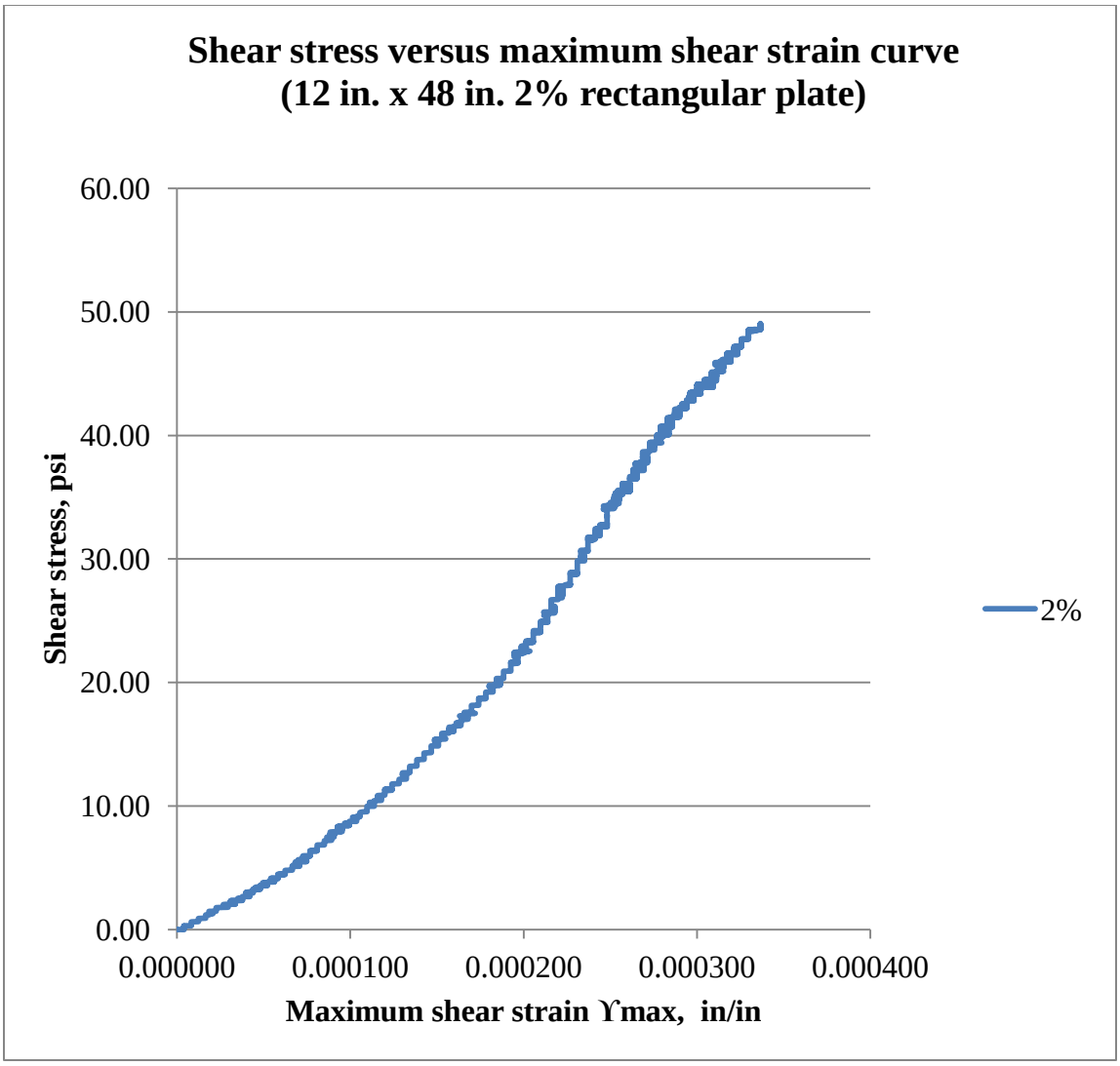

Figure 8.2.6: Shear stress versus maximum rosette shear strain curve for 2% HSSFRC rectangular plate (12 in. x 48 in.) under longitudinal line load

8.2.7.4 Cylinder compressive strength test results

As indicated in previous section, the concrete cylinder specimens that were used for compressive strength tests were taken from the same batch that the corresponding plates were made. The cylinders were tested, for compressive strength, within 24 hours of testing the corresponding plates. During the testing process both applied compression load and the corresponding longitudinal strain of cylinders were obtained.

www.manaraa.com

The average compressive stress versus longitudinal strain curves for 0%, 1% and 2% steel fiber reinforced concrete cylinders are presented in Figure 8.2.7.

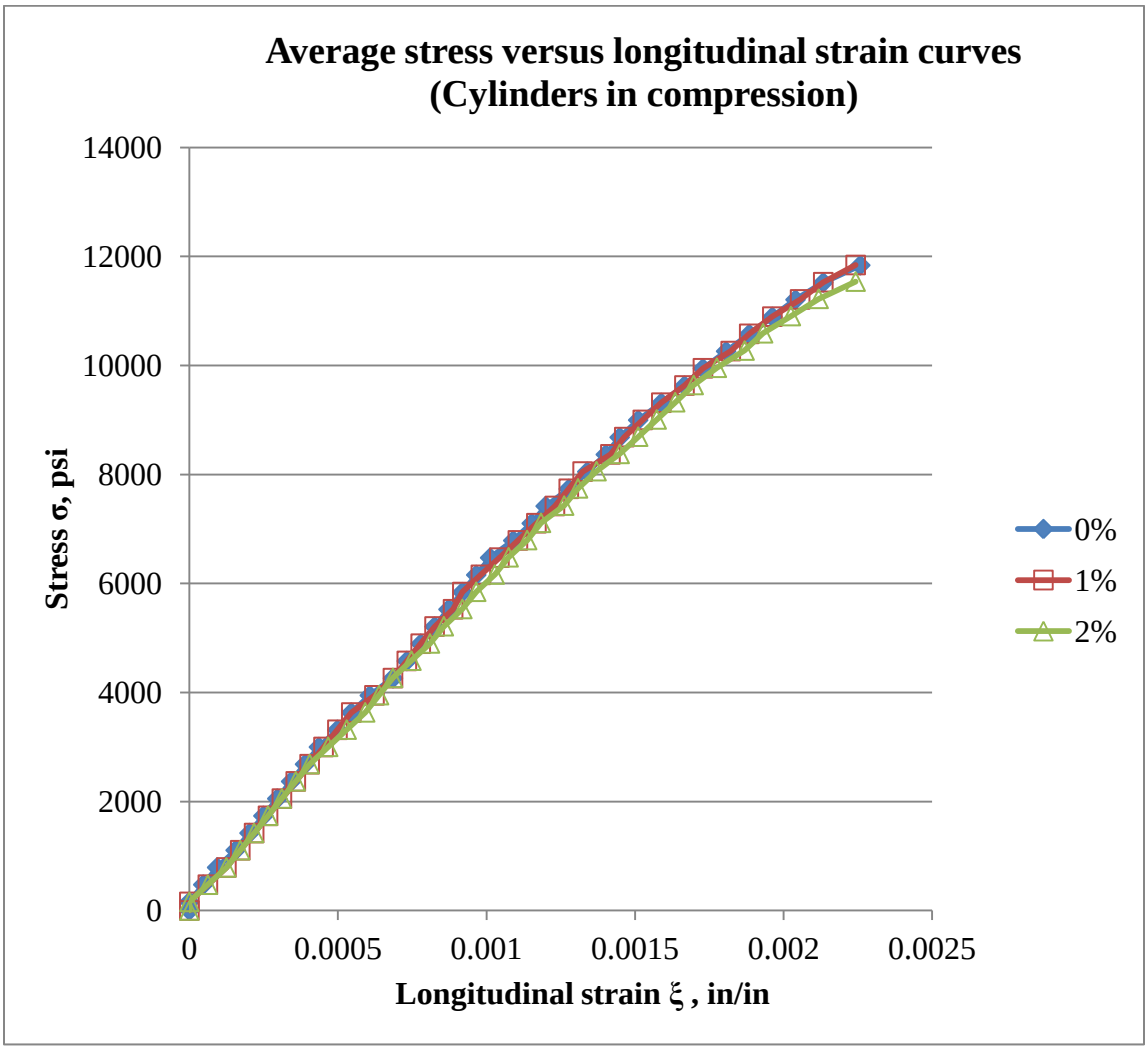

Figure 8.2.7: Average compressive stress versus longitudinal strain curves for 0%, 1% and 2% HSSFRC cylinders (4 in. x 8in.), casted with rectangular plates (12 in. x 48 in.)

The average compression strength and modulus of elasticity test results for 0%, 1% and 2% high strength steel fiber reinforced concrete cylinders under compression load are

www.manaraa.com

presented in Table 8.2.2. The compressive strength and modulus of elasticity results were calculated using procedures in Sections 4.4.1 and 4.4.2, respectively.

Table 8.2.2: Average compressive strength and modulus of elasticity results for 0%, 1% and 2% HSSFRC cylinders (4 in. x 8 in.) casted with rectangular plates, (12 in. x 48 in.)

Cylinder	Compressive stress MPa (psi)	Percentage increase from 0% steel fiber	Modulus of elasticity MPa (ksi)	Percentage increase from 0% steel fiber
0%	85		44,071	
	(12,359)	0%	(6,392)	0%
1%	84		43,658	
	(12,129)	-2%	(6,332)	-0.9%
2%	84		42,410	
	(12,238)	-1%	(6,151)	-3.8%

8.2.7.5 Cylinder splitting tensile strength results

The average splitting tensile strength test results for 0%, 1% and 2% high strength steel fiber reinforced concrete cylinders are presented in Table 8.2.3, while the splitting tensile figures are presented in Figure 8.2.8. Splitting tensile strength results were computed using Equation 4.3. The splitting tensile strength of HSSFRC cylinders increased as the SFVF increased.

www.manaraa.com

Table 8.2.3: Average splitting tensile strength results for 0%, 1% and 2% HSSFRC cylinders (4 in. x 8 in.) casted with rectangular plates (12 in. x 48 in.)

Cylinder	Splitting tensile stress MPa (psi)	Percentage increase from 0% steel fiber	Splitting tensile to compression strength ratio
0%	5.89		
	(855)	0%	0.07
1%	7.51		
	(1,089)	27%	0.09
2%	13.09		
	(1,898)	122%	0.16

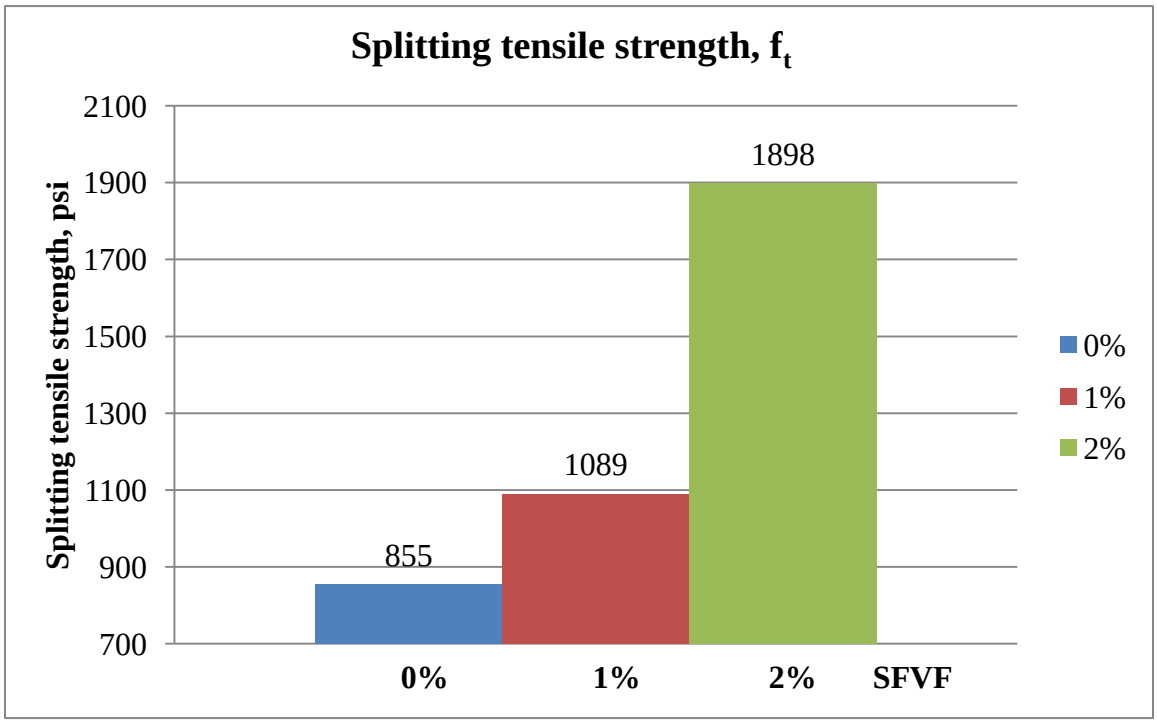

Figure 8.2.8: Average splitting tensile strength results for 0%, 1% and 2% HSSFRC cylinders (4 in. x 8 in.) casted with rectangular plates (12 in. x 48 in.)

www.manaraa.com

8.2.7.6 Stress-strain analysis and test results

Longitudinal and transverse strains at first crack and calculated stress results for 0%, 1% and 2% HSSFRC rectangular plates (12 in. x48 in.) are presented in Table 8.2.4. Stress results for the rectangular plates were calculated using Equation 8.3 in Section 8.1.2 and modulus of elasticity values from cylinders in compression. The flexural stresses at first noticeable crack, as shown in Table 8.2.4, are comparable to the spitting tensile stress results of HSSFRC cylinders.

www.manaraa.com

Table 8.2.4: Stress–strain results for 0%, 1% and 2% HSSFRC rectangular plates (12 in. x 48 in.) at first crack under longitudinal line load

Plate	Load N (lb)	f_t MPa (psi)	Strain (Measured) ε_x (10^{-6})	Strain (Measured) ε_y (10^{-6})	Stress, σ_x (Calculated) MPa (psi)
0%	7,482 (1,682)	5.90 (855)	124	-8	5.71 (828)
1%	8,372 (1,882)	7.51 (1,089)	148	-14	6.66 (965)
2%	18,247 (4,162)	13.10 (1,898)	301	-112	12.34 (1,789)

Where: P = applied transverse load at first noticeable crack, lb

f_t = splitting tensile strength of HSSFRC cylinders (from Table 8.2.3), psi

ε_x, ε_y = measured longitudinal and transverse strains of the rectangular plates, in/in

σ_x = calculated stress along the span of the rectangular plates, psi.

8.2.7.7 Failure modes

Refer to Section 8.1.7.7 for discussion on failure modes of short span HSSFRC rectangular plates. Failure and crack patters for 0%, 1% and 2% short span HSSFRC rectangular plates are presented in Figures 8.2.9 through 8.2.12.

www.manaraa.com

Figure 8.2.9: Failure patterns for short span 0% HSSFRC rectangular plates under longitudinal line load

www.manaraa.com

Figure 8.2.10: Failure patterns for short span 1% HSSFRC rectangular plates under longitudinal line load

www.manaraa.com

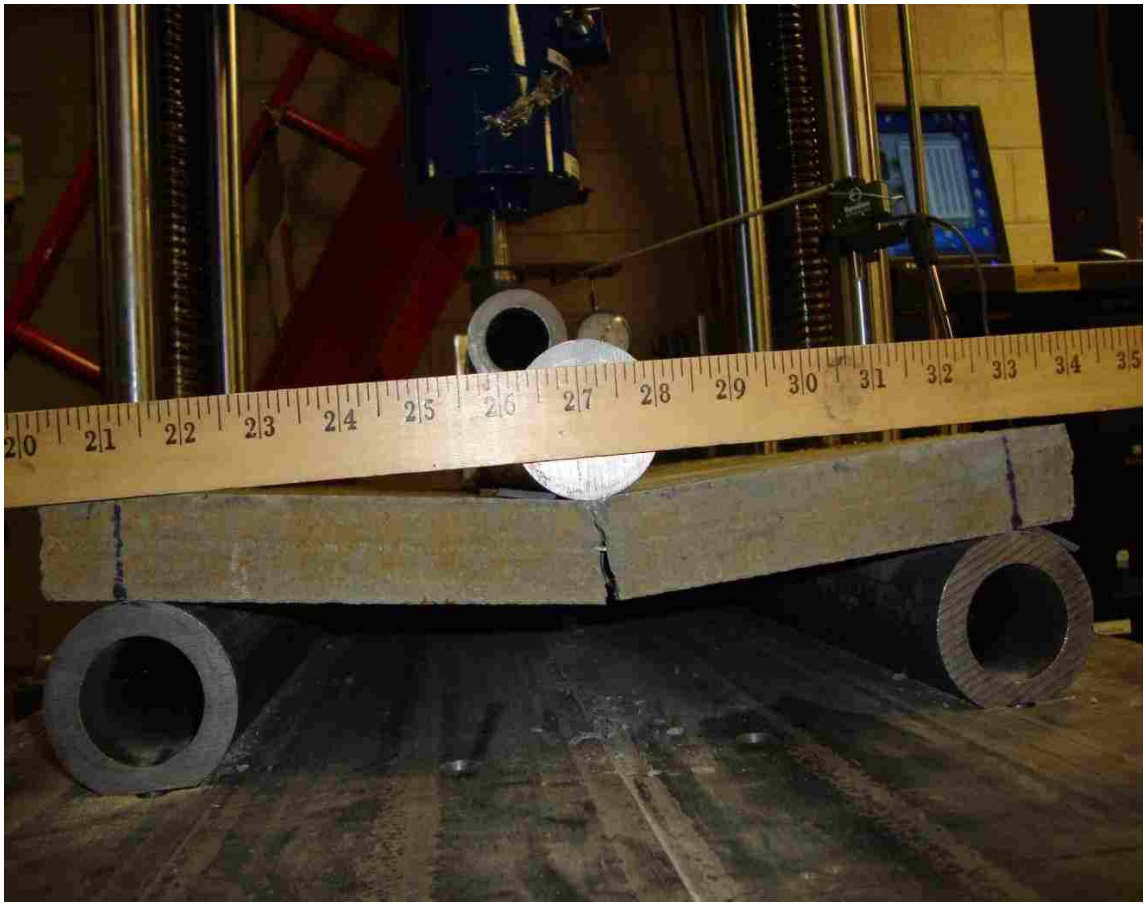

Figure 8.2.11: Failure patterns for short span 2% HSSFRC rectangular plates under longitudinal line load

www.manaraa.com

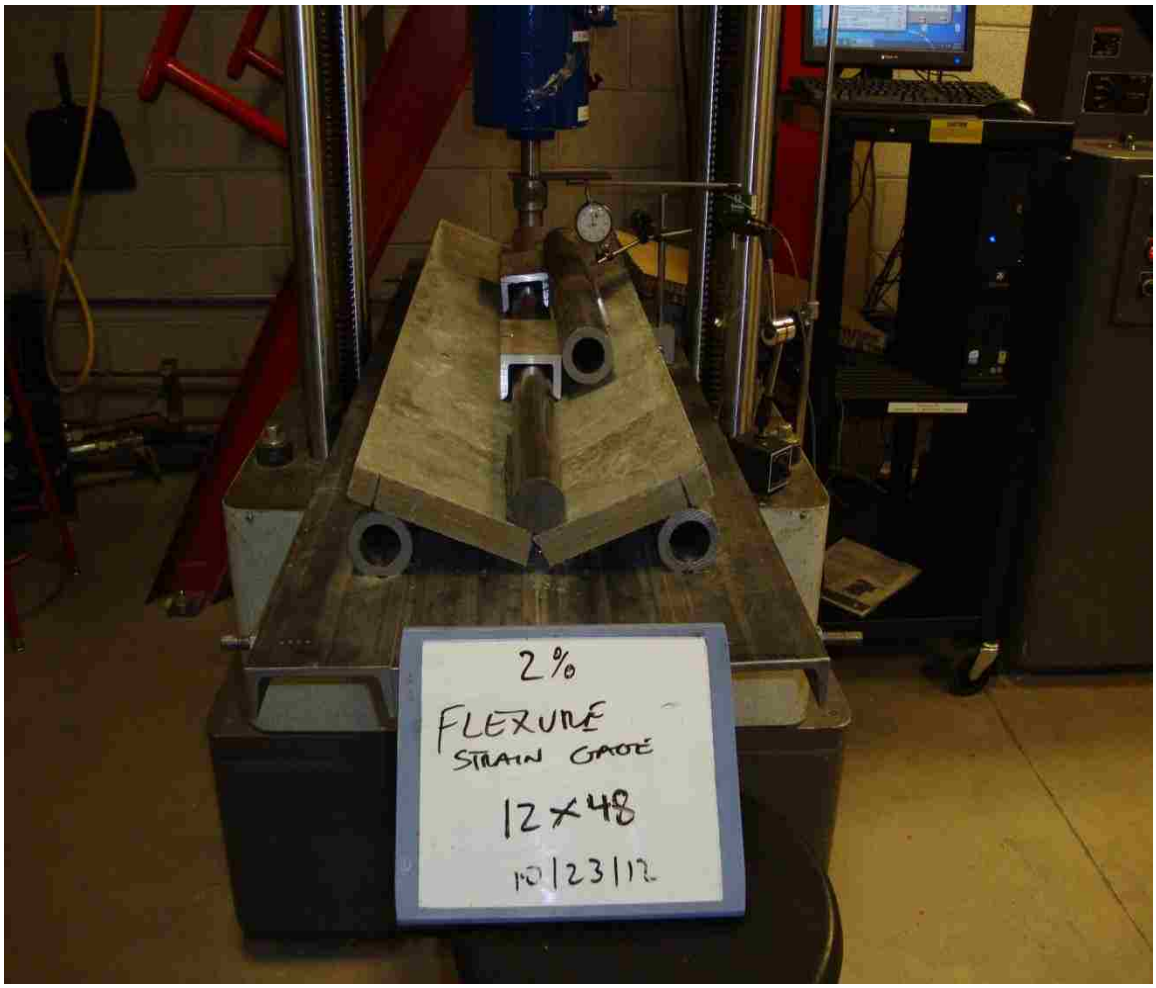

Figure 8.2.12: Failure patterns for short span 2% HSSFRC rectangular plates under longitudinal line load

8.2.7.8 Energy absorption (toughness)

The energy absorption (toughness), the area under the load versus deflection curves, for 0%, 1% and 2% HSSFRC short span rectangular plates were calculated as 138, 671 and 1,028 in-lb, respectively. The load versus deflection curves are shown in Figure 8.2.2. The energy absorption of HSSFRC short span rectangular plates increased as the steel fiber content increased: 386% and 645% for 1% and 2% SFVF plates, respectively over the 0% SFVF plates.

www.manaraa.com

8.2.7.9 Discussion of test results

The capacity of short span HSSFRC rectangular plates to accommodate longitudinal central line load increased as the steel fiber by volume fraction (SFVF) increased from 0%, to 1% and 2%. The load-carrying capacity of short span HSSFRC rectangular plates increased by 56% and 127% for 1% and 2% SFVF, respectively compared to 0% (plain) HSSFRC rectangular plates.

The deflection of short span HSSFRC rectangular plates increased as the SFVF increased from 0% to 1% and 2%. Even though, the deflection at which all SFVF plates initially cracked is very comparable, the ultimate deflection at which the plates failed completely varied by a large margin. The higher value of deflection was exhibited by the higher SFVF, 2%. The total deflection at complete failure for the short span rectangular plates at mid span increased by 232% and 353% for 1% and 2% SFVF, respectively compared to 0% (plain) rectangular plates.

The ductility of the short span HSSFRC rectangular plates increased as the SFVF increased from 0% to 1% and 2%. The ratio of deflection at complete failure to the deflection at first crack increased from 1.0 for 0% to 7.03 and 6.87 for 1% and 2% SFVF, respectively. This shows greatly enhanced ductility and toughness capacities.

The splitting tensile strength of HSSFRC cylinders increased by 27% and 122% for 1% and 2% SFVF, respectively compared to 0% (plain) HSSFRC cylinders.

The young's modulus results for 0%, 1% and 2% HSSFRC cylinders remained roughly the same for all three SFVF at ±4.0%. The compressive strength results for all three SFVF are within ±2.0%. Therefore, the effect on young's modulus and compressive strength due to the addition of steel fibers is very small, almost flat. It can be concluded

www.manaraa.com

that, the addition of steel fibers to the plain mixture did not affect the behavior with respect to young's modulus and compressive strength in this case. It should be stressed that the amount of High Range Water Reducer (HRWR) that is suitable for 0% mixture was used to prepare all 0%, 1% and 2% concrete mixtures. The effect of HRWR on young's modulus and compressive strength are shown in Phase (1b) of the research.

The stress-strain diagram for cylinders in compression showed curves for all three SFVF samples being nearly identical, which is consistent with modulus of elasticity results.

The transverse strain gage reading were continuously in tension while the longitudinal strain gages were mostly subjected to compression due to Poisson's effect during the entire testing process. Longitudinal strains were smaller in magnitude than the transverse strains (perpendicular to the line of load).

The experimental tensile stress results for 0%, 1% and 2% HSSFRC short span rectangular plates at the first crack load correspond to the splitting tensile strength of 0%, 1% and 2% HSSFRC cylinders.

The theoretical elastic deflection results, for all three steel fiber by volume fractions, were consistently smaller than experimental values, even though the results seem to coincide within the 30% to 40% of the peak load. Theoretical deflection formulas tend to overestimate the stiffness of the plates.

The area under the load-deflection curves for HSSFRC rectangular plates with higher steel fiber by volume fraction exhibited higher energy absorption capacity (toughness) than the lower SFVF plates.

www.manaraa.com

CHAPTER 9

HIGH STRENGTH STEEL FIBER REINFORCED CONCRETE SQUARE PLATES WITH FOUR EDGES SIMPLY SUPPORTED UNDER CENTER POINT LOAD

9.1 Introduction

In this chapter the behavior of simply supported high strength steel fiber reinforced concrete (HSSFRC) square plates with 0%, 1% and 2% steel fiber by volume fractions (SFVF) subjected to a concentrated load at the geometric center is presented. The square plates are predominantly subjected to bi-axial flexural stress due to the plate dimensions, length to width ratio of 1:1, and the location of the point load and supports. The significance of the test is to study the flexural behavior of HSSFRC plates under bi-axial flexure stress.

All constituents for the three types of concrete mixtures (0%, 1% and 2% SFVF), used for the making of plates and cylinders, are the same except for the content of steel fibers. The thin square plates have dimensions of 483 mm (19 in.) long by 483 mm (19 in.) wide and 32 mm (1.25 in.) thick. The plates are simply supported at all sides by 457 mm (18 in.) long by 457 mm (18 in.) wide metal supports and subjected to a concentrated center load, as shown in Figure 9.1.

www.manaraa.com

Figure 9.1: HSSFRC square plate subjected to concentrated load at the geometric center

Two strain gages, perpendicular to one another, for each type of steel fiber by volume fraction mixture, are placed at the center bottom surface of the plate to measure the strain activities at the extreme fiber of the plate in relation to the applied load. One rosette strain gage, for each steel fiber by volume fraction mixture, is placed on the side of the plate right at the support to measure the shear strain activity at the plate support.

www.manaraa.com

The chapter presents HSSFRC specimen preparation, testing procedures and experiment results such as load versus deflection, load versus flexural and shear strains and mode of failure of square plates. The chapter discusses the influence of steel fibers on: flexural and shear capacity, mode of failure and ductility of thin plates; and modulus of elasticity, compression and splitting tensile strength of cylinders prepared from the same mixtures used for the making of plates.

Comparisons are made between centrally loaded square plates with various steel fiber by volume fractions with respect to the mechanical properties such as flexural capacity, deflection, ductility, and mode of failure. The elastic analysis results corresponding to the first crack load such as stress, strain and deflection are presented. Test results are discussed and conclusions drown.

9.2 Preparation of test specimens - cylinders and square plates

Two types of test specimens, square plates and cylinders, were prepared for each test (0%, 1% and 2% SFVF) from the same concrete batch:

- Three thin square plates for each SFVF with dimensions of 483 mm (19 in.) wide by 483 mm (19 in.) long and 32 mm (1.25 in.) thick. Therefore, a total of nine plate specimens were prepared.
- Six 102 mm (4 in.) diameter by 203 mm (8 in.) long cylinders for each SFVF. Three cylinders each were used for compressive and splitting tensile strength tests, respectively. Therefore, a total of eighteen cylinders were prepared.

www.manaraa.com

To form the square plates, a crate with dimensions of approximately 483 mm (19 in.) long and 483 mm (19 in.) wide was made by nailing 32 mm (1.25 in.) thick plywood strip around the perimeter of the base board.

The ingredients for all concrete mixtures were kept the same except for the amount of steel fibers used by volume fraction in each concrete mixture type. The ingredients for the 0%, 1% and 2% steel fiber concrete mixtures are given in Table 9.1.

Refer to Section 8.1.3 for concrete and specimen preparations. Plates and cylinders were cured for 56-days.

www.manaraa.com

Table 9.1: Concrete batch constituents for 0%, 1% and 2% HSSFRC square plates (18 in. x 18 in.) and cylinders

Mixture Components		**0%**	**1%**	**2%**
Batch Volume		**1.5 ft^3**	**1.5 ft^3**	**1.5 ft^3**
3/8" Coarse Aggregate (lb)		34.2	34.2	34.2
#4 Coarse Aggregate (lb)		33.6	33.6	33.6
Fine Aggregate, FA3* (lb)		86.4	86.4	86.4
Water (lb)		17.4	17.4	17.4
Cement Type V (lb)		37.5	37.5	37.5
Silica Fume (lb)		2.85	2.85	2.85
Fly Ash (lb)		16.05	16.05	16.05
Total Cementitious (lb)		56.4	56.4	56.4
Water to Cement Ratio		0.46	0.46	0.46
Water / Cementitious Ratio		0.31	0.31	0.31
Gravel : Sand Ratio		0.44 : 0.56	0.44 : 0.56	0.44 : 0.56
HRWR ADVA540 (lb)		0.588	0.588	0.588
Steel Fiber by Volume %		0%	1%	2%
Steel Fiber by weight (lb)		0	7.5	15
Concrete Total Weight (lb)		228.59	236.09	243.59
Concrete Unit weight (pcf)		152.4	157.4	162.4

*Fine aggregate with fineness modulus of 2.05

www.manaraa.com

9.3 Types of strain gage used

The size and type of strain gages depend on the maximum aggregate size. Two types of strain gages, which were recommended by the manufacturer, were used:

1. N2A-06-10CBE-350/E – is an individual strain gage, which measures strain in a single direction. It can be installed, as shown in Figure 9.2, individually or in group to measure strain in one or multiple directions, respectively.
2. CEA-06-250UR-120 – is a rosette, group, type strain gage with three grids oriented 45° apart, angularly, from each other; refer to Figures 8.1.3 and 9.3 for rosette orientation. Refer to Section 8.1.4 for full description of both types of strain gages.

Figure 9.2: Strain gages located at the center bottom surface of the 18 in. x 18 in. square plates

www.manaraa.com

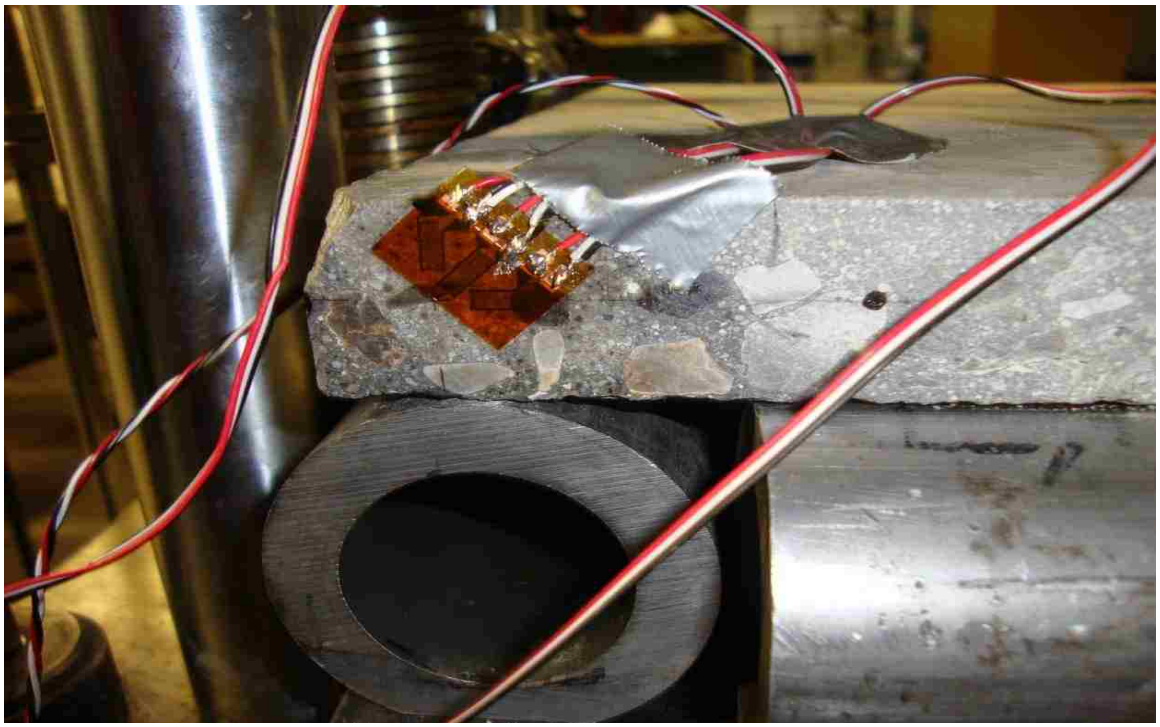

Figure 9.3: 45°- rectangular rosette placed at the support of HSSFRC 18 in. x 18 in. square plates

9.4 Location and orientation of strain gages on the test specimens

The strain gage arrangements for every test plate were determined by the capability of the data acquisition system to accommodate rosette and strain gage output, deflection measurements and load input combined.

At the end of the 56-day, both plate and cylinder specimens were pulled out of the curing room. The plate specimens were prepared as follows:

- Plate #1 had no strain gages on it. Vertical deflection was measured at the point of load application. The load and vertical deflection readings were electronically linked.

www.manaraa.com

- Plate #2 was furnished with two independent orthogonally placed strain gages, as shown in Figure 9.4.
- Plate #3 was equipped with one 45°- rectangular rosette with three grids spaced at 45° interval, as shown in Figure 9.5.

Refer to Section 8.1.5 for the locations and arrangements of both types of strain gages, since the strain gage set up were the same as long span rectangular plates.

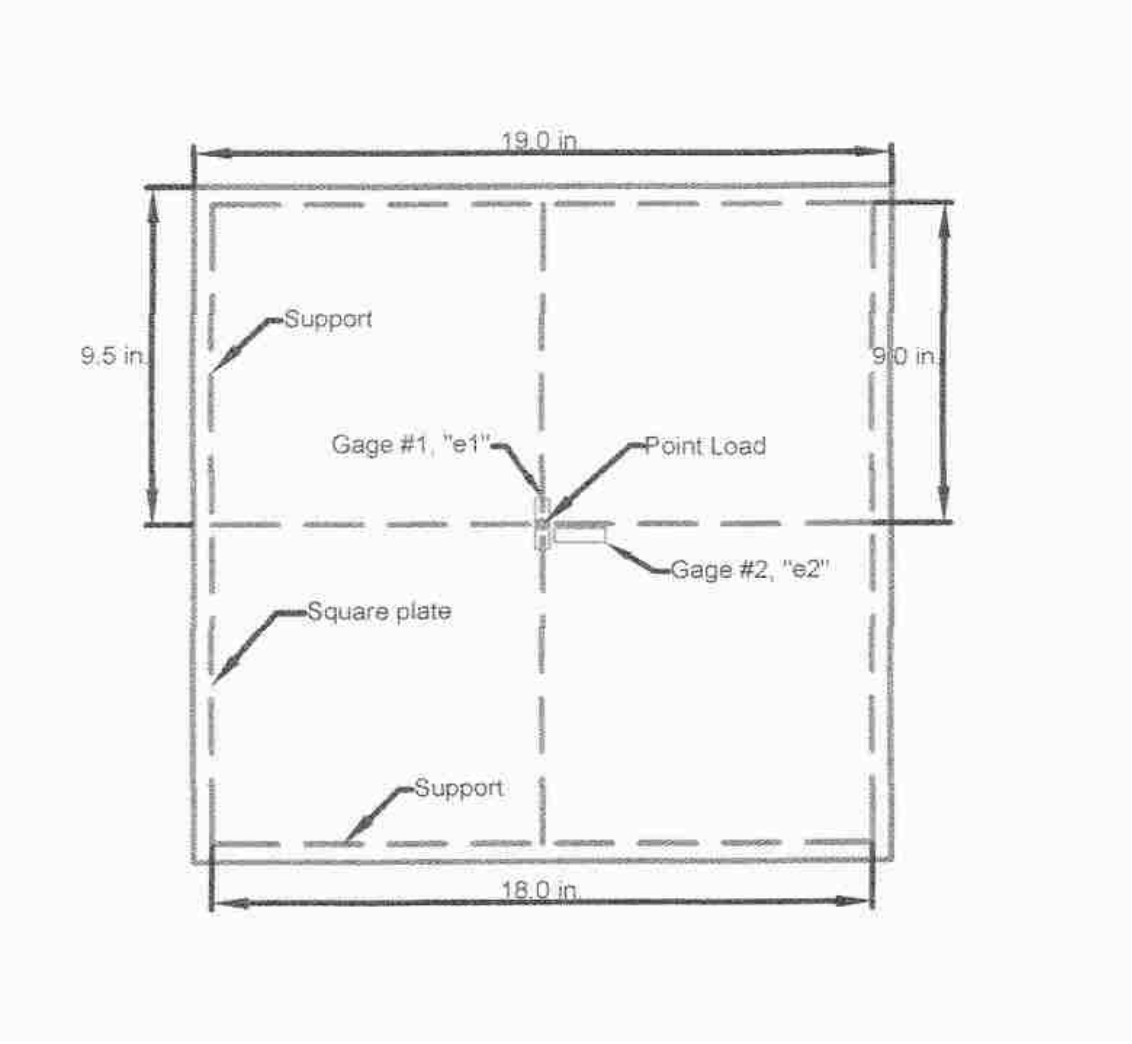

Figure 9.4: Strain gages located at the bottom surface of HSSFRC square plate

www.manaraa.com

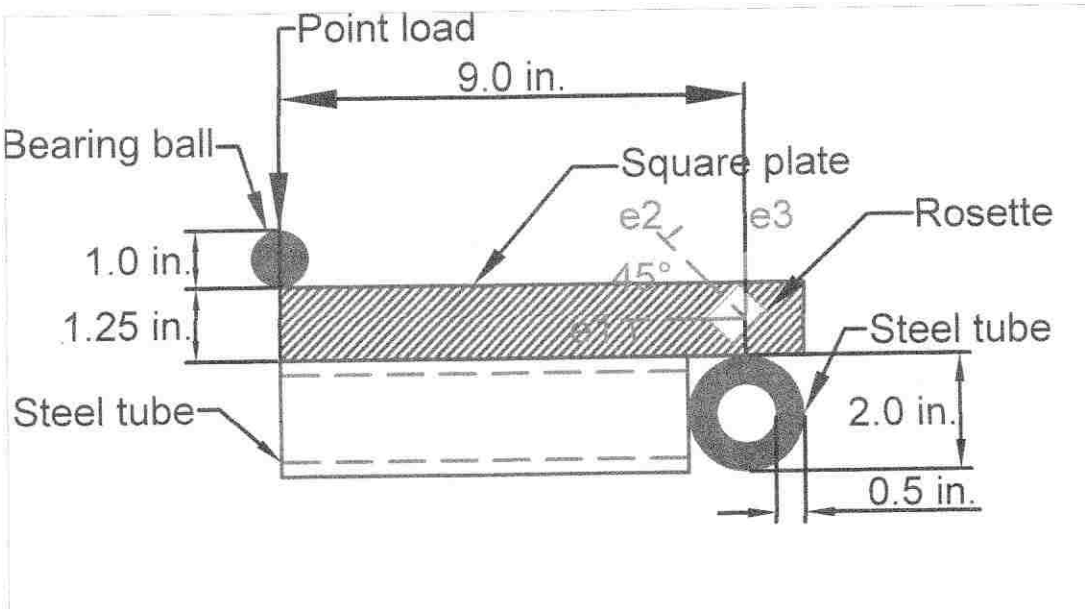

Figure 9.5: Rosette strain gage located on the side of the square plate

9.5 Test apparatus and procedures for square plates

Once the specimens were fitted with strain gages, they were ready for testing. The strain gages and rosettes were installed per manufacturer's recommendation as stated in Section 4.4.6. The apparatus involved were:

1. Tinius-Olsen testing machine (50,000 lb maximum capacity).
2. Steel base/platform.
3. Four 12.75 mm (0.5 in.) thick and 50.8 mm (2 in.) diameter steel tube supports.
4. 25.4 mm (1 in.) diameter spherical bearing ball, part of the load assembly.

   Support system and load assembly sizes and dimensions are presented in Figure 9.5.
5. Extensometer to measure deflection of plates.

www.manaraa.com

The test set up for plates was assembled as follows:

1. First, the steel platform was placed flat on a very strong testing base.
2. Four support tubes were pinned on the steel platform to form 457 mm (18 in.) by 457 mm (18 in.) square.
3. The specimen was laid flat on the top of the tubes spanning between the four supports.
4. The bearing ball was placed at the geometric center of the specimen.
5. The entire test set up and all contact surfaces were checked for any kind of rocking or gap (lack of contact) between the test specimen supports and the test specimen. All gaps were shimmed to ensure full contact and uniform load transfer between units.
6. Finally, the load cell was lowered slowly just to make contact with the loading unit (bearing ball) and thereafter the load was applied at a steady rate of 0.025 – 0.051 mm/minute (0.001 – 0.002 in./min) till the first major failure or crack occurred and increased to 0.076 – 0.127 mm/minute (0.003 – 0.005 in./minute) till complete failure of the specimen.

The HSSFRC cylinders, which were cast from the same concrete mixture used for plates, were tested for compressive and splitting tensile strength according to the test procedures that are presented in Sections 4.4.1 and 4.4.4, respectively. During the testing process for cylinders and plates: load, deflection and strain data were collected; failure and failure modes were noted.

www.manaraa.com

9.6 Experiment results for simply supported HSSFRC square plates under transverse center point load

9.6.1 Load versus deflection results

Load versus vertical deflection data were collected during the testing process for HSSFRC square plates, with 0% to 2% steel fiber by volume fractions (SFVF), under concentrated center load. Deflection of plates was measured at plate center. Average load versus deflection curves for 0%, 1% and 2% HSSFRC square plates under concentrated center load are presented in Figure 9.6. Each load versus deflection curve represents an average result of three HSSFRC square plate specimens for each SFVF, a total of nine specimens for 0%, 1% and 2% SFVF. Table 9.2 presents the peak concentrated load, deflection of the square plate at the peak load and maximum deflection of the square plate at complete failure for 0%, 1% and 2% SFVF. Values in Table 9.2 were obtained from the average load versus deflection curves in Figure 9.6.

www.manaraa.com

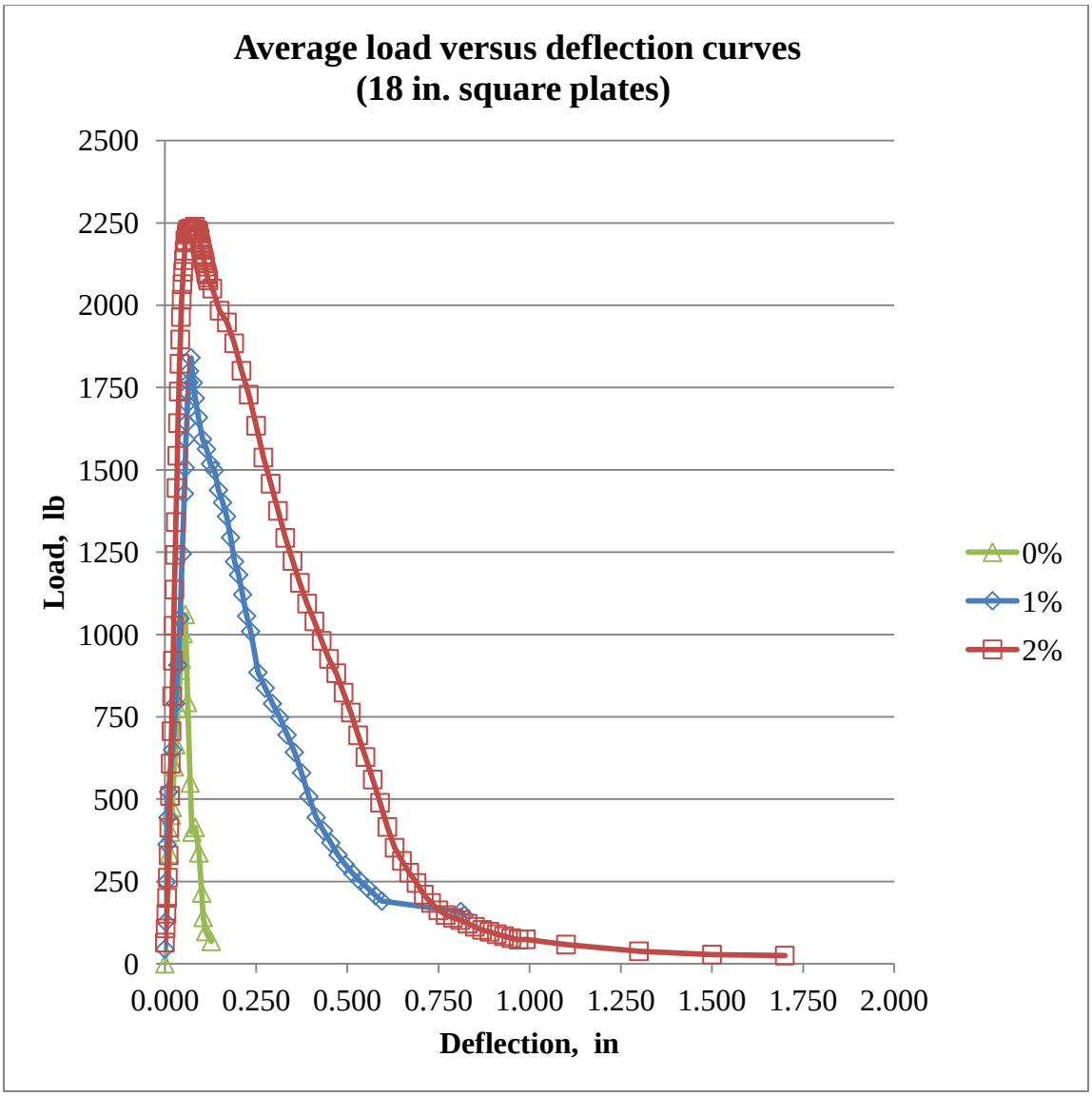

Figure 9.6: Average load versus deflection curves for 0%, 1% and 2% HSSFRC square plates (18 in. x 18 in.) under central point load

www.manaraa.com

Table 9.2: Maximum load and deflection results for 0%, 1% and 2% HSSFRC square plates (18 in. x 18 in.) under center point load

Plate	P_{Max} N (lb)	Percentage increase in deflection	Δ at P_{Max} mm (in.)	$\Delta_{failure}$ mm (in.)	Percentage increase in deflection	$\Delta_{failure}/\Delta$
0%	4,542 (1,021)	0%	1.42 (0.056)	3.23 (0.127)	0%	2.27
1%	8,185 (1,840)	80%	1.83 (0.072)	20.50 (0.807)	535%	11.21
2%	9,933 (2,233)	119%	1.83 (0.072)	43.46 (1.711)	1,247%	23.76

Where: P_{Max} = peak concentrated load, N (lb)

Δ = plate deflection corresponding to the peak load, mm (in.)

$\Delta_{failure}$ = maximum deflection of the plate at complete failure, mm (in.).

9.6.2 Test results for strain gages located at mid span

Load versus strain of square plates (18 in. x 18 in.) with 0%, 1% and 2% high strength steel fiber concrete loaded at the geometric center are presented in Figure 9.7. The strains were measured at the center bottom surface of the square plates. Figures 9.7 shows 2% SFVF specimen exhibited larger elastic range, ductile response and re-distribution of stress after initial crack than 0% and 1% SFVF specimen.

www.manaraa.com

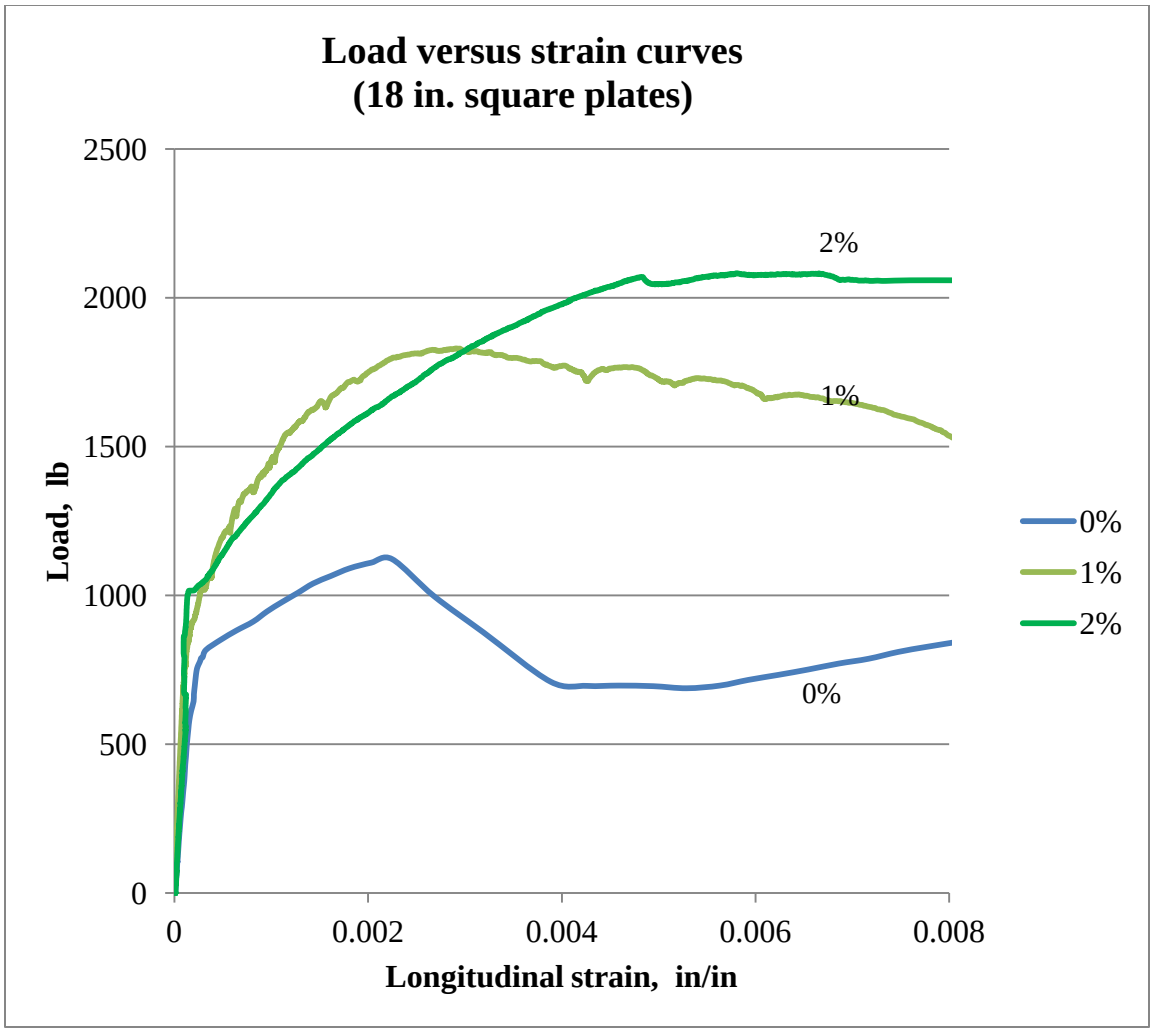

Figure 9.7: Load versus strain curves for 0%, 1% and 2% HSSFRC square plates (18 in. x 18 in.) under center point load

9.6.3 Test results for rosette strain gages located at the support

Load versus rosette strain results for 2% HSSFRC square plate (18 in. x 18 in.) are shown in Figure 9.8. The rosette strains were measured at the support on the plane coinciding with the depth and length of the square plate. "E_1", "E_2" and "E_3" correspond to strains at 0°, 45° and 90° angle, respectively. Rosette strain results for 0% and 1% were similar to 2% and are not shown.

www.manaraa.com

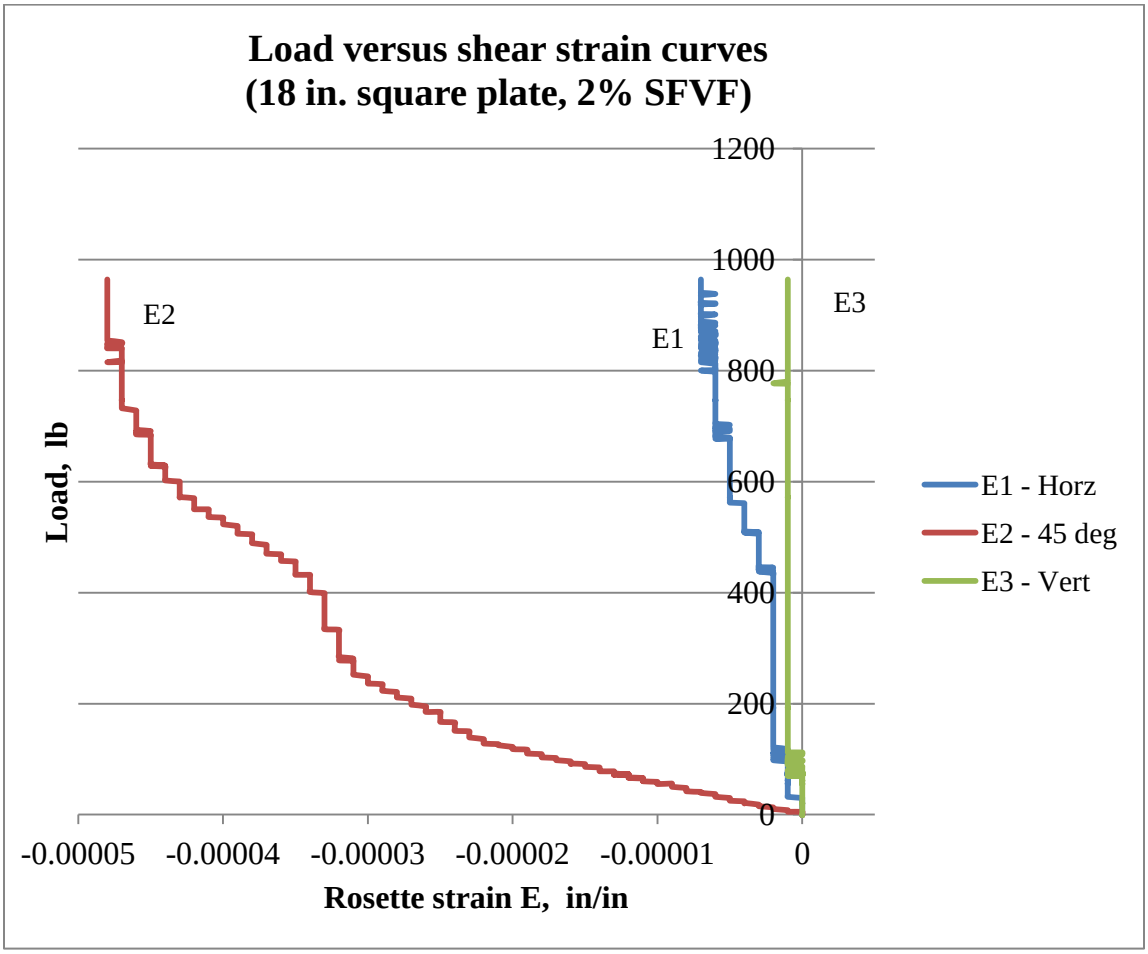

Figure 9.8: Load versus rosette strain results for 2% HSSFRC square plate (18 in. x 18 in.) under center point load

Load versus maximum shear strain curve for 2% HSSFRC square plate (18 in. x 18 in.) is presented in Figure 9.9. Maximum shear strains were calculated using Equation 8.12 in Section 8.1.4 with strain values from Figure 9.8. Referring to Figure 9.8, rosette strain "E_2" (45°) dominates both strains "E_1" and "E_3". The principal shear strain in Figure 9.9 therefore, took predominantly the shape of rosette strain "E_2".

www.manaraa.com

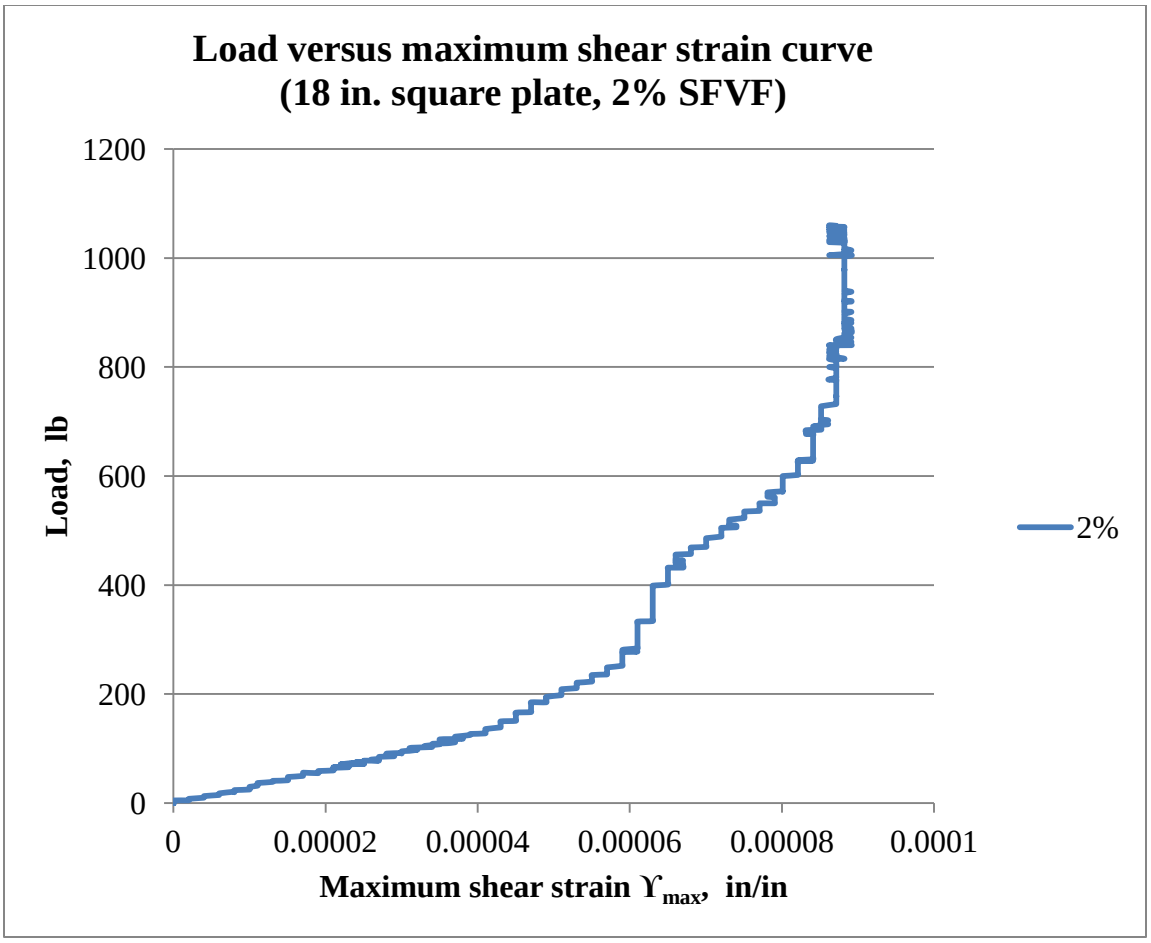

Figure 9.9: Load versus maximum shear strain results for 2% HSSFRC square plate (18 in. x 18 in.) under center point load

9.6.4 Cylinder compressive strength test results

As noted before, the concrete cylinder specimens that were used for compressive strength tests were taken from the same batch of concrete from which the corresponding plates were made. The cylinders were tested, for compressive strength, within 24 hours of testing the corresponding plates. During the testing process both applied compression load and the corresponding longitudinal strain of cylinders were obtained.

The average compressive stress versus longitudinal strain curves for 0%, 1% and 2% high strength steel fiber reinforced concrete cylinders are presented in Figure 9.10.

www.manaraa.com

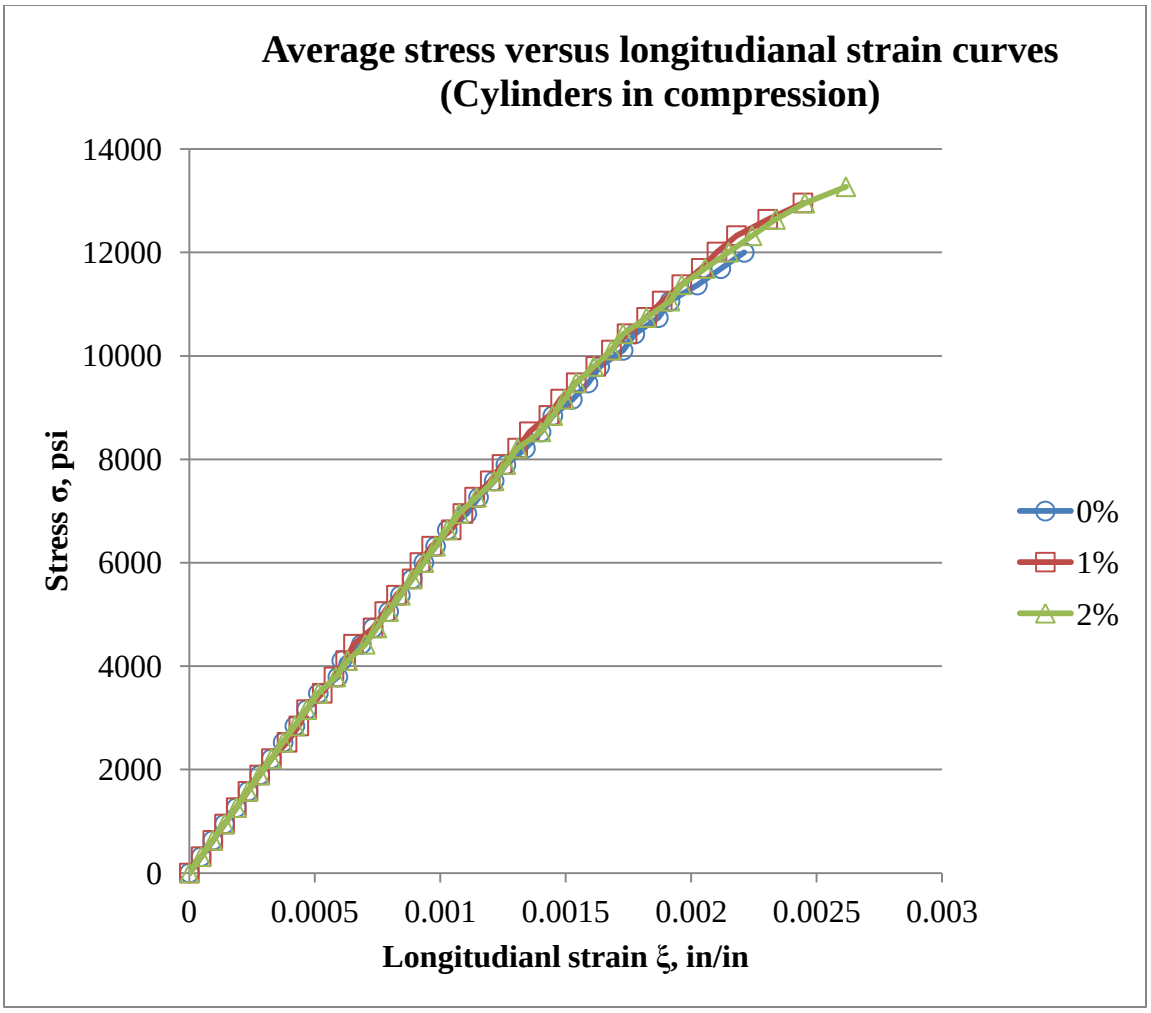

Figure 9.10: Average compressive stress versus longitudinal strain curves for 0%, 1% and 2% HSSFRC cylinders (4 in. x 8in.), casted with square plates (18 x 18 in.)

The average compressive strength and modulus of elasticity test results for 0%, 1% and 2% high strength steel fiber reinforced concrete cylinders under compression load are presented in Table 9.3. The compressive strength and modulus of elasticity results were calculated using procedures in Sections 4.4.1 and 4.4.2, respectively.

www.manaraa.com

Table 9.3: Compressive strength and modulus of elasticity results for 0%, 1% and 2% HSSFRC cylinders (4 in. x 8 in.) casted with square plates (18 in. x 18 in.)

Cylinder	Compressive strength MPa (psi)	Percentage increase from 0% steel fiber	Modulus of elasticity MPa (ksi)	Percentage increase from 0% steel fiber
0%	88		44,950	
	(12,826)	0%	(6,519)	0%
1%	91		45,168	
	(13,259)	3%	(6,551)	0.5%
2%	92		44,406	
	(13,374)	4%	(6,441)	-1.2%

9.6.5 Cylinder splitting tensile strength results

The average splitting tensile strength results for 0%, 1% and 2% high strength steel fiber reinforced concrete cylinders are presented in Table 9.4, while the splitting tensile strength figures are presented in Figure 9.11. Splitting tensile strength results were computed using Equation 4.3. The splitting tensile strength of HSSFRC cylinders increased as the SFVF increased.

www.manaraa.com

Table 9.4: Average splitting tensile strength results for 0%, 1% and 2% HSSFRC cylinders (4 in. x 8 in.) casted with square plates (18 in. x 18 in.)

Cylinder	Splitting tensile Strength MPa (psi)	Percentage increase from 0%	Splitting tensile to compression strength ratio
0%	8.88	steel fiber	
	(1,288)	0%	0.10
1%	10.73		
	(1,556)	21%	0.12
2%	14.91		
	(2,163)	68%	0.16

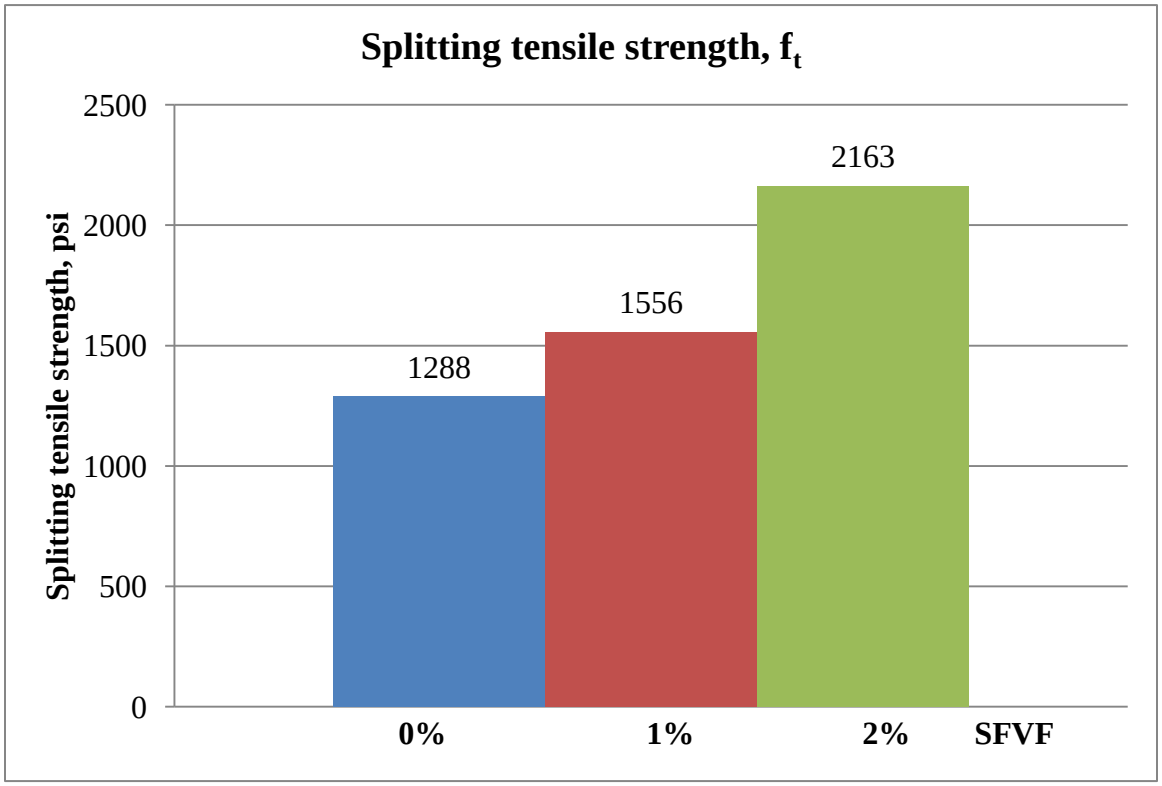

Figure 9.11: Average splitting tensile strength results for 0%, 1% and 2% HSSFRC cylinders casted with square plates (18 in. x 18 in.)

www.manaraa.com

9.7 Stress-strain analysis and test results

Longitudinal and transverse strains at first crack and calculated stress results for 0%, 1% and 2% square plates (18 in. x 18 in.) are presented in Table 9.5. Stress results for the square plates were calculated using Equation 8.3 in Section 8.1.2 and modulus of elasticity values from cylinders in compression. The flexural stresses at first noticeable crack, as shown in Table 9.5, are comparable to the spitting tensile stress results of HSSFRC cylinders.

Table 9.5: Stress–strain results for 0%, 1% and 2% HSSFRC square plates (18 in. x 18 in.) at first crack under center point load

Plate	Load N (lb)	f_t MPa (psi)	Strain (Measured) $\varepsilon_x = \varepsilon_y$ (10^{-6})	Stress, σ_x (Calculated) MPa (psi)
0%	2,669 (600)	8.89 (1,288)	143	8.47 (1,227)
1%	4,110 (924)	10.74 (1,556)	161	10 (1,388)
2%	4,857 (1,092)	14.92 (2,163)	233	13.28 (1,924)

Where: P = applied transverse point load at first noticeable crack, lb

f_t = splitting tensile strength of HSSFRC cylinders (from Table 9.4), psi

ε_x, ε_y = measured longitudinal and transverse strains of the square plates, in/in

www.manaraa.com

σ_x = calculated stress along the span of the square plates, psi

9.8 Failure modes

The load versus deflection curves in Figure 9.6 show that the square plates under concentrated load responded elastically till they reached the first crack load (peak load). Once the square plates reached the first crack load, they exhibited gradual deterioration of resistance for 1% and 2% SFVF and steep loss of resistance for 0% SFVF square plates.

Due to the proximity of the square plates to the testing platform and support locations, it was not possible to observe the development and propagation of cracks at the bottom surface of the square plates during the testing process. Therefore, the cracks were seen and noted when they reached the edges of the square plates.

The cracks at the edges of the square plates were observed to occur after the peak load had been reached and when the deflection of the plates were at approximately 6%, 10-20% and 10-40% of the total thickness of the specimens for 0%, 1% and 2% HSSFRC square plates, respectively.

After the formation of cracks at the edge of square plates, as the loading process progressed and the deflection of the plate increased, the corners of the plates start lifting about the cracks. The crack lines actually acted as hinges and the plate pieces in between the cracks rotated or curled about the hinge causing some of the plate sections and corners to lift. The hinges at the support being a point of zero deflection.

Crack formations at the bottom surface of the plates were mostly:

(a) For 0% SFRV - 66% T-shaped and 33% cross-shaped

(b) For 1% SFVF - 66% T-shaped and 33% mixed, cross and diagonal shaped

www.manaraa.com

(c) For 2% SFVF - almost all crack formations were diagonal in shape.

Crushing of concrete was not observed at any time during testing process, neither at the supports nor at the point concentrated load application.

Top surface cracks were observed on 1% and 2% HSSFRC square plates only, none on 0% SFVF specimens. Duration of the test process was about 90 minutes for 0% compared to 210 minutes for 1% and 2% SFVF HSSFRC square plates. Refer to Figures 9.12 through 9.15 for failure and crack patterns of 0%, 1% and 2% HSSFRC square plates.

Figure 9.12: Failure patterns for 0% HSSFRC square plates under center point load

www.manaraa.com

Figure 9.13: Crack patterns for 1% HSSFRC square plates under center point load

www.manaraa.com

Figure 9.14: Crack sizes and patterns for 2% HSSFRC square plates under center point load

www.manaraa.com

Figure 9.15: Lifting of corners and crack patterns for 2% HSSFRC square plates under center point load

9.9 Energy absorption (toughness)

The energy absorption (toughness), the area under the load versus deflection curves, for 0%, 1% and 2% HSSFRC square plates were calculated as 59, 523 and 903 in-lb, respectively. The load versus deflection curves are shown in Figure 9.6. The energy absorption of HSSFRC square plates increased as the steel fiber content increased: 786% and 1,431% for 1% and 2% SFVF plates, respectively over the 0% SFVF plates.

www.manaraa.com

9.10 Discussion of test results

9.10.1 Load versus deflection

The capacity of simply supported HSSFRC square plates to withstand a concentrated center load increased as the steel fiber by volume fraction (SFVF) increased from 0% to 1% and 2%. The capacity of the HSSFRC square plates to support a concentrated center load increased by 80% and 119% for 1% and 2% SFVF, respectively compared to 0% (plain) HSSFRC square plates. The sharp increase in capacity, by 80%, was between the ranges of 0% and 1% HSSFRC square plates. The increase in capacity between 1% and 2% HSSFRC square plates was 39%.

The deflections of HSSFRC square plates at peak load, which corresponds to the first crack load, were very comparable for all three SFVF. The deflections at the peak load were 1.42 mm (0.06 in.) for 0% and 1.83 mm (0.07 in.) for 1% and 2% SFVF square plates. But, the maximum deflection of HSSFRC square plates, which corresponds to the deflection at failure, for all three SFVF, differed by a large margin. The deflection of HSSFRC square plates increased as the SFVF increased from 0% to 1% and 2%. The higher deflection value was exhibited by the higher SFVF, which is 2%. The maximum deflection of the HSSFRC square plates at mid span increased by 535% and 1,247% for 1% and 2% SFVF, respectively compared to 0% (plain) HSSFRC square plates.

The ductility of HSSFRC square plates increased as the SFVF increased from 0% to 1% and 2%. The ratio of HSSFRC square plate deflection at complete failure to that of deflection at first crack increased from 2.27 for 0% to 11.21 and 23.76 for 1% and 2% SFVF, respectively. This was an increase of 394% and 947% for 1% and 2% SFVF, respectively in contrast to 0% HSSFRC square plates, respectively.

www.manaraa.com

9.10.2 Splitting tensile strength, compressive strength and modulus of elasticity for HSSFRC cylinders

The splitting tensile strength of HSSFRC cylinders increased by 21% and 68% for 1% and 2% SFVF, respectively compared to 0% (plain) HSSFRC cylinders.

The young's modulus values for 0%, 1% and 2% HSSFRC cylinders remained roughly the same for all three SFVF at ±1.2%. The compressive strength results for all three SFVF are within ±4.0%. Therefore, the increase in young's modulus and compressive strength due the addition of steel fibers is very small, almost flat. It should be stressed that the amount of High Range Water Reducer (HRWR) suitable for 0% mixture was used to prepare all 0%, 1% and 2% concrete mixtures. The effect of HRWR on young's modulus and compressive strength are shown in Phase (1b) of the research.

The stress versus strain diagrams for cylinders in compression showed curves for all three SFVF samples being nearly identical, which is consistent with modulus of elasticity results.

9.10.3 Flexural and shear strains

Load versus flexural strain relationship for 0%, 1% and 2% HSSFRC square plates appeared to be identical for most part of the linear portion of 0% SFVF curve, which is consistent with load versus deflection behavior. As expected, 2% HSSFRC square plates sustained the largest load and strain followed by 1% and 0% SFVF square plates.
The diagonal shear strain (E_2) was by far larger in magnitude than the horizontal (E_1) and vertical (E_3). The shear strain is dominated by the diagonal shear strain (E_2). The

www.manaraa.com

maximum shear strain and consequently shear stress seemed to correspond to the maximum capacity of the 2% HSSFRC square plates.

9.10.4 Analysis results

The experimental tensile stress results for 0%, 1% and 2% HSSFRC square plates at the first crack load correspond to the splitting tensile strength of 0%, 1% and 2% HSSFRC cylinders. In regard to post-crack behavior, for the same longitudinal strain, the resistance of the plate increased with the increase in steel fiber by volume fraction.

The theoretical elastic deflection results, for all three steel fiber by volume fractions, are consistently smaller than the experimental values. Theoretical deflection formulas tend to overestimate the stiffness of the plates.

9.10.5 Energy absorption (Toughness)

The area under the load versus deflection curves for HSSFRC square plates with higher steel fiber by volume fraction exhibited higher energy absorption capacity (toughness) than the lower SFVF plates.

www.manaraa.com

CHAPTER 10

HIGH STRENGTH STEEL FIBER REINFORCED CONCRETE SQUARE PLATES SUPPORTED AT OPPOSITE CORNERS AND THE OTHER TWO UNDER CONCENTRATED LOADS

10.1 Introduction

The behavior of simply supported high strength steel fiber reinforced concrete (HSSFRC) square plates with 0%, 1% and 2% steel fiber by volume fractions (SFVF) subjected to concentrated loads at opposite corners (two up and two down) is presented in this chapter. The plates are predominantly subjected to shear stresses due to the plate loading condition and support location, as shown in Figure 10.1. The significance of the test is to study the torsional/shear behavior of HSSFRC corner loaded plates.

All constituents for the three types of concrete mixtures (0%, 1% and 2% SFVF), used for the making of plates and cylinders, are the same except for the content of steel fibers. The thin square plates have an overall dimensions of 508 mm (20 in.) long by 508 mm (20 in.) wide and 32 mm (1.25 in.) thick, with length to width ratio of 1:1. The plates are discretely supported at opposite corners and subjected to concentrated loads at opposite and unsupported corners, as shown in Figure 10.1. The supports are 25 mm (1 in.) away from the edges of the corner.

www.manaraa.com

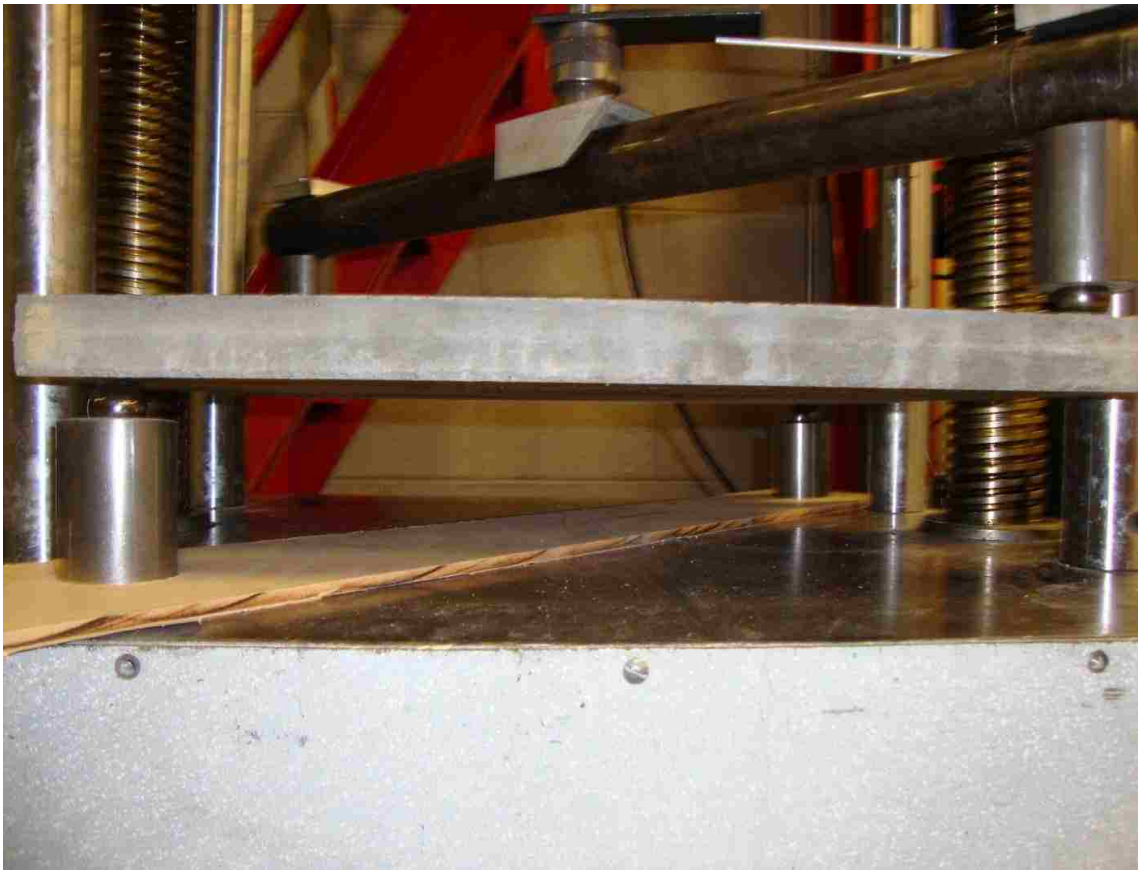

Figure 10.1: HSSFRC square plate subjected to transverse opposite corner loads

Two strain gages, perpendicular to one another, for each type of steel fiber by volume fraction mixture, are placed on the top surface of the plate to measure the strain activities at the extreme fiber of the plate in relation to the applied load. The strain gages are aligned along the diagonal line at the center of adjacent quadrants. A single rosette strain gage, for each steel fiber by volume fraction mixture, is placed on the side of the plate close to the support to measure the shear strain activity at the plate support.

This chapter presents HSSFRC specimen preparation, testing procedures and experiment results such as load versus deflection, load versus flexural and shear strains and mode of failure of square plates. The chapter discusses the influence of steel fibers

www.manaraa.com

on: flexural and shear capacity, mode of failure and ductility of thin square plates; and modulus of elasticity, compression and splitting tensile strength of cylinders prepared from the same mixtures used for the making of plates.

Comparisons are made between opposite corners loaded square plates with various steel fiber by volume with respect to the mechanical properties such as flexural capacity, deflection, ductility, and mode of failure. The elastic analysis results corresponding to the first crack load such as stress, strain and deflection are presented. Test results are discussed and conclusions drown.

10.2 Theoretical background of square plates under opposite transverse corner loads

The governing differential equation for deflection of thin plates is defined as (Ugural 2009)

$$\frac{\partial^4 w}{\partial x^4} + 2\frac{\partial^4 w}{\partial x^2 \partial y^2} + \frac{\partial^4 w}{\partial y^4} = \frac{p_o}{D} \qquad (10.1)$$

$p_o = 0$, since there is no distributed load. Boundary conditions such as moment on the free edges and shear forces at the center are equal to zero. The twisting moment and shear stress can be expressed as:

$$p = -2M_{xy} \qquad (10.2)$$

$$\tau_{xy} = \frac{-3p}{t^2} \qquad (10.3)$$

Where: D = flexural rigidity, $Et^3/12(1-\nu^2)$

t = plate thickness

ν = Poisson's ratio

www.manaraa.com

p = corner load

E = modulus of elasticity

M_{xy} = twisting moment

τ_{xy} = shear stress.

10.3 Preparation of test specimens - cylinders and plates

Two types of test specimens, square plates and cylinders, were prepared for each test (0%, 1% and 2% SFVF) from the same concrete batch:

- Three thin square plates for each SFVF with dimensions of 508 mm (20 in.) wide by 508 mm (20 in.) long and 32 mm (1.25 in.) thick. Therefore, a total of nine plate specimens were prepared.
- Six 102 mm (4 in.) diameter by 203 mm (8 in.) long cylinders for each SFVF. Three cylinders each were used for compressive and splitting tensile strength tests, respectively. Therefore, a total of eighteen cylinders were prepared.

To form the square plates, a crate with dimensions of approximately 508 mm (20 in.) long and 508 mm (20 in.) wide was made by nailing 32 mm (1.25 in.) thick plywood strip around the perimeter of base board.

The ingredients for all concrete mixtures were kept the same except for the amount of steel fibers used by volume fraction in each concrete mixture type. The ingredients for 0%, 1% and 2% steel fiber concrete mixtures are given in Table 10.1.

Refer to Section 8.1.3 for concrete and specimen preparations. Plates and cylinders were cured for 28-days.

www.manaraa.com

Table 10.1: Concrete batch constituents for 0%, 1% and 2% HSSFRC square plates (20 in. x 20 in.) and cylinders

Mix Components		**0%**	**1%**	**2%**
Batch Volume		**1.5 ft^3**	**1.5 ft^3**	**1.5 ft^3**
3/8" Coarse Aggregate	(lb)	34.2	34.2	34.2
#4 Coarse Aggregate	(lb)	33.6	33.6	33.6
Fine Aggregate, FA3*	(lb)	86.4	86.4	86.4
Water	(lb)	17.4	17.4	17.4
Cement Type V	(lb)	37.5	37.5	37.5
Silica Fume	(lb)	2.85	2.85	2.85
Fly Ash	(lb)	16.05	16.05	16.05
Total Cementitious	(lb)	56.4	56.4	56.4
Water to Cement Ratio		0.46	0.46	0.46
Water / Cementitious Ratio		0.31	0.31	0.31
Gravel : Sand Ratio		0.44 : 0.56	0.44 : 0.56	0.44 : 0.56
HRWR ADVA540	(lb)	0.588	0.588	0.588
Steel Fiber by Volume	%	0%	1%	2%
Steel Fiber by weight	(lb)	0	7.5	15
Concrete Total Weight	(lb)	228.59	236.09	243.59
Concrete Unit weight	(pcf)	152.4	157.4	162.4

*Fine aggregate with fineness modulus of 2.05

www.manaraa.com

10.4 Types of strain gages used

The size and type of strain gages depend on the maximum aggregate size. Two types of strain gages, which were recommended by the manufacturer, were used:

1. N2A-06-10CBE-350/E – is an individual strain gage, which measures strain in a single direction. It can be installed, as shown in Figure 10.2, individually or in group to measure strain in one or multiple directions, respectively.
2. CEA-06-250UR-120 – is a rosette, group, type strain gage with three grids oriented 45° apart, angularly, from each other, refer to Figures 8.1.3 and 10.3 for rosette orientation.

Refer to Section 8.1.4 for full description of both types of strain gages.

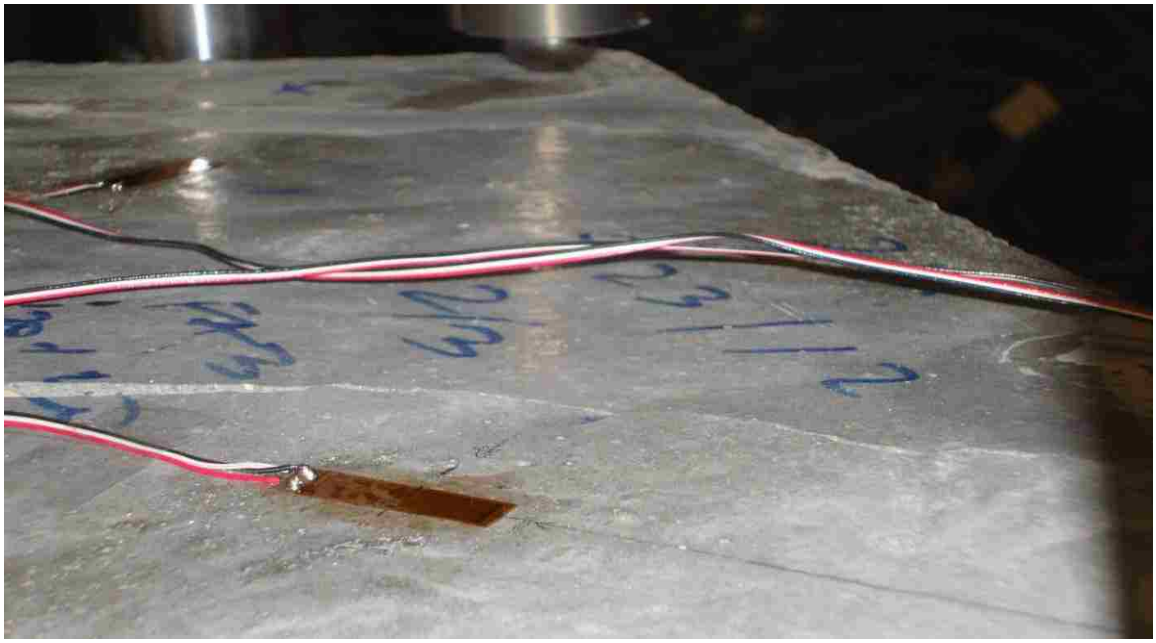

Figure 10.2: Two N2A-06-10CBE-350/E type strain gages located at ± 45 degree from the horizontal axis

www.manaraa.com

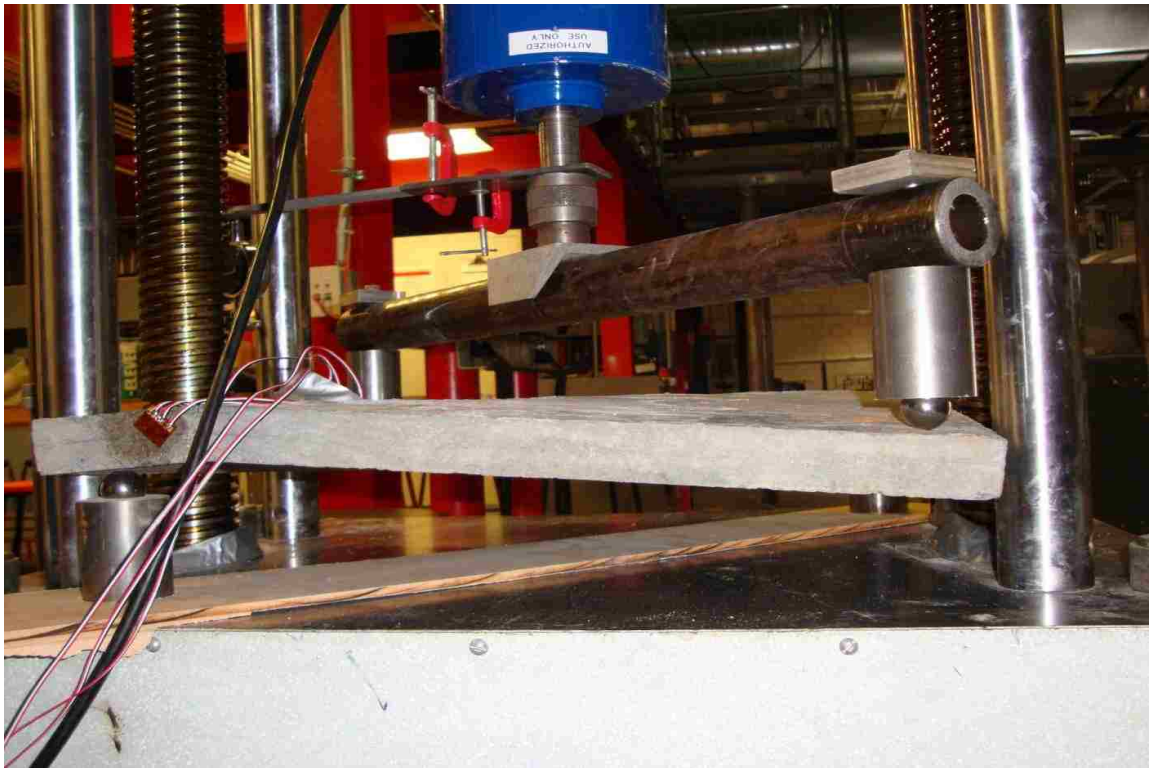

Figure 10.3: 45°- rectangular rosette located on the side of the square plate close to the support point

10.5 Location and orientation of strain gages on the test specimens

The strain gage arrangements for every test plate were determined by the capability of the data acquisition system to accommodate rosette and strain gage output, deflection measurements and load input combined.

At the end of the 28-day, both plate and cylinder specimens were pulled out of the curing room, and the plate specimens were prepared as follows:

1. Plate #1 was not provided with strain gages. It was used strictly to measure load versus vertical deflection behavior of plates under opposite corner loads. Vertical deflection was measured at the point of load application. The load and vertical deflection readings were electronically linked.

www.manaraa.com

2. Plate #2 was furnished with two independently placed strain gages. The strain gages were placed at midpoint of the diagonal line between the plate center and the support and the plate center and point of load, on adjacent quadrants. The strain gages were 90 degrees apart. The strain gages were used to measure the strain activities on the top of the square plates. See Figure 10.4 for strain gage locations.
3. Plate #3 was equipped with one 45°- rectangular rosette with three grids spaced at 45° interval. The rosette was place on the side of the plate #3 adjacent to the support location. The edge of the rosette was placed about 32 mm (1 ¼") away from the support point to avoid destruction during the loading process. The intention was to measure the shear strain of the plate at the support location. A vertical dial gage was used to measure the vertical deflection of the plate at the point of load. For location of the rosette strain gage on the plate refer to Figures 10.3 and 10.5.

www.manaraa.com

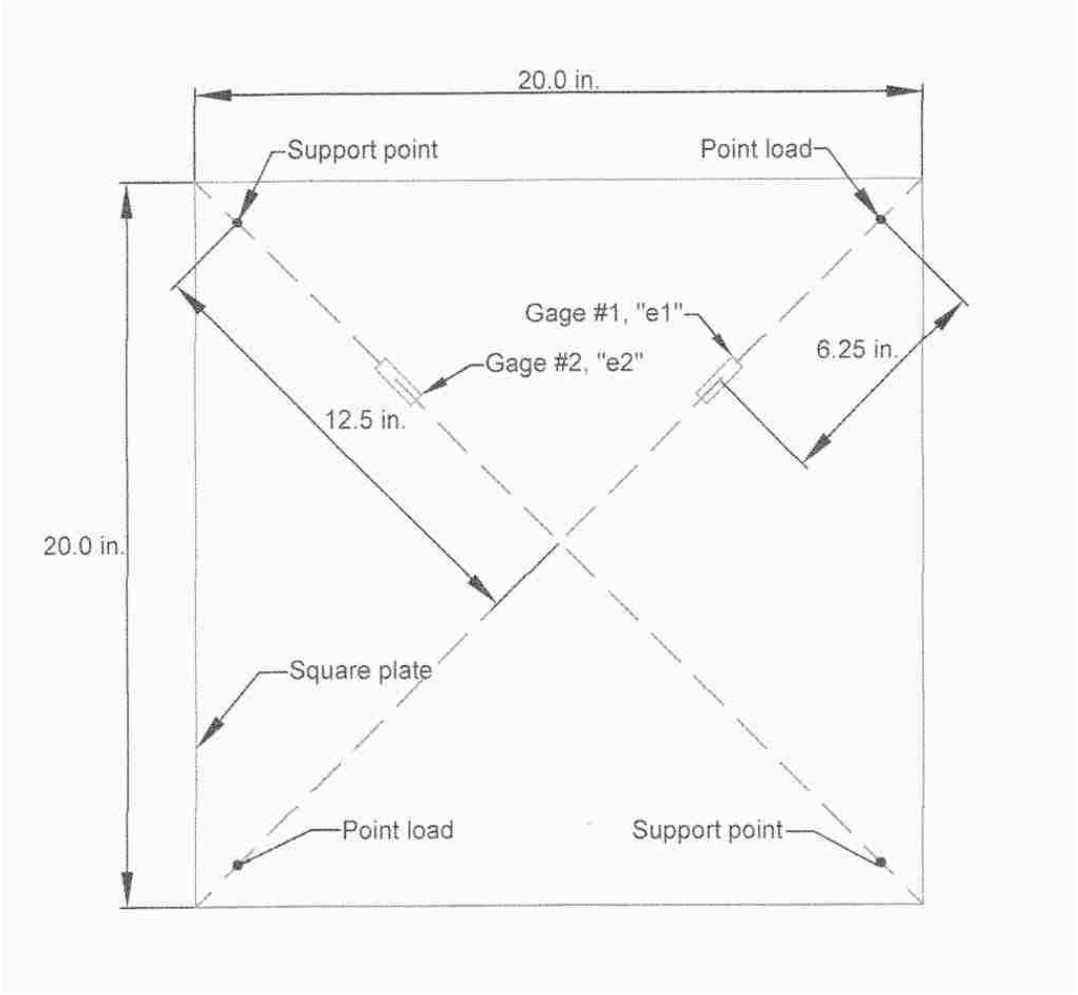

Figure 10.4: Strain gages located on the top surface of the HSSFRC square plate

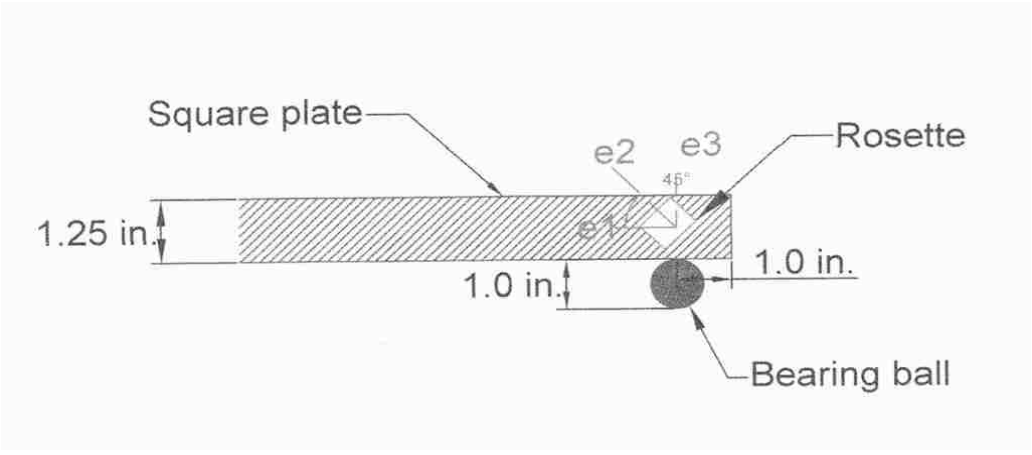

Figure 10.5: Rosette strain gage located on the side of the HSSFRC square plate

www.manaraa.com

10.6 Test apparatus and procedures for square plates

Once the specimens were fitted with strain gages, they were ready for testing. The strain gages and rosettes were installed per manufacturer's recommendation as stated in Section 4.4.6. The apparatus involved were:

1) Tinius-Olsen testing machine (50,000 lb maximum capacity).
2) Solid cylindrical steel stub/bar and bearing ball combination that were used as part of load application and support system. The solid cylindrical steel stubs had a portion of sphere indentation/impression on the flat side of it, where the bearing ball would seat. The impression was created by milling out a portion of the sphere, from the steel stub using a computerized drill machine. Refer to Figure 10.5 for sizes and dimensions of the support system.
3) Four 25.4 mm (1 in.) diameter spherical bearing ball, part of the load and support assembly.
4) Load applicator bar consisting of 2.5 in. (63.5 mm) diameter long hallow steel bar and two 2.5 in. (63.5 mm) long solid cylindrical steel stub/bar from step 2. The steel stubs were bolted at each end of the load applicator bar, 635 mm (25 in.) apart.
5) Strip of plywood with two circular slots, equal to the diameter of the support solid cylindrical steel bar, cut out. The slots were spaced 635 mm (25 in.) apart. The plywood was used to secure the steel support pieces in place and maintain spacing during the specimen set up and loading process.

www.manaraa.com

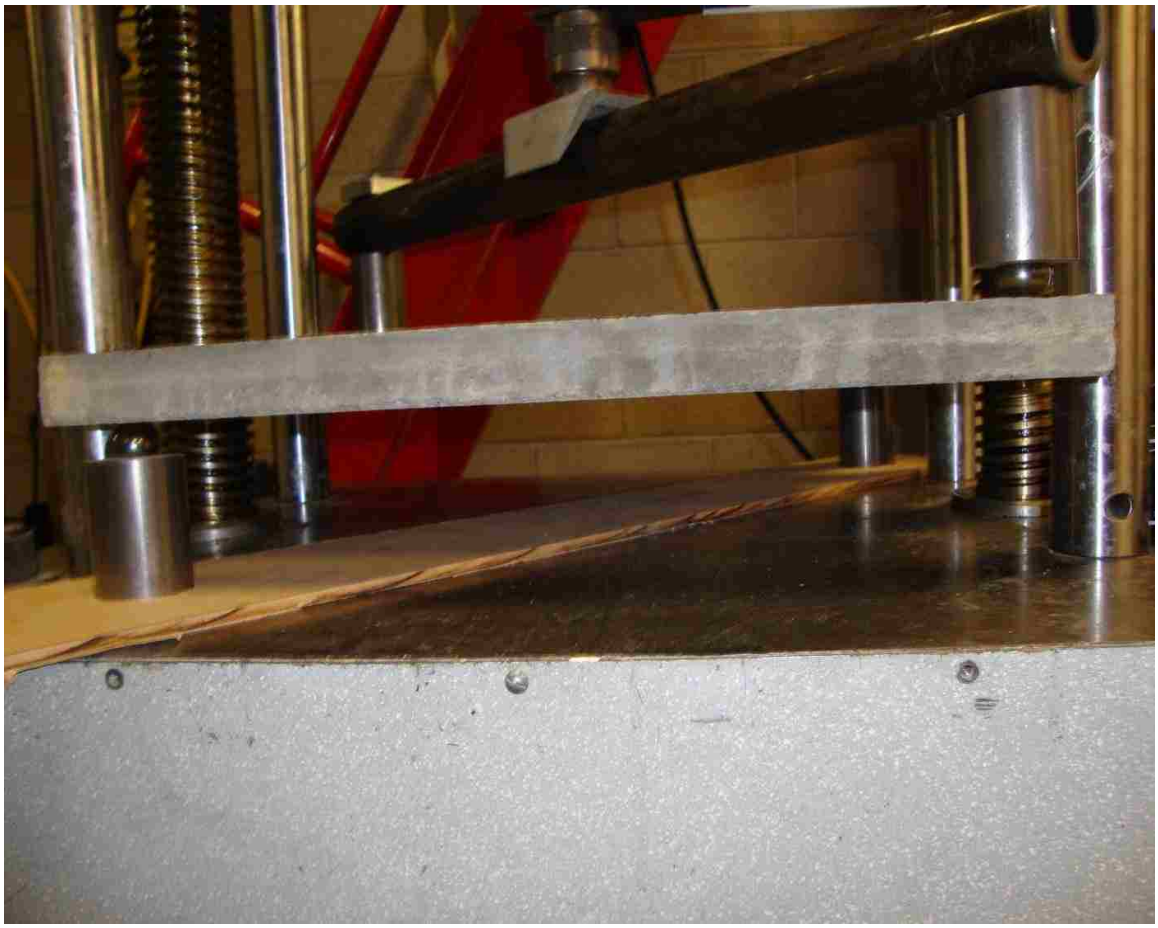

Figure 10.6: Test apparatus and specimen set up for opposite corner loads

The test set up for plates, as shown in Figure 10.6, was assembled as follows:

1) First, the plywood strip was placed flat on a very strong testing base.
2) Two solid cylindrical steel stubs/bars were inserted into the preformed slots.
3) One bearing ball was placed on the top of each cylindrical steel bar, where the partial shape of the bearing was milled out.
4) The square plate was placed on the bearing ball supports; the supports were positioned on opposite corners.

www.manaraa.com

5) Two bearing balls were placed on the top side of the square plate but on the opposite corners to the support points.
6) The load assembly, strong hallow steel bar fitted with cylindrical steel bar similar to the support unit, was placed on the top of the bearing balls.
7) The load cell was lowered enough just to engage the square plate. Before the actual loading process started: the plate, support, the entire test set up and all contact surfaces were checked for any kind of rocking or gap (lack of contact) between the test specimen supports and test specimen.
8) All gaps were shimmed to ensure full contact and uniform load transfer between units. Finally, the load was applied at a steady rate of 0.025 – 0.051 mm/minute (0.001 – 0.002 in./min) till the first major failure or crack occurred and increased to 0.076 – 0.203 mm/minute (0.003 – 0.008 in./minute) till complete failure of the specimen.

The HSSFRC cylinders, which were cast from the same concrete mixture used for plates, were tested for compressive and splitting tensile strength according to the test procedures that are presented in Sections 4.4.1 and 4.4.4, respectively. During the testing process for cylinders and plates: load, deflection and strain data were collected; failure and failure modes were noted.

www.manaraa.com

10.7 Experiment results for square plates supported at opposite corners and the other two under concentrated loads

10.7.1 Load versus deflection results

Load versus vertical deflection data were collected during the testing process for HSSFRC square plates, with 0% to 2% steel fiber by volume fractions (SFVF), under concentrated opposite corner loads. The deflection was measured at the point of load application/corners. The load versus deflection curves for 0%, 1% and 2% HSSFRC square plates under opposite corner loads are presented in Figure 10.7. Each load versus deflection curve represents an average result of three HSSFRC square plate specimens for each SFVF, a total of nine specimens for 0%, 1% and 2% SFVF. Table 10.2, presents the peak concentrated load, deflection of the square plate at the peak load and maximum deflection of the square plate at complete failure for 0%, 1% and 2% SFVF. Values in Table 10.2 were obtained from the load versus deflection curves in Figure 10.7.

www.manaraa.com

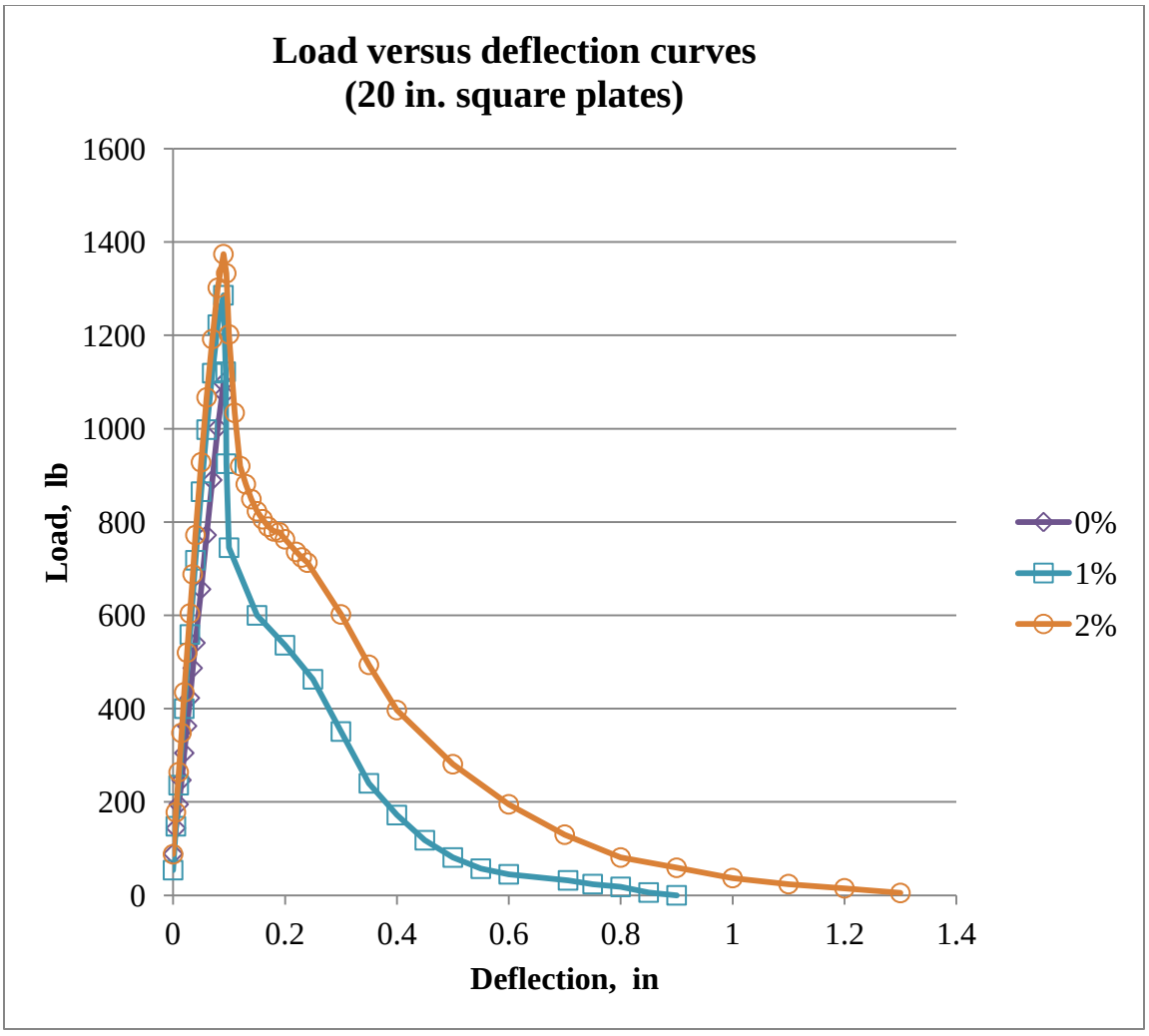

Figure 10.7: Load versus deflection curves for 0%, 1% and 2% HSSFRC square plates (20 in. x 20 in.) under opposite concentrated corner loads

www.manaraa.com

Table 10.2: Maximum load and deflection results of HSSFRC square plates (20 in. x 20 in.) under opposite concentrated corner loads

Plate	P_{Max} N (lb)	Percentage increase in load	Δ at P_{Max} mm (in.)	$\Delta_{failure}$ mm (in.)	Percentage increase in deflection	$\Delta_{failure}/\Delta$
0%	4,911 (1,104)	0%	2.34 (0.092)	2.34 (0.092)	0%	1.00
1%	5,720 (1,286)	16%	2.21 (0.087)	23.50 (0.925)	905%	10.63
2%	6,161 (1,385)	25%	2.34 (0.092)	33.02 (1.300)	1,313%	14.13

Where: P_{Max} = peak concentrated load, N (lb.)

Δ = plate deflection corresponding to the peak load, mm (in.)

$\Delta_{failure}$ = maximum deflection of the plate at complete failure, mm (in.).

10.7.2 Test results of strain gages

Two strain gages were placed at the center of adjacent quadrants on the top surface of the HSSFRC square plates. The gages were installed 90° from each other, that is, at 45°and 135° from the horizontal axis, respectively. Load versus strain curves of both strain gages for HSSFRC square plates with 0%, 1% and 2% SFVF under opposite corner loads are presented in Figure 10.8. The graphs show that, while one of the strain gages

www.manaraa.com

was continuously in tension (elongation); the other strain gage was continuously in compression (contraction). Strains from both gages exhibited near symmetrical response for all SFVF as was expected due to the symmetry of the load and support conditions.

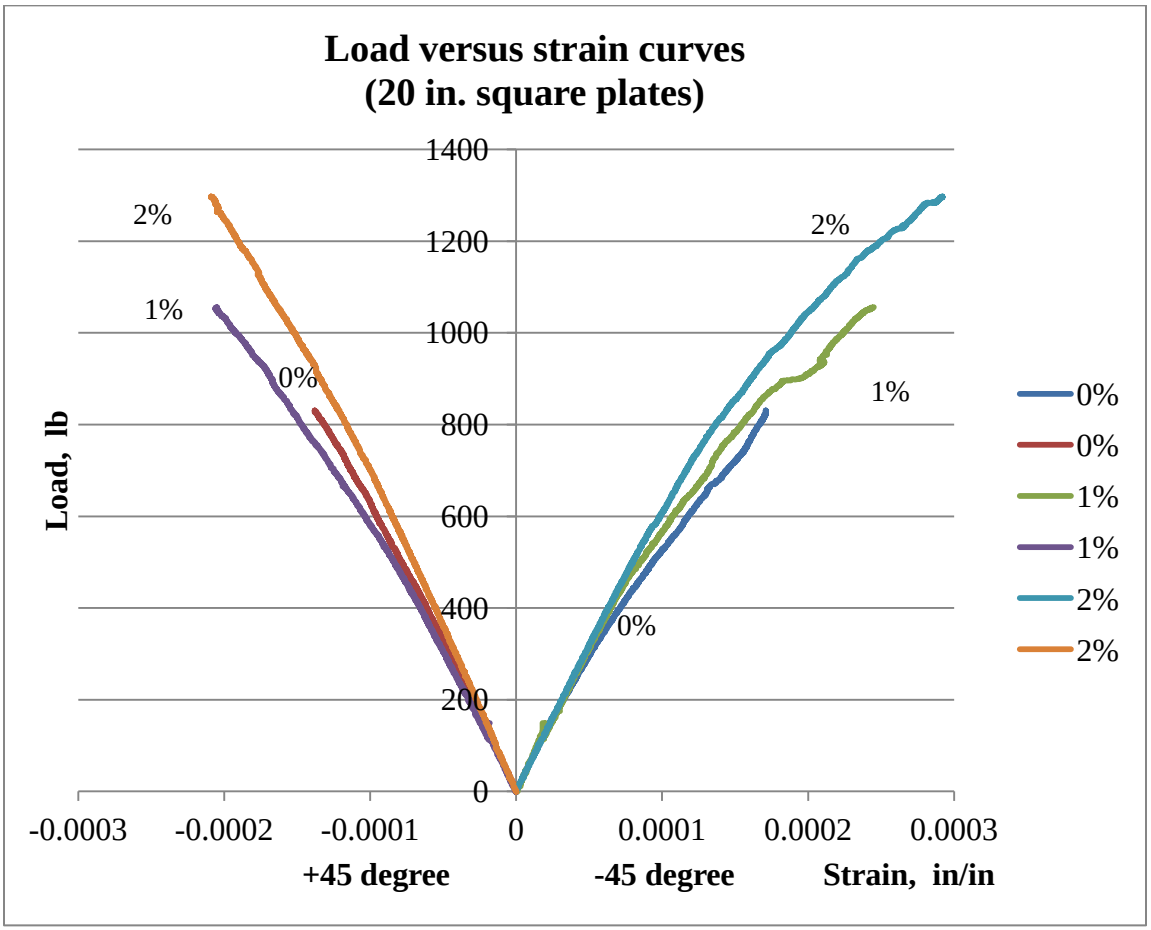

Figure 10.8: Strain gage results for 0%, 1% and 2% HSSFRC square plates (20 in. x 20 in.) under opposite concentrated corner loads

www.manaraa.com

10.7.3 Test results for rosette strain gages at support

Load versus maximum shear strain curves for 0% and 2% HSSFRC square plates (20 in. x 20 in.) loaded in the transverse direction at opposite corners are presented in Figure 10.9. The maximum shear strains were calculated per Equation 8.12 in Section 8.1.4, using strains measured by rosette strain gages located close to the supports.

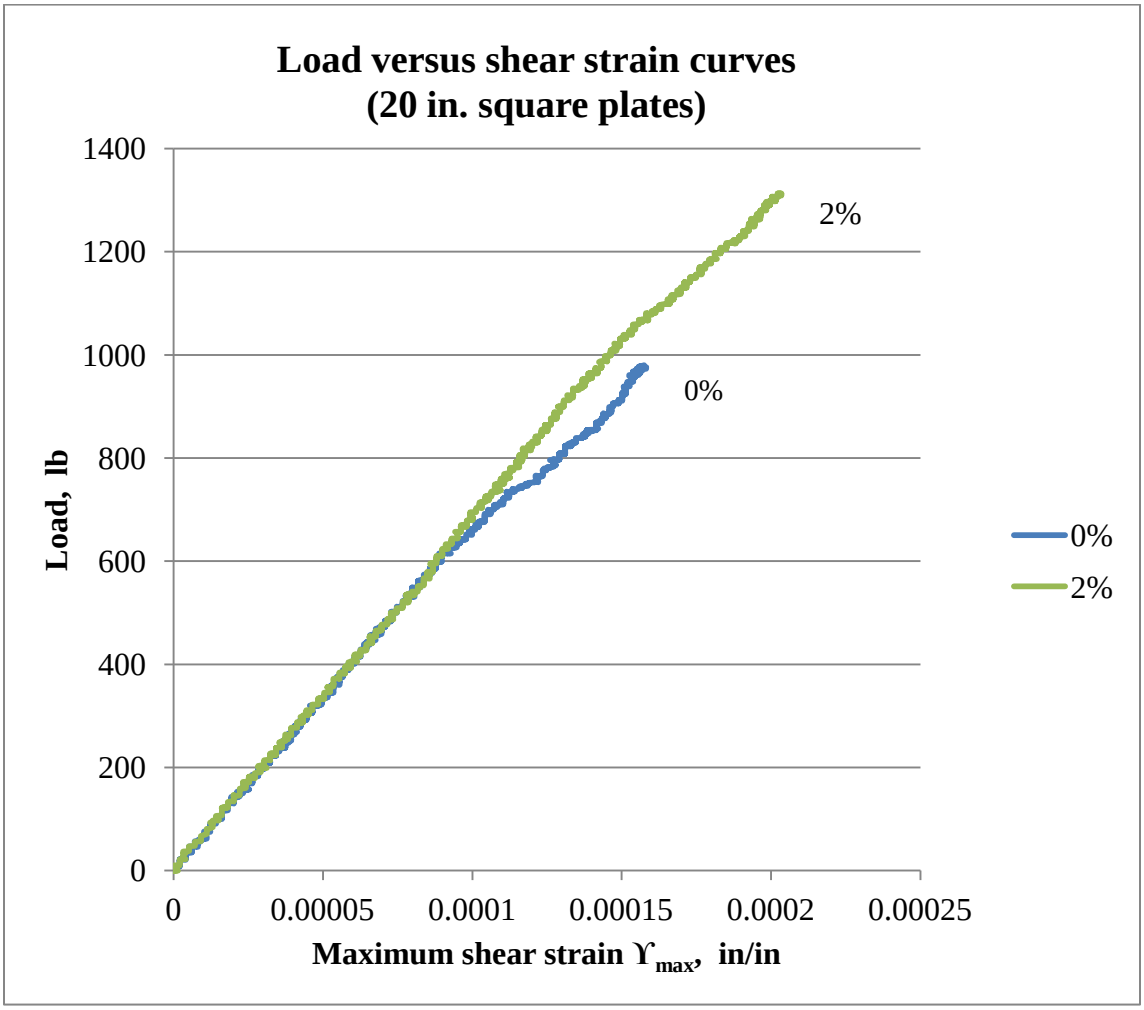

Figure 10.9: Load versus maximum shear strain curves for 0% and 2% HSSFRC square plates (20 in. x 20 in.) under concentrated opposite corner loads

www.manaraa.com

10.7.4 Cylinder compressive strength test results

As described in previous section, the HSSFRC cylinder specimens used for compressive strength tests were prepared from the same batch of concrete the corresponding plates were made from. The cylinders were tested, for compressive strength, within 24 hours of testing the corresponding plates. During the testing process both applied compression load and the corresponding longitudinal strain of cylinders were obtained.

The average compressive stress versus longitudinal strain curves for 0%, 1% and 2% high strength steel fiber reinforced concrete cylinders are presented in Figure 10.10.

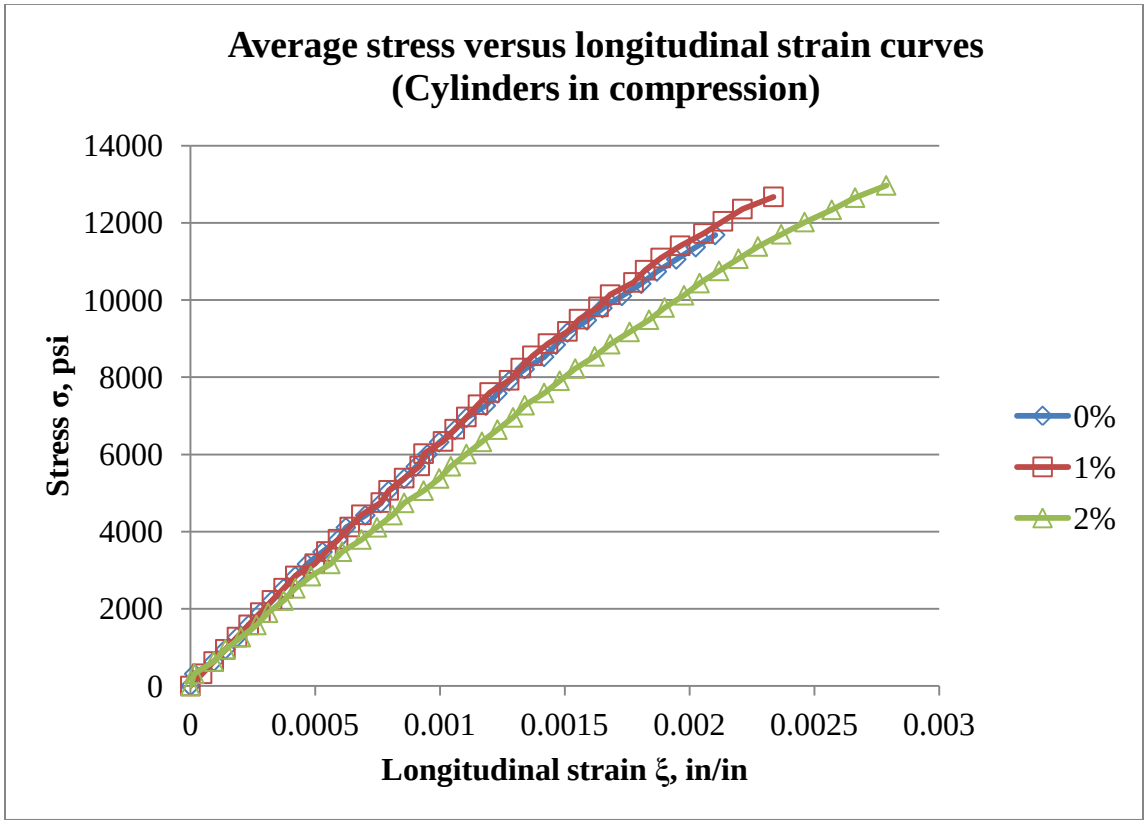

Figure 10.10: Average compressive stress versus strain curves for 0%, 1% and 2% HSSFRC cylinders casted with square plates (20 in. x 20 in.)

www.manaraa.com

The average compressive strength and modulus of elasticity test results for 0%, 1% and 2% high strength steel fiber reinforced concrete cylinders under compression load are presented in Table 10.3. The compressive strength and modulus of elasticity results were calculated using procedures in Sections 4.4.1 and 4.4.2, respectively. It is noted that while the compressive strength increases with the increase in steel fiber content, up to 5%, the modulus of elasticity decreases up to -16.5%.

Table 10.3: Average compressive strength and modulus of elasticity for 0%, 1% and 2% HSSFRC cylinders casted with square plates (20 in. x 20 in.)

Cylinder	Compressive strength MPa (psi)	Percentage increase from 0% steel fiber	Modulus of elasticity MPa (ksi)	Percentage increase from 0% steel fiber
0%	88		45,038	
	(12,809)	0%	(6,532)	0%
1%	91		43,434	
	(13,143)	3%	(6,300)	-3.6%
2%	93		37,620	
	(13,483)	5%	(5,456)	-16.5%

www.manaraa.com

10.7.5 Cylinder splitting tensile strength results

The average splitting tensile strength test results for 0%, 1% and 2% high strength steel fiber reinforced concrete cylinders are presented in Table 10.4, while the splitting tensile strength figures are presented in Figure 10.11. Splitting tensile strength results were computed using Equation 4.3. The splitting tensile strength of HSSFRC cylinders increased as the SFVF increased.

Table 10.4: Average splitting tensile strength for 0%, 1% and 2% HSSFRC cylinders (4 in. x 8 in.) casted with square plates (20 in. x 20 in.)

Cylinder	Splitting tensile strength MPa (psi)	Percentage increase from 0% steel fiber	Splitting tensile to compression strength ratio
0%	9.07		
	(1,316)	0%	0.10
1%	10.77		
	(1,561)	19%	0.12
2%	12.76		
	(1,851)	41%	0.14

www.manaraa.com

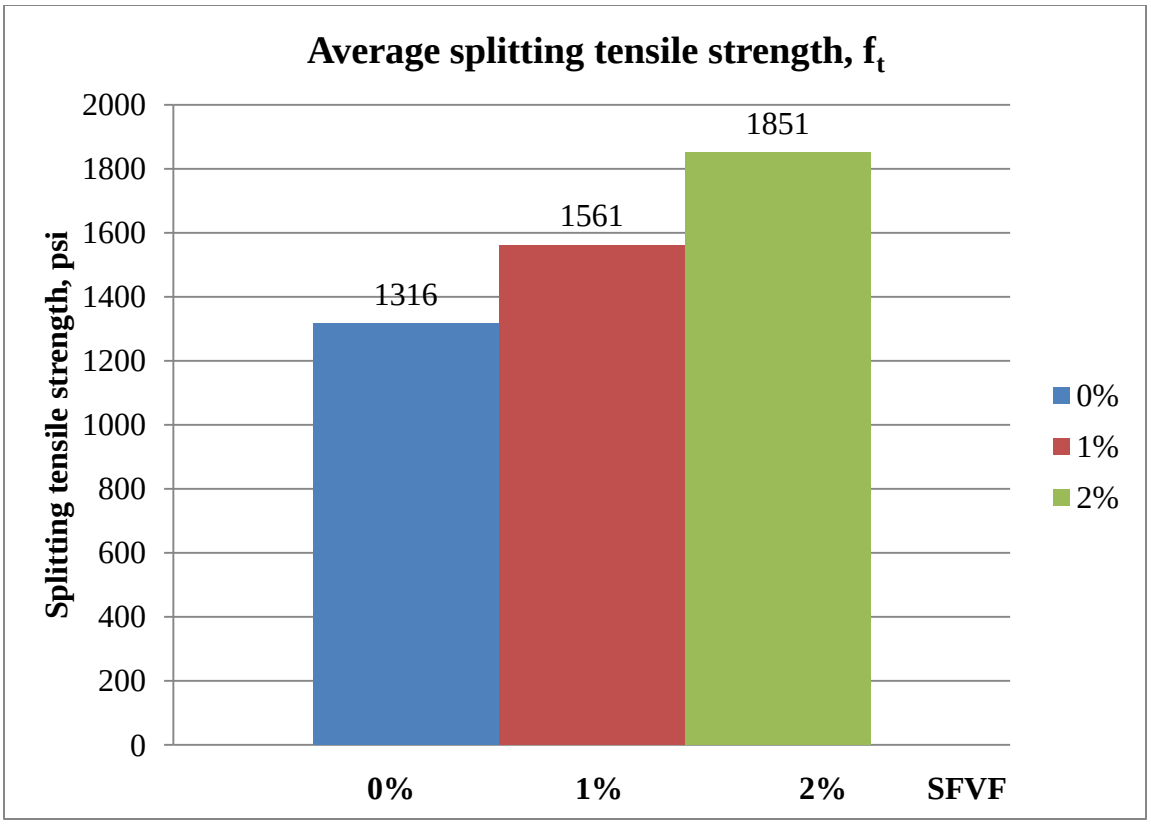

Figure 10.11: Average splitting tensile strength results for 0%, 1% and 2% HSSFRC cylinders (4 in. x 8 in.) casted with square plates (20 in. x 20 in.)

10.8 Stress-strain analysis and test results

Longitudinal and transverse strains at first crack and calculated stress results for 0%, 1% and 2% HSSFRC square plates (20 in. x 20 in.) are presented in Table 10.5. Stress results for the square plates were calculated using Equations 8.3 and 10.3 and modulus of elasticity values from cylinders in compression. The flexural stresses at first noticeable crack, as shown in Table 10.5, are comparable to the spitting tensile stress results of HSSFRC cylinders.

www.manaraa.com

Table 10.5: Stress–strain results for 0%, 1% and 2% HSSFRC square plates (20 in. x 20 in.) at first crack under opposite concentrated corner loads

Plate	Load N (lb)	f_t MPa (psi)	Strains (Measured) ε_x (10^{-6}) ε_y (10^{-6})	Stress, σ_x (Calc.) MPa (psi)	$\tau_{xy} = 3P/2t^2$ (Calculated) MPa (psi)
0%	3,981 (895)	9.07 (1,316)	171 -137	7.29 (1,057)	5.48 (788)
1%	4,964 (1,116)	10.77 (1,561)	254 -214	9.35 (1,355)	7.00 (1,016)
2%	6,161 (1,385)	12.76 (1,851)	316 -226	10.45 (1,515)	8.70 (1,262)

Where: P = applied transverse point load at first noticeable crack, lb

f_t = splitting tensile strength of HSSFRC cylinders (Table 10.4), psi

ε_x, ε_y =measured longitudinal and transverse strains of the square plates, in/in

σ_x = calculated stress along the span of the square plates, psi

τ_{xy} = calculated shear stress, psi (Equation 10.2).

10.9 Failure modes

The load versus deflection curves in Figure 10.7 show that square plates under opposite corner loads responded elastically till the first crack load (peak load) was reached. Once the first crack load of square plates was reached, the resistance to the load decreased gradually for 1% and 2% SFVF but there was a sudden loss of resistance for

www.manaraa.com

0% SFVF square plates. In Figure 10.7, load versus deflection curves, all three HSSFRC square plates, showed almost identical response for most part of the elastic range, up to the development of major tensile cracks, despite the variation in SFVF. During the test, there was no sign of crushing of concrete neither at the point of load application nor at support locations due to the concentrated nature of the load and support system.

The cracks on the surface of the square plates appeared at the point when the peak load was reached and when the corner deflection were at approximately 5% to 8% of the total thickness of the specimens for both 1% and 2% HSSFRC square plates. Most of the cracks were straight line, diagonal and on the top surface perpendicular to the tensile stress field. On one occasion only did bottom crack occur for 2% SFVF. When top cracks occurred, the cracks run across the support points; whereas when the bottom crack occurred, the crack run across the points of load application, at the other two opposite corners.

The 0% HSSFRC square plates exhibited the following behaviors:

- Sudden failure.
- Vertical crack planes were straight, smooth and 90 degrees with the bottom and top surfaces. Refer to Figures 10.12 and 10.13 for failure and crack patterns.
- For most part (2 out of 3 specimens) a single failure plane developed.
- The test duration for 0% HSSFRC square plates was between 45 to 55 minutes, a lot shorter than for 1% and 2% specimens, which were 225 and 255 minutes, respectively since these plates continued to deflect after the initiation of major cracks.

www.manaraa.com

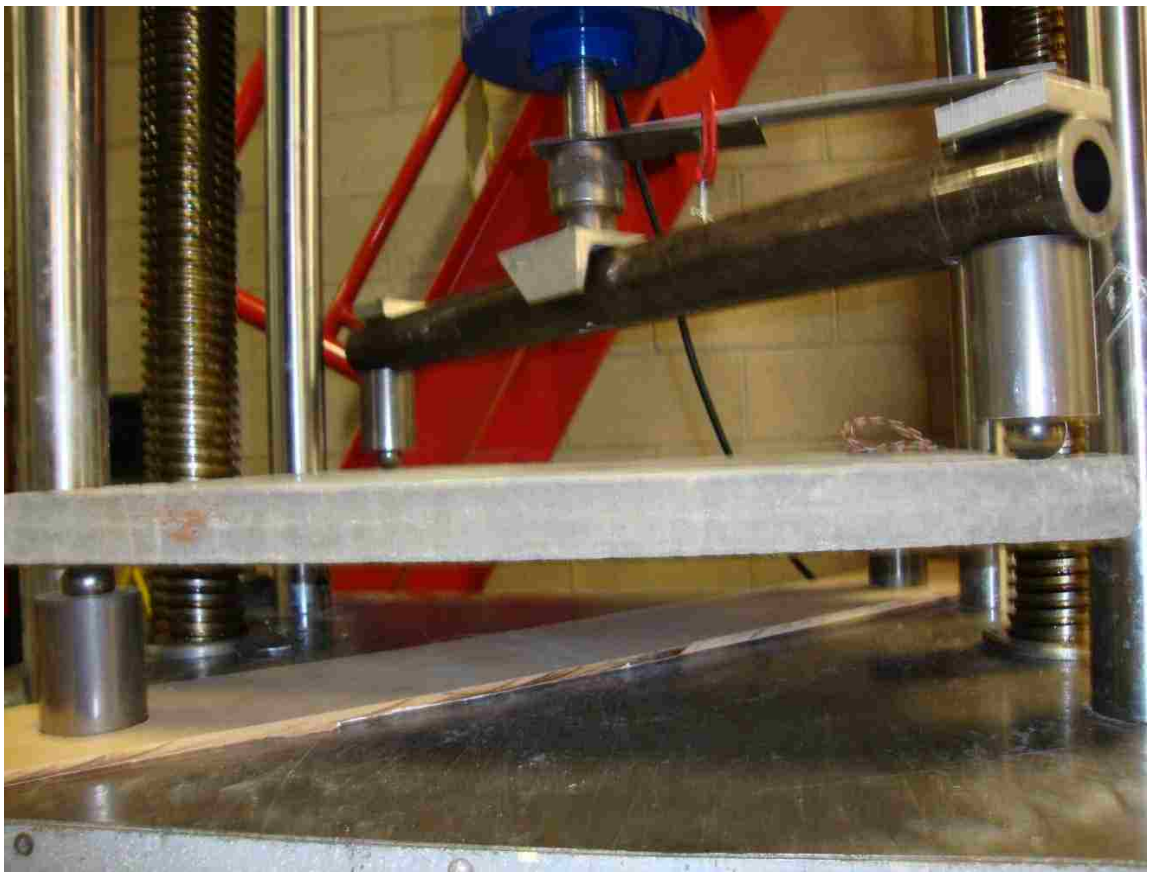

Figure 10.12: Shape and condition of 0% HSSFRC square plates subjected to concentrated opposite corner loads just before failure

www.manaraa.com

Figure 10.13: Crack and failure patterns for 0% HSSFRC square plates under concentrated opposite corner loads

The 1% and 2% HSSFRC square plates demonstrated the following behaviors:

- Both types of plates showed more ductile failure behavior by undergoing large deflections and gradual loss of capacity without instant failure.
- The plates did not break into pieces at the end of the test; they stayed in one piece with large and visible cracks.
- The cracks did penetrate the whole depth of the plates, which indicates the failure was slow and resistance to the applied load continued till the whole thickness of

www.manaraa.com

the plates was exhausted. This indicated the energy needed to fail the plates increased from 0% to 1% and 2% SFVF drastically.

- There were multiple and segmented failure planes (cracks) on HSSFRC square plates in comparison to plain (0%) SFVF square plates. Also, the failure planes were not straight and perpendicular lines to the top and bottom surfaces, they were rather ragged.
- Maximum plate deflections, at full failure, for 1% and 2% HSSFRC square plates were observed to be 23 mm (0.92 in.) and 35 mm (1.38 in.), respectively.
- It was also noted that, the maximum crack width, at the plate surfaces, for 1% and 2% HSSFRC square plates were 4.0 mm (0.16 in.) and 9.5 mm (0.375 in.), respectively. Refer to Figures 10.14, 10.15 and 10.6 for failure and crack patterns.

www.manaraa.com

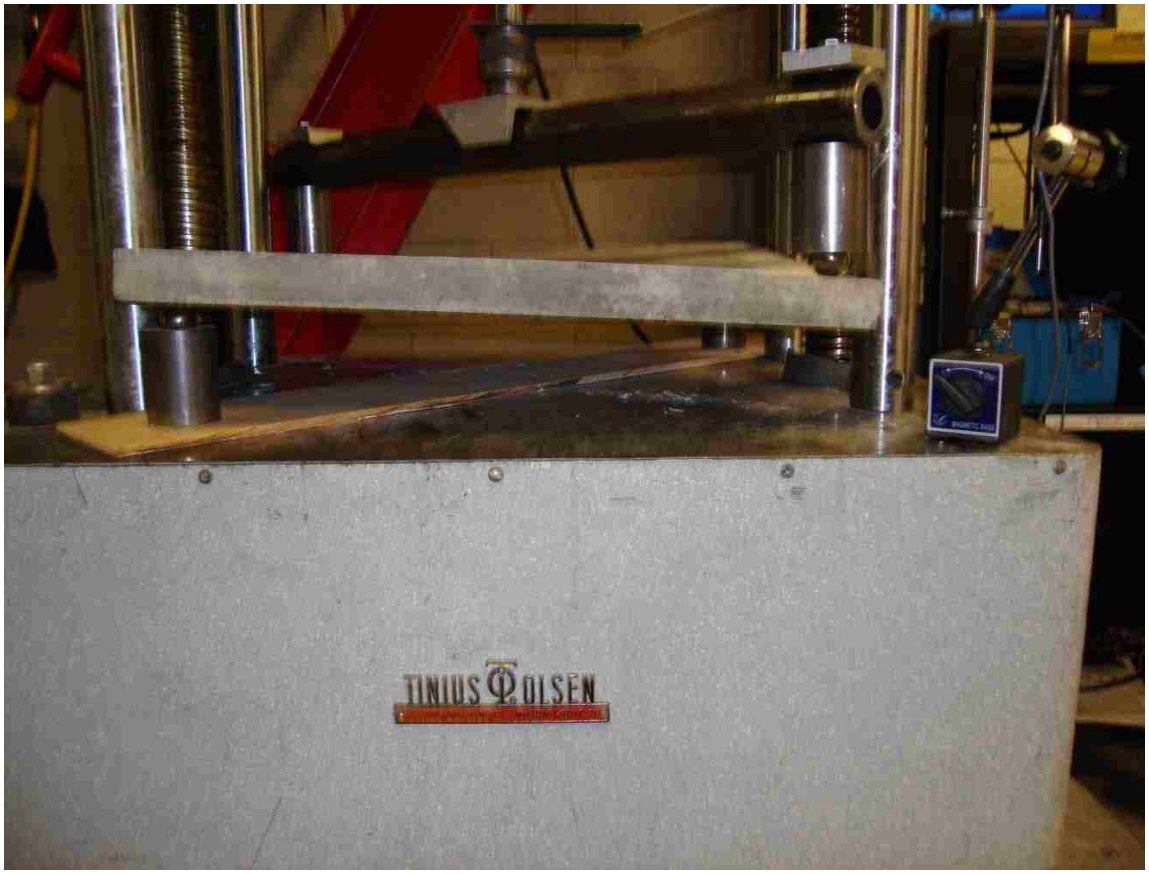

Figure 10.14: Failure patterns for 1% HSSFRC square plates under concentrated opposite corner loads

www.manaraa.com

Figure 10.15: Crack pattern at the bottom surface for 1% HSSFRC square plates under concentrated opposite corner loads

www.manaraa.com

Figure 10.16: Failure and crack patterns for 2% HSSFRC square plates under concentrated opposite corner loads

10.10 Energy absorption (toughness)

The energy absorption (toughness), the area under the load versus deflection curves, for 0%, 1% and 2% HSSFRC square plates were calculated as 56, 235 and 393 in-lb, respectively. The load versus deflection curves are shown in Figure 10.7. The energy absorption of HSSFRC square plates increased as the steel fiber content increased: 320% and 602% for 1% and 2% SFVF plates, respectively over the 0% SFVF plates.

www.manaraa.com

10.11 Discussion of test results

10.11.1 Load versus deflection

The capacity of HSSFRC square plates to carry opposite corner loads increased as the steel fiber volume fraction (SFVF) increased from 0% to 1% and 2%. The capacity of HSSFRC square plates to carry opposite corner loads increased by 16% and 25% for 1% and 2% SFVF in comparison to 0% (plain) HSSFRC square plates, respectively. The increase in capacity of HSSFRC square plates between 0% and 1% SFVF is greater than the increase between 1% and 2% SFVF.

The deflection for 0%, 1% and 2% HSSFRC square plates at peak load, which corresponds to the first crack load, were very comparable for all three SFVF. The deflections at peak load were 2.34 mm (0.092 in.) for 0% and 2% and 2.21 mm (0.087 in.) for 1% SFVF. But, the maximum deflection of HSSFRC square plates, which corresponds to the point of complete failure, differed by a large margin for all three SFVF. The deflection for HSSFRC square plates increased as the SFVF increased from 0% to 1% and 2%. The higher deflection value was exhibited by the higher SFVF, which is 2%. The maximum deflection of the HSSFRC square plates increased by 905% and 1313% for 1% and 2% SFVF, respectively compared to 0% (plain) HSSFRC square plates.

The ductility of HSSFRC square plates increased as the SFVF increased from 0% to 1% and 2%. The ratio of HSSFRC square plate deflection at complete failure to the deflection at first crack increased from 1.00 for 0% to 10.63 and 14.13 for 1% and 2% SFVF, respectively. The increase in the ductility of the HSSFRC plates is evident from the load-deflection curves. While 1% and 2% SFVF plates reached a maximum central

www.manaraa.com

deflection of 22.9 mm (0.9 in.) and 33 mm (1.3 in.), respectively in a slow and steady mode of failure; 0% SFVF plates failed abruptly at 2.8 mm (0.11 in.) which shows the great advantage of HSSFRC.

The plate mode of failure showed that, total collapse occurred when major cracks developed. Failure occurred suddenly in 0% SFVF plates; while 1% and 2% SFVF plates failed slowly and went into large deflection.

10.11.2 Splitting tensile strength, compressive strength and modulus of elasticity for HSSFRC cylinders

The Splitting tensile strength results of HSSFRC cylinders showed an increase of 19% and 41% for 1% and 2% SFVF, respectively compared to 0% (plain) cylinders.

It is noted that, while the compressive strength increased with the increase in steel fibers, up to 5%. The young's modulus values for 0% and 1% HSSFRC cylinders remained roughly the same at -3.6%; the results for 2% SFVF decreased by 16.5%. Therefore, the variation in young's modulus and compressive strength results due to the addition of steel fibers were very small, almost flat. It can be concluded that, the addition of steel fibers to the plain concrete mixture did not affect the behavior with respect to young's modulus and compressive strength in this case. It should be stresses that the amount of High Range Water Reducer (HRWR) suitable for 0% mixture was used to prepare all 0%, 1% and 2% concrete mixtures. The effect of HRWR on young's modulus and compressive strength are shown in Phase (1b) of the research.

The stress-strain diagram for cylinders in compression showed that curves for 0% and 1% SFVF samples being nearly identical.

www.manaraa.com

10.11.3 Flexural and shear strains

Load versus shear strain relationship for 0%, 1% and 2% HSSFRC square plates appears to be linear till the peak load, which is consistent with load versus deflection behavior. As expected, 2% HSSFRC square plates sustained the largest load than the lower SFVF square plates.

Flexural strain results showed that, the behavior of HSSFRC plates were nearly linear in compression and almost fully linear in tension and that both gages stopped recording at the same time as major crack leading to failure developed orthogonal to the strain gage in tension. Test results verified the conclusions obtained from plate theory since the reversed corner loading condition (two opposite forces up and the other two down) leads to positive bending in one direction and negative bending in the other direction. More importantly, results showed that the HSSFRC plates behaved symmetrically in two orthogonal directions like a quasi homogenous orthotropic material.

10.11.4 Analysis results

The experimental tensile stress results for 0%, 1% and 2% HSSFRC square plates at the first crack load correspond to the splitting tensile strength for 0%, 1% and 2% HSSFRC cylinders. In regard to pre-crack behavior, the strains for 0%, 1% and 2% HSSFRC square plates were linear and fell on the same slope. The theoretical elastic deflection results, for all three steel fiber by volume fraction, were consistently smaller than the experimental values. Theoretical deflection formulas tend to overestimate the stiffness of the plates.

www.manaraa.com

10.11.5 Energy absorption (toughness)

The area under the load-deflection curves for HSSFRC square plates with higher steel fiber by volume fraction exhibited higher energy absorption capacity (toughness) than the lower SFVF plates.

www.manaraa.com

CHAPTER 11

HIGH STRENGTH STEEL FIBER REINFORCED CONCRETE CIRCULAR PLATES SUPPORTED AT THREE POINTS AND SUBJECTED TO A CONCENTRATED CENTER LOAD (ASTM C 1550)

11.1 Introduction

In this chapter the behavior of simply supported high strength steel fiber reinforced concrete (HSSFRC) circular plates with 0%, 1% and 2% steel fiber by volume fraction (SFVF) supported at three points and subjected to a concentrated center load is presented. The significance of this test is, per ASTM Standard 1550-08 (ASTM C 1550 2008), "Such test panels experience bi-axial bending in response to central point loads and exhibit a mode of failure related to the *in situ* behavior of structures. The post crack performance of round panels subject to a central point load can be represented by the energy absorbed by the panel up to a specified central deflection. In this test method the energy absorbed is taken to represent the ability of fiber reinforced concrete to redistribute stress following crack."

All constituents for the three types of concrete mixtures (0%, 1% and 2% SFVF), used for the making of plates and cylinders, are the same except for the content of steel fibers. The circular plates are 508 mm (20 in.) in diameter and 76 mm (3 in.) thick. The plates are simply supported at three locations; the supports are equidistant from the geometric center, 120° apart and 25 mm (1 in.) shy from the edges. The plates are subjected to a concentrated load at the geometric center, as shown in Figure 11.1.

www.manaraa.com

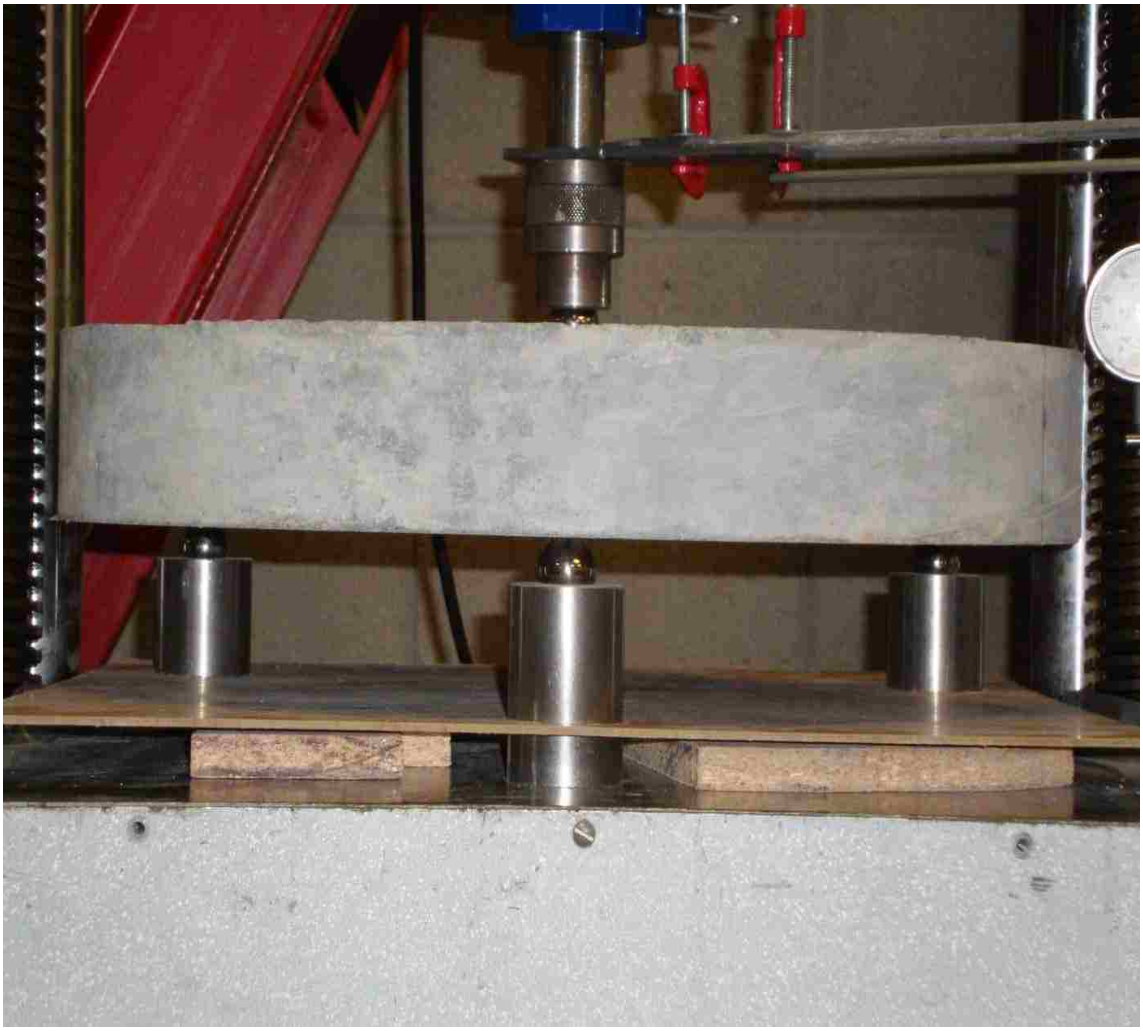

Figure 11.1: HSSFRC circular plate subjected to a transverse concentrated center load

Two strain gages, perpendicular to one another, for each type of steel fiber mixture, are placed on the circular plates to measure the strain activities at the extreme fiber of the plate in relation to the applied load. The first strain gage is placed at the center bottom surface of the plate while, the other is placed at the top surface of the plate by the support. One rosette strain gage, for each steel fiber by volume fraction mixture, is placed on the

www.manaraa.com

side of the plate right at the support to measure the shear strain activities at the plate support.

The chapter presents HSSFRC specimen preparation, testing procedures and experiment results such as load versus deflection, load versus flexural and shear strains and mode of failure of circular plates. The chapter discusses the influence of steel fibers on: flexural and shear capacity, mode of failure and ductility of moderately thick plates (t/D = 0.15); and modulus of elasticity, compression and splitting tensile strength of cylinders prepared from the same mixtures used for the making of plates.

Comparisons are made between circular plates with various steel fiber by volume fractions with respect to the mechanical properties such as flexural capacity, deflection, ductility, and mode of failure. The elastic analysis results corresponding to the first crack load such as stress, strain and deflection are presented. Test results are discussed and conclusions drown.

11.2 Theoretical background of circular plates under center point load

The governing differential equation for plate deflection in polar coordinates (r, θ) is given as (Ugural 2009) (page 130):

$$\nabla^4 w = \left[\frac{\partial^2}{\partial r^2} + \frac{1}{r}\frac{\partial}{\partial r} + \frac{1}{r^2}\frac{\partial^2}{\partial \theta^2}\right]\left[\frac{\partial w^2}{\partial r^2} + \frac{1}{r}\frac{\partial w}{\partial r} + \frac{1}{r^2}\frac{\partial^2 w}{\partial \theta^2}\right] = \frac{p}{D} \qquad (11.1)$$

Where: D = flexural rigidity, $Et^3/12(1-\nu^2)$

t = plate thickness

ν = Poisson's ratio

w = vertical deflections of the plate

www.manaraa.com

p = uniformly distributed load, equal zero for this case.

Stresses on circular plates can be expressed as:

$$\sigma_r = \frac{E}{(1-\nu^2)}(\varepsilon_r + \nu\varepsilon_\theta) \quad (11.2)$$

$$\sigma_\theta = \frac{E}{1-\nu^2}(\varepsilon_\theta + \nu\varepsilon_r) \quad (11.3)$$

$$\tau_\theta = G\gamma_\theta \quad (11.4)$$

Where: G = shear modulus, E/2(1+ν)

γ_θ = shear strain

E = modulus of elasticity

σ_r, σ_θ = circumferential and diametral normal stresses in horizontal plane

ε_r, ε_θ = circumferential and diametral normal strains.

11.3 Preparation of test specimens - cylinders and plates

Two types of test specimens, circular plates and cylinders, were prepared for each test (0%, 1% and 2% SFVF) from the same concrete batch:

- Three circular plates for each SFVF with dimensions of 508 mm (20 in.) diameter by 76 mm (3 in.) thickness. Therefore, a total of nine plate specimens were prepared.
- Six 102 mm (4 in.) diameter by 203 mm (8 in.) long cylinders for each SFVF. Three cylinders each were used for compressive and splitting tensile strength tests, respectively. Therefore, a total of eighteen cylinders were prepared.

www.manaraa.com

To make the circular plates, a Sonotube, commercially available hollow tube made of thick paper products, with approximately 508 mm (20 in.) diameter was obtained. The tube was cut at 76 mm (3 in.) interval to produce a cylinder shape formworks with a diameter of 508 mm (20 in.) and height of 76 mm (3 in.).

The ingredients for all concrete mixtures were kept the same except for the amount of steel fibers used by volume fraction in each concrete mixture type. The ingredients for the 0%, 1% and 2% steel fiber concrete mixtures are given in Table 11.1.

Refer to Section 8.1.3 for concrete and specimen preparations. Plates and cylinders were cured for 28-days.

11.4 Types of strain gages used (Circular plates)

The size and type of strain gages depend on the maximum aggregate size. Two types of strain gages, which were recommended by the manufacturer, were used:

1. N2A-06-10CBE-350/E – is an individual strain gage, which measures strain in a single direction. It can be installed, as shown in Figures 11.2 and 11.3, individually or in group to measure strain in one or multiple directions, respectively.
2. CEA-06-250UR-120 – is a rosette, group, type strain gage with three grids oriented 45° apart, angularly, from each other, refer to Figures 8.1.3 and 11.4 for rosette orientation.

Refer to Section 8.1.4 for full description of both types of strain gages.

www.manaraa.com

Table 11.1: Concrete batch constituents for 0%, 1% and 2% HSSFRC circular plates (20 in. diameter x 3 in. thick) and cylinders

Mixture Components			**0%**	**1%**	**2%**
Batch Volume			**2.2 ft^3**	**2.2 ft^3**	**2.2 ft^3**
3/8" Coarse Aggregate	(lb)		50.16	50.16	50.16
#4 Coarse Aggregate	(lb)		49.28	49.28	49.28
Fine Aggregate, FA4*	(lb)		126.72	126.72	126.72
Water	(lb)		25.52	25.52	25.52
Cement Type V	(lb)		55.00	55.00	55.00
Silica Fume	(lb)		4.18	4.18	4.18
Fly Ash	(lb)		23.54	23.54	23.54
Total Cementitious	(lb)		82.72	82.72	82.72
Water to Cement Ratio			0.46	0.46	0.46
Water / Cementitious Ratio			0.31	0.31	0.31
Gravel : Sand Ratio			0.44 : 0.56	0.44 : 0.56	0.44 : 0.56
HRWR ADVA540	(lb)		0.864	0.864	0.864
Steel Fiber by Volume	%		0%	1%	2%
Steel Fiber by weight	(lb)		0	11	22
Concrete Total Weight	(lb)		335.26	346.26	357.26
Concrete Unit weight	(pcf)		152.4	157.4	162.4

*Fine aggregate with fineness modulus of 2.05

www.manaraa.com

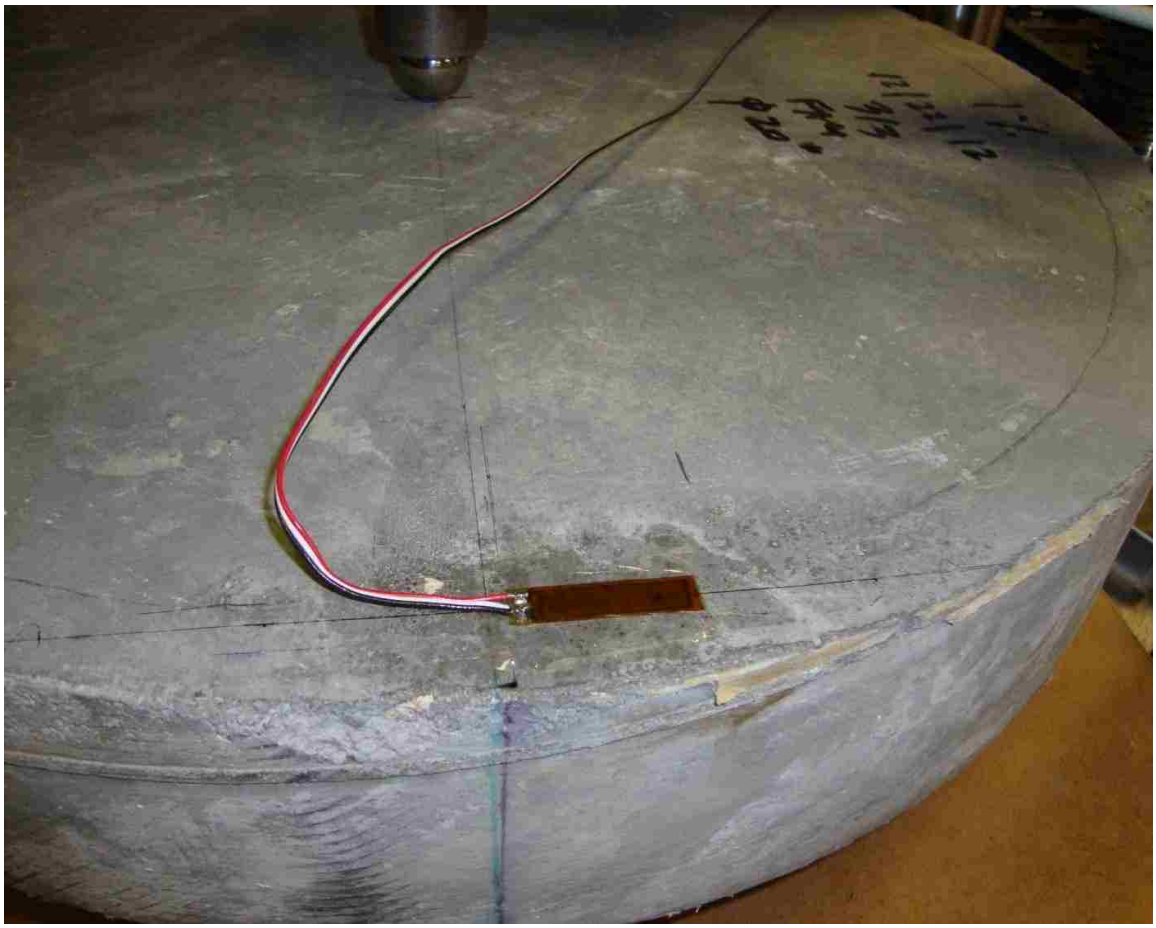

Figure 11.2: N2A-06-10CBE-350/E type strain gage located on the top surface of the circular plate and 3 mm (0.125 in.) away from the support point

www.manaraa.com

Figure 11.3: N2A-06-10CBE-350/E type strain gages located at the bottom surface of the circular plate and 3 mm (0.125 in.) away from the center point

www.manaraa.com

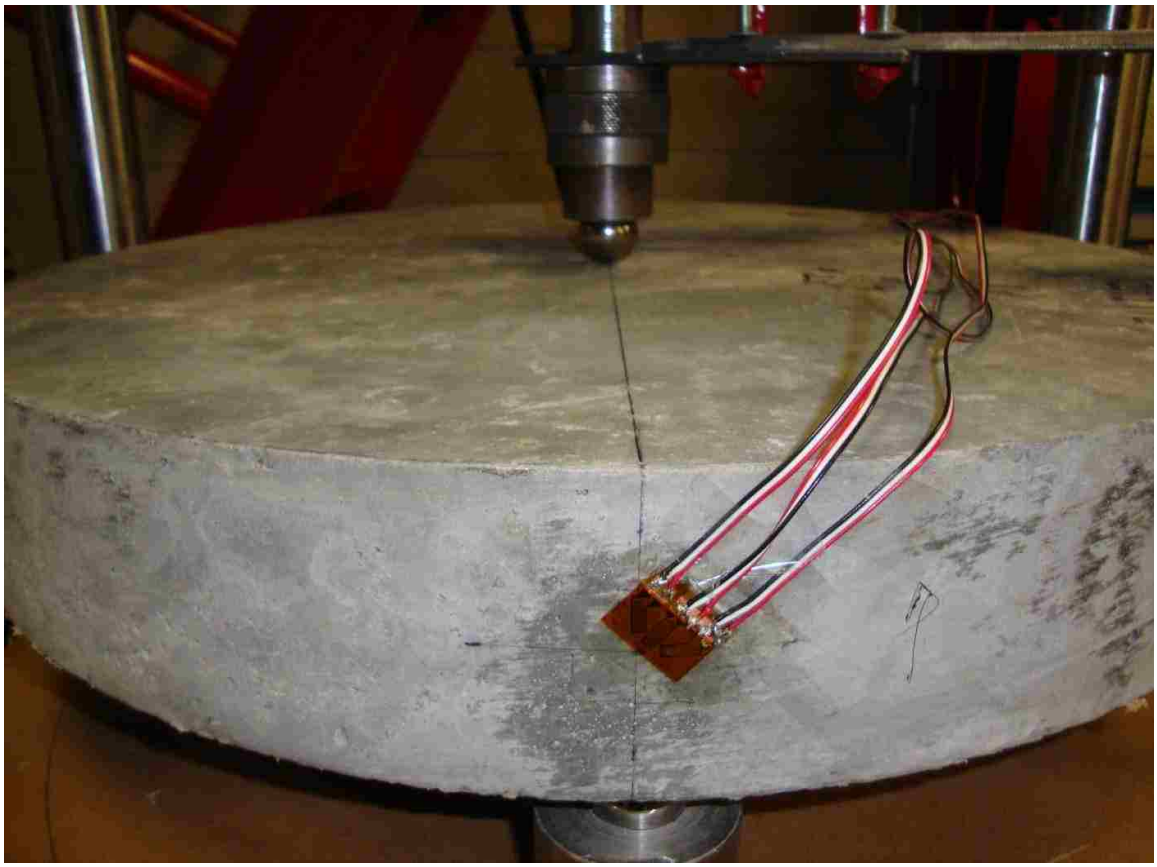

Figure 11.4: 45°- rectangular rosette located at mid depth of the circular plates

11.5 Location and orientation of strain gages on the test specimens

The strain gage arrangements for every test plate were determined by the capability of the data acquisition system to accommodate rosette and strain gage output, deflection measurements and load input combined.

At the end of the 28-day, both plate and cylinder specimens were pulled out of the curing room, and the plate specimens were prepared as follows:

1) Plate #1 had no strain gage attached to it. Plate #1 was used strictly to measure load versus vertical deflection behavior of plates under center point load. Vertical

www.manaraa.com

deflection was measured at the center of the circular plate. The load and vertical deflection readings were electronically linked.

2) Plate #2 was furnished with two independently placed strain gages. Plate #2, in addition to measuring load versus vertical deflection, it also measured the top and bottom surfaces strain activities of the plate. Strain gage #1 was placed at the bottom surface of the plate and parallel to the straight line connecting center point and one of the support points. The center point of the strain gage was aligned with the center of the plate but with an offset of 3 mm (0.125 in.) from the center of the plate to the edge of the strain gage. Strain gage #2 was placed on the top surface of the plate directly above the support point; where the longitudinal axis of the gage is perpendicular to the alignment of the bottom surface strain gage. The edge of the strain gage was offset by 3 mm (0.125 in.) from the support point. Refer to Figures 11.2, 11.3 and 11.5 for strain gage layout. The strain gages were placed 3 mm (0.125 in.) away from the point of load or support to minimize damage or distraction of strain gages during the loading process.

3) Plate #3 was equipped with one 45°- rectangular rosette, with three grids spaced at 45° interval. Refer to Section 8.1.4 for the properties, size and arrangement of rosettes. The rosette was placed on the side of plate #3 adjacent to the support location. The center axis of the rosette was on the same vertical plane as the center of the support. Grid #1 (e_1) of the rosette was aligned with the neutral axis of the plate so that only shear strain of the plate at the support location can be measured. For plate #3, a dial gage, not extensometer, was used to measure the

www.manaraa.com

vertical deflection at the plate center. For the location and layout of the rosette (shear strain gage) on the circular plates, refer to Figures 11.4 and 11.6.

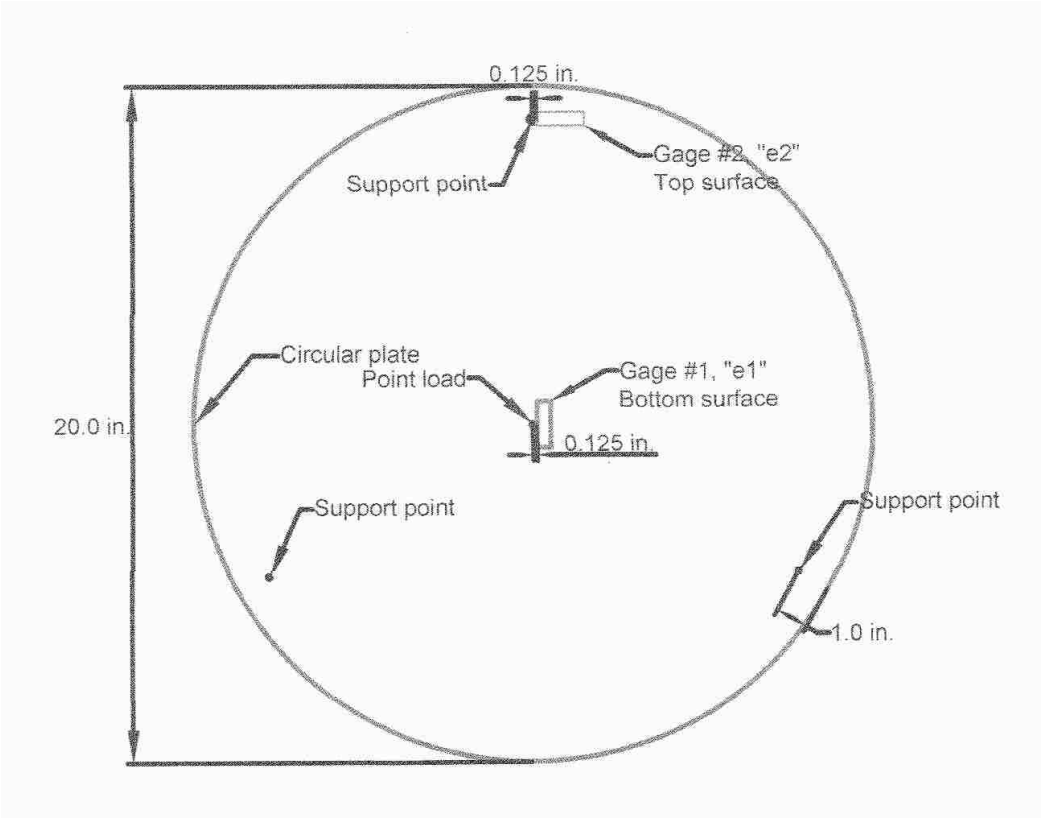

Figure 11.5: Strain gages located on the top and bottom surfaces of HSSFRC circular plate

www.manaraa.com

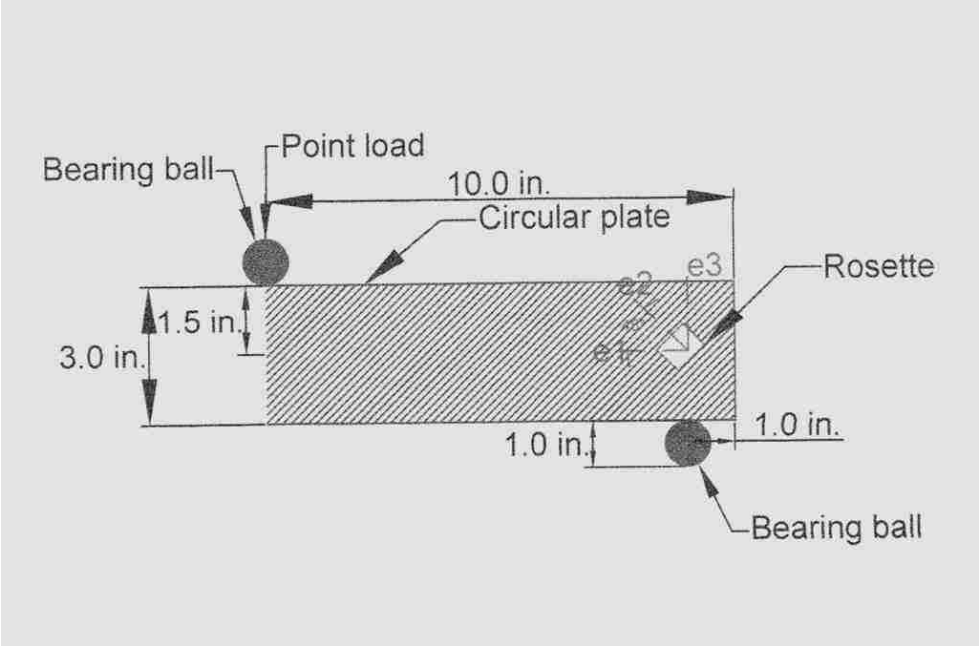

Figure 11.6: Rosette strain gage located on the side of the HSSFRC circular plate

11.6 Test apparatus and procedures for circular plates

Once the specimens were fitted with strain gages, they were ready for testing. The strain gages and rosettes were installed per manufacturer's recommendation as stated in Section 4.4.6. The apparatus involved were:

1. Tinius-Olsen testing machine (50,000 lb maximum capacity)
2. Solid cylindrical steel stub/bar and bearing ball combination that were used as part of load application and support system. The solid cylindrical steel stubs had a portion of sphere indentation/impression, where the bearing ball would seat. The impression was created by milling out a portion of the sphere from the steel stub using a computerized drill machine. Refer to Figure 11.6 for sizes and dimensions of the support system.

www.manaraa.com

3. Four 25.4 mm (1 in.) diameter spherical bearing balls, part of the load and support assembly.
4. Strip of rectangular plywood with three circular slots, equal in diameter to the support solid cylindrical steel bar, cut out. The slots were spaced equally at 120° apart and at the perimeter of 457 mm (18 in.) diameter circle. The plywood was used to secure the steel support pieces in place and maintain spacing during the specimen set up and loading process. Refer to Figure 11.7 for test specimen set up.

Figure 11.7: Test apparatus and specimen set up for circular plates under a concentrated center load

www.manaraa.com

The test set up for plates was assembled as follows:

1) First, the plywood strip was placed flat on a very strong testing base.
2) Three solid cylindrical steel bars were inserted into the preformed slots.
3) One bearing ball was placed on the top of each cylindrical steel bar, where the partial shape of the bearing was milled out.
4) The circular plate was placed on three bearing ball supports.
5) One bearing ball, part of the load assembly, was placed on the top surface and center of the circular plate.
6) The load cell was lowered enough to just engage the circular plate. The extensometer was set up and set to zero. Before the actual loading process started: the plate, support, entire test set up and all contact surfaces were checked for any kind of rocking or gap (lack of contact) between the test specimen supports and test specimen. All gaps were shimmed to ensure full contact and uniform load transfer between units.
7) Finally, the load was applied at a steady rate of 0.025 – 0.051 mm/minute (0.001 – 0.002 in./min) till the first major failure or crack occurred and increased to 0.076 – 0.203 mm/minute (0.003 – 0.008 in./minute) till complete failure of the specimen.

The HSSFRC cylinders, which were cast from the same concrete mixture used for plates, were tested for compressive and splitting tensile strength according to the test procedures that are presented in Sections 4.4.1 and 4.4.4, respectively. During the testing process for cylinders and plates: load, deflection and strain data were collected; failure and failure modes were noted.

www.manaraa.com

11.7 Experiment results for circular plates supported at three points and under a concentrated center load

11.7.1 Load versus deflection results

Load versus vertical deflection data were collected during the testing process for HSSFRC circular plates, with 0% to 2% steel fiber by volume fractions (SFVF), under a concentrated center load. The deflection was measured at the center of the plates. The load versus deflection curves for 0%, 1% and 2% HSFRC circular plates, supported at three equally spaced locations, under a concentrated center load are presented in Figure 11.8. Each load versus deflection curve represents an average result of three HSSFRC circular plate specimens for each SFVF, a total of nine specimens for 0%, 1% and 2% SFVF. Table 11.2, presents the peak concentrated load, deflection of the circular plate at the peak load and maximum deflection of the circular plate at complete failure for 0%, 1% and 2% SFVF. Values in Table 11.2 were obtained from load versus vertical deflection curves in Figure 11.8.

www.manaraa.com

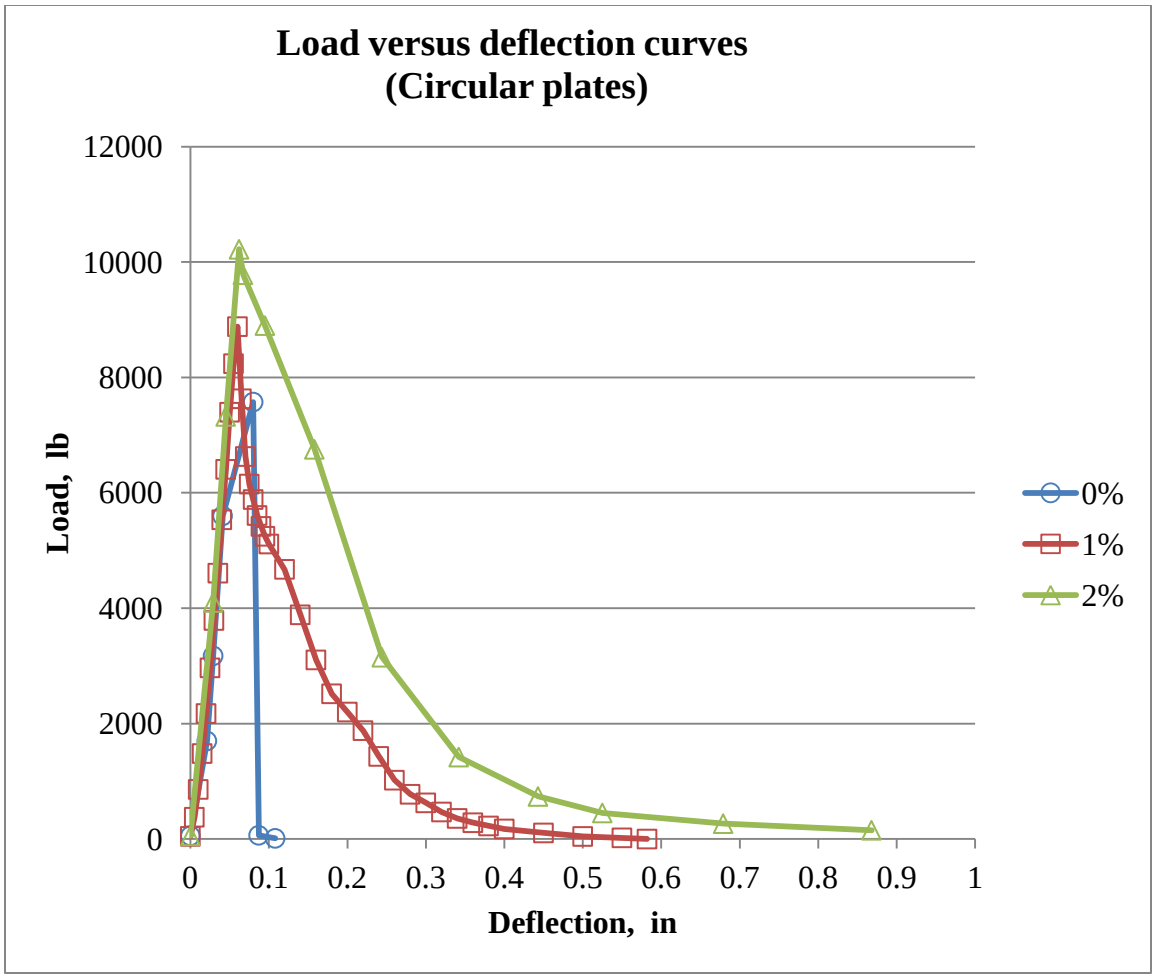

Figure 11.8: Load versus deflection curves for 0%, 1% and 2% HSSFRC circular plates (20 in. diameter x 3 in. thick) under a concentrated center load

www.manaraa.com

Table 11.2: Maximum load and deflection results for 0%, 1% and 2% HSSFRC circular plates (20 in. diameter x 3 in. thick) under a concentrated center load

Plate	P_{Max} N (lb)	Percentage increase from 0% steel fiber	Δ at P_{Max} Mm (in.)	Δ_{Max} Mm (in.)	Percentage increase from 0% steel fiber	$\Delta_{Max\,/\,\Delta}$
0%	33,121 (7,446)	0%	1.57 (0.062)	3.76 (0.148)		2.39
1%	39,571 (8,898)	19%	1.52 (0.060)	14.73 (0.580)	292%	9.67
2%	44,887 (10,091)	36%	1.80 (0.071)	36.58 (1.440)	873%	20.28

Where: P_{Max} = peak concentrated load, N (lb.)

Δ = plate deflection corresponding to the peak load, mm (in.)

$\Delta_{failure}$ = maximum deflection of the plate at complete failure, mm (in.).

11.7.2 Test results of strain gages

As mentioned in Section 11.5, two N2A-06-10CBE-350/E type strain gages were provided to measure the flexural strains of the circular plate. Strain gage #1, was located at the center bottom surface of the circular plate, whereas strain gage #2 was located at the support and top surface of the circular plate. The load versus strain curves for strain gages located at center and support of the circular plates are given in Figures 11.9 and

www.manaraa.com

11.10, respectively. Both figures show 2% SFVF specimen exhibited larger elastic range, ductile response and re-distribution of stress after the initial crack.

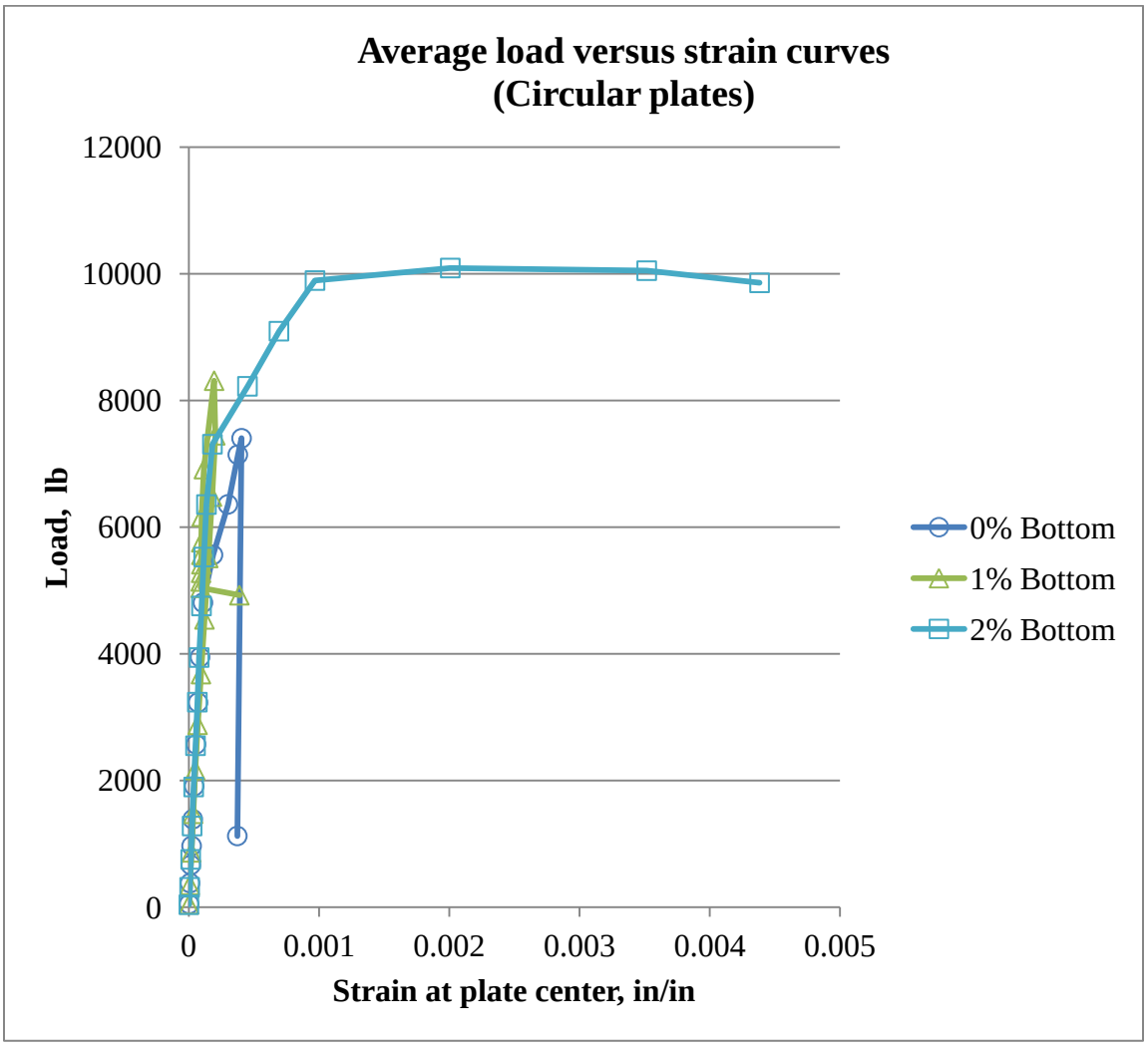

Figure 11.9: Load versus strain (at plate center, bottom) curves for 0%, 1% and 2% HSSFRC circular plates (20 in. dia. x 3 thick in.) under a concentrated center load

www.manaraa.com

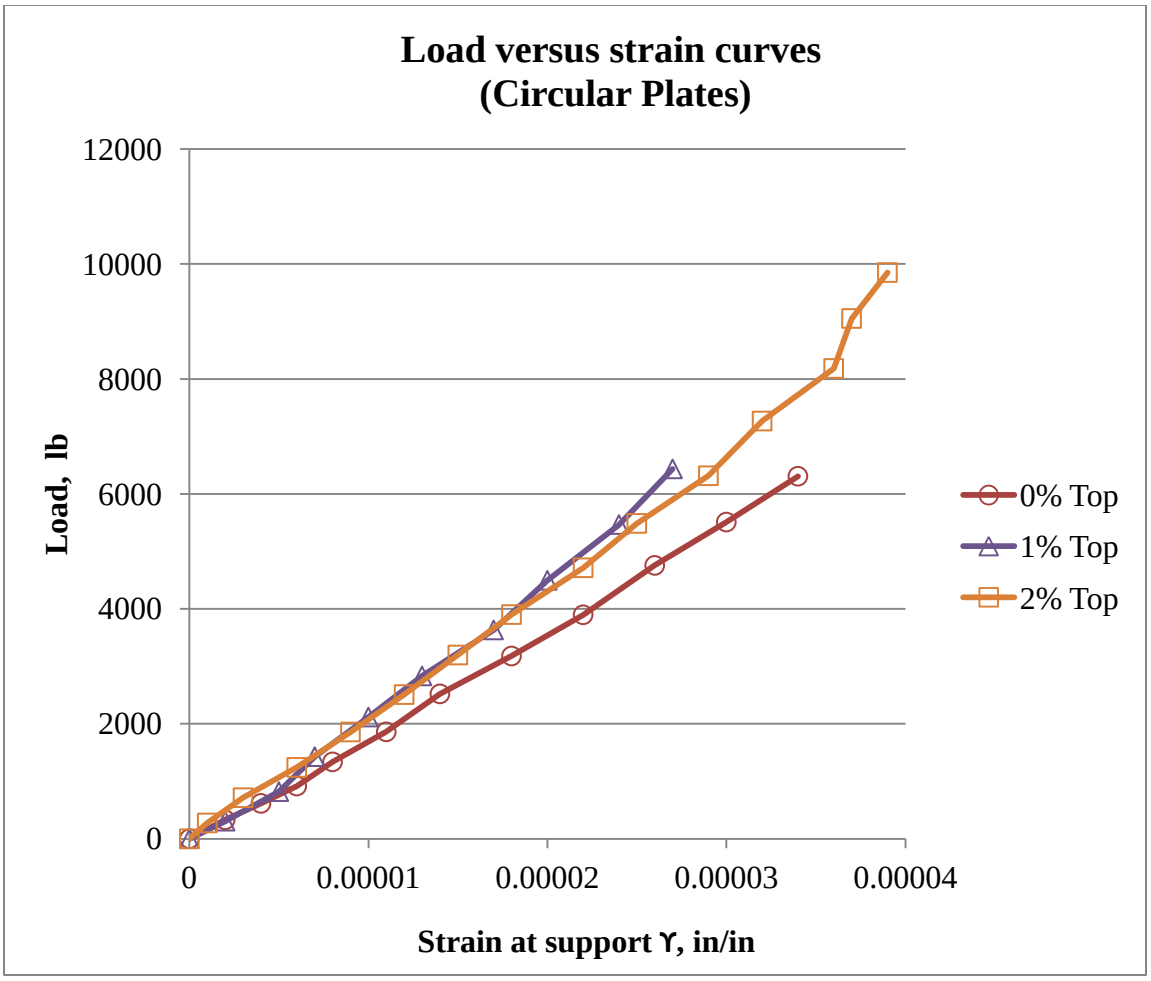

Figure 11.10: Load versus strain (at support, top) curves for 0%, 1% and 2% HSSFRC circular plates (20 in. dia. x 3 in. thick) under a concentrated center load

11.7.3 Test results for rosette strain gages at support

Load versus maximum shear strain curves for 0%, 1% and 2% HSSFRC circular plates loaded in the transverse direction at the plate center are presented in Figure 11.11. The maximum shear strains were calculated per Equation 8.12 in Section 8.1.4, using strains measured by rosette strain gages located close to the supports. Figure 11.11 shows a linear range till the initial crack for all steel fiber volume fractions.

www.manaraa.com

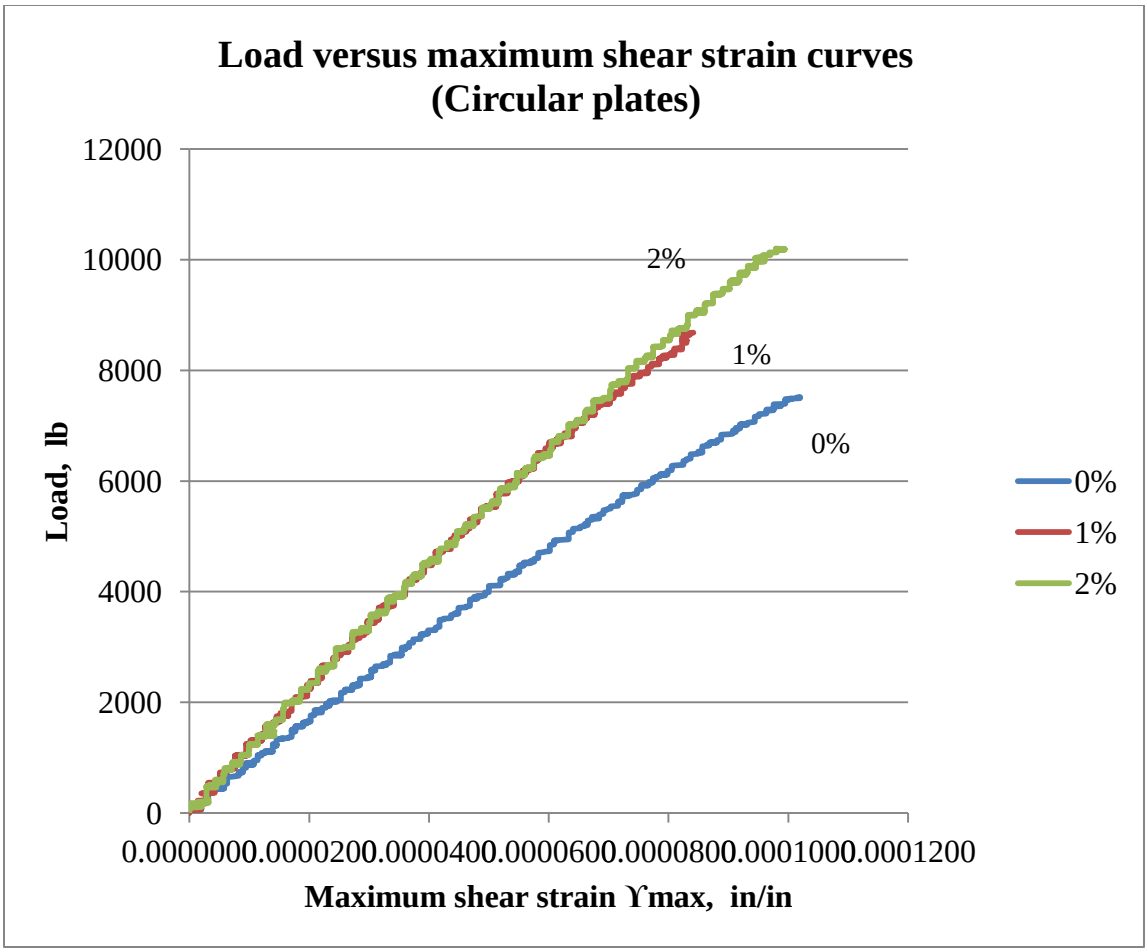

Figure 11.11: Load versus maximum shear strain curves for 0%, 1% and 2% HSSFRC circular plates (20 in. dia. x 3 in. thick) under a concentrated center load

11.7.4 Cylinder compressive strength test results

11.7.4.1 Longitudinal strain and modulus of elasticity of HSSFRC cylinder

As noted before, HSSFRC cylinder specimens that were used for compressive strength tests were prepared from the same batch of concrete the corresponding plates were made. The cylinders were tested, for compressive strength, within 24 hours of testing the corresponding plates. During the testing process applied compression load and the corresponding longitudinal and transverse strains of cylinders were collected.

www.manaraa.com

The average compressive stress versus longitudinal strain curves for 0%, 1% and 2% high strength steel fiber reinforced concrete cylinders are presented in Figure 11.12.

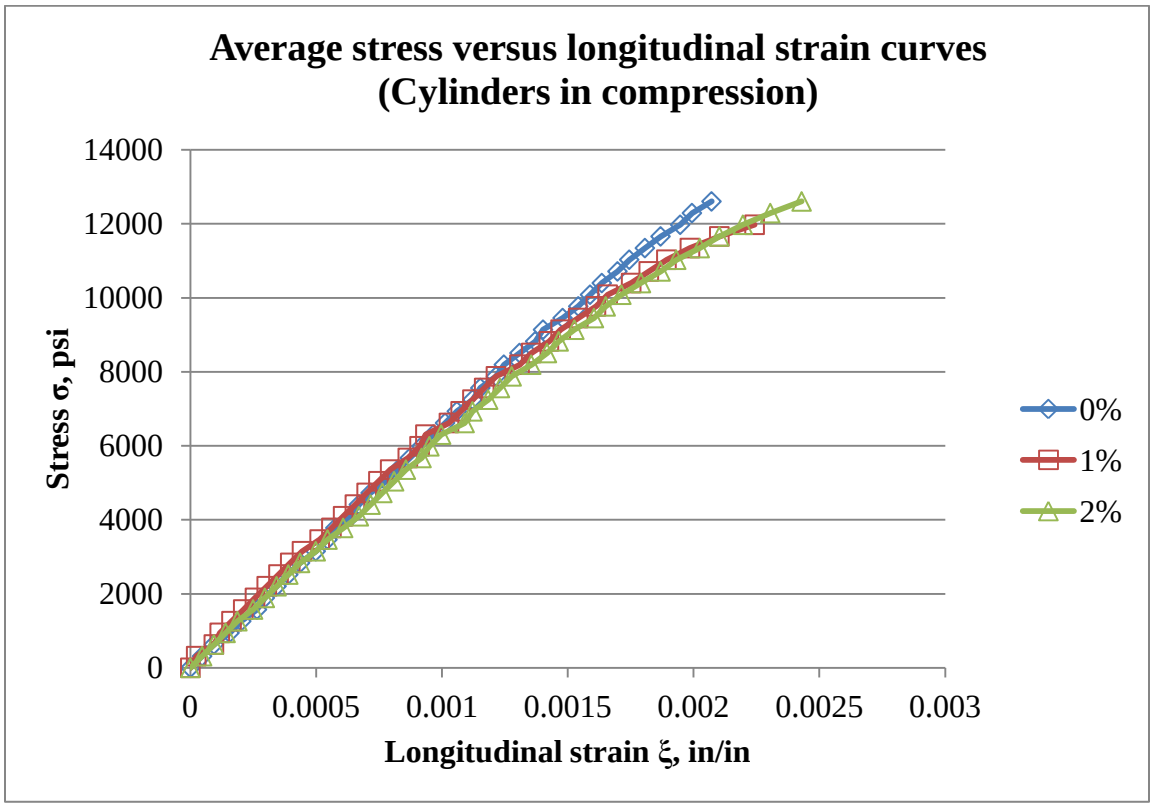

Figure 11.12: Average compressive stress versus longitudinal strain curves for 0%, 1% and 2% HSSFRC cylinders (4 in. x 8 in.) casted with circular plates

The average compressive strength and modulus of elasticity test results for 0%, 1% and 2% high strength steel fiber reinforced concrete cylinders under compression load are presented in Table 11.3. The compressive strength and modulus of elasticity results were calculated using procedures in Sections 4.4.1 and 4.4.2, respectively.

www.manaraa.com

Table 11.3: Average compressive strength and modulus of elasticity for 0%, 1% and 2% HSSFRC cylinders (4 in. x 8 in.) casted with circular plates

Cylinder	Compressive strength MPa (psi)	Percentage increase from 0% steel fiber	Modulus of elasticity MPa (ksi)	Percentage increase from 0% steel fiber
0%	89		44,176	
	(12,883)	0%	(6,407)	0%
1%	85		46,076	
	(12,325)	-4%	(6,683)	4.3%
2%	88		43,100	
	(12,757)	-1%	(6,251)	-2.4%

11.7.4.2 Transverse strain and Poisson's ratio of HSSFRC cylinders

The average compressive stress versus transverse strain curves for 0%, 1% and 2% HSSFRC cylinders are presented in Figure 11.13. While compressive stress versus Poisson's ratio curves for 0% and 2% HSSFRC cylinders are shown in Figure 11.14. The Poisson's ratio results for 0% and 2% HSSFRC cylinders were calculated using procedures in Section 4.4.3. The Poisson's ratio curves in Figure 11.14 show that 0% and 2% HSSFRC cylinders responded in similar fashion at the lower to mid stress range and converged to the same values at the higher end of the stress range.

www.manaraa.com

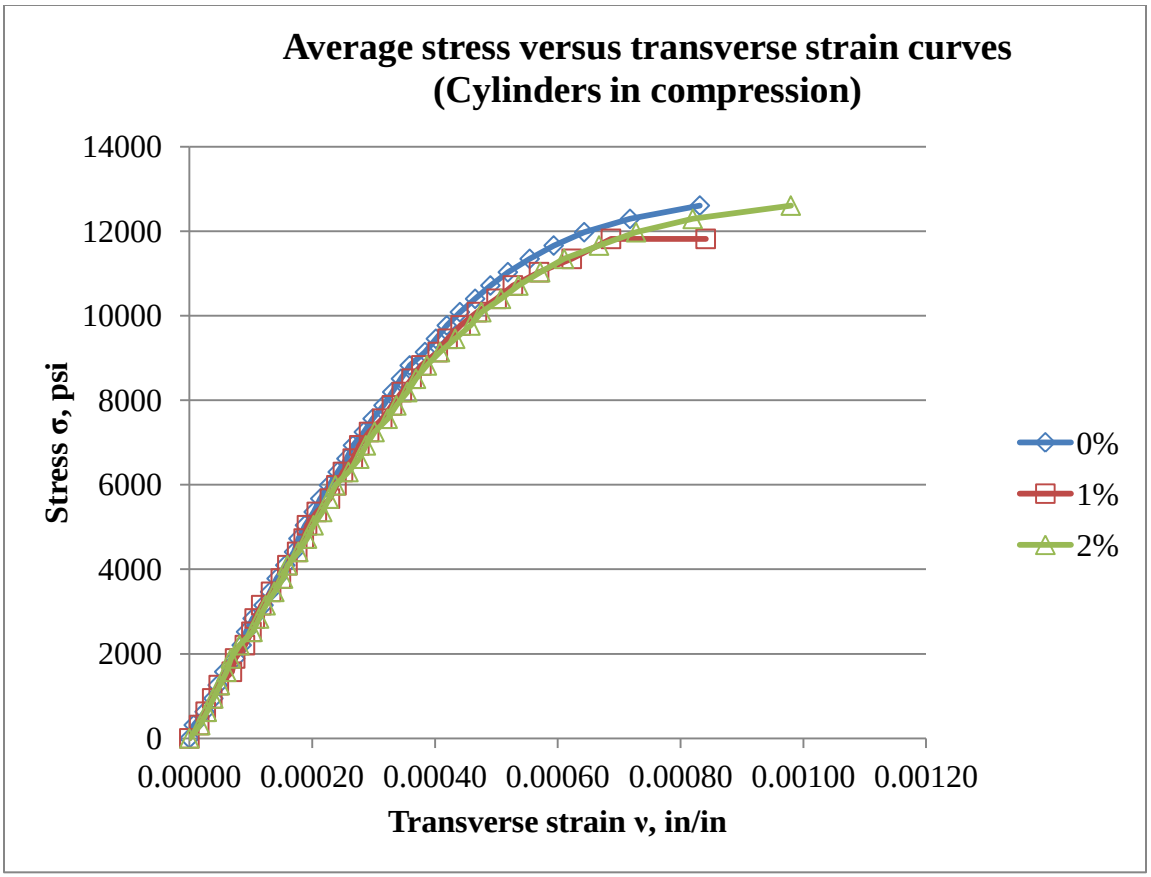

Figure 11.13: Compressive stress versus transverse strain curves for 0%, 1% and 2% HSSFRC cylinders (4 in. x 8 in.) casted with circular plates

www.manaraa.com

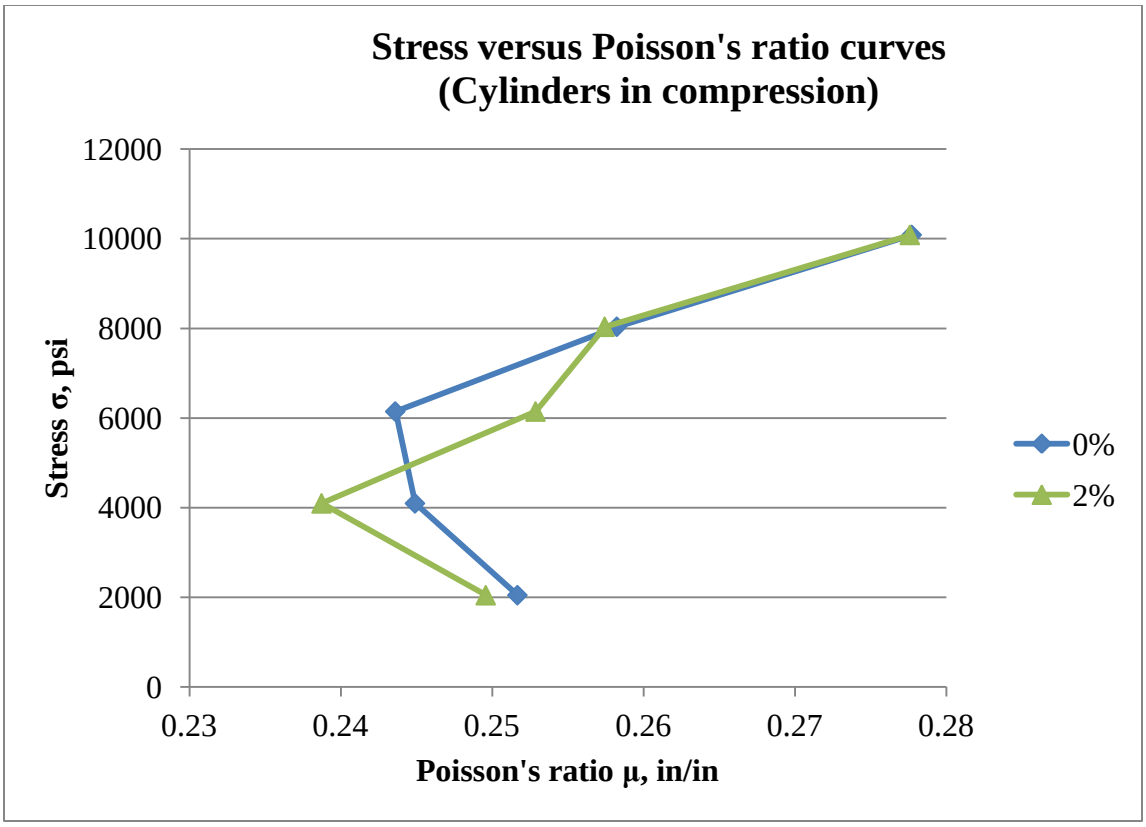

Figure 11.14: Avergae compressice stress versus Poisson's ratio curves for 0% and 2% HSSFRC cylinders (4 in. x 8 in.) casted with circular plates

11.7.5 Cylinder splitting tensile strength results

The average splitting tensile strength test results of 0%, 1% and 2% high strength steel fiber reinforced concrete cylinders are presented in Table 11.4 and Figure 11.15. Splitting tensile strength results were computed using Equation 4.3.

www.manaraa.com

Table 11.4: Average splitting tensile strength for 0%, 1% and 2% HSSFRC cylinders (4 in. x 8 in.) casted with circular plates

Cylinder	Splitting tensile strength MPa (psi)	Percentage increase from 0% steel fiber	Splitting tensile to compression strength ratio
0%	8.63		
	(1,252)	0%	0.10
1%	9.34		
	(1,354)	8%	0.11
2%	11.74		
	(1,703)	36%	0.13

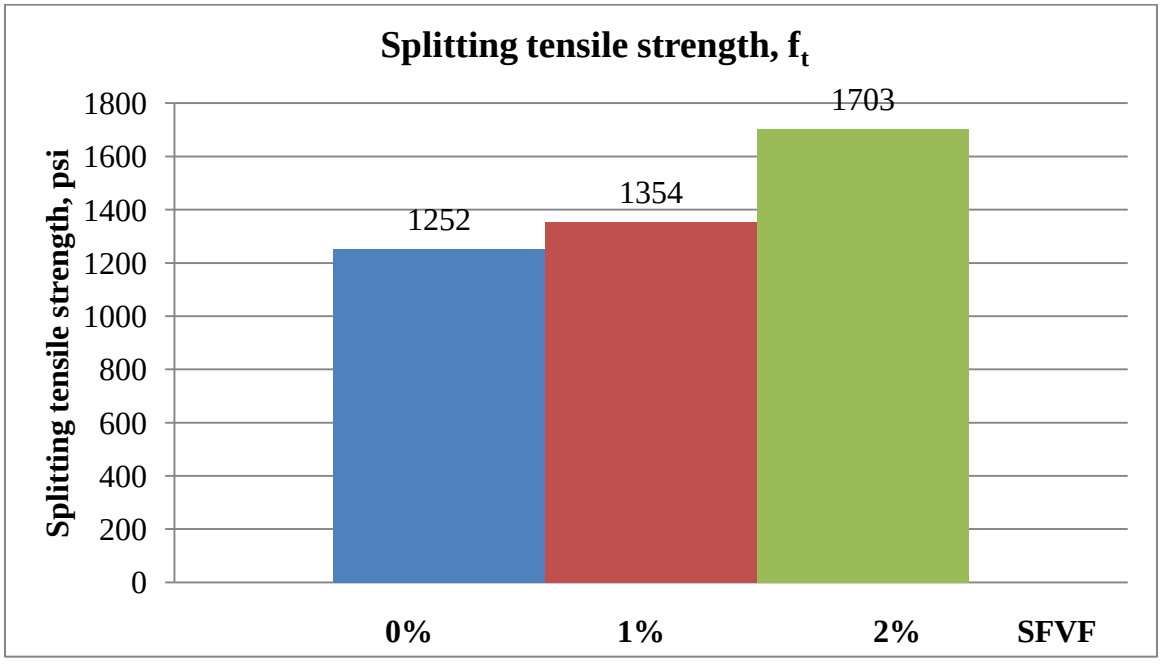

Figure 11.15: Average splitting tensile strength results for 0%, 1% and 2% HSSFRC cylinders (4 in. x 8 in.) casted with circular plates

www.manaraa.com

11.8 Stress-strain analysis and test results

Longitudinal and transverse strains at first crack and the corresponding plate deflection and calculated stress results for 0%, 1% and 2% HSSFRC circular plates (20 in. Dia x 3 in. thick) are presented in Table 11.5. Stress results for the circular plates were calculated using Equation 8.3 in Section 8.1.2 and modulus of elasticity values from cylinders in compression. The flexural stresses at first noticeable crack, as shown in Table 11.5, are comparable to the spitting tensile stress results of HSSFRC cylinders.

Table 11.5: Stress–strain results for 0%, 1% and 2% HSSFRC circular plates (20 in. diameter x 3 in. thick) at first crack under a concentrated center load

Plate	Load N (lb)	f_t MPa (psi)	Strain (Measured) ε_x (10^{-6})	Strain (Measured) ε_y (10^{-6})	Stress, σ_x (Calculated) MPa (psi)
0%	23,536 (5,291)	8.63 (1,252)	144	29	7.18 (1,041)
1%	37,098 (8,340)	9.34 (1,354)	192	27	9.84 (1,426)
2%	34,367 (7,726)	11.74 (1,703)	245	33	11.73 (1,700)

Where: P = applied transverse point load at first noticeable crack, lb

f_t = splitting tensile strength of HSSFRC cylinders (from Table 11.4), psi

www.manaraa.com

ε_x, ε_y =measured longitudinal and transverse strains of the circular plates, in/in

σ_x = calculated stress along the span of the circular plates, psi

11.9 Failure modes

The load versus deflection curves in Figure 11.8 showed that circular plates under center point load responded elastically till the first crack load (peak load) was reached, at which point, the resistance to the load decreased gradually for 1% and 2% SFVF however, there was a sudden loss of resistance for 0% SFVF circular plates. In Figure 11.8, load versus deflection curves, all three HSSFRC circular plates, showed similar responses for most part of the elastic range despite the variation in SFVF. During the test, there was no sign of crushing of concrete neither at the point of load application nor at support locations. All edge cracks, for all three SFVF circular plates, occurred in between supports in the radial direction where the maximum circumferential bending occurred.

The 0% HSSFRC circular plates exhibited the following behaviors:

- Sudden failure.
- Cracks occur as the peak load was reached followed by a sudden loss of resistance.
- Crack planes were straight, smooth and 90 degrees with the bottom and top surfaces.
- All cracks or failure planes developed at the bottom surface of the plates where maximum tension occurred.

www.manaraa.com

- In two out of three specimens, three cracks from the plate edge to the plate center occurred simultaneously and in almost symmetrical fashion. Refer to Figure 11.16 for failure and crack patterns.
- The test duration for 0% HSSFRC circular plates was 54 minutes on average, a lot shorter than for 1% and 2% SFVF specimens, which were 169 and 237 minutes, respectively.

Figure 11.16: Crack and failure patterns for 0% HSSFRC circular plates under a concentrated center load

www.manaraa.com

The 1% and 2% HSSFRC circular plates demonstrated the following behaviors:

- Both types of plates showed more ductile failure behavior by demonstrating to undergo large deflections without complete failure and slow loss of resistance.
- The plates did not break into pieces at the end of the test; they stayed in one piece having developed large and deep cracks.
- The cracks did penetrate the whole depth of the plates, which indicates the failure was slow and resistance to the applied load continued till the whole thickness of the plates was exhausted. This indicated the energy needed to break circular plates increased drastically with the increase in SFVF.
- The failure planes were not straight and perpendicular to the top and bottom surfaces. Cracks were ragged and more of parabolic shape.
- Maximum plate deflection of 15mm (0.58 in.) and 37mm (1.44 in.) were observed for 1% and 2% SFVF HSSFRC circular plates, respectively.

- It was also noted that, the maximum crack width for 1% and 2% HSSFRC circular plates were 12.7 mm (0.50 in.) and 15.5 mm (0.61 in.), respectively. Refer to Figures 11.17 and 11.18 for failure and crack patterns.

www.manaraa.com

Figure 11.17: Crack and failure patterns for 1% HSSFRC circular plates under a concentrated center load

www.manaraa.com

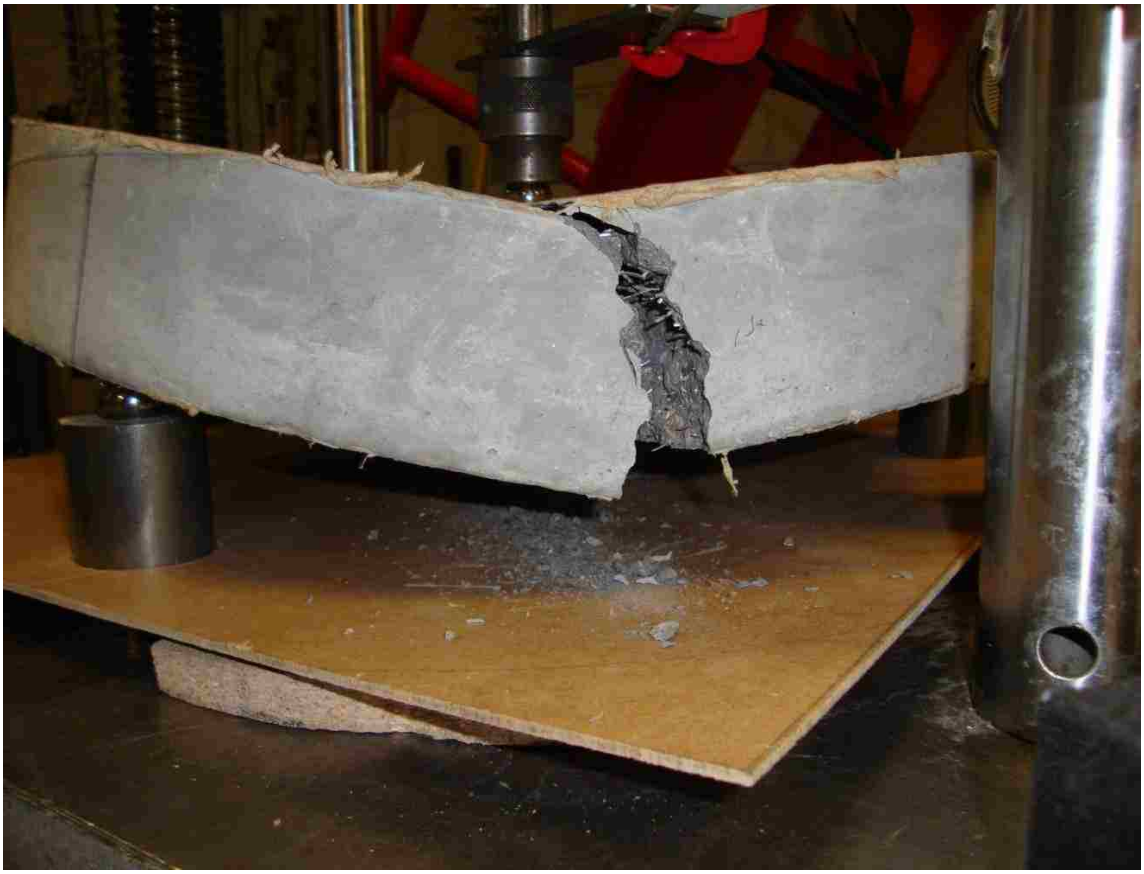

Figure 11.18: Crack and failure patterns for 2% HSSFRC circular plates under a concentrated center load

11.10 Energy absorption (toughness)

The energy absorption (toughness), the area under the load versus deflection curves, for 0%, 1% and 2% HSSFRC circular plates were calculated as 375, 1,023 and 2,008 in-lb, respectively. The load versus deflection curves are shown in Figure 11.8. The energy absorption of HSSFRC circular plates increased as the steel fiber content increased: 173% and 435% for 1% and 2% SFVF plates, respectively over the 0% SFVF plates.

www.manaraa.com

11.11 Discussion of test results

11.11.1 Load versus deflection

The capacity of HSSFRC circular plates to carry or accommodate a concentrated center load increased as the steel fiber by volume fraction (SFVF) increased. The capacity of HSSFRC circular plates increased by 19% and 36% for 1% and 2% SFVF, respectively from 0% (plain) HSSFRC plates.

The ultimate deflection of HSSFRC circular plates increased as the SFVF increased for 0%, 1% and 2% SFVF. Even though, the deflection at which all SFVF circular plates initially cracked was similar, the final deflection at which the HSSFRC circular plates failed completely were different. The higher ultimate deflection values were exhibited by the higher SFVF, which is 2%. The total deflection of HSSFRC circular plates, at the plate center, increased by 292% and 873% for 1% and 2% SFVF, respectively compared to 0% (plain) HSSFRC circular plates.

The ductility of HSSFRC circular plates increased as the SFVF increased. The ratio of HSSFRC circular plate deflection at complete failure to the deflection at first crack increased from 2.39 for 0% SFVF to 9.67 and 20.28 for 1% and 2% SFVF, respectively.

11.11.2 Splitting tensile strength, modulus of elasticity, compressive strength and Poisson's ratio for HSSFRC cylinders

The Splitting tensile strength results for HSSFRC cylinders exhibited an increase of 8% and 36% for 1% and 2% SFVF, respectively in comparison to 0% (plain) HSSFRC cylinders.

www.manaraa.com

The young's modulus values for 0% though 2% HSSFRC cylinders remained roughly close, within ±4.3%.

The compressive strength results for all three SFVF were within ±4.0%. Therefore, the variation in young's modulus and compressive strength results due to the addition of steel fibers was small. It could be concluded that, the addition of steel fibers to the plain concrete mixture did not affect the behavior of HSSFRC circular plates with respect to young's modulus and compressive strength in this case. It should be stresses that the amount of High Range Water Reducer (HRWR) suitable for 0% mixture was used to prepare all 0%, 1% and 2% concrete mixtures. The effect of HRWR on young's modulus and compressive strength are shown in Phase (1b) of the research.

The stress versus strain curves for HSSFRC cylinders in compression showed that curves for 1% and 2% SFVF samples being similar.

The Poisson's ratio curves for all three SFVF cylinders exhibited similar shape response and converged as the stress level increased.

11.11.3 Flexural and shear strains

The strains at plate center were consistently positive indicating tension throughout the loading process till failure. As for strains at the support, the strains were under tension until the peak load was reached, and then the stress reversed to compression till complete plate failure due to stress release at the plate center after crack initiation.

www.manaraa.com

11.11.4 Analysis results

The maximum experimental tensile stress results correspond to the splitting tensile strength of the HSSFRC 0%, 1% and 2% SFVF circular plates. With respect to pre-crack behavior, the strains for 0%, 1% and 2% HSSFRC circular plates were linear and fell on the same slope. The theoretical elastic deflection results, for all three SFVF, were consistently smaller than the experimental values. Theoretical deflection formulas tend to overestimate the stiffness of the plates.

11.11.5 Energy absorption (toughness)

The area under the load versus deflection curves for HSSFRC circular plates with higher steel fiber by volume fraction (SFVF) exhibited higher energy absorption capacity (toughness) than the lower SFVF plates.

www.manaraa.com

CHAPTER 12

HIGH STRENGTH STEEL FIBER REINFORCED CONCRETE CIRCULAR CYLINDRICAL SHELLS UNDER OPPOSITE CONCENTRATED CENTER LOADS

12.1 Introduction

The behavior of high strength steel fiber reinforced concrete (HSSFRC) circular cylindrical shells with 0%, 1% and 2% steel fiber by volume fractions (SFVF) subjected to a pinching center load is presented in this chapter. The significance of the test is to study the pre and post crack behavior of circular cylindrical shells and pipes subjected to the most severe loading condition, a pinching load. The circular cylindrical shells are subjected to high local bending stresses at the point of load application combined with circumferential stresses.

All constituents for the three types of concrete mixtures (0%, 1% and 2% SFVF), used for the making of shells and cylinders, are the same except for the content of steel fibers. The circular cylindrical shells are 305 mm (12 in.) long, 22 mm (0.875 in.) thick and have an interior diameter of 254 mm (10 in.). The steel fiber length did not exceed the thickness of the shell. The circular cylindrical shells are supported and loaded by pinching loads applied at the shell center from the top and bottom ends of the shell diameter, as shown in Figure 12.1.

Three strain gages, for each type of steel fiber by volume fraction mixture, are placed on the circular cylindrical shells to measure the strain activities at the extreme fiber of the shell in relation to the applied load. Two strain gages are placed along the longitudinal

www.manaraa.com

and circumferential axes, perpendicular to each other, on the top surface of the shell very close to the point of load application. The third strain gage is placed at the mid height (waist) along the circumferential axis of the shell. Vertical and horizontal deflections of the circular cylindrical shells are also gathered.

Figure 12.1: HSSFRC circular cylindrical shell subjected to a pinching center load

The chapter presents HSSFRC specimen preparation, testing procedures and experiment results such as load versus deflection, load versus flexural strain and mode of failure of circular cylindrical shells. The chapter discusses the influence of steel fibers on:

www.manaraa.com

flexural and shear capacity, mode of failure and ductility of thin shells; and modulus of elasticity, compression and splitting tensile strength of cylinders prepared from the same mixtures used for the making of shells.

Comparisons are made between circular cylindrical shell test specimens with various steel fiber by volume fractions with respect to the mechanical properties such as flexural capacity, deflection, ductility, and mode of failure. The elastic analysis results corresponding to the first crack load such as stress, strain and deflection are presented. Test results are discussed and conclusions drown.

12.2 Preparation of test specimens - cylinders and circular cylindrical shells

Two types of test specimens, shells and cylinders, were prepared for each test (0%, 1% and 2% SFVF) from the same concrete batch:

- Three circular cylindrical shells for each SFVF with dimensions of 254 mm (10 in.) interior diameter, 300 mm (11.75 in.) exterior diameter, 22 mm (0.875 in.) thickness and 305 mm (12 in.) long. Therefore, a total of nine shell specimens were prepared.
- Six 102 mm (4 in.) diameter by 203 mm (8 in.) long cylinders for each SFVF. Three cylinders each were used for compressive and splitting tensile strength tests, respectively.

To form the circular cylindrical shells, two Sonotubes, commercially available hollow tube made of thick paper product, with external diameters of 305 mm (12 in.) and 254 mm (10 in.) were obtained. The tubes were cut at 305 mm (12 in.) long interval. Four strips of plywood with a width of 22 mm (0.875 in.) and 305 mm (12 in.) long were

www.manaraa.com

prepared. Initially, the larger tube was placed on a flat surface. Then, the smaller diameter tube was placed inside the larger diameter tube. The wood strips, used as spacer to create a hollow uniform space, were inserted in between the tubes at four equally spaced locations, as shown in Figure 12.2. To measure the horizontal deflection of the circular cylindrical shells, the relative movement of two pieces, rod and tube, was used. To begin with, 3.15 mm (0.124 in.) diameter solid metal rod was inserted into a larger hollow plastic tube with an outer diameter of 6.43 mm (0.253 in.). While the rod was still partially inside the plastic tube, one end of the rod and the opposite end of the tube were embedded at opposite ends of the Sonotube diameter, as shown in Figures 12.2 and 12.5. As the circular cylindrical shell was loaded and deformed horizontally, the relative movement between the rod and tube was measured using extensometer as total horizontal displacement of the shell. Refer to Section 12.4 for dimension and details of the circular cylindrical shell. The entire set was then secured at the base to prevent the set from shifting during the concrete pour process. The concrete mixture was poured from the top side of the form to fill up the shell, while the spacers were lifted as the pour process continued without any external mechanical vibration.

www.manaraa.com

Figure 12.2: Formwork for circular cylindrical shells

The ingredients for all concrete mixtures were kept the same except for the amount of steel fibers used by volume fraction in each concrete mixture type. The ingredients for the 0%, 1% and 2% steel fiber concrete mixtures are given in Table 12.1.

Refer to Section 8.1.3 for concrete and specimen preparations. Shells and cylinders were cured for 28-days.

www.manaraa.com

Table 12.1: Concrete batch constituents for 0%, 1% and 2% HSSFRC circular cylindrical shells (10 in. diameter x 0.875 in. thick) and cylinders

Mixture Components		**0%**	**1%**	**2%**
Batch Volume		**1.3 ft^3**	**1.3 ft^3**	**1.3 ft^3**
3/8" Coarse Aggregate (lb)		29.64	29.64	29.64
#4 Coarse Aggregate (lb)		29.12	29.12	29.12
Fine Aggregate, FA4* (lb)		74.88	74.88	74.88
Water (lb)		15.08	15.08	15.08
Cement Type V (lb)		32.50	32.50	32.50
Silica Fume (lb)		2.47	2.47	2.47
Fly Ash (lb)		13.91	13.91	13.91
Total Cementitious (lb)		48.88	48.88	48.88
Water to Cement Ratio		0.46	0.46	0.46
Water / Cementitious Ratio		0.31	0.31	0.31
Gravel : Sand Ratio		0.44 : 0.56	0.44 : 0.56	0.44 : 0.56
HRWR ADVA540 (lb)		0.510	0.510	0.510
Steel Fiber by Volume %		0%	1%	2%
Steel Fiber by weight (lb)		0	6.5	13
Concrete Total Weight (lb)		198.11	204.61	211.11
Concrete Unit weight (pcf)		152.4	157.4	162.4

*Fine aggregate with fineness modulus of 2.05

www.manaraa.com

12.3 Type of strain gage used

One type of strain gage, N2A-06-10CBE-350/E, was used. Refer to Figures 12.3 and 12.4 for strain gage alignments and locations. The size of the strain gage, which is dependent on maximum aggregate size, was recommended by the manufacturer. Refer to Section 12.4 for location and Section 8.1.4 for full description of strain gages.

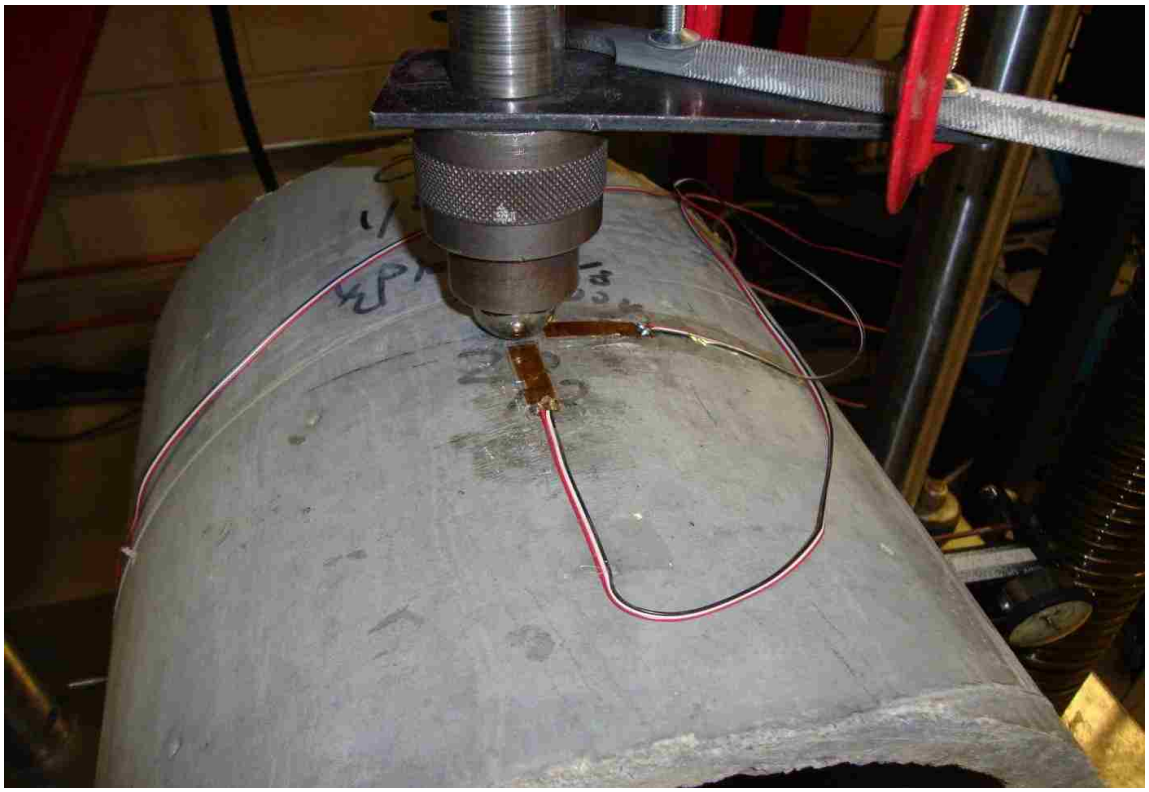

Figure 12.3: N2A-06-10CBE-350/E type strain gages located on the top surface of the circular cylindrical shell and 3 mm (0.125 in.) away from the center point load

www.manaraa.com

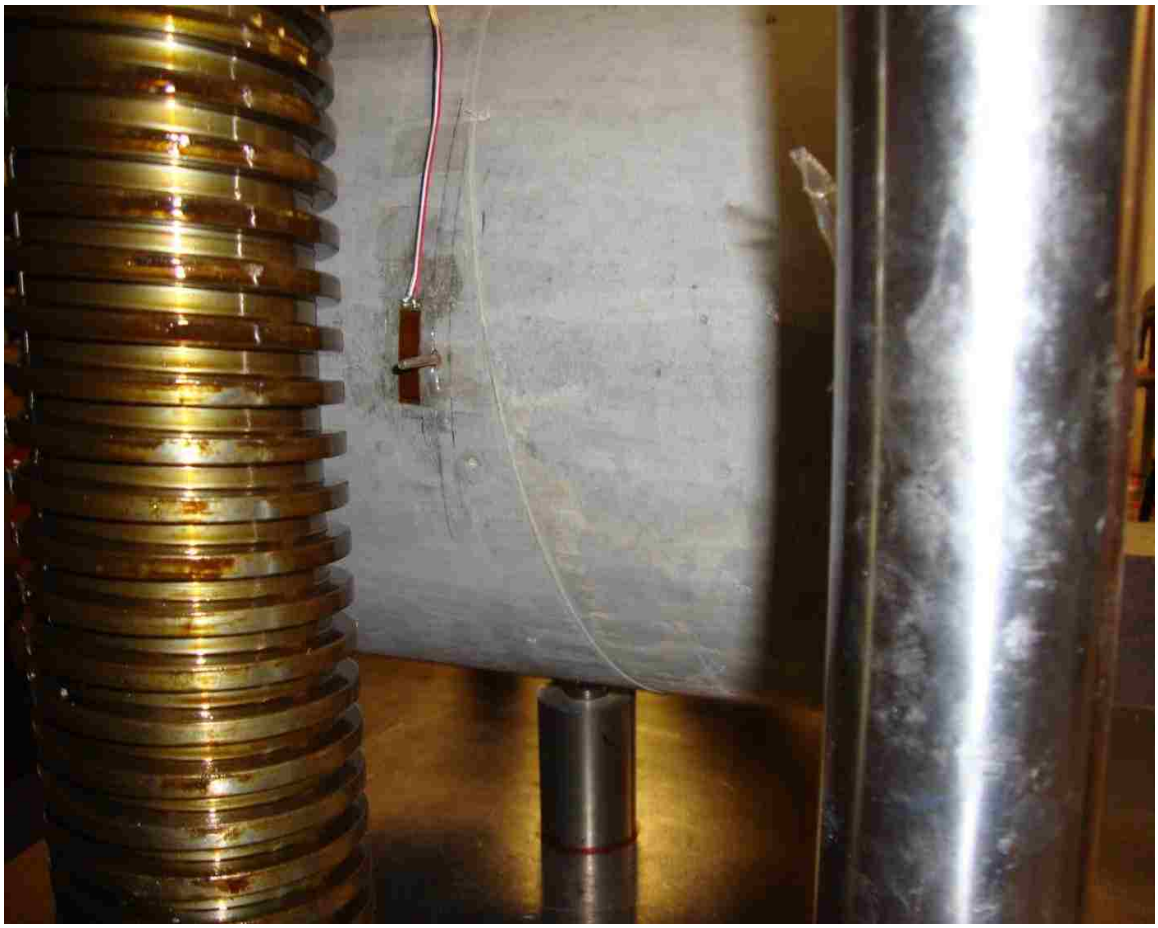

Figure 12.4: N2A-06-10CBE-350/E type strain gage located on the side of the circular cylindrical shell

12.4 Location and orientation of strain gages on the test specimens

The strain gage arrangements for every test were determined by the capability of the data acquisition system to accommodate strain gage output, deflection measurements and load input combined.

At the end of the 28-day, both circular cylindrical shell and cylinder specimens were pulled out of the curing room; and the shell specimens were prepared as follows:

1) Circular cylindrical shell #1 and #2 had no strain gages attached to them. Circular cylindrical shell #1 and #2 were used strictly to measure load versus vertical and

www.manaraa.com

horizontal deflection behavior of circular cylindrical shells under pinching loads. The load and vertical deflection readings were electronically linked.

2) Circular cylindrical shell #3 was furnished with three independently placed strain gages. The strain gages were placed in three different locations on the outer surface of the circular cylindrical shell. Strain gage #1 and #2 were located close to the point of load application. Strain gage #1 was placed along the length of the circular cylindrical shell (longitudinal axis). Strain gage #2 was placed perpendicular to the strain gage #1, along the perimeter of circular cylindrical shell cross section (circumferential axis). Both gages were offset about 3 mm (0.125 in.) from the point of load application along their respective directions as shown in Figure 12.3. Strain gage #3 was installed at mid height on the perimeter of the circular cylindrical shell, along the circumferential axis that connects the load and support points, with an offset of 3 mm (0.125 in.), as shown in Figure 12.4. Strain gages #2 and #3 were aligned parallel to each other. Refer to Figure 12.6 for strain gage layout.

www.manaraa.com

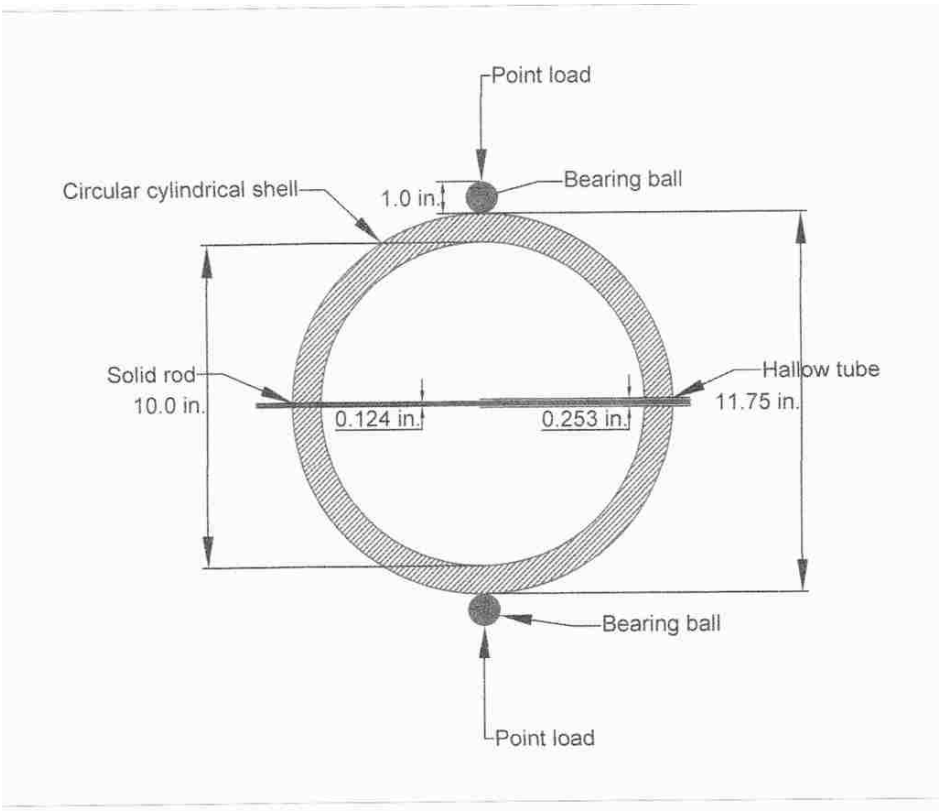

Figure 12.5: Section view of the HSSFRC Circular cylindrical shell set up

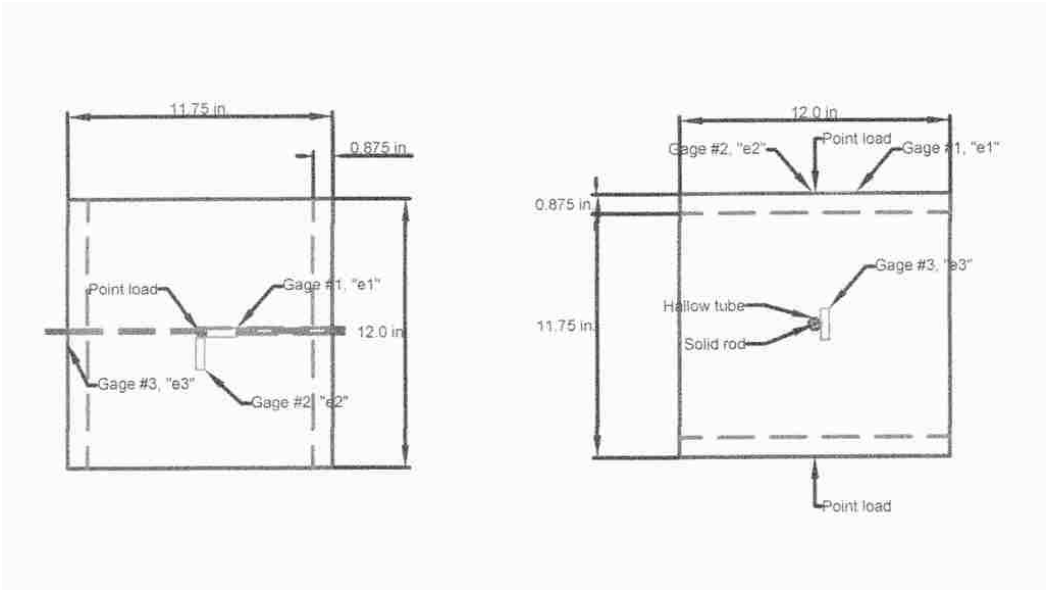

a) Top view **b) Side view**

Figure 12.6: Location of strain gages on the outside surface of the circular cylindrical shells

www.manaraa.com

12.5 Test apparatus and procedures for circular cylindrical shells

Once the specimens were fitted with strain gages, they were ready for testing. The strain gages were installed per manufacturer's recommendation as stated in Section 4.4.6. The apparatus involved were:

1. Tinius-Olsen testing machine (50,000 lb maximum capacity).
2. Solid cylindrical steel stub/bar and bearing ball combination that were used as part of load application and support system. The solid cylindrical steel had a portion of sphere indentation/impression, where the bearing ball would seat. The impression was created by milling out a portion of the sphere from the steel stub using a computerized drill machine. Refer to Figure 12.5 for sizes and dimensions of the support system.
3. Two 25.4 mm (1 in.) diameter spherical bearing balls. Single bearing ball each for the load and support assemblies.

www.manaraa.com

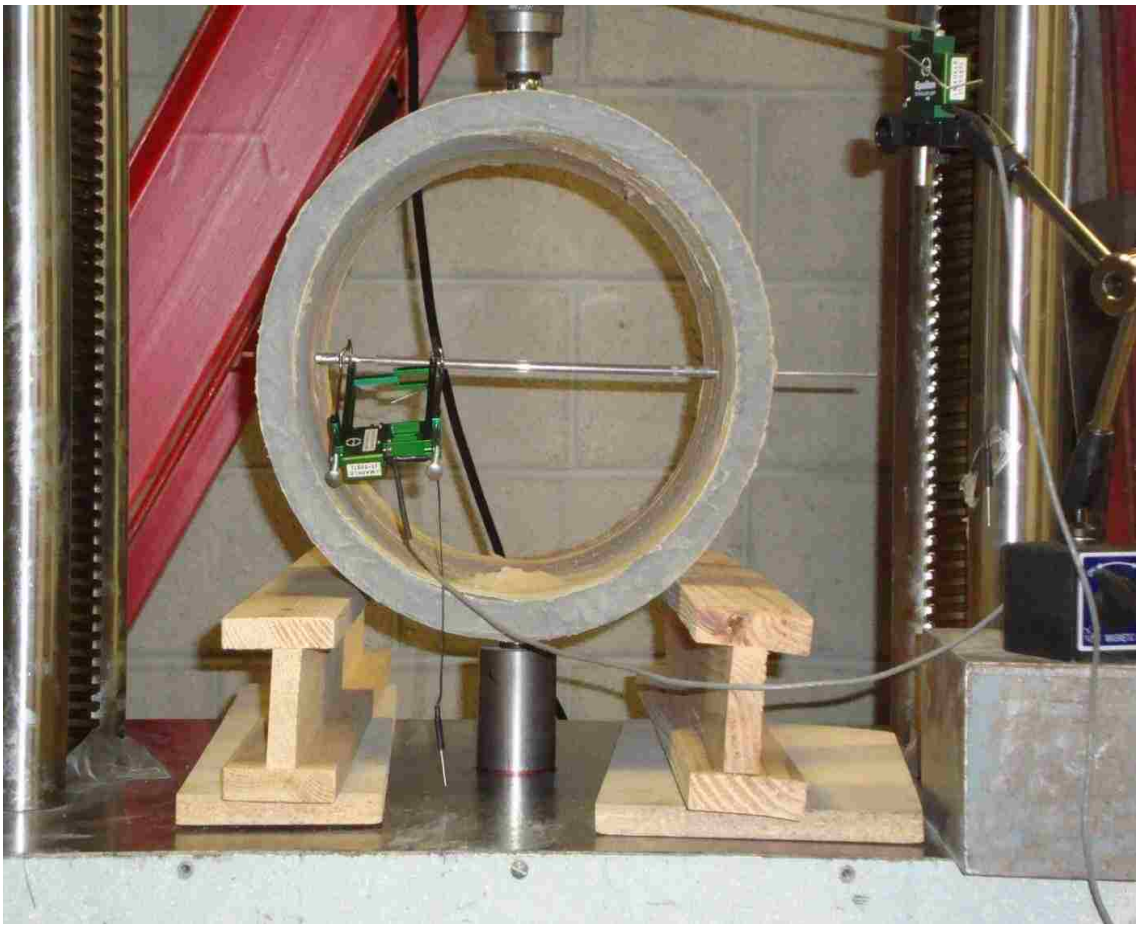

Figure 12.7: Test apparatus and specimen set up for circular cylindrical shells under pinching center loads

The test set up for circular cylindrical shells was assembled as follows (Figure 12.7):

1) One solid cylindrical steel stub/bar was placed on a strong testing base. A bearing ball was placed on the top of the steel bar where the partial shape of the bearing was milled out.
2) The circular cylindrical shell was placed on the solid cylindrical steel stub/bar and bearing ball assembly in such a way that the center of the circular cylindrical shell is aligned with the center of the bearing ball. Temporary support was provided to hold the circular cylindrical shell in place.

www.manaraa.com

3) One bearing ball, part of the load assembly, was placed on the top side and center of the circular cylindrical shell.
4) The load cell was lowered enough to just engage the circular cylindrical shell. Both horizontal and vertical extensometers were set up. The horizontal extensometer was place inside the circular cylindrical shell. It was clamped at one end to the solid bar and at the other end to the hollow tube, which are part of the horizontal deflection measurement apparatus. Before the actual loading process started: the circular cylindrical shell, supports, the entire test set up and all contact surfaces were checked for any kind of rocking. All temporary supports were removed.
5) Finally, the load was applied at a steady rate of 0.03 – 0.05 mm/minute (0.001 – 0.002 in. /minute) till the first major failure or crack occurred and increased to 0.08 – 0.20 mm/minute (0.003 – 0.008 in. /minute) till complete failure of the specimen.

The HSSFRC cylinders, which were cast from the same concrete mixture used for shells, were tested for compressive and splitting tensile strength according to the test procedures that are presented in Sections 4.4.1 and 4.4.4, respectively. During the testing process for cylinders and shells: load, deflection and strain data were collected; failure and failure modes were noted.

www.manaraa.com

12.6 Experiment results for circular cylindrical shells under pinching load

12.6.1 Load versus deflection results

Load versus vertical and horizontal deflection data were collected for HSSFRC circular cylindrical shells, with 0%, 1% to 2% steel fiber by volume fractions (SFVF), under concentrated center loads (pinching load). The vertical deflection was measured at the center of the circular cylindrical shell where the load was applied. The horizontal deflection was measured at the diameter perpendicular to the vertical axis. The average load versus vertical and horizontal deflection curves for 0%, 1% and 2% HSSFRC circular cylindrical shells under concentrated centers load are presented in Figures 12.8 and 12.9, respectively. Each load versus deflection curve represents an average result of three HSSFRC circular cylindrical shell specimens for each SFVF, a total of nine specimens for 0%, 1% and 2% SFVF. Table 12.2, presents the peak concentrated load, vertical deflection of the circular cylindrical shell at the peak load and maximum deflection of the circular cylindrical shell at complete failure for 0%, 1% and 2% SFVF. Values in Table 12.2 were obtained from load versus vertical deflection curves in Figure 12.8.

www.manaraa.com

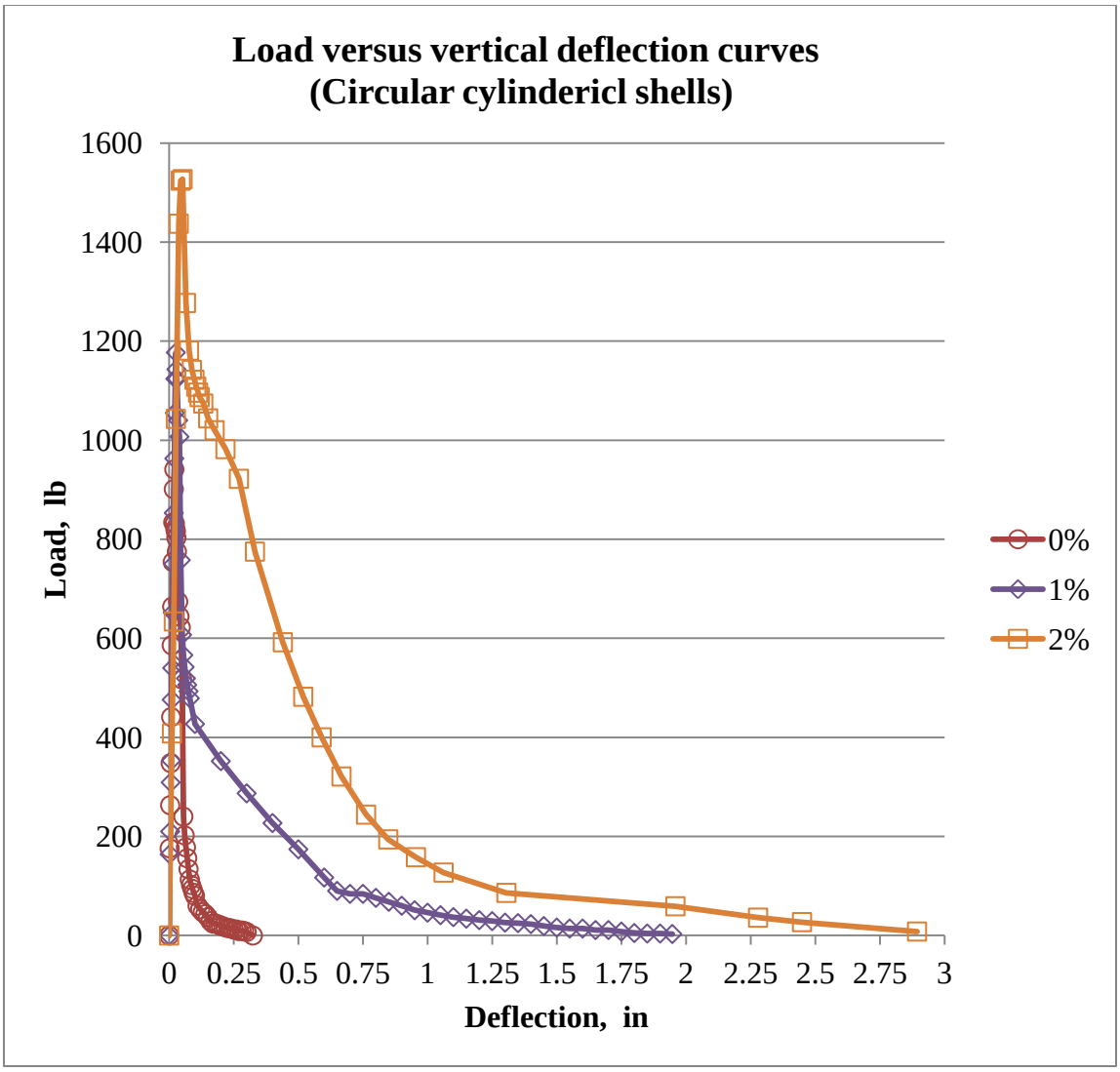

Figure 12.8: Load versus vertical deflection curves for 0%, 1% and 2% HSSFRC circular cylindrical shells under concentrated (pinching) center loads

www.manaraa.com

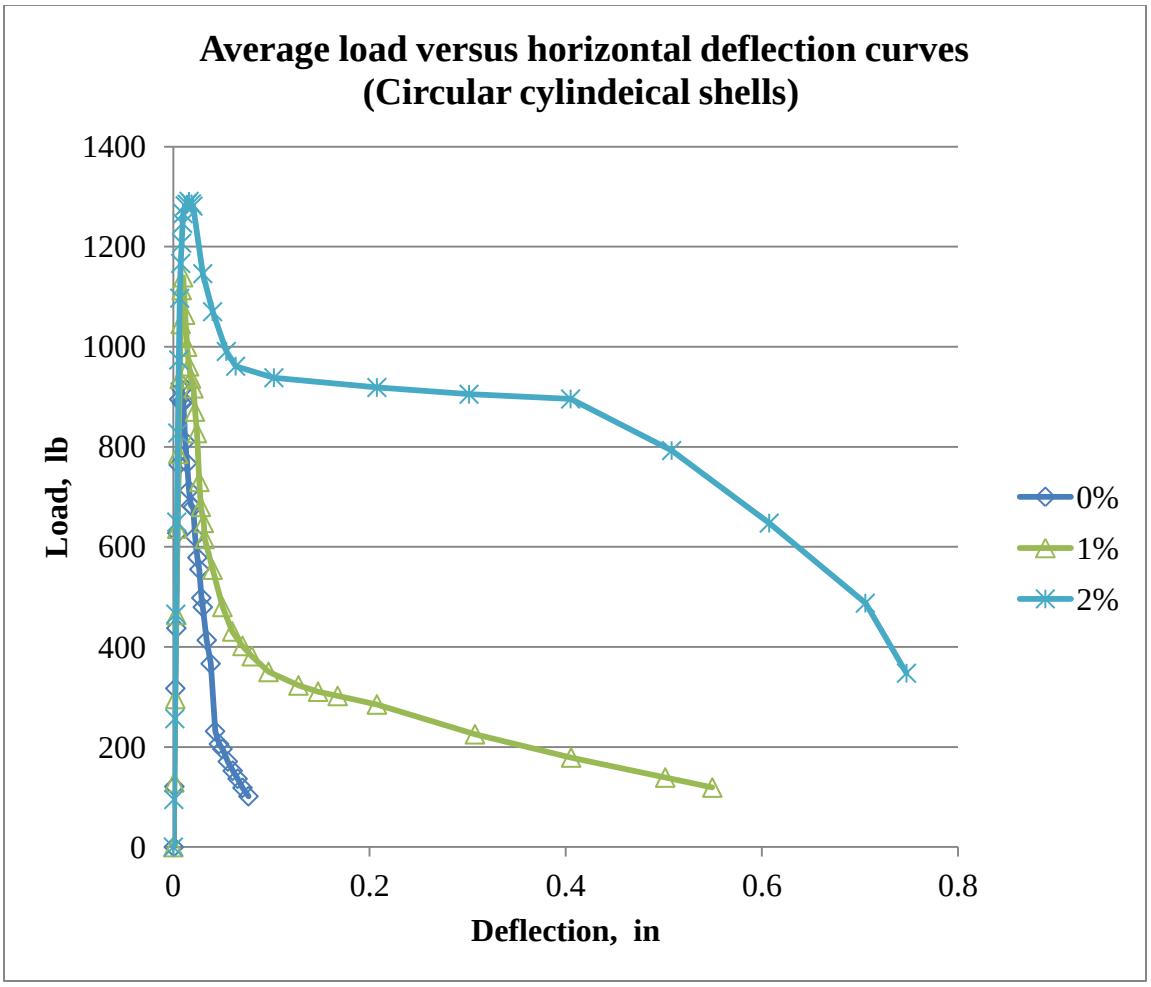

Figure 12.9: Average load versus horizontal deflection curves for 0%, 1% and 2% HSSFRC circular cylindrical shells under concentrated (pinching) center loads

www.manaraa.com

Table 12.2: Maximum load and vertical deflection results for 0%, 1% and 2% HSSFRC circular cylindrical shells under concentrated center (pinching) loads

Shell	P_{Max} N (lb)	Percentage increase in load	Δ at P_{Max} mm (in.)	$\Delta_{failure}$ mm (in.)	Percentage increase in deflection	$\Delta_{failure}/\Delta$
0%	4,186 (941)	0%	0.51 (0.020)	8.20 (0.323)	0%	16.15
1%	5,334 (1,199)	27%	0.69 (0.027)	47.90 (1.886)	484%	69.85
2%	6,793 (1,527)	62%	1.32 (0.052)	73.51 (2.894)	796%	55.65

Where: P_{Max} = peak concentrated load, N (lb.)

Δ = shell vertical deflection corresponding to the peak load, mm (in.)

$\Delta_{failure}$ = maximum deflection of the shell at complete failure, mm (in.).

12.6.2 Test results of strain gages

The location and layout of the strain gages on the circular cylindrical shells are presented in Section 12.4. The strain measured along the length of the circular cylindrical shell and close to the point of load application was labeled as "e1". The load versus strain (e1) curves for 0%, 1% and 2% HSSFRC circular cylindrical shells are presented in Figure 12.10. The strain along the perimeter of the circular cylindrical shell and close to the point of load application but perpendicular to "e1" was labeled as "e2". The load

www.manaraa.com

versus strain (e2) curves for 0%, 1% and 2% HSSFRC circular cylindrical shells are presented in Figure 12.11. The strain along the perimeter of the circular cylindrical shell and at mid height and parallel to "e2" was labeled as "e3". The load versus strain (e3) curves for 0%, 1% and 2% HSSFRC circular cylindrical shells are presented in Figure 12.12. Strains "e1" and "e2" are continuously in compression while strain "e3" is continuously in tension.

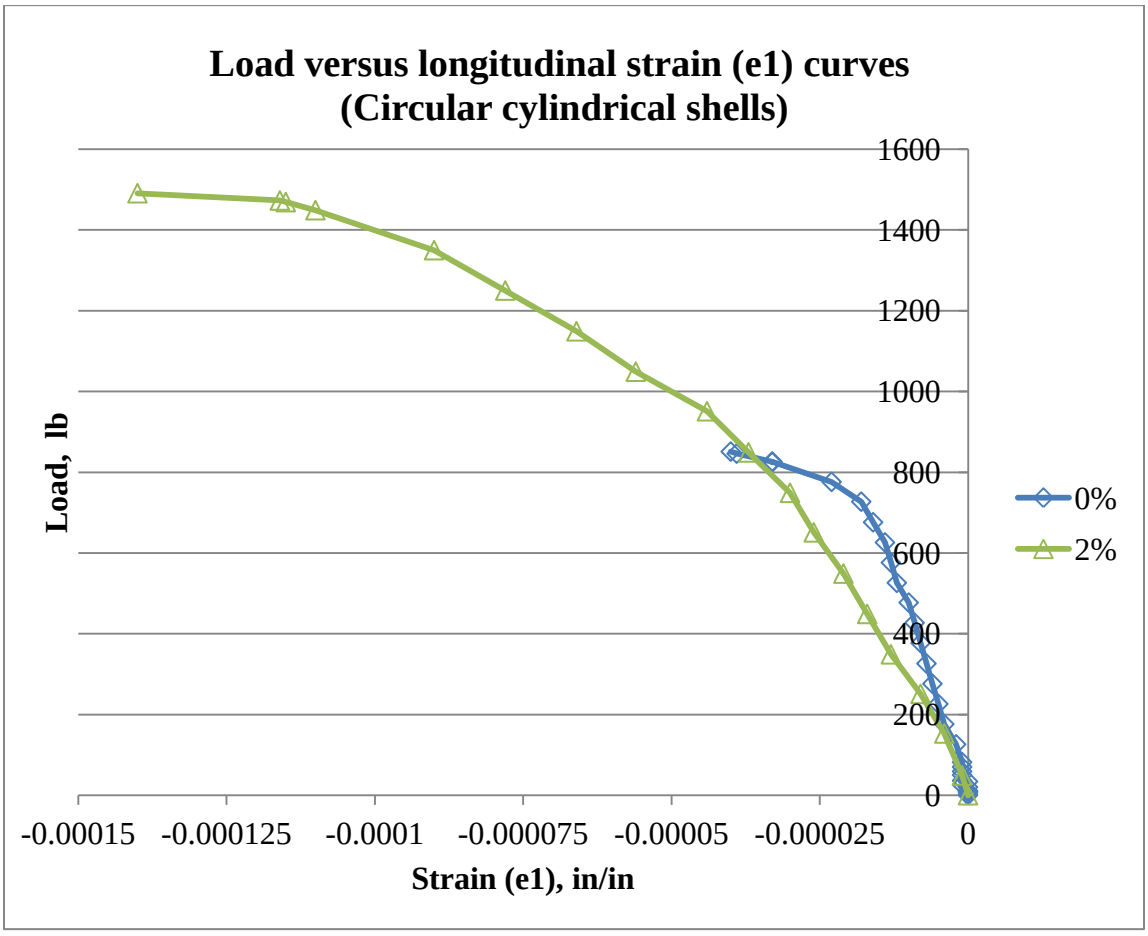

Figure 12.10: Load versus longitudinal strain (e1) results for 0%, 1% and 2% HSSFRC circular cylindrical shells under concentrated center (pinching) loads

www.manaraa.com

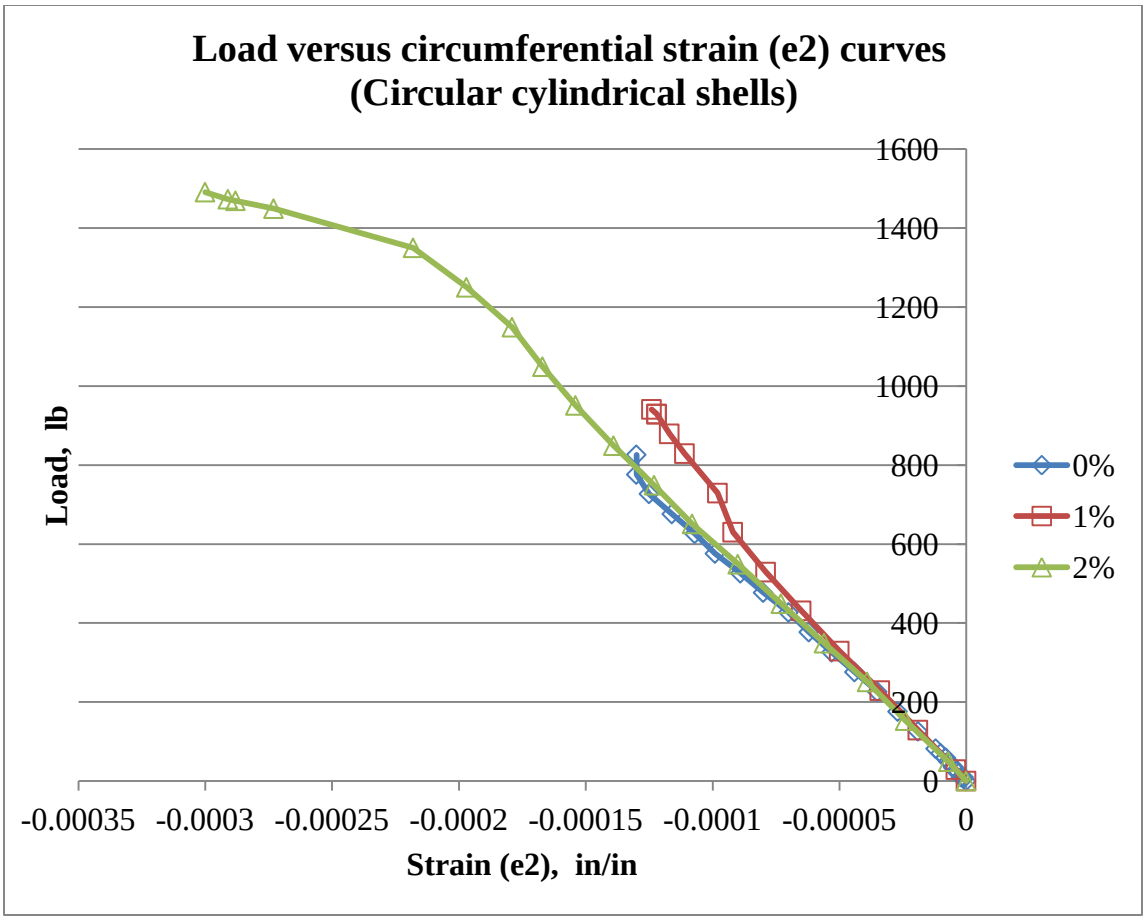

Figure 12.11: Load versus circumferential strain (e2) results for 0%, 1% and 2% HSSFRC circular cylindrical shells under concentrated center (pinching) loads

www.manaraa.com

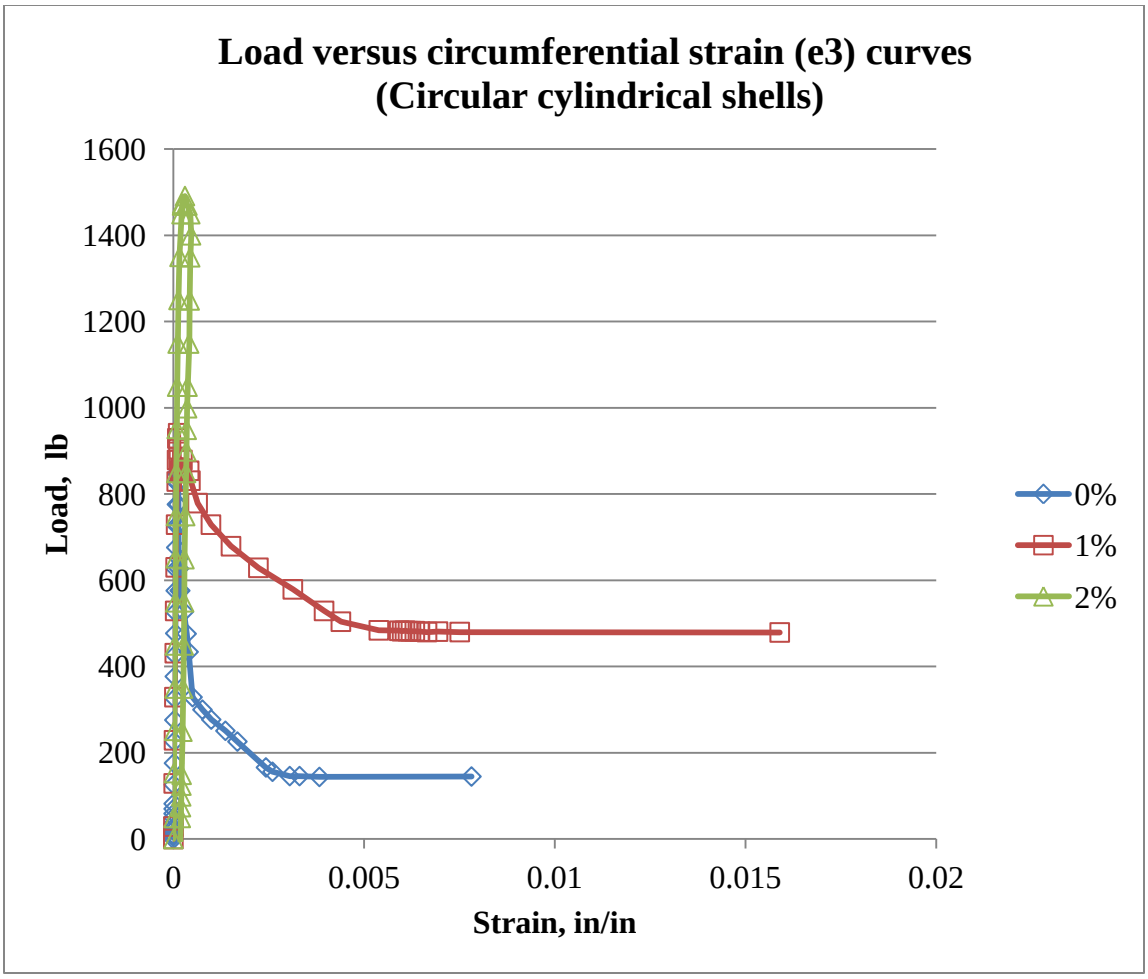

Figure 12.12: Load versus circumferential strain (e3) results for 0%, 1% and 2% HSSFRC circular cylindrical shells under concentrated center (pinching) loads

12.6.3 Cylinder compressive strength test results

12.6.3.1 Longitudinal strain and modulus of elasticity of HSSFRC cylinders

As indicated in previous section, HSSFRC cylinder specimens that were used for compressive strength test were prepared from the same batch of concrete the corresponding circular cylindrical shells were made from. The cylinders were tested, for compressive strength, within 24 hours of testing the corresponding circular cylindrical

www.manaraa.com

shells. During the testing process applied compression load and the corresponding longitudinal and transverse strains of cylinders were recorded.

The average compressive stress versus longitudinal strain curves for 0%, 1% and 2% high strength steel fiber reinforced concrete cylinders are presented in Figure 12.13.

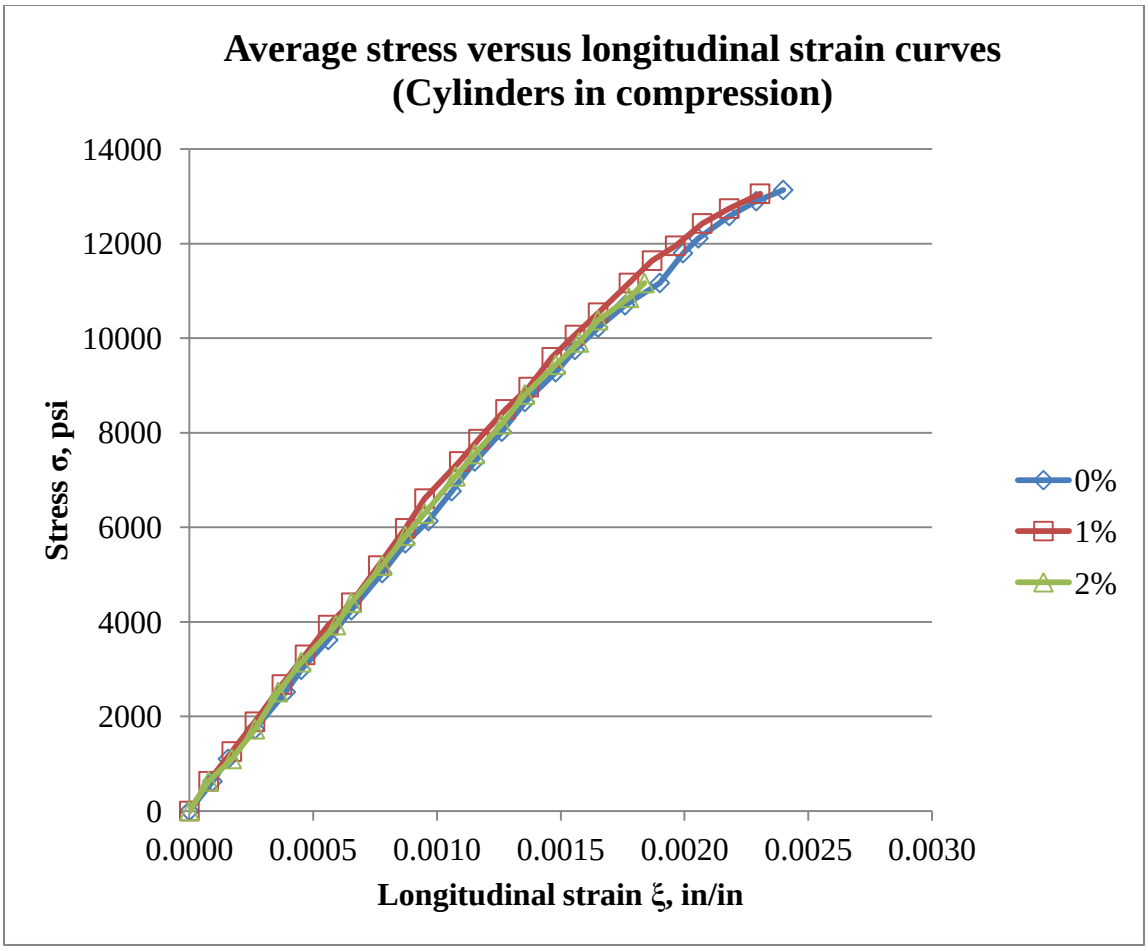

Figure 12.13: Average compressive stress versus longitudinal strain curves for 0%, 1% and 2% HSSFRC cylinders (4 in. x 8 in.) casted with circular cylindrical shells

The average compressive strength and modulus of elasticity test results for 0%, 1% and 2% high strength steel fiber reinforced concrete cylinders under compression load are

www.manaraa.com

presented in Table 12.3. The compressive strength and modulus of elasticity results were calculated using procedures in Sections 4.4.1 and 4.4.2, respectively.

Table 12.3: Average compressive strength and modulus of elasticity for 0%, 1% and 2% HSSFRC cylinders (4 in. x 8 in.) casted with circular cylindrical shell

Cylinder	Compressive strength MPa (psi)	Percentage increase from 0% steel fiber	Modulus of elasticity MPa (ksi)	Percentage increase from 0% steel fiber
0%	93		44,761	
	(13,448)	0%	(6,492)	0%
1%	92		47,251	
	(13,400)	0%	(6,853)	5.6%
2%	90		45,454	
	(13,065)	-3%	(6,593)	1.5%

12.6.3.2 Transverse strain and Poisson's ratio of HSSFRC cylinders

The average compressive stress versus transverse strain curves for 0%, 1% and 2% HSSFRC cylinders are presented in Figure 12.14 while, compressive stress versus Poisson's ratio curves of 0% and 2% HSSFRC cylinders are shown in Figure 12.15. The Poisson's ratio results for 0% and 2% HSSFRC cylinders were calculated using procedures in Section 4.4.3. The Poisson's ratio curves in Figure 12.15 show that 0% and

www.manaraa.com

2% HSSFRC cylinders responded in similar fashion and converged to the same values at the higher end of the stress range.

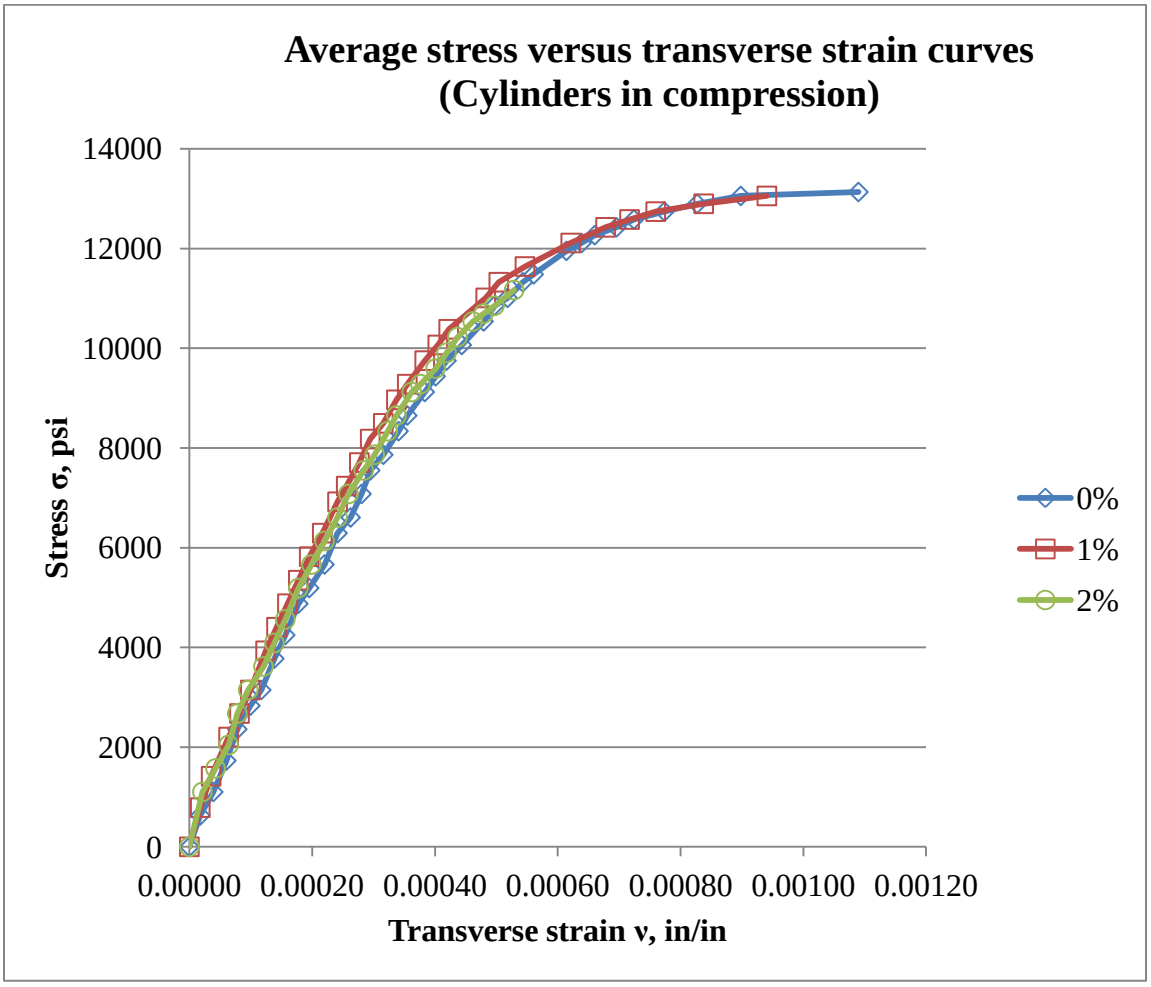

Figure 12.14: Average compressive stress versus transverse strain curves for 0%, 1% and 2% HSSFRC cylinders (4 in. x 8 in.) casted with circular cylindrical shells

www.manaraa.com

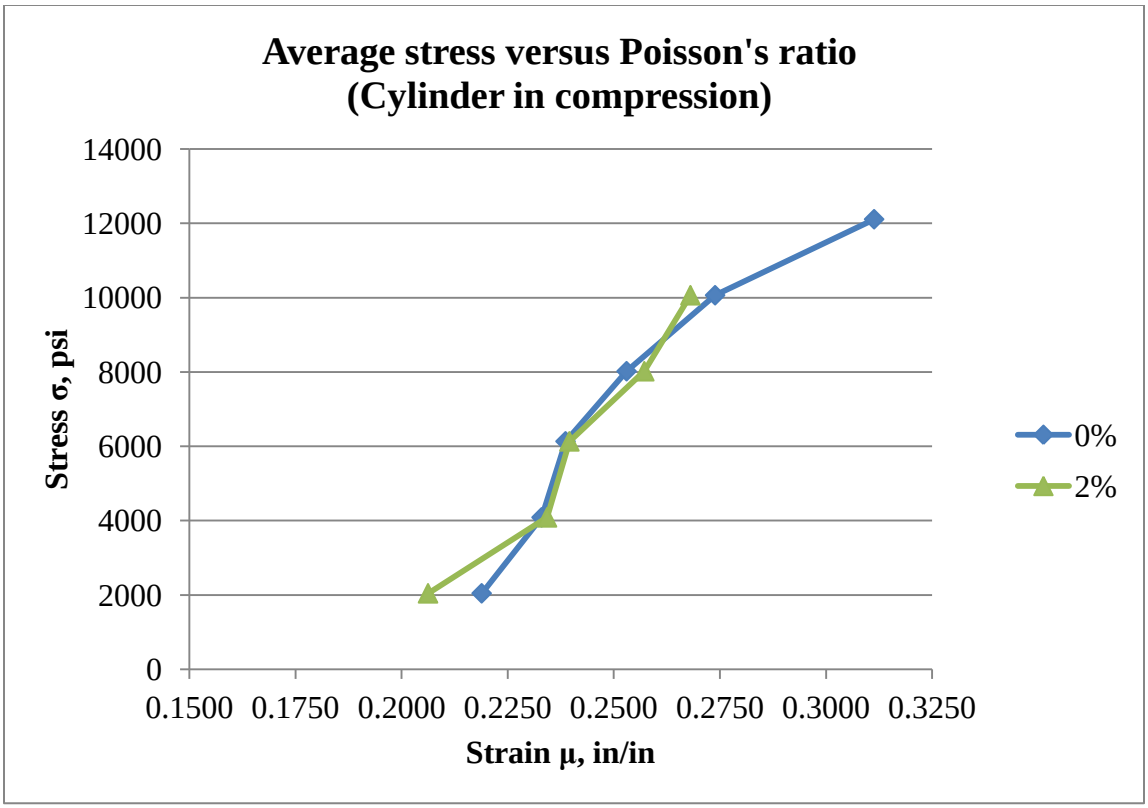

Figure 12.15: Average compressive stress versus Poisson's ratio curves for 0% and 2% HSSFRC cylinders (4 in. x 8 in.) casted with circular cylindrical shells

12.6.4 Cylinder splitting tensile strength results

The average splitting tensile strength test results for 0%, 1% and 2% high strength steel fiber reinforced concrete cylinders are presented in Table 12.4 and Figure 12.16. Splitting tensile strength results were computed using Equation 4.3. The splitting tensile strength of HSSFRC cylinders increased as the SFVF increased.

www.manaraa.com

Table 12.4: Average splitting tensile strength results for 0%, 1% and 2% HSSFRC cylinders (4 in. x 8 in.) casted with circular cylindrical shells

Cylinder	Splitting tensile strength MPa (psi)	Percentage increase from 0% steel fiber	Splitting tensile to compression strength ratio
0%	7.53		
	(1,092)	0%	0.08
1%	10.30		
	(1,495)	37%	0.11
2%	10.98		
	(1,592)	46%	0.12

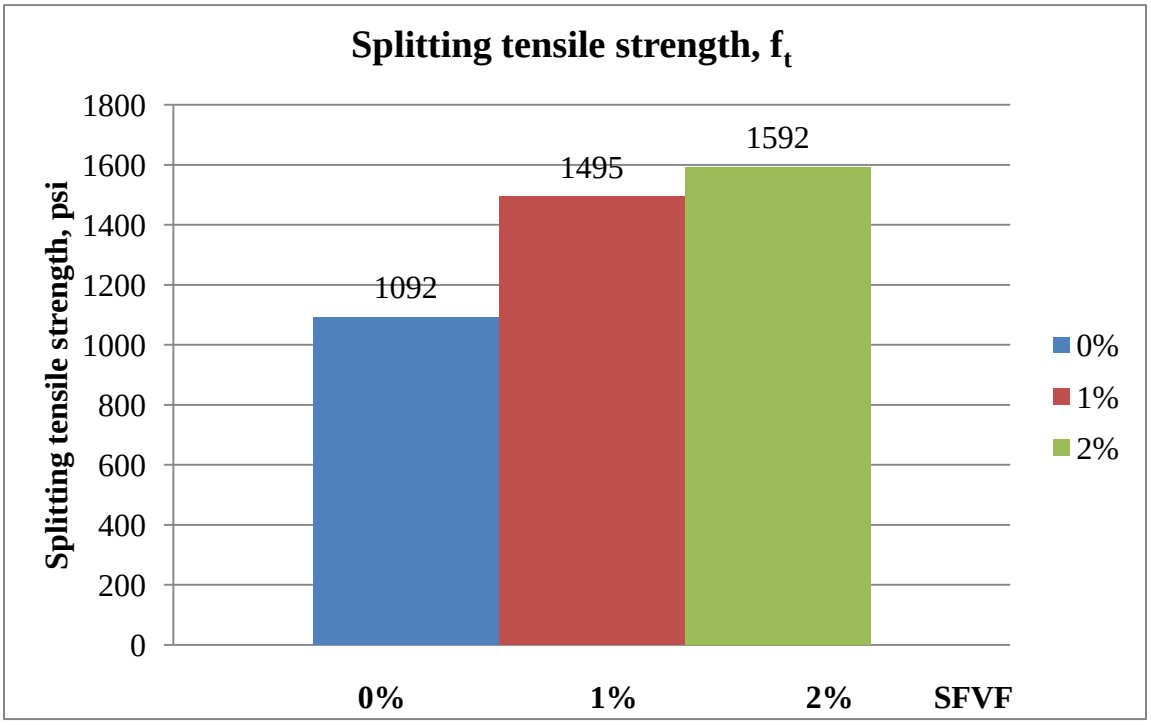

Figure 12.16: Average splitting tensile strength results for 0%, 1% and 2% HSSFRC cylinders (4 in. x 8 in.) casted with circular cylindrical shells

www.manaraa.com

12.7 Stress-strain analysis and test results

Longitudinal strain at first crack and the corresponding strain and calculated stress results for 0%, 1% and 2% HSSFRC circular cylindrical shells are presented in Table 12.5. Stress results for the circular cylindrical shells were calculated using Equation 8.3 in Section 8.1.2 and modulus of elasticity values from cylinders in compression. The flexural stresses at first noticeable crack, as shown in Table 12.5, are comparable to the spitting tensile stress results of HSSFRC cylinders.

Table 12.5: Stress–strain results for 0%, 1% and 2% HSSFRC circular cylindrical shells at first crack under concentrated center (pinching) load

Shell	Load N (lb)	f_t MPa (psi)	Strain (Measured) ε_x (10^{-6})	Stress, σ_x (Calculated) MPa (psi)
0%	4,115 (925)	7.53 (1,092)	117	5.62 (815)
1%	4,502 (1,012)	10.30 (1,495)	128	6.49 (941)
2%	6,748 (1,517)	10.98 (1,592)	225	10.98 (1,591)

Where: P = applied pinching center load at first noticeable crack, lb

f_t = splitting tensile strength of HSSFRC cylinders (from Table 12.4), psi

www.manaraa.com

ε_x, ε_y = measured longitudinal and transverse strains of the circular cylindrical shells, in/in

σ_x = calculated circumferential stress along perimeter of the circular cylindrical shells, psi.

12.8 Failure modes

The load versus deflection curves in Figures 12.8 and 12.9 showed that HSSFRC circular cylindrical shells under pinching center loads responded elastically till the first crack load (peak load) was reached. Once the first crack load (peak load) of the circular cylindrical shells was reached, the resistance to the load decreased gradually for 2% SFVF, but 58% and 34% loss of resistance for 0% and 1% SFVF, respectively. In Figure 12.8, load versus deflection curves, all three HSSFRC circular cylindrical shells showed almost identical response for most part of the elastic range despite the variation in SFVF. During the test, there was no sign of crushing of concrete neither at the point of load application nor at support location due to the concentrated nature of the load and support system.

The 0%, 1% and 2% HSSFRC circular cylindrical shells exhibited the following behaviors:

- Cracks appear to occur as the first crack load (peak load) was reached followed by 58%, 34% and 2% loss of resistance for 0%, 1% and 2% SFVF, respectively.
- Slow loss of resistance after the initial failure.
- Sequence of failure process was as follows:

www.manaraa.com

1. First crack to emerge was at the point of load application. The crack appeared on the inside surface of the shell.
2. The crack propagated from the center towards the edges, on both directions along the length, as the loading process continued.
3. After substantial vertical deflection of the shell, cracks developed on the left and right mid-height of the shell near plane of load application. The cracks appeared on the outside surface of the shell.
4. The crack propagated from the center towards the edges, on both directions along the length, as the loading process continued.
5. Near the end of the loading process, the cracks crossed over from the inside to the outside surfaces at the top and bottom section of the shell; and from the outside to inside surfaces on the left and right mid-height section of the shell.
6. As the process of loading continued the original circular shape of the shell assumed an oval shape.
7. Near the very end of the test, the top and bottom end of the shell flattened in addition to having an oval shape.

- At the end of the test process, 1% and 2% SFVF circular cylindrical shells remained in one piece however cracked, twisted and buttered. 0% SFVF circular cylindrical shells however, reduced into four pieces. Refer to Figures 12.17 through 12.20 for failure and crack patterns of 0%, 1% and 2% HSSFRC circular cylindrical shells.
- Maximum crack width were 3.8 mm (0.15 in.), 6.1 mm (0.24 in.) and 6.6 mm (0.26 in.) on the outside surface of the shell at mid-height and 3.3 mm (0.13 in.),

www.manaraa.com

5.8 mm (0.23 in.), and 6.4 mm (0.25 in.) on the inside surface of the shell at the point of load application for 0%, 1% and 2% HSSFRC circular cylindrical shells, respectively.

- The test duration for 0% HSSFRC circular cylindrical shells was on average 90 minutes, a lot shorter than for 1% and 2% SFVF specimens, which were 195 and 275 minutes, respectively.
- The unique behavior exhibited by 2% HSSFRC circular cylindrical shells were:
    a. The ability of the shell to distribute the failure plane by formation of tributaries of small cracks as the test processed than a formation of one large failure plane.
    b. The ability of the specimen to absorb large amount of energy right after the initial failure dropping only 4% in load resistance followed by a plateau and gradual degradation of resistance.

www.manaraa.com

Figure 12.17: Shape and condition of 0% HSSFRC circular cylindrical shells, just before failure, subjected to concentrated center (pinching) loads

www.manaraa.com

Figure 12.18: Crack and failure patterns for 0% HSSFRC circular cylindrical shells under concentrated center (pinching) loads

www.manaraa.com

Figure 12.19: Crack and failure patterns for 1% HSSFRC circular cylindrical shells under concentrated center (pinching) loads

www.manaraa.com

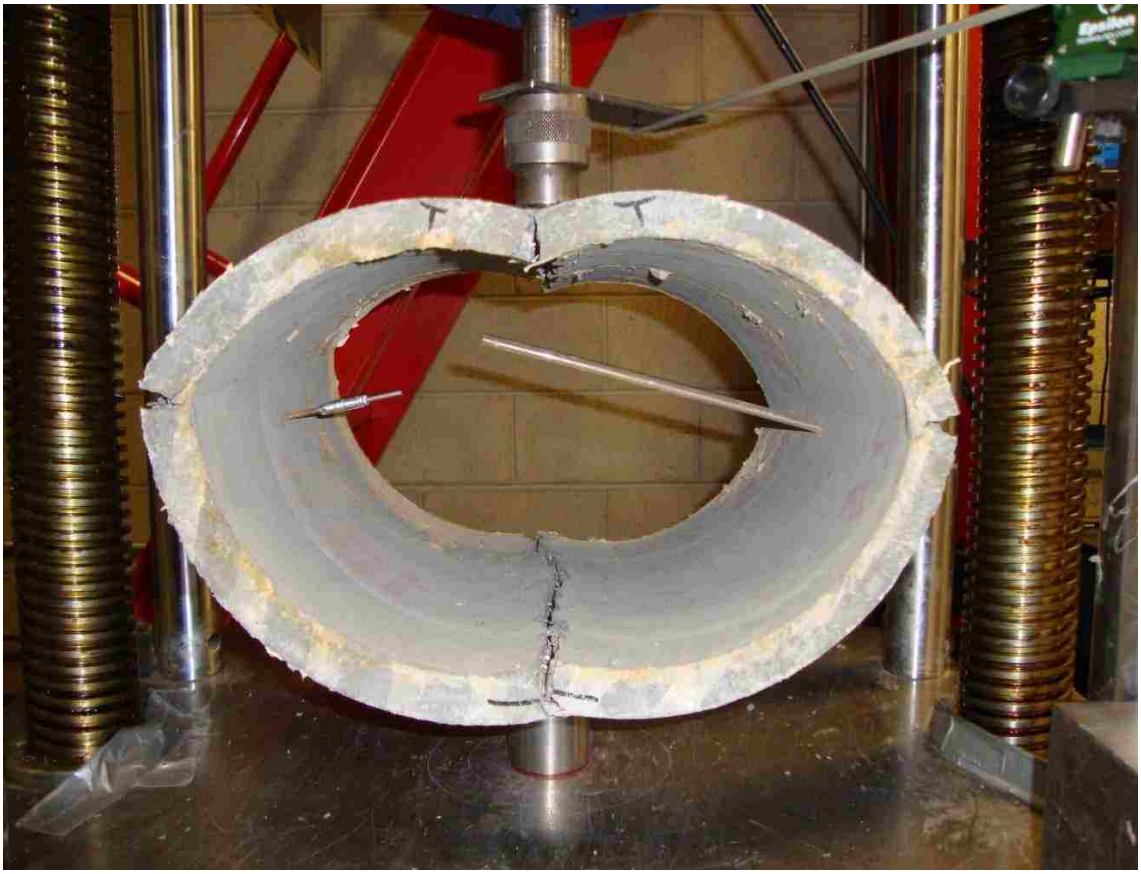

Figure 12.20: Crack and failure patterns for 2% HSSFRC circular cylindrical shells under concentrated center (pinching) loads

www.manaraa.com

12.9 Energy absorption (toughness)

The energy absorption (toughness), the area under the load versus deflection curves, for 0%, 1% and 2% HSSFRC circular cylindrical shells were calculated as 45, 234 and 573 in-lb, respectively. The load versus deflection curves are shown in Figure 12.8. The energy absorption of HSSFRC circular cylindrical shells increased as the steel fiber content increased: 420% and 1,173% for 1% and 2% SFVF shells, respectively over the 0% SFVF shells.

12.10 Discussion of test results

12.10.1 Load versus deflection

The capacity of HSSFRC circular cylindrical shells to accommodate concentrated center (pinching) loads increased as the steel fiber by volume fraction (SFVF) increased from 0% through 2%. The capacity of HSSFRC circular cylindrical shells increased by 27% and 62% for 1% and 2% SFVF, respectively from 0% (plain) HSSFRC circular cylindrical shells.

The ultimate vertical and horizontal deflection of the HSSFRC circular cylindrical shells increased as the SFVF increased from 0% to 1% and 2%. Even though, the deflection at which all SFVF circular cylindrical shells initially cracked was similar for 0% and 1% SFVF, the final deflection at which the circular cylindrical shells completely failed were different by a large margin. Higher ultimate vertical and horizontal deflection values were exhibited by the higher SFVF, which is 2%. The total vertical deflection of HSSFRC circular cylindrical shells increased by 484% and 796% for 1% and 2% SFVF, respectively compared to 0% (plain) HSSFRC circular cylindrical shells.

www.manaraa.com

The ductility of HSSFRC circular cylindrical shells increased as the SFVF increased from 0% to 1% and 2%. The ratio of circular cylindrical shells vertical deflection at complete failure to the vertical deflection at first crack increased from 16.15 for 0% to 69.85 and 55.65 for 1% and 2% SFVF, respectively.

12.10.2 Splitting tensile strength, modulus of elasticity, compressive strength and Poisson's ratio for HSSFRC cylinders

The Splitting tensile strength of HSSFRC cylinders increased by 37% and 46% for 1% and 2% SFVF, respectively compared to 0% (plain) HSSFRC cylinders.

The young's modulus values for 0% through 2% HSSFRC cylinders remained roughly close within ±5.6%.

The compressive strength results, for all three SFVF were within ±3.0%. Therefore, the variation in young's modulus and compressive strength results due to the addition of steel fibers was very small, almost flat. It can be concluded that, the addition of steel fibers to the plain concrete mixture did not affect the behavior of HSSFRC circular cylindrical shells with respect to young's modulus and compressive strength in this case. However, it should be stresses that the amount of High Range Water Reducer (HRWR) suitable for 0% mixture was used to prepare all 0%, 1% and 2% concrete mixtures. The effect of HRWR on young's modulus and compressive strength are shown in Phase (1b) of the research.

The stress versus strain curves for HSSFRC cylinders in compression showed curves for 0%, 1% and 2% SFVF samples being closely similar within the elastic range.

www.manaraa.com

The Poisson's ratio curves for all three SFVF cylinders exhibited similar shape response and converged as the stress level increased.

12.10.3 Flexural strains

Flexural strains "e1" and "e2", close to the point of load, were consistently in compression till peak load was reached. Circumferential strain "e3" was consistently in tension till peak load was reached and stayed in tension afterwards. 1% SFVF specimen showed stiffer response that 0% and 2% specimens; this could be due to the effect of HRWR used.

12.10.4 Analysis results

The maximum experimental tensile stress results correspond to the splitting tensile strength of the HSSFRC 0%, 1% and 2% SFVF circular cylindrical shells. With respect to pre-crack behavior, the strains for 0%, 1% and 2% HSSFRC circular cylindrical shells were linear and fell on the same slope. The theoretical elastic deflection results, for all three SFVF, are consistently smaller than the experimental values. Theoretical deflection formulas tend to overestimate the stiffness of the shells.

12.10.5 Energy absorption (Toughness)

The area under the load versus deflection curves indicated that, HSSFRC circular cylindrical shells with higher steel fiber by volume fraction (SFVF) exhibited higher energy absorption capacity (toughness) than the lower SFVF shells.

www.manaraa.com

CHAPTER 13

HIGH STRENGTH STEEL FIBER REINFORCED CONCRETE HYPERBOLIC PARABOLOID SHELLS SIMPLY SUPPORTED AT FOUR SIDES AND UNDER A UNIFORMLY DISTRIBUTED LOAD

13.1 Introduction

In this chapter the behavior of simply supported high strength steel fiber reinforced concrete (HSSFRC) hyperbolic paraboloid shells with 0%, 1% and 2% steel fiber by volume fractions (SFVF) subjected to a uniformly distributed load is presented. A hyperbolic paraboloid shell carries the entire distributed load, initially, in constant in-plane shear. Therefore, the in-plane shear behavior of HSSFRC hyperbolic paraboloid shells with various steel fiber by volume fractions is studied. However, at ±45° from the edges, stress transformations result in tensile and compressive stress fields orthogonal to each other and equal in intensity to the shear stress. The in-plane stress condition discussed is due to the membrane theory of hyperbolic paraboloid shells and applies only to loads that produce stresses in the linear range of the shear stress – shear strain diagram for the shells well below cracking stresses. When the stresses exceed their linear range, moments – M_x, M_y, M_{xy} and vertical shears Q_x and Q_y will develop and the resulting failure mode is due to a combination of stresses from the in-plane shear and flexural stresses as will be amply discussed at the end of the chapter.

All constituents for the three types of concrete mixtures (0%, 1% and 2% SFVF), used for the making of shells and cylinders, are the same except for the content of steel

www.manaraa.com

fibers. The thin hyperbolic paraboloid shells have a projected length and width of 508 mm (20 in.) and thickness of 32 mm (1.25 in.). The shells have two adjacent straight edges and two tilted ones with a pitch of 95 mm (3.75 in.). The shells are simply supported at all sides by a metal support with projected dimensions of 457 mm (18 in.) long by 457 mm (18 in.) wide and a pitch of to match the shell, as shown in Figure 13.1.

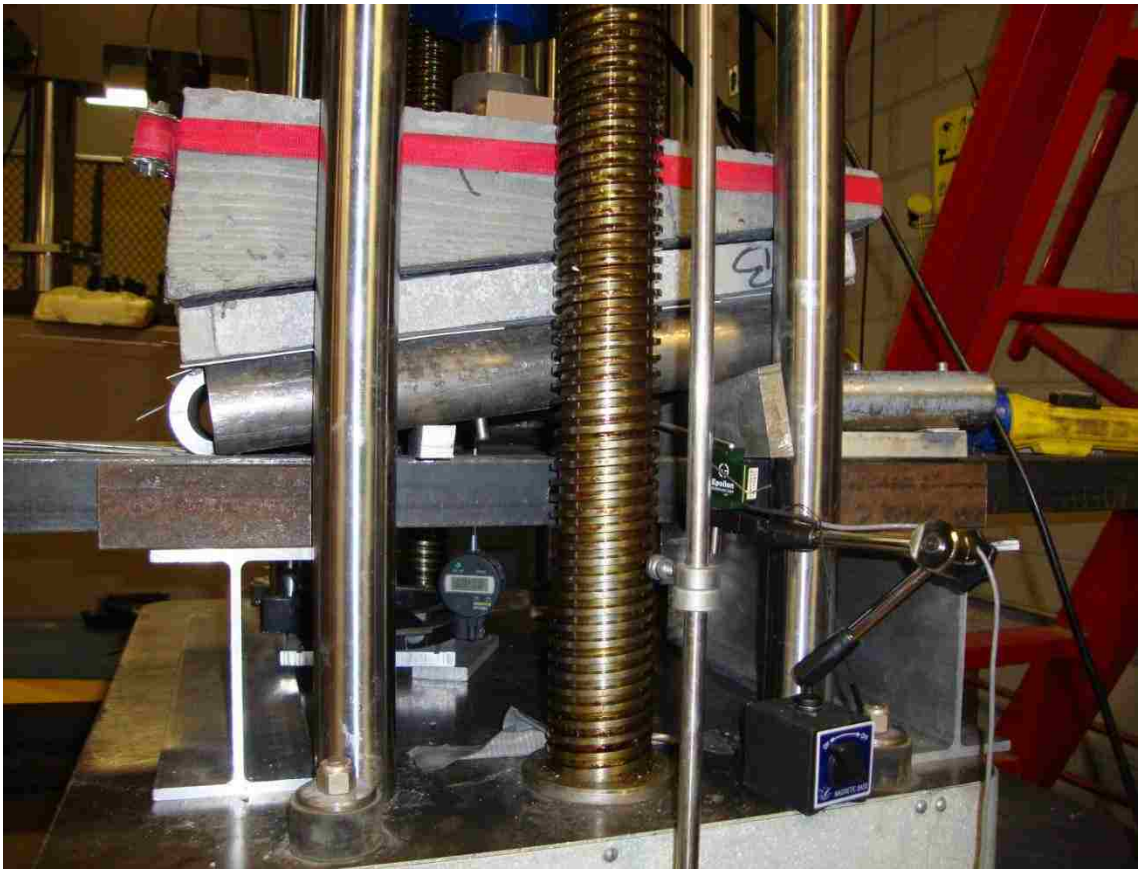

Figure 13.1: Test set up for HSSFRC Hyperbolic paraboloid shell structure subjected to a vertically applied uniformly distributed load, showing the steel supports and silica sand inside the concrete ring

Two rosette strain gages, for each type of steel fiber by volume fraction mixture, are placed on the hyperbolic paraboloid shell surfaces. The first rosette is placed at the center

www.manaraa.com

bottom surface of shell #1 and the second rosette is placed at mid-span bottom surface of shell #2 close to the flat support.

The chapter presents HSSFRC hyperbolic paraboloid shell specimen preparation, testing procedures and experiment results such as load versus deflection, load versus flexural strain and stress and mode of failure of hyperbolic parabolic shells. The chapter discusses the influence of steel fibers on: flexural and shear capacity, mode of failure and ductility of thin shells; and modulus of elasticity, compression and splitting tensile strength of cylinders prepared from the same mixtures used for the making of shells.

Comparisons are made between hyperbolic parabolic shells with various steel fiber by volume fractions with respect to the mechanical properties such as flexural capacity, deflection, ductility, and mode of failure. The elastic analysis results corresponding to the first crack load such as stress, strain and deflection are presented. Test results are discussed and conclusions drown.

13.2 Theoretical background of hyperbolic paraboloid shells under a uniformly distributed load

The governing differential equation for membrane forces of shells using stress function is (Timoshenko 1987) (page 461-465)

$$\frac{\partial^2 F}{\partial x^2}\frac{\partial^2 z}{\partial y^2} - 2\frac{\partial^2 F}{\partial x\,\partial y}\frac{\partial^2 z}{\partial x\,\partial y} + \frac{\partial^2 F}{\partial y^2}\frac{\partial^2 z}{\partial x^2} = q \qquad (13.1)$$

Refer to Figure 13.2 for forces acting on the shell membrane.

www.manaraa.com

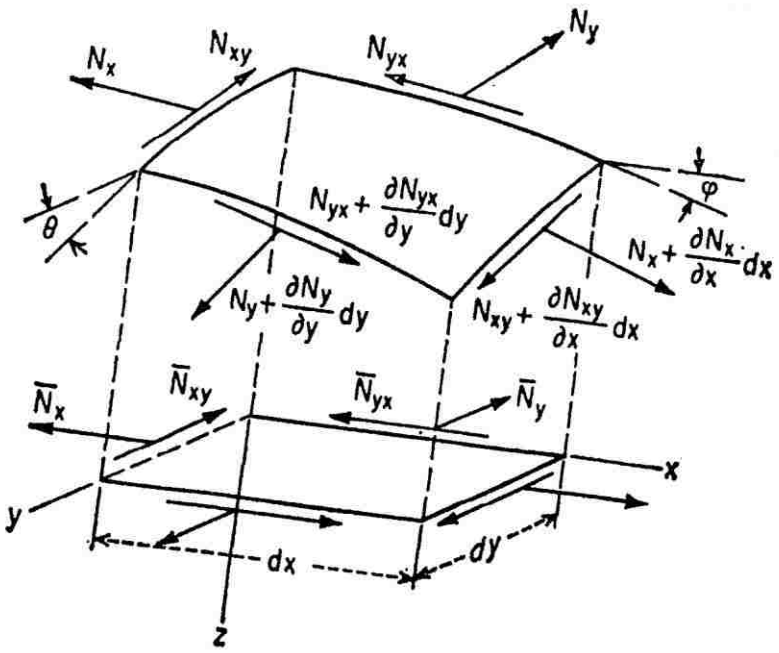

Figure 13.2: Forces acting on hyperbolic paraboloid shell

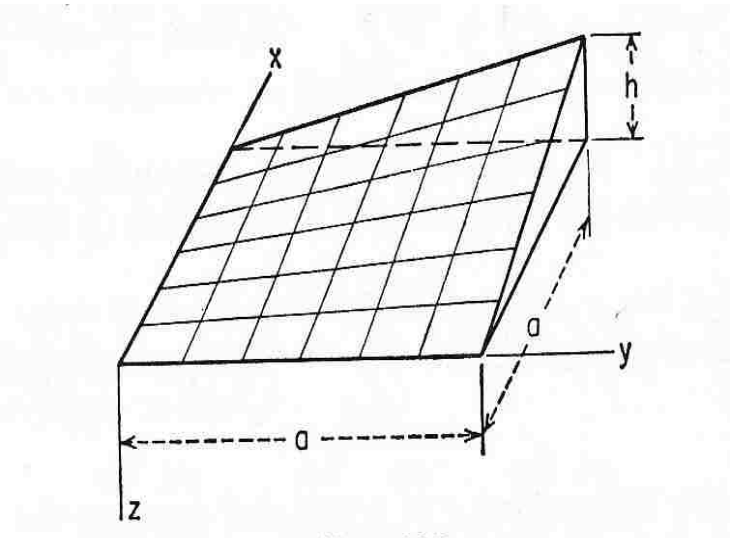

Figure 13.3: Hyperbolic paraboloid shell

www.manaraa.com

In case of hyperbolic paraboloid, where the middle surface is given by

$$z = -\frac{xy}{c} \tag{13.2}$$

and the origin of the coordinates are placed at the projected edge of the shell.

Hence,

$$\frac{\partial z}{\partial x} = -\frac{y}{c} \qquad \frac{\partial z}{\partial x} = -\frac{x}{c} \qquad \frac{\partial^2 z}{\partial x^2} = \frac{\partial^2 z}{\partial y^2} = 0 \qquad \frac{\partial^2 z}{\partial x\,\partial y} = -\frac{1}{c} \tag{13.3}$$

(a) For vertical loading,

$$\frac{2}{c}\frac{\partial^2 F}{\partial x\ \partial y} = q \tag{13.4}$$

Which yields,

$$N_{xy} = \frac{qc}{2} = \frac{qa^2}{2h} \quad \text{and} \quad N_x = N_y = 0, \text{every where} \tag{13.5}$$

(b) Considering shell own weight,

$$N_{xy} = \frac{q_o}{2}\sqrt{x^2 + y^2 + c^2} \tag{13.6}$$

$$\overline{N}_x = -\frac{q_o y}{2}\log\frac{x + \sqrt{x^2 + y^2 + c^2}}{\sqrt{y^2 + c^2}} \tag{13.7}$$

$$\overline{N}_y = -\frac{q_o x}{2}\log\frac{y + \sqrt{x^2 + y^2 + c^2}}{\sqrt{x^2 + c^2}} \tag{13.8}$$

Where: F = Stress function, F(x,y)

$c = a^2/h$

q = uniformly distributed vertical loading over the shell horizontal projection

q_o = shell own weight

www.manaraa.com

$N_x = \bar{N}_x . \cos \theta / \cos \varphi$

$N_y = \bar{N}_y . \cos \varphi / \cos \theta$

$N_{xy} = \bar{N}_{xy}$

$\varphi = \tan^{-1} \frac{\partial z}{\partial x}$

$\theta = \tan^{-1} \frac{\partial z}{\partial y}$

h = rise on one corner of the shell over its projected plane, Figure 13.3.

13.3 Preparation of test specimens - cylinders and hyperbolic paraboloid shells

Two types of test specimens, shells and plates, were prepared for each test (0%, 1% and 2% SFVF) from the same concrete batch:

- Three hyperbolic paraboloid shells for each SFVF with overall dimensions of 508 mm (20 in.) long by 508 mm (20 in.) wide, 32 mm (1.25 in.) thick and a pitch of 95mm (3.75 in.). Therefore, a total of nine shell specimens were prepared.
- Six 102 mm (4 in.) diameter by 203 mm (8 in.) long cylinders for each SFVF. Three cylinders each were used for compressive and splitting tensile strength tests, respectively. Therefore, a total of eighteen cylinders were prepared.

To form the hyperbolic paraboloid shells:

1. Two 32 mm (1.25 in.) thick wood strips were laid flat perpendicular to each other and nailed to a flat plywood base board, forming L-shaped base.
2. Two 508 mm (20 in.) long trapezoidal shaped plywood strips with heights of 32 mm (1.25 in.) at one end and 95 mm (3.75 in.) at the opposite end were prepared.

www.manaraa.com

3. The short ends of the trapezoidal wood strips were butted against the flat 32 mm (1.25 in.) thick wood strips at 508 mm (20 in.) from the corner of the L-shaped base. While, the tall ends of the trapezoidal wood strips were butted against each other to form an enclosed area of 508 mm (20 in.) by 508 mm (20 in.) at the base. The formwork would have two flat and two inclined edges.
4. All pieces were secured by nailing them to the base board.
5. HSSFRC was deposited inside the formwork and leveled with a metal bar. The metal bar was swung back and forth parallel to the flat side of the hyperbolic paraboloid form repeatedly, one flat side of the hyperbolic paraboloid form at a time, till smooth hyperbolic parabolic surface was obtained. This surface was labeled as surface #1.
6. Once the concrete was cured, it was covered with plastic film and encased by a wood formwork, 140 mm (5.5 in.) high, 508 mm (20 in.) long and 508 mm (20 in.) wide square prism.
7. HSSFRC was poured, on the top of the hyperbolic paraboloid surface #1, all the way to the top of the formwork to form hyperbolic paraboloid surface #2. The two surfaces needed to make the hyperbolic paraboloid formwork were now complete.
8. The two surfaces were aligned parallel to each other with a separation of 32 mm (1.25 in.). The hallow space created between the two surfaces would have a shape of a hyperbolic paraboloid shell with a thickness of 32 mm (1.25 in.).
9. The three edges of the hyperbolic paraboloid formwork were covered with plywood strips leaving one side open. Refer to Figure 13.4.

www.manaraa.com

10. The set up was secured with clamps and straps leaving the open side of the formwork on the top position.
11. The entire set was then secured to prevent it from shifting during the concrete pour process.

Figure 13.4: Formwork set up for hyperbolic paraboloid shells

The ingredients for all concrete mixtures were kept the same except for the amount of steel fibers used by volume fraction (0%, 1% and 2%) in each concrete mixture type. The ingredients for the 0%, 1% and 2% steel fiber concrete mixtures are given in Table 13.1.

Refer to Section 8.1.3 for concrete and specimen preparations. Shells and cylinders were cured for 28-days.

Table 13.1: Concrete batch constituents for 0%, 1% and 2% HSSFRC hyperbolic paraboloid shells (20 in. square x 1.25 in. thick) and cylinders

www.manaraa.com

Mixture Components			0%	1%	2%
Batch Volume			**1.5 ft^3**	**1.5 ft^3**	**1.5 ft^3**
3/8" Coarse Aggregate	(lb)		34.20	34.20	34.20
#4 Coarse Aggregate	(lb)		33.60	33.60	33.60
Fine Aggregate, FA4*	(lb)		86.4	86.4	86.4
Water	(lb)		17.4	17.4	17.4
Cement Type V	(lb)		37.5	37.5	37.5
Silica Fume	(lb)		2.85	2.85	2.85
Fly Ash	(lb)		16.05	16.05	16.05
Total Cementitious	(lb)		56.40	56.40	56.40
Water to Cement Ratio			0.46	0.46	0.46
Water / Cementitious Ratio			0.31	0.31	0.31
Gravel : Sand Ratio			0.44 : 0.56	0.44 : 0.56	0.44 : 0.56
HRWR ADVA540	(lb)		0.588	0.588	0.588
Steel Fiber by Volume	%		0%	1%	2%
Steel Fiber by weight	(lb)		0	7.5	15
Concrete Total Weight	(lb)		228.59	236.09	243.59
Concrete Unit weight	(pcf)		152.4	157.4	162.4

*Fine aggregate with fineness modulus of 2.05

www.manaraa.com

13.4 Type of strain gage used

One type of rosette strain gage, CEA-06-250UR-120, was used. Refer to Figures 8.1.3, 13.5 and 13.6 for rosette strain gage alignment and location. The size of the rosette strain gage, which is dependent on maximum aggregate size, was recommended by the manufacturer. Refer to Section 13.5 for location and Section 8.1.4 for full description of rosette strain gages.

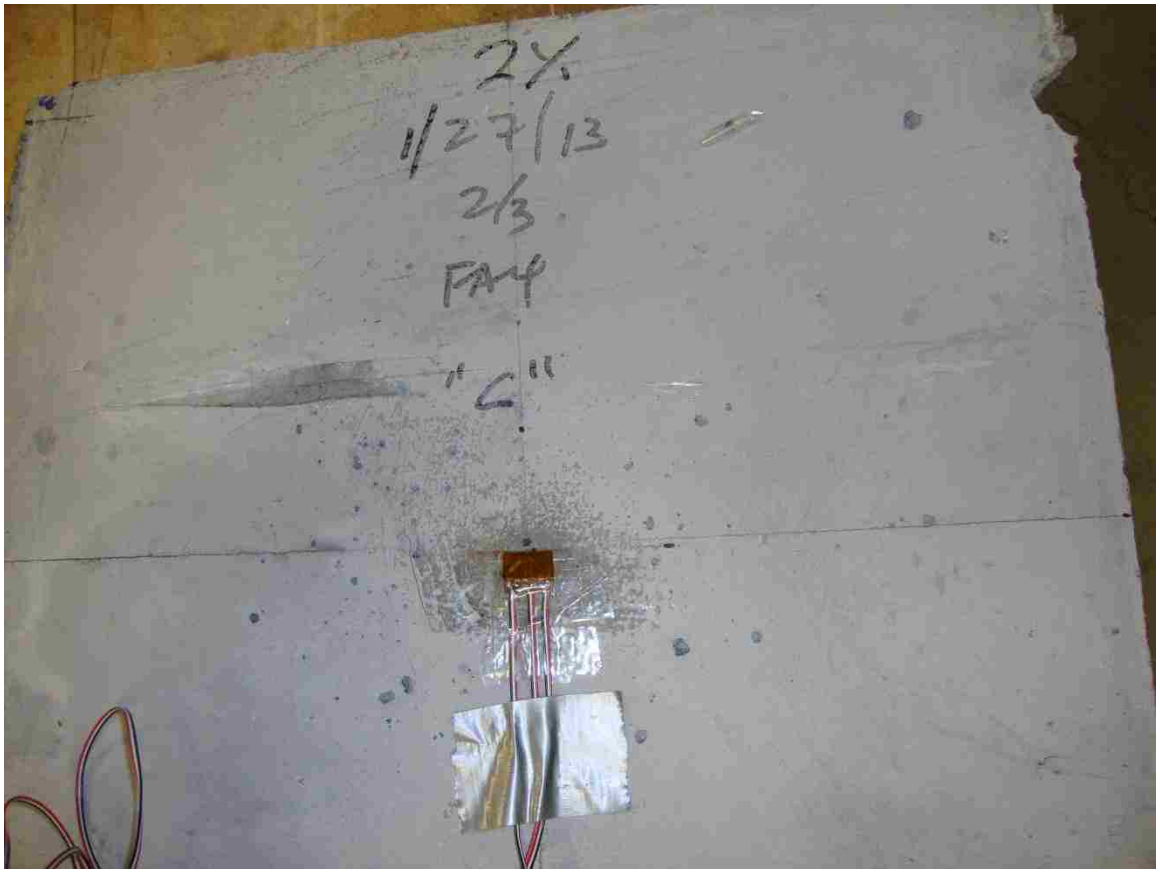

Figure 13.5: Rosette located at the center bottom surface of the hyperbolic paraboloid shell, 3 mm (0.125 in.) off the center line

www.manaraa.com

Figure 13.6: Rosette located, at bottom surface, 32 mm (1.25 in.) from the edge of the hyperbolic paraboloid shell

13.5 Location and orientation of strain gages on the test specimen

The strain gage arrangements for every test were determined by the capability of the data acquisition system to accommodate rosette strain gage output, deflection measurements and load input combined.

At the end of the 28-day, both hyperbolic paraboloid shell and cylinder specimens were pulled out of the curing room; and the hyperbolic paraboloid shell specimens were prepared as follows:

www.manaraa.com

1) Hyperbolic paraboloid shell #1 had no strain gages attached to it. It was used strictly to measure the relationship between load and vertical deflection behavior of hyperbolic paraboloid shells under a uniformly distributed load. The load and vertical deflection readings were electronically linked.
2) Hyperbolic paraboloid shells #2 and #3 were furnished with single rosette strain gage each. In the case of hyperbolic paraboloid shell #2, the rosette was placed 32 mm (1.25 in.) off the flat edge of the hyperbolic paraboloid shell and its center was aligned with the center line of the hyperbolic paraboloid shell as shown in Figure 13.6.
3) In the case of hyperbolic paraboloid shell #3, the rosette was located close to the hyperbolic paraboloid shell center, 3 mm (0.125 in.) off from the center line. The center of the rosette was also aligned with the center of the hyperbolic paraboloid shell as shown in Figure 13.5. The vertical deflection reading for hyperbolic paraboloid shells #2 and #3 were measured using a dial gage.

13.6 Test apparatus and procedures for hyperbolic paraboloid shells

Once the specimens were fitted with strain gages, they were ready for testing. The rosettes were installed per manufacturer's recommendation as stated in Section 4.4.6. The apparatus involved were:

1. Tinius-Olsen testing machine (50,000 lb maximum capacity).
2. Steel platform.
3. Four 50.8 mm (2 in.) diameter, 6.35 mm (0.25 in.) thick and 508 mm (20 in.) long steel tube supports.

www.manaraa.com

4. One 51 mm (2 in.) thick high strength steel fiber reinforced concrete square ring. The ring is a hollow square piece that, when laid on the top of the hyperbolic paraboloid shell, fits the hyperbolic paraboloid shell surface perfectly while remaining flat on the top side. It is part of the load system used to confine soil (silica sand) pressure to the hyperbolic paraboloid shell, see Figure 13.7.
5. 432 mm (17 in.) by 432 mm (17 in.) and 6.4 mm (1/4 in.) thick square steel plate.
6. 3 mm (0.125 in.) thick polycarbonate (rubber) that was placed between the silica sand and the hyperbolic paraboloid shell to reduce friction between the two surfaces.
7. Fine silica sand.

www.manaraa.com

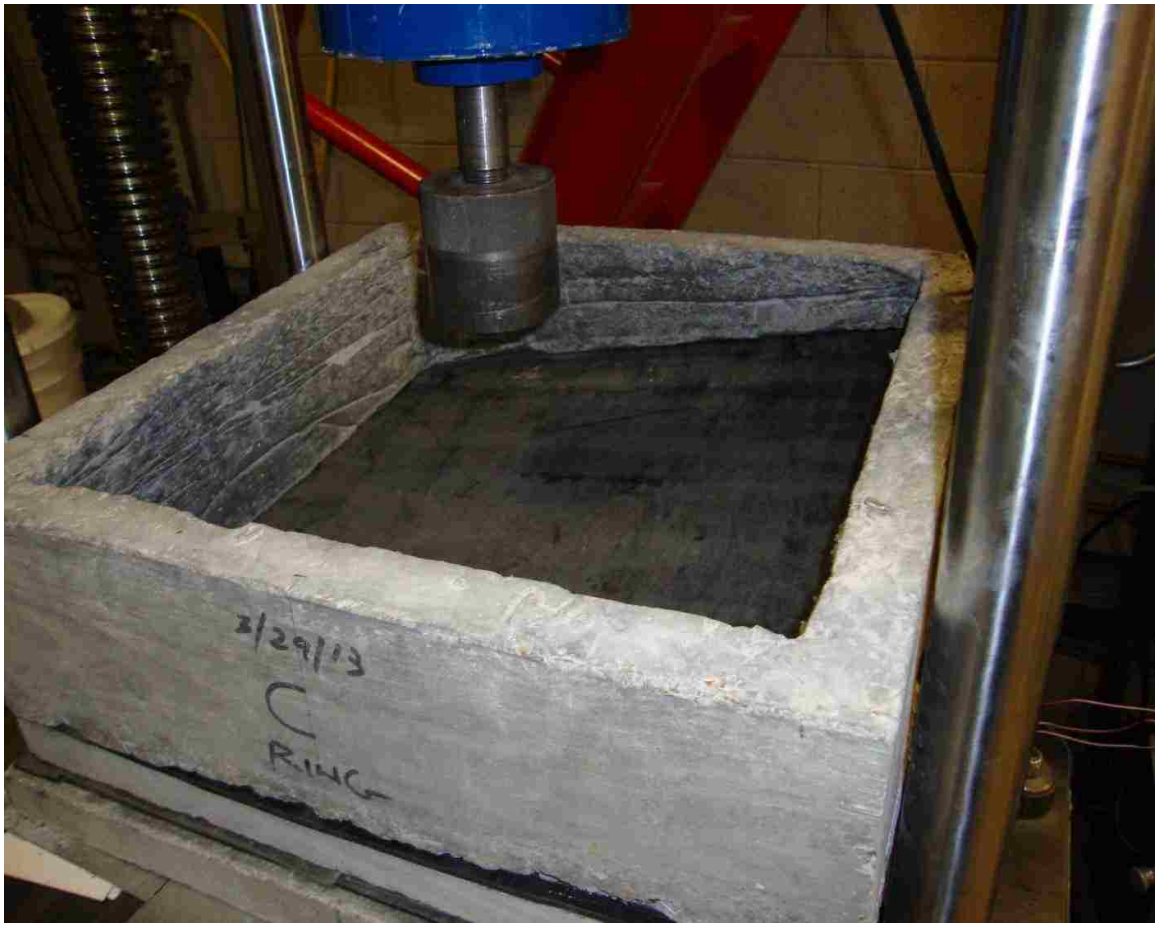

Figure 13.7: Test apparatus and specimen set up for hyperbolic paraboloid shell under a uniformly distributed load showing 51 mm (2 in.) thick high strength steel fiber reinforced concrete square ring

The test set up for hyperbolic paraboloid shells was assembled as follows:

1) The steel platform was assembled and placed on a hard surface of the Tinius-Olsen test machine.
2) Four tube supports were placed on the steel platform. Two adjacent supports were flat and the other two were inclined with a pitch of 95 mm (3.75 in.).

www.manaraa.com

3) The hyperbolic paraboloid shell was placed on the support system. The inclined supports were adjusted to make full contact with the hyperbolic paraboloid shell; shims were also used to assure full contact between the supports and the hyperbolic paraboloid shell.
4) Two layers of polycarbonate (rubber) were laid on the top of the hyperbolic paraboloid shell to reduce friction between the hyperbolic paraboloid shell and the silica sand which was used to transfer the load to the shell.
5) A hollow square concrete ring was placed on the top of the rubber and support system.
6) The concrete ring was then filled to the top with silica sand.
7) Thick steel plate was placed on the top of the silica sand. Very thick steel block was placed between the steel plate and the load cell to facilitate the distribution of the applied load.
8) The load cell was lowered and just engaged the hyperbolic paraboloid shell. Before the actual loading process started: the shell, support, entire test set up and all contact surfaces were checked for any kind of rocking or gap (lack of contact) between the test specimen supports and the test specimen. All gaps were shimmed to ensure full contact and uniform load transfer between units.
9) Finally, the load was applied at a steady rate of 0.03 – 0.08 mm/minute (0.001 – 0.002 in./minute).

The HSSFRC cylinders, which were cast from the same concrete mixture used for shells, were tested for compressive and splitting tensile strength according to the test procedures that are presented in Sections 4.4.1 and 4.4.4, respectively. During the testing

www.manaraa.com

process for cylinders and shells: load, deflection and strain data were collected; failure and failure modes were noted.

13.7 Experiment results for hyperbolic paraboloid shell under a vertically applied uniformly distributed load

13.7.1 Load versus deflection and Load versus strain results

Load versus vertical deflection data were collected for HSSFRC hyperbolic paraboloid shells, with 0% to 2% steel fiber by volume fractions (SFVF), subjected to a uniformly distributed load. The vertical deflection was measured at the geometric center of the hyperbolic paraboloid shells. The average load versus deflection curves for 0%, 1% and 2% HSSFRC hyperbolic paraboloid shells under a uniformly distributed load are presented in Figure 13.8. Each load versus deflection curve represents an average result of three HSSFRC hyperbolic paraboloid shell specimens for each SFVF, a total of nine specimens for 0%, 1% and 2% SFVF. Table 13.2 presents, the load at first crack, peak load, vertical deflection of the hyperbolic paraboloid shells at first crack load and maximum deflection of the hyperbolic paraboloid shell for 0%, 1% and 2% SFVF. The values in Table 13.2 were obtained from the average load versus vertical deflection curves in Figure 13.8.

www.manaraa.com

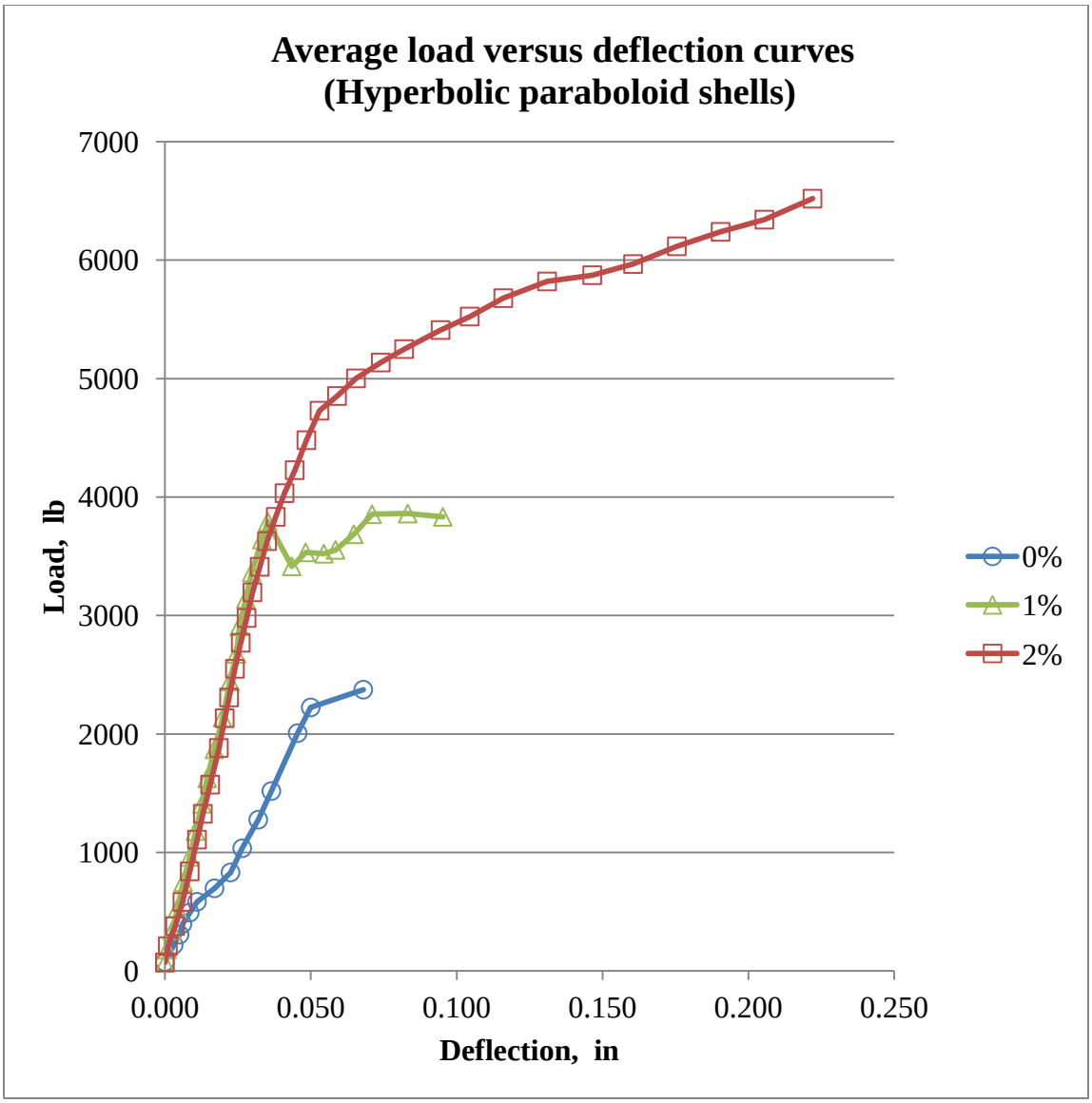

Figure 13.8: Average load versus deflection curves for 0%, 1% and 2% HSSFRC hyperbolic paraboloid shells under a uniformly distributed load

www.manaraa.com

Table 13.2: Load and vertical deflection results for 0%, 1% and 2% HSSFRC hyperbolic paraboloid shells under a uniformly distributed load

Shell	$P_{elastic}$ N (lb)	P_{Max} N (lb)	Percentage increase in load	Δ_y mm (in.)	Δ_{Max} mm (in.)	Percentage increase in deflection
0%	9,786 (2,200)	10,560 (2,374)	0%	0.23 (0.009)	1.73 (0.068)	0%
1%	15,124 (3,400)	17,050 (3,833)	61%	0.89 (0.035)	2.41 (0.095)	40%
2%	20,017 (4,500)	28,998 (6,519)	175%	1.24 (0.049)	5.64 (0.222)	226%

Where: P_{Max}, $P_{elastic}$ = peak and elastic loads, N (lb.)

Δ_y = shell deflection corresponding to the first crack load, mm (in.)

$\Delta_{failure}$ = maximum deflection of the shell at complete failure, mm (in.).

13.7.2 Test results for rosette strain gages

The location and layout of the rosette strain gages on the hyperbolic paraboloid shells are presented in Section 13.5. The shear stress versus maximum shear strain curves, for rosette strain gages located close to the support, for 0% and 2% HSSFRC hyperbolic paraboloid shells are presented in Figure 13.9. The shear stresses were calculated using Equation 13.5. The maximum shear strains were calculated per Equation 8.12 in Section 8.1.4, using shear strains measured by rosette strain gages located close to the support of HSSFRC shells. The 2% HSSFRC shells exhibited higher shear modulus than the lower

www.manaraa.com

SFVF shells. Shear resistance of the shell structures increased as the SFVF increased. The ragged shape of the curves in Figure 13.9 can be attributed to potential slip of the shells as the loading processed.

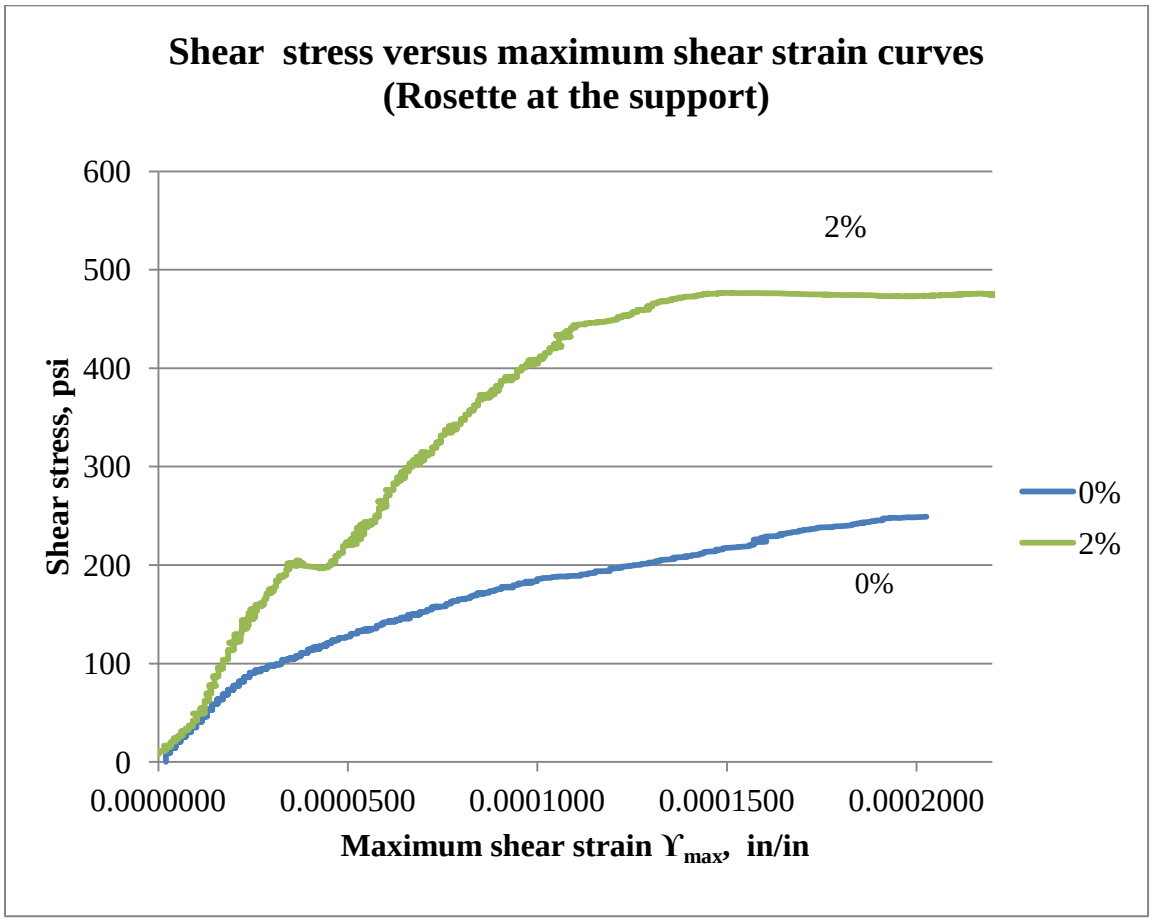

Figure 13.9: Shear stress versus maximum shear strain curves for 0%, 1% and 2% HSSFRC hyperbolic paraboloid shells under a uniformly distributed load (rosette located close to the support)

The load versus strain curves for rosette strain gages located close to the support are presented in Figures 13.10, 13.11 and 13.12 for 0%, 1% and 2% HSSFRC hyperbolic paraboloid shells, respectively. Strains "e1", "e2" and "e3" represent strains in grids

www.manaraa.com

aligned to 45°, 90° and 135° axes from the support base line, rotating about the intersection point between the shell center and support base lines.

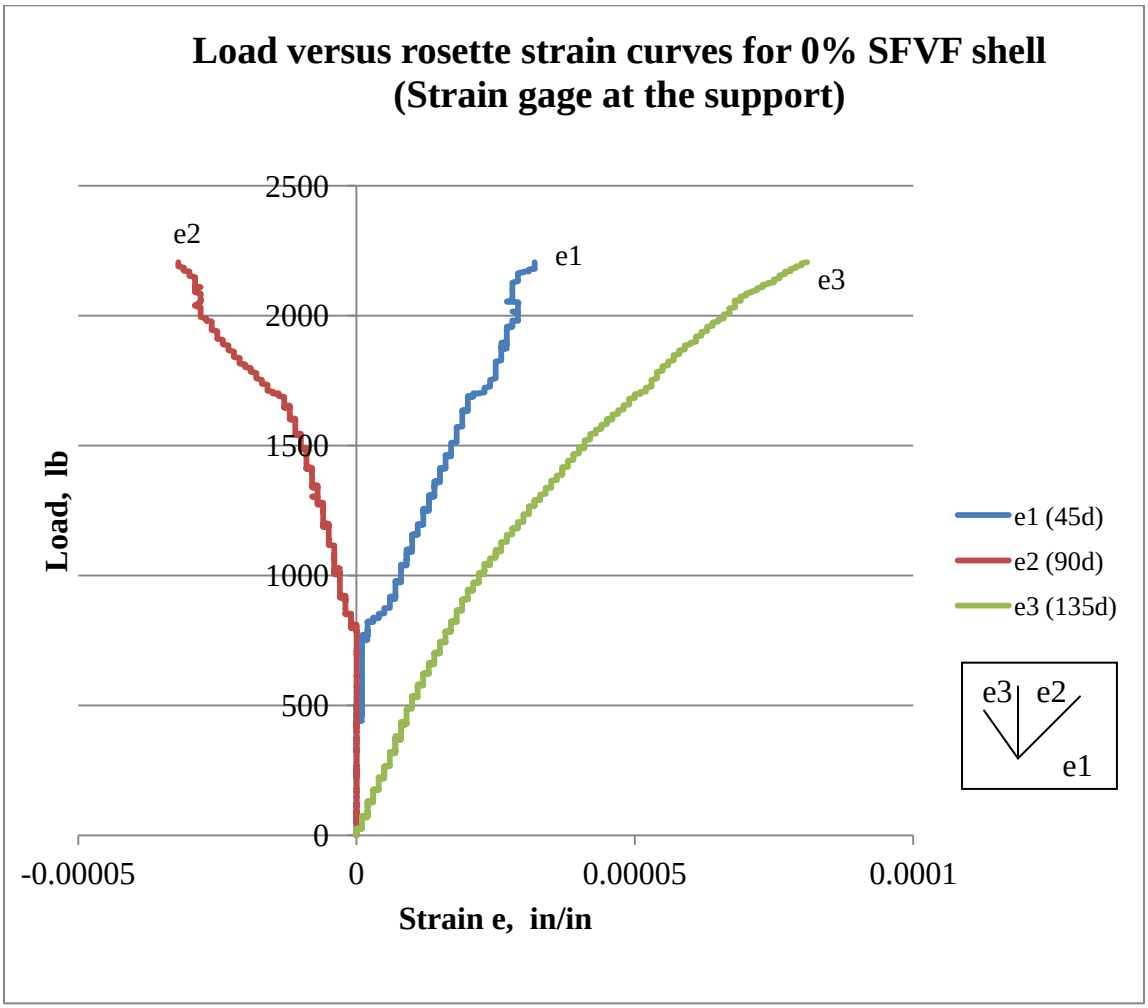

Figure 13.10: Load versus rosette shear strain curves for 0% HSSFRC hyperbolic paraboloid shell under a uniformly distributed load (rosette located close to the support)

www.manaraa.com

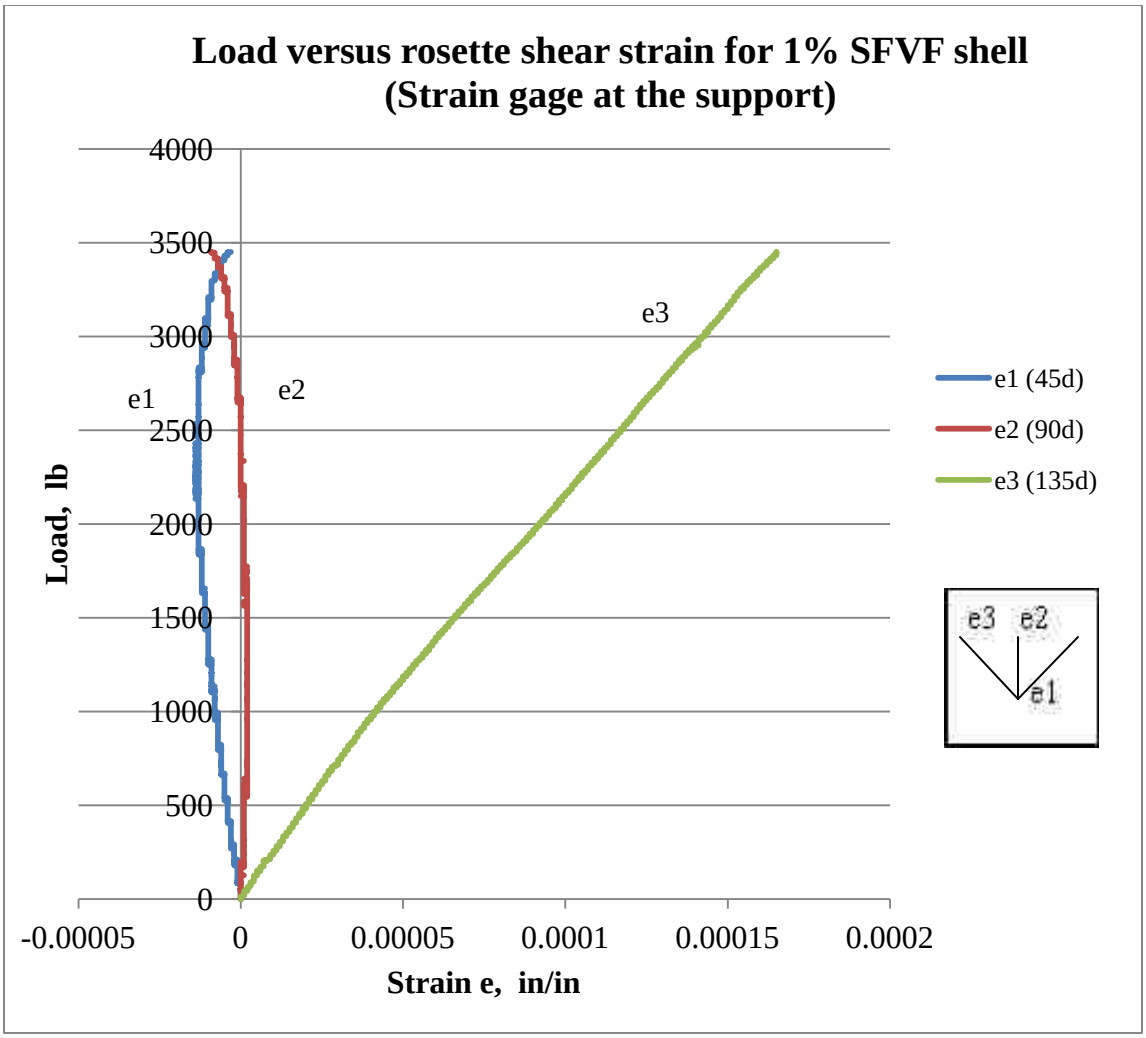

Figure 13.11: Load versus rosette shear strain curves for 1% HSSFRC hyperbolic paraboloid shell under a uniformly distributed load (rosette located close to the support)

www.manaraa.com

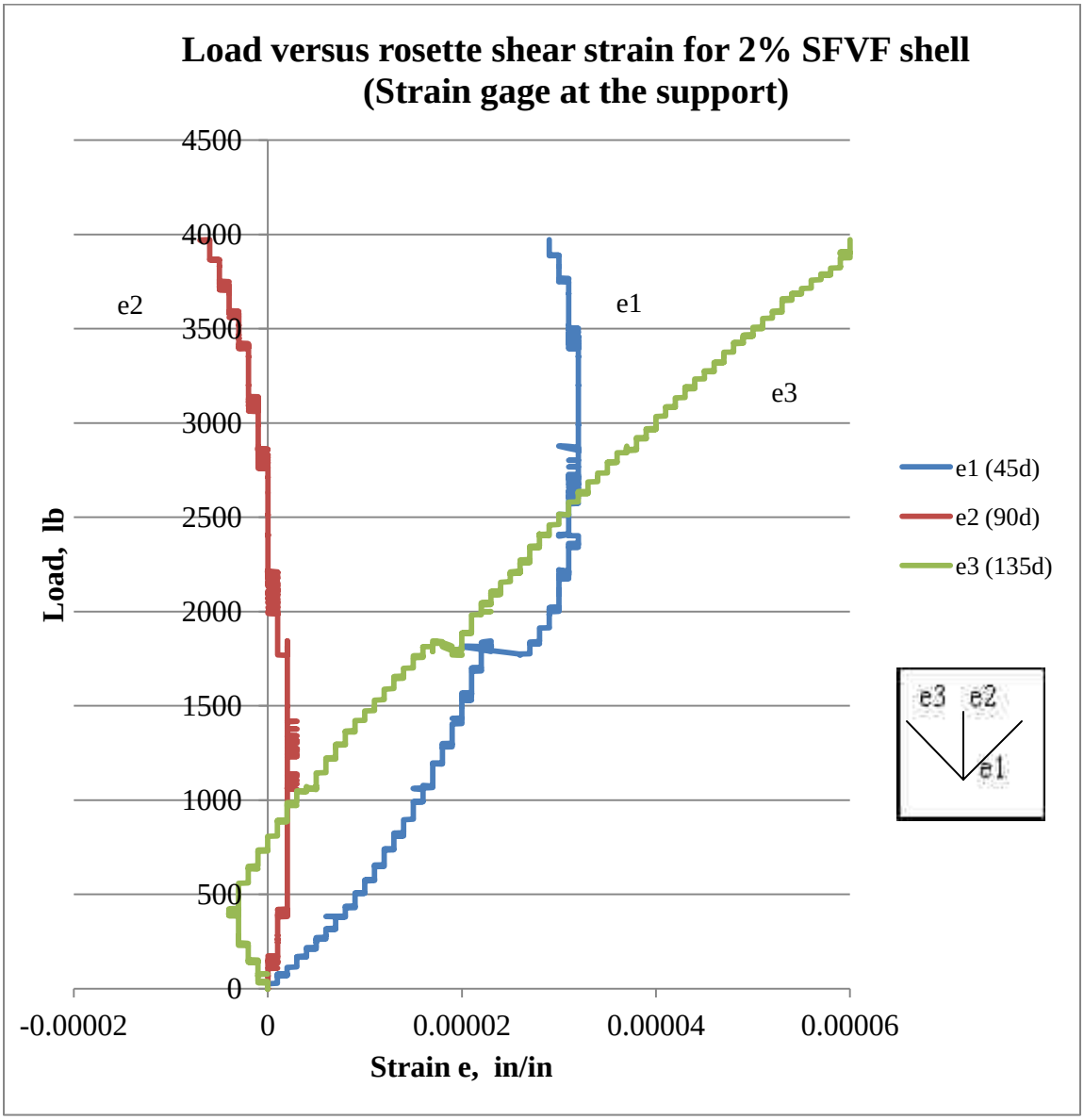

Figure 13.12: Load versus rosette shear strain curves for 2% HSSFRC hyperbolic paraboloid shell under a uniformly distributed load (rosette located close to the support)

www.manaraa.com

13.7.3 Cylinder compressive strength test results

13.7.3.1 Longitudinal strain and modulus of elasticity of HSSFRC cylinders

HSSFRC cylinders that were used for compressive strength tests were taken from the same batch of concrete the corresponding hyperbolic paraboloid shells were made. The cylinders were tested, for compressive strength, within 24 hours of testing the corresponding hyperbolic paraboloid shells. During the testing process, the applied compression load and corresponding longitudinal and transverse strains of HSSFRC cylinders were obtained.

The average compressive stress versus longitudinal strain curves for 0%, 1% and 2% high strength steel fiber reinforced concrete cylinders are presented in Figure 13.13.

www.manaraa.com

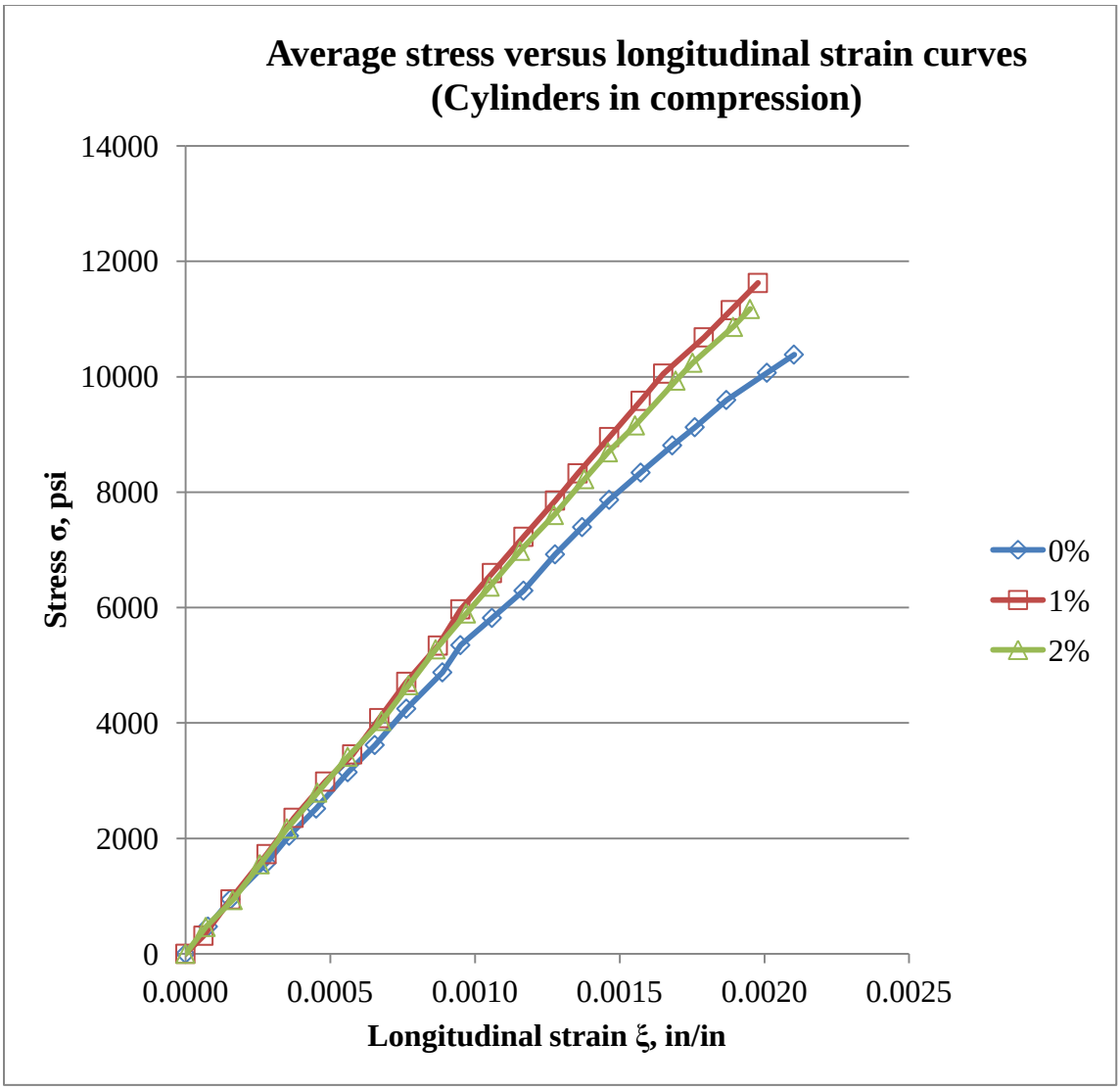

Figure 13.13: Average compressive stress versus longitudinal strain curves for 0%, 1% and 2% HSSFRC cylinders (4 in. x 8 in.) casted with hyperbolic paraboloid shells

www.manaraa.com

The average compressive strength and modulus of elasticity test results for 0%, 1% and 2% high strength steel fiber reinforced concrete cylinders are presented in Table 13.3. The compressive strength and modulus of elasticity results were calculated using procedures in Sections 4.4.1 and 4.4.2, respectively.

Table 13.3: Average compressive strength and modulus of elasticity results for 0%, 1% and 2% HSSFRC cylinders (4 in. x 8 in.) casted with hyperbolic paraboloid shells

Cylinder	Compressive strength MPa (psi)	Percentage increase from 0% steel fiber	Modulus of elasticity MPa (ksi)	Percentage increase from 0% steel fiber
0%	78		43,101	
	(11,366)	0%	(6,251)	0%
1%	95		42,946	
	(13,712)	21%	(6,229)	-0.4%
2%	89		42,415	
	(12,971)	14%	(6,152)	-1.6%

13.7.3.2 Transverse strain and Poisson's ratio of HSSFRC cylinders

The average compressive stress versus transverse strain curves for 0%, 1% and 2% HSSFRC cylinders are presented in Figure 13.14. Compressive stress versus Poisson's ratio curves for 0% and 2% HSSFRC cylinders are shown in Figure 13.15. The Poisson's ratio results for 0% and 2% HSSFRC cylinders were calculated using procedures in

www.manaraa.com

Section 4.4.3. The Poisson's ratio curves in Figure 13.15 show that 0% and 2% HSSFRC cylinders responded in similar fashion at the lower to mid stress range and converged to the same values at the higher end of the stress range.

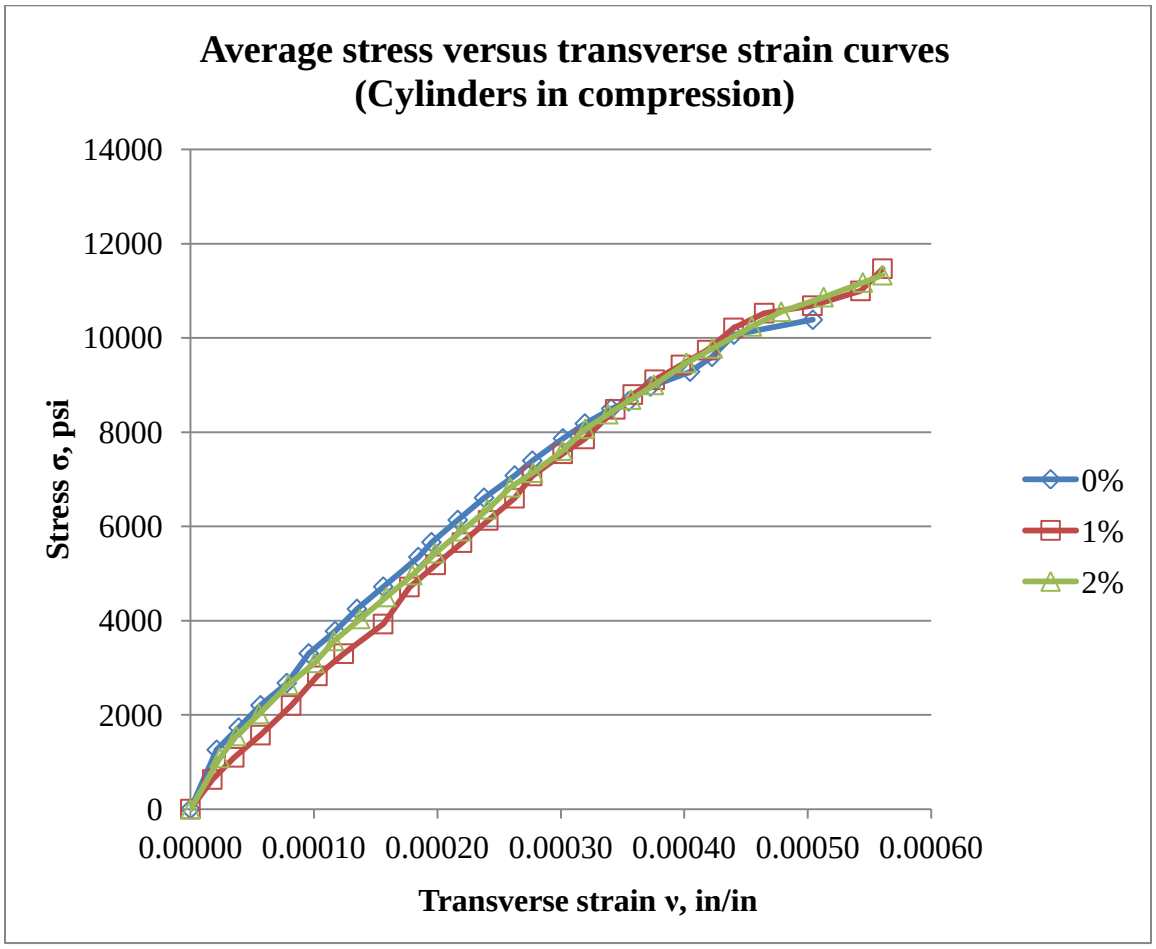

Figure 13.14: Average compressive stress versus transverse strain curves for 0%, 1% and 2% HSSFRC cylinders (4 in. x 8 in.) casted with hyperbolic paraboloid shells

www.manaraa.com

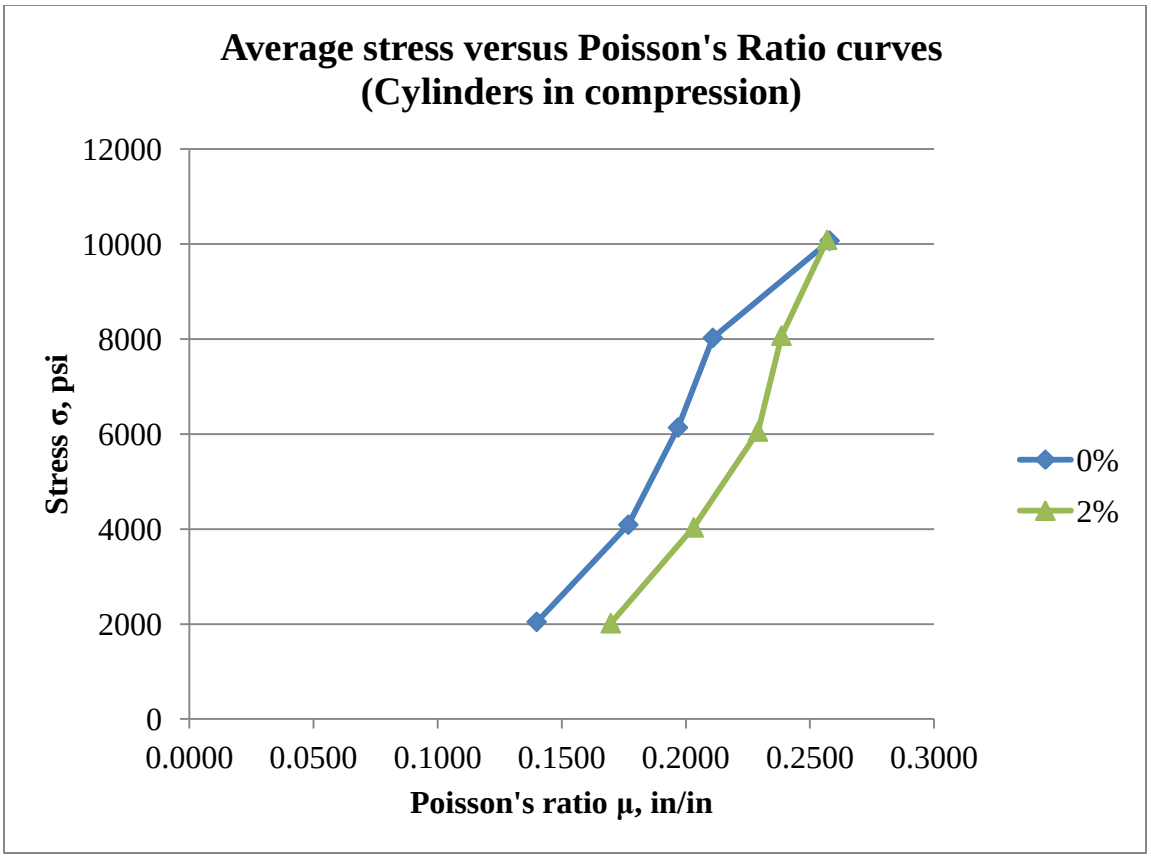

Figure 13.15: Average compressive stress versus Poisson's ratio curves for 0% and 2% HSSFRC cylinders (4 in. x 8 in.) casted with hyperbolic paraboloid shells

13.7.4 Cylinder splitting tensile strength results

The average splitting tensile strength for 0%, 1% and 2% high strength steel fiber reinforced concrete cylinders are presented in Table 13.4 and Figure 13.16. Splitting tensile strength results were computed using Equation 4.3. The splitting tensile strength of HSSFRC cylinders increased as the SFVF increased.

www.manaraa.com

Table 13.4: Average splitting tensile strength results for 0%, 1% and 2% HSSFRC cylinders (4 in. x 8 in.) casted with hyperbolic paraboloid shells

Cylinder	Splitting tensile strength MPa (psi)	Percentage increase from 0% steel fiber	Splitting tensile to compression strength ratio
0%	7.53		
	(1,092)	0%	0.10
1%	10.38		
	(1,506)	38%	0.11
2%	12.03		
	(1,745)	60%	0.13

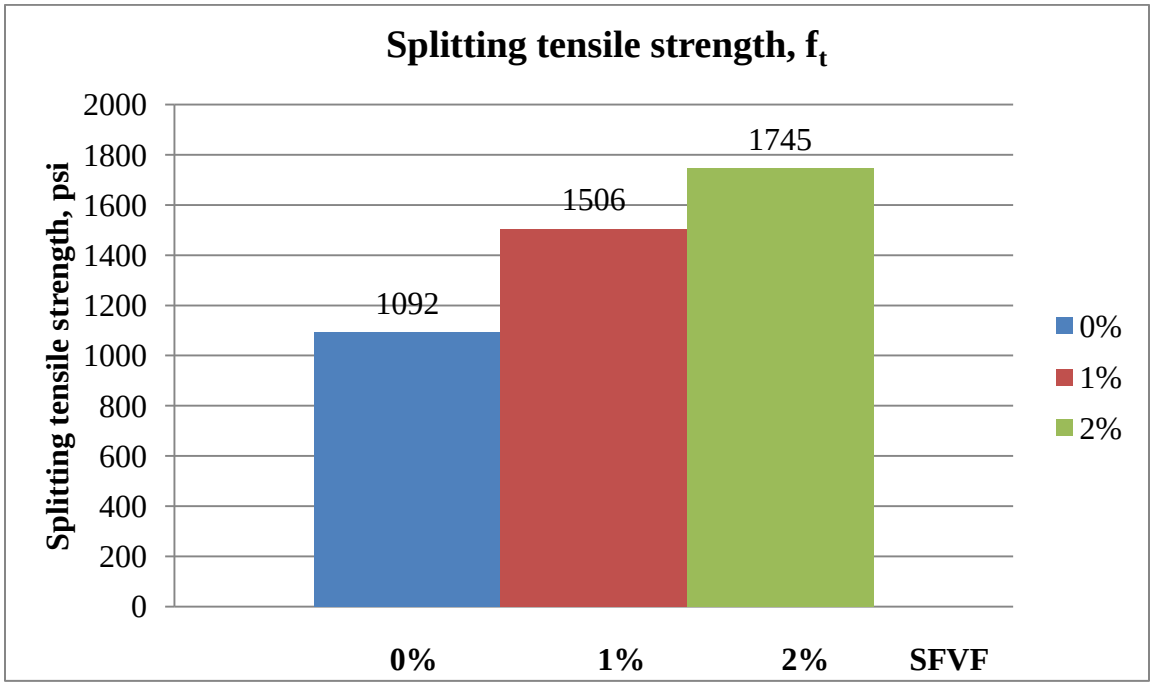

Figure 13.16: Average splitting tensile strength results for 0%, 1% and 2% HSSFRC cylinders (4 in. x 8 in.) casted with hyperbolic paraboloid shells

www.manaraa.com

13.8 Stress-strain analysis and test results

As seen in the membrane theory of hyperbolic paraboloid shells presented by Timoshenko and Ugural (Ugural 2009) Equations 13.2 – 13.8, the hyperbolic paraboloid shell carries distributed applied loads initially in constant shear,

$$N_{xy} = \frac{qc}{2} = \frac{qa^2}{2h} \qquad (13.5)$$

The shear stress therefore is,

$$\tau_{xy} = \frac{N_{xy}}{t} = \frac{qa^2}{2ht} \qquad (13.9)$$

This equation is quite accurate near the simply supported edges of the shell, where $\sigma_x = \sigma_y = 0$ and $M_x = M_y = 0$. It's seen that bending stresses will develop, that combined with the constant shear stresses will lead to initial cracks at the center of the shell as shown in Section 13.9. These initial cracks develop at the center, normal to the tensile stress field, and continue towards the corners. As shown in Table 13.2 and Figure 13.8 for deflections and Figure 13.9 for shear strains, the nearly linear (elastic) behavior of the shells stopped at $P_{elastic}$ = (2,200 lb) for 0%, (3,400 lb) for 1% and (4,500) lb for 2% HSSFRC shells, respectively. The shear stresses, shear strains and shear modulii corresponding to the $P_{elastic}$ for 0%, 1% and 2% HSSFRC shells are presented in Table 13.5.

At 45° the constant shear stress state produces principal stress $\sigma_x' = -\sigma_y' = \tau_{xy}$. It is obvious from the results that as the initial cracks develop at the center of the shell, stress redistribution occurs and flexural stresses develop up to failure in tensile cracking. Since the tensile failure stress is known from cylinder splitting tensile tests, the flexural stresses f_{bt} at maximum loading are calculated as follows:

$$f_{bt} = f_t - \frac{P_{elastic}}{2ht} \qquad (13.10)$$

www.manaraa.com

Where f_{bt} is the tensile flexural stress at the center of the hyperbolic paraboloid shell, $P_{elastic}$ is load at the end of the linear range and f_t is tensile strength taken from Table 13.4. These values are shown in Table 13.6.

Table 13.5: Stress–strain results for 0%, 1% and 2% HSSFRC hyperbolic paraboloid shells at first crack under a uniformly distributed load

Shell	$P_{elastic}$ N (lb)	τ_{xy} (Calculated) MPa (psi)	Shear strain (Calculated) Υ_{xy} (10^{-6})	G_{xy} (Calculated) MPa (ksi)
0%	9,786 (2,200)	1.62 (235)	205	7,899 (1,145)
1%	15,124 (3,400)	2.50 (363)	240	10,427 (1,511)
2%	20,017 (4,500)	3.31 (480)	110	30,109 (4,364)

Where: $P_{elastic}$ = applied uniformly load, lb

τ_{xy} = shear stress (Equation 13.9), psi

Υ_{xy} = shear strain of HSSFRC shell corresponding to $P_{elastic}$ (Equation 8.12)

G_{xy} = shear stress calculated (Equation 8.5) using Poisson's ratio from Figure 13.15.

www.manaraa.com

Table 13.6: Flexural tensile stress f_{bt} at the center of 0%, 1% and 2% HSSFRC hyperbolic paraboloid shells at first crack under a uniformly distributed load

Shell	$P_{elastic}$ N (lb)	f_t MPa (psi)	τ_{xy} (Calculated) MPa (psi)	f_{bt} (Calculated) MPa (psi)
0%	9,786 (2,200)	7.53 (1,092)	1.62 (235)	6.04 (875)
1%	15,124 (3,400)	10.38 (1,506)	2.50 (363)	7.89 (1,143)
2%	20,017 (4,500)	12.03 (1,745)	3.31 (480)	8.73 (1,265)

Where: f_{bt} = flexural tensile stress at the center of the HSSFRC shells at first noticeable crack, psi

f_t = splitting tensile strength of HSSFRC cylinders (from Table 13.4), psi , psi

As a final note to the analysis of structural behavior of HSSFRC hyperbolic paraboloid shells, if the loading is such that the in-plane shear stress and shear strains are within the linear range of stress-strain curves, then the loading ratio $P_{elastic}$ to P_{Max} are 0.927, 0.887 and 0.690 for 0%, 1% and 2% SFVF, respectively.

www.manaraa.com

13.9 Failure modes

The load versus deflection curves in Figure 13.8 show that, 0% and 1% HSSFRC hyperbolic paraboloid shells under a uniformly distributed load responded linearly till about 90% of their maximum capacity; while 2% SFVF shells exhibited elasto-plastic (bi-linear) behavior starting at 70% of their maximum capacity. In Figure 13.8, average load versus deflection curves, for 1% and 2% SFVF HSSFRC hyperbolic paraboloid shells, showed identical response for most part of the linear range despite the variation in SFVF. The 0% HSSFRC hyperbolic paraboloid shells have half the linear range of 1% and 2% shells. This validates the positive influence of steel fibers on the shear capacity of shells.

Due to the proximity of the square shells to the testing platform and support locations, it was not possible to observe the development and propagation of cracks at the bottom surface of the shells during the testing process; however, shells were examined after the test ended as shown in Figures 13.17, 13.18 and 13.19. Therefore, the cracks were seen and noted when they reached the edges of the hyperbolic paraboloid shells.

After the formation of cracks at the edge of shell, as the loading process progressed and the deflection of the shell increased, the corners of the shell started lifting about the crack lines. The crack lines actually acted as hinges and the shell pieces in between the cracks rotated or curled about the hinges causing some of the corners to lift. The hinges at the support being a point of zero deflection. As the loading process continued, the corners broke off due to excessive deflection (rotation) countered by the uniformly distributed load.

www.manaraa.com

The failure patterns for 0%, 1% and 2% HSSFRC hyperbolic paraboloid shells subjected to a uniformly distributed load show that a primary central crack at 45° extending to the corners and secondary cracks extending from primary cracks towards the edges and corners. Crushing of concrete was not observed at any time during the testing process of the hyperbolic paraboloid shells. Duration of the test process, till the first crack, was about 30, 35 and 48 minutes for 0%, 1% and 2% HSSFRC hyperbolic paraboloid shells, respectively.

Figure 13.17: Primary (center) and secondary (corner) crack patterns at failure for 0% HSSFRC shells under a uniformly distributed load

www.manaraa.com

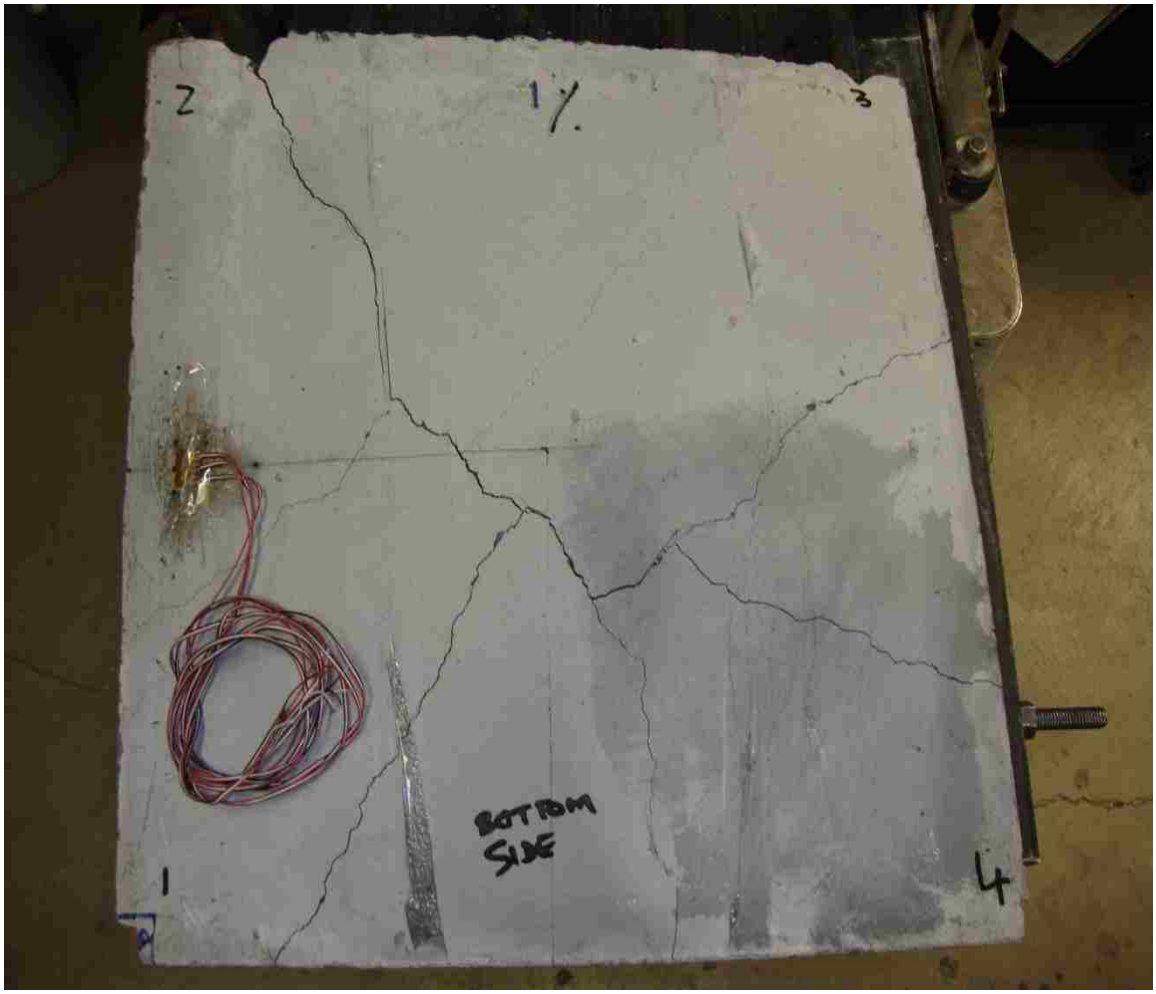

Figure 13.18: Primary (center) and secondary (corner) crack patterns at failure for 1% HSSFRC shells under a uniformly distributed load

www.manaraa.com

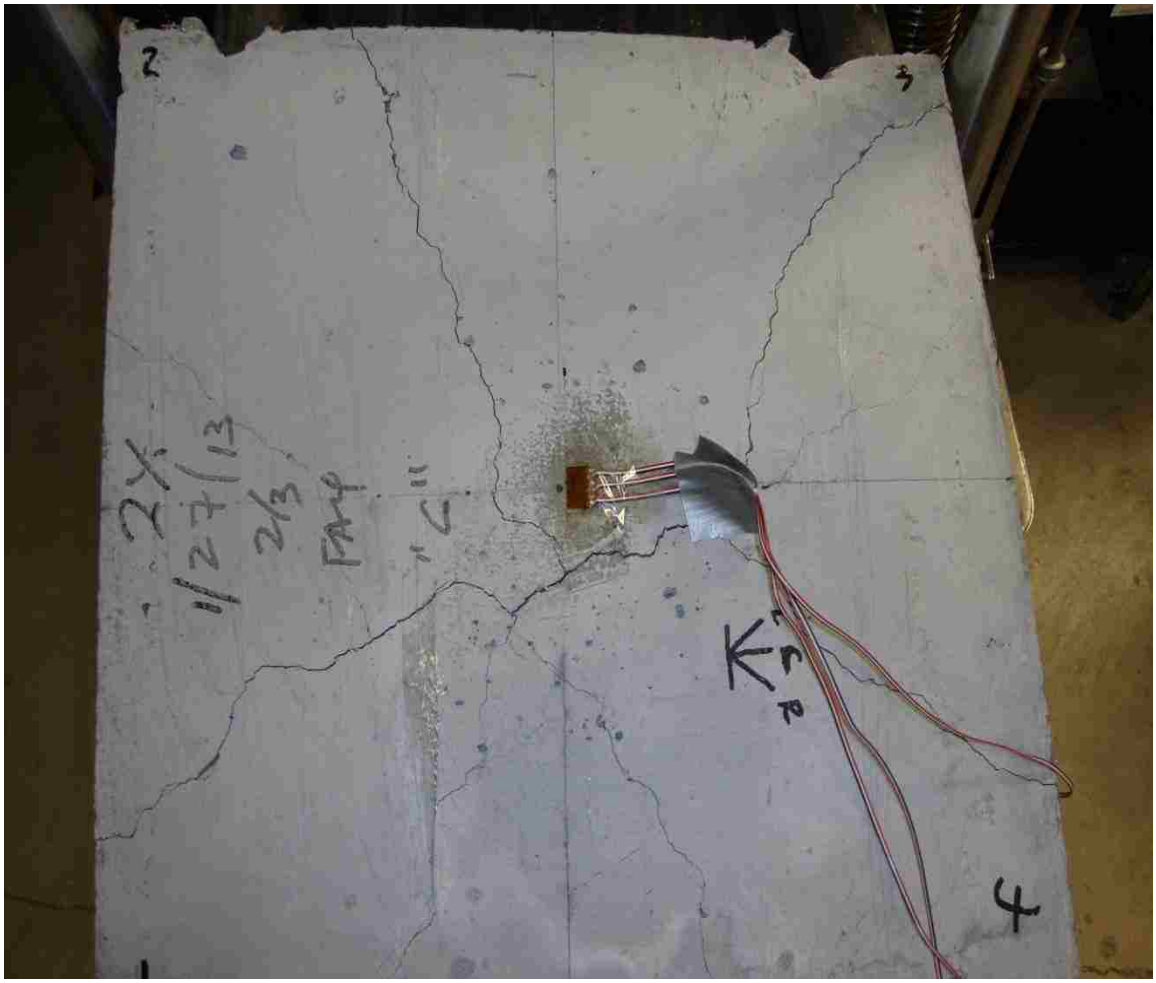

Figure 13.19: Primary (center) and secondary (corner) crack patterns at failure for 2% HSSFRC shells under a uniformly distributed load

13.10 Energy absorption

The energy absorption (toughness), the area under the load versus deflection curves, for 0%, 1% and 2% HSSFRC hyperbolic paraboloid shells were calculated as 95, 291 and 1,114 in-lb, respectively. The load versus deflection curves are shown in Figure 13.8. The energy absorption of HSSFRC hyperbolic paraboloid shells increased as the steel fiber content increased: 206% and 1,073% for 1% and 2% SFVF shells, respectively over the 0% SFVF shells.

www.manaraa.com

13.11 Summary of load capacity increase for plates and shells

Table 13.7 presents a summary of increase in load-carrying capacity of plate and shell structures subjected to various loading and support conditions as the steel fiber by volume fraction increases from 0% to 1% and 2%. Table 13.7 helps to compare the effectiveness of steel fibers in plate and shell structures.

Table 13.7: A summary of increase in load capacity for 1% and 2% HSSFRC plate and shell structures over 0% SFVF

	Structure type	1% SFVF, percent increase from 0% steel fiber	2% SFVF, percent increase from 0% steel fiber
1	Short span rectangular plates*	70%	125%
2	Square plates under central loading *	80%	119%
3	Square plates with opposite corner loads*	16%	25%
4	Circular plates under central loading **	19%	36%
5	Circular cylindrical shells under pinching loads *	27%	62%
6	Hyperbolic paraboloid shells*	61%	175%

www.manaraa.com

* Thickness of the structure = 32 mm (1.25 in.)

** Thickness of the structure = 76 mm (3.0 in.)

13.12 Discussion of test results

13.12.1 Capacity of hyperbolic paraboloid shells under a uniformly distributed load

The capacity of HSSFRC hyperbolic paraboloid shells to accommodate a uniformly distributed load increased as the steel fiber by volume fraction (SFVF) increased from 0% through 2%. The load capacity of HSSFRC hyperbolic paraboloid shells increased by 61% and 175% for 1% and 2% SFVF, respectively compared to 0% (plain) HSSFRC hyperbolic paraboloid shells.

The ultimate vertical deflection and vertical deflection of the hyperbolic paraboloid shells at first crack formation increased as the SFVF increased from 0% to 1% and ultimately to 2%. The vertical deflection of the hyperbolic paraboloid shells at first crack formation increased by 289% and 444% for 1% and 2% SFVF, respectively with respect to 0% (plain) hyperbolic paraboloid shells. The ultimate vertical deflection of hyperbolic paraboloid shells increased by 40% and 226% for 1% and 2% SFVF, respectively with respect to 0% (plain) hyperbolic paraboloid shells.

13.12.2 Strain–stress analysis

Shear strains at the support of the HSSFRC shells were much larger in magnitude than shear strains at shell center. For the same load, HSSFRC shells with high SFVF exhibited smaller shear strain; therefore, higher shear strength.

www.manaraa.com

When the values for calculated modulus of elasticity, using shear stress and Poisson's ratio from Section 13.8, were compared to those obtained from the compression cylinder tests, it was noted that the shear modulus was not linearly related to the young's modulus as is the case for non-homogeneous materials. It was also observed that the shear modulus of HSSFRC mixture increased steadily with the increase in steel fiber by volume fraction.

13.12.3 Splitting tensile strength, modulus of elasticity, compressive strength and Poisson's ratio for HSSFRC cylinders

The Splitting tensile strength results for HSSFRC cylinders increased by 38% and 60% for 1% and 2% SFVF, respectively with respect to 0% (plain) cylinders.

The young's modulus values for 0% through 2% HSSFRC cylinders in compression remained roughly close within ±1.6%.

The average stress versus longitudinal strain curves for cylinders in compression showed that 1% and 2% SFVF cylinders are initially nearly identical; while, stress-strain curve for 0% SFVF cylinders are slightly shallower than both 1% and 2% SFVF curves.

The average stress versus transverse strain curves for cylinders in compression showed, 0%, 1% and 2% SFVF behavior nearly identical. The Poisson's ratio curves for all three SFVF cylinders exhibited similar shape responses but different values initially and converged to 0.25 as the stress level increased.

www.manaraa.com

13.12.4 Energy absorption (Toughness)

The area under the load-deflection curves for hyperbolic paraboloid shells with higher steel fiber by volume fraction (SFVF) exhibited higher energy absorption capacity (toughness) than the lower SFVF shells.

www.manaraa.com

CHAPTER 14

CONCLUSIONS

14.1 Fresh properties of high strength steel fiber concrete

High range water reducing agent (HRWR) increases slump flow, slump and chances of bleeding. HRWR should be adjusted as steel fiber by volume fraction (SFVF) increases to achieve desirable SCC/Flow-able HSSFRC mixtures.

Viscosity modifying agent (VMA) does enhance the flow ability and deformation of HSSFRC mixture. VMA does also tend to: slow the flow ability, shrink the spread diameter and slow the spread flow of HSSFRC mixture. Therefore, the amount of VMA to be used should be negotiated between the flow ability and slump diameter of the concrete mixture.

Small amount of steel fiber by volume fraction, $\leq$ 1%, may not have much effect on the flow ability of HSSFRC mixtures. But, large volume (> 1.5% SFVF) does affect fresh properties of HSSFRC mixtures such as flow ability to a large extent. If high volume steel fiber is to be used, other factors that enhance the flow ability and fresh properties of HSSFRC mixture in general, should be implemented to get the desired flow ability without aggregate separation. When SFVF increases, flow ability decreases. This applies to other fresh properties such as J-ring, V-Funnel and U-Box, as well. HSSFRC mixture can meet all or most of the standard SCC requirements depending on the amount of SFVF used. For concrete mixtures with 3% and 4% steel fiber by volume fractions, minimal mechanical vibration may be necessary to help the consolidation of the mixture, especially for fine aggregates with higher fineness modulus.

www.manaraa.com

The effect of coarse to fine aggregate ratio on the flow ability is eminent from the test results. When slump diameter is too small or there is a presence of honeycombing; coarse to fine aggregate ratio could be lowered and/or fine aggregate with lower fineness modulus could be used to mitigate the problem.

Finally, the SCC standards should be adjusted for high percentage steel fiber concrete mixtures with 2% and higher SFVF since such mixtures may not be able to meet all the standard SCC requirements for normal concrete.

14.2 Hardened properties of high strength steel fiber concrete

High range water reducer (HRWR) agents play a major role in the mechanical properties of HSSFRC mixture such as compressive strength, splitting tensile strength, modulus of elasticity and Poisson's ratio, in addition to the fresh properties. When HRWR is adjusted in accordance with the amount of SFVF of the HSSFRC mixture, improved and better hardened properties of HSSFRC mixture can be achieved. When HRWR was adjusted along with the SFVF, the compressive strength of HSSFRC cylinders increased by 11% and 19% for 1% and 2% SFVF, respectively. When HRWR was kept constant however, a modest increase of 3.5% and 3.3% was observed for 1% and 2% SFVF, respectively.

Splitting tensile strength and modulus of elasticity are also affected positively when HRWR is applied in correspondence with the amount of SFVF used.

Steel fibers enhanced mechanical properties such as compressive strength, splitting tensile strength and modulus of elasticity of HSSFRC mixture. In addition, the steel fibers improved ductility and mode of failure characteristics of HSSFRC cylinders.

www.manaraa.com

The mode of failure of HSSFRC cylinders under compressive and splitting tensile forces have improved from a brittle to a ductile mode by the introduction of steel fibers to the SCC or flow-able concrete mixtures.

14.3 Beams, plates and shell structures

14.3.1 Beams

The modulus of rupture (MOR) of HSSFRC beams increased by 10% as the content of steel fibers increased by 1% up to 3% SFVF however, only 2% increase in MOR from 3% to 4% SFVF. It can be concluded that, as far as MOR is concerned, the addition of steel fibers is recommended up to 3% SFVF, beyond which the effect of the steel fibers on MOR is minimal. The 4% HSSFRC beams provided the highest level of ductility in their failure mode.

14.3.2 Simply supported long span HSSFRC rectangular plates under central line load

The ability of simply supported long span HSSFRC rectangular plates to withstand unidirectional bending under central line load increased with the increase in steel fiber by volume fraction between 0% and 2%. The capacity of long span HSSFRC rectangular plates increased by 5% and 18% for 1% and 2% SFVF, respectively.

The ductile behavior of long span HSSFRC rectangular plates improved substantially under unidirectional bending as the steel fiber by volume fraction increased, with deflection at failure increasing by 707% and 890% for 1% and 2% SFVF, respectively. The steel fibers also enabled the rectangular plate structures to undergo large post crack

www.manaraa.com

deformations and rotations therefore, allowing the plates to have a ductile flexural mode of failure and in the process increasing the energy absorption capacity by 331% and 378% for 1% and 2% SFVF, respectively.

In general, it can be concluded that the introduction of 1% and 2% steel fibers to high strength flow-able or SCC concrete mixtures improved: the bending capacity, provided a ductile mode of failure and increased the energy absorption (toughness) capacity of HSSFRC rectangular plates under unidirectional bending.

14.3.3 Simply supported short span HSSFRC rectangular plates under central line load

The ability of simply supported short span HSSFRC rectangular plates to support unidirectional bending under central line load increased with the increase in steel fiber by volume fraction, between 0% and 2%. The capacity of short span HSSFRC rectangular plates increased by 70% and 125% for 1% and 2% SFVF, respectively.

The ductile behavior of short span HSSFRC rectangular plates improved considerably, with respect to unidirectional bending, as the steel fiber by volume fraction increased with deflection at failure increasing by 232% and 353% for 1% and 2% SFVF, respectively. The steel fibers also enabled the rectangular plate structures to undergo large post crack deformations and rotations therefore, allowing the plates to have a ductile flexural mode of failure and in a process increasing the energy absorption capacity by 386% and 645% for 1% and 2% SFVF, respectively.

In general, it can be concluded that the introduction of 1% and 2% steel fibers to high strength flow-able or SCC concrete mixtures improved: the bending capacity, provided a

www.manaraa.com

ductile mode of failure and increased the energy absorption (toughness) capacity of HSSFRC rectangular plates under unidirectional bending.

14.3.4 Simply supported HSSFRC square plates under center point load

The capacity of simply supported HSSFRC square plates to resist bi-axial bending under a concentrated center load increased with the increase in steel fiber by volume fraction, from 0% to 1% and 2% SFVF. The capacity of simply supported HSSFRC square plates increased by 80% and 119% for 1% and 2% SFVF, respectively.

The ductile behavior of HSSFRC square plates improved substantially, with respect to bi-axial bending, as the steel fiber by volume fraction increased to 1% and 2% with deflection at failure increasing by 535% and 1,247% for 1% and 2% SFVF, respectively. The steel fibers enabled the HSSFRC square plate structures to undergo large post crack deformations and rotations therefore, allowing the plates to have a ductile flexural mode of failure and in the process increasing the energy absorption capacity by 786% and 1,431% for 1% and 2% SFVF, respectively.

In general, it can be concluded that the introduction of steel fibers to high strength flow-able or SCC concrete mixtures improved: the bi-axial bending capacity, provided a ductile mode of failure and increased the energy absorption capacity of HSSFRC square plates under bi-axial bending.

14.3.5 HSSFRC square plates under opposite corner loads

The capacity of HSSFRC square plates, supported at opposite corners, to support concentrated opposite corner loads increased with the increase in steel fiber by volume

www.manaraa.com

fraction. Since the applied corner loading subjects the plates to a constant twisting moment which resulted in a state of shear stress and strain condition, it is concluded that the addition of steel fibers increased the torsional (twisting moment) capacity of HSSFRC square plates loaded in opposite corners by 16% and 25% for 1% and 2% SFVF, respectively.

The ductile behavior of HSSFRC square plates improved by a considerable amount with respect to a twisting moment and shear loading as the steel fiber by volume fraction increased; the deflection at failure increasing by 905% and 1,313% for 1% and 2% SFVF, respectively. The steel fibers enabled the HSSFRC square plate structures to undergo large post crack deformations and rotations therefore, enabling the plates to have a ductile mode of failure under torsional stresses and in a process increasing the energy absorption capacity by 320% and 602% for 1% and 2% SFVF, respectively.

In general, it is concluded that the introduction of steel fibers to high strength flow-able or SCC concrete mixtures in thin plates improved: twisting moment capacity, provided a ductile mode of failure and increased the energy absorption (toughness) capacity of HSSFRC square plates in twisting moment loading.

14.3.6 Circular plates under center point load

The ability of moderately thick, thickness to diameter (t/D) ratio of 0.15, HSSFRC circular plates supported at three equally spaced discrete locations, to carry or accommodate a concentrated center load by bi-axial bending increased with the increase in steel fiber by volume fraction. The capacity of simply supported HSSFRC circular plates increased by 19% and 36% for 1% and 2% SFVF, respectively.

www.manaraa.com

The ductile behavior of HSSFRC circular plates improved considerably, with respect to bi-axial bending, as the steel fiber by volume fraction increased; the deflection at failure increasing by 292% and 873% for 1% and 2% SFVF, respectively. The steel fibers enabled the HSSFRC circular plate structures to undergo large post crack deformations and rotations therefore, enabling the plates to have a ductile mode of failure under bi-axial stress and in a process increasing the energy absorption capacity by 173% and 435% for 1% and 2% SFVF, respectively.

In general, it can be concluded that the introduction of steel fibers to high strength flow-able or SCC concrete mixtures improved: bi-axial bending capacity, provided a ductile mode of failure and increased the energy absorption (toughness) capacity of HSSFRC circular plates under bi-axial bending.

14.3.7 Circular cylindrical shells under pinching central load

The capacity of HSSFRC circular cylindrical shells to accommodate a pinching central load increased as the steel fiber by volume fraction (SFVF) increased from 0% to 1% and 2%. The capacity of HSSFRC circular cylindrical shells increased by 27% and 62% for 1% and 2% SFVF, respectively.

The ductile behavior of HSSFRC circular cylindrical shells improved greatly under a highly concentrated central load with deformations at failure increasing by 484% and 796% for 1% and 2% SFVF, respectively as the steel fiber by volume fraction increased from 0% to 1% and 2%. The steel fibers facilitated the HSSFRC circular cylindrical structure to undergo large post crack deformations and rotations therefore, enabling the shells to have a ductile mode of failure under a severe pinching point load and in a

www.manaraa.com

process increasing the energy absorption capacity by 420% and 1,173% for 1% and 2% SFVF, respectively.

In general, it can be concluded that the introduction of steel fibers to high strength flow-able or SCC concrete mixtures improved: load capacity, provided a ductile mode of failure and enhanced the energy absorption (toughness) capacity of HSSFRC circular cylindrical shells subjected to a severe pinching point loads.

14.3.8 Hyperbolic paraboloid shells under a vertically applied uniformly distributed load

The capacity of HSSFRC hyperbolic paraboloid shells to support a uniformly distributed load by mainly in-plane shear increased by 61% and 175% for 1% and 2% SFVF, respectively as the steel fiber by volume fraction (SFVF) increased from 0% to 1% and 2%..

The ductile behavior of HSSFRC hyperbolic paraboloid shells improved greatly, with respect to in-plane shear, with deformations at failure increasing by 40% and 226% for 1% and 2% SFVF, respectively as the steel fiber by volume fraction increased. The steel fibers aided the HSSFRC hyperbolic paraboloid shells to undergo large post crack deformations and rotations therefore, enabling the shells to have a ductile mode of failure under in-plane shear stress and in a process increasing the energy absorption capacity by 206% and 1,073% for 1% and 2% SFVF, respectively.

In general, it can be concluded that the introduction of steel fibers to high strength flow-able or SCC concrete mixtures improved: in-plane shear capacity, provided a ductile

www.manaraa.com

mode of failure and enhanced the energy absorption (toughness) capacity of HSSFRC hyperbolic paraboloid shells under a uniformly distributed load.

As a generally conclusion, for concrete mixtures with a *constant* HRWR, it is deduced from the performance of HSSFRC cylinders and structures that, the introduction of steel fibers to high strength (70 MPa/10 ksi) flow-able or SCC concrete mixtures resulted in:

- An impressive increase in the tensile and shear strength of the steel fiber concrete structures.
- An impressive increase in ductility and energy absorption (toughness) capacity.
- Moderate effect on the compressive strength and young's modulus.
- Moderate-to-no effect on the first major crack loads.
- Steel fibers were mostly effective for in-plane shear resistance followed by bi-axial and uni-axial flexural resistance.

www.manaraa.com

Bibliography

ACI 237R-07. *Self-Consolidating Concrete.* ACI 237R-07, American Concrerte Institute, 2008.

ACI Commettee 544.3R. *Guide for Specifying, proportioning, and Production of Fiber-Reinforced Concrete.* American Concrete Institute, 2008.

ACI Committee 544.2R. *Measurement of Properties of Fiber Reinforced Concrete.* American Concrete Institute, 2008.

Ahmed, A. *"Characterization of Steel Fiber and/or Polymer Concrete Mixes and Applications to Slender Rectangular and I-Beams".* PhD Thesis, University of Nevada, Las Vegas, 2001.

Ahmed, A.and Ladkany, S. "Effects of Adverse Hot Weather Curing Conditions on Plain and Polymer-Modified Concrete Mixes Used in Foundations and Basements." *Proceedings of the 38th symposium of Engineering Geology and Geotecnical Engineering.* University of Nevada, Reno, 2003. 197-201.

Aoude, H., Cook,W.D., and Mitchell, D. "Behavior of columns constructed with fibers and self-consolidating concrete." *ACI Structural Journal*, 2009: Vol 106, Issue 3, Pages 349-357.

ASTM A 820. *Standard Specification for Steel Fibers for Fiber-Reinforced Concrete.* Standard, West Conshohocken: ASTM, 2006.

ASTM C 1550. *Flexural Toughness of Fiber Reinforced Concrete (Using Centrally Loaded Round Panel).* Standard, ASTM, 2008.

ASTM C 1611. *"Standard Test Method for Slump Flow of Self-Consolidating Concrete".* ASTM International, Conshohocken, 2009.

www.manaraa.com

ASTM C 39. *"Standard Test Method for Compressive Strength of Cylindrical Concrete Specimens"*. West Conshohocken, PA: ASTM Standards, 2001.

ASTM C 469. *"Standard Test Method for Static Modulus of Elasticity and Poisson's Ratio of Concrete in Compression"*. West Conshohocken, PA: ASTM, 1994.

ASTM C 496. *"Standard Test Method for Solitting Tensile Strength of Cylinderical Concrete Specimens"*. West Conshohocken, PA: ASTM Standards, 1996.

ASTM C 78. *"Standards Test Method for Flexural Strength of Concrete (Using Simple Beam with Third-Point Loading)"*. West Conshohocken, PA: ASTM Standards, 2000.

ASTM C09.47. *"Self-Consolidating Concrete"*. ASTM International Sub committee C09.47 on Concrete and Concrete Aggregates, 2009.

ASTM C09.47, American Society for Testing and Materials. *"Self-Consolidating Concrete"*. ASTM International Sub committee C09.47 on Concrete and Concrete Aggregates, 2009.

ASTM C1611, American Society for Testing and Materials. *"Standard Test Method for Slump Flow of Self-Consolidating Concrete"*. ASTM International, Conshohocken, 2009.

ASTM C1621. *"Standard Test Method for Passing Ability of Self-Consolidation Concrete by J-Ring"*. ASTM International, Conshohocken, 2009.

ASTM C1621, American Society for Testing and Materials. *"Standard Test Method for Passing Ability of Self-Consolidation Concrete by J-Ring"*. ASTM International, Conshohocken, 2009.

Bayramov, F., Tasdemir, C. and Tasdemir, M.A. "Optimisation of steel fibre reinforced concretes by means of statistical response surface method." *Cement & Concrete Composites 26*, 2004: 26, Page 665-675.

www.manaraa.com

Casanova, P. and Rossi, P. "Analysis of metallic fibre-reinforced concrete beams submitted to bending." *Materials and Structures 29.* 1996. 354-361.

Colombo, M et al. "Mechanical properties of steel fibre reinforced conocrete exposed at high temperatures." *Material and Structures 43.* 2010. 475-491.

Derucher, K. N., Korfiatis, G. P., and Ezeldin, A. S. *Materials for Civil & Highway Engineers.* Prentice Hall, 1998.

Destree, Xavier. *Structural application of steel fibre as only reinforcing in free suspended elevated slabs.* Varenna, Italy: Symposium, 6th RILEM, pp. 1073-1082, 2004.

Diawara, Hamidou. *Parametric study of self-consolidating concrete.* Ph.D. Dissertation, Las Vegas: University of Nevada, 2008.

Doli, V.and Ladkany, S.G. *The influence of cementitious materials and steel fiber reinforcement on the strength of self consolidating concrete.* Master's Thesis, Las Vegas: Unlversity of Nevada, 2004.

Eren, O., Marar, K. and Celik, T. "Effects of Silicaa Fume and Steel Fibers on Some Mechanical Properties of High-Strength Fiber-Reinforced Concrete." *Journal of Testing and Evaluation*, 1999: 27 (6), Pages 380-387.

Ganesan, N., Indira, P.V., and Abraham, R. "Steel fibre reinforced high performance concrete beam-column joints subjected to cyclic loading." *ISET Jounal of Earthquake Technology*, 2007: Vol 44; Pages 445-456.

Garcia-Taengua, E., Marti-vargas, J.R.and Serna-Ros, P. "Statistical Approach to Effect of Factors Involved in Bond Performance of SteelFiber-Reinforced Concrete." *ACI Structural Journal*, 2011: Vol. 108, No. 4, Pages 461-468.

www.manaraa.com

Greenough, Tom, Nehdi & Moncef. "Shear Behavior of Fiber-Reinforced Self-Consolidating Concrete Slender Beams." *ACI Materials Journal*, 2008.

Grunewald, S and Walraven, J.C. "Parameter-study on the influence of steel fibers and coarse aggregate content on the fresh properties of self-compacting concrete." *Cement and Concrete Research 31*, 2001: Pages 1793-1798.

Johnston, Colin D. *Fiber-reinforced cements and concretes.* Amsterdam: Gordon and Breach Science Publishers, 2001.

Kasper, T., Edvardsen, C., Wittneben, G., and Neumann, D. "Lining design for the district heating tunnel in Copenhagen with steel fiber reinforced concrete segments." *Tunnelling and Underground Space Technology*, 2007.

Kearns, C.F. and McConnell, G.M. "Structural behaviour of thin planar and curved microconcret plates reinforced conventionally and with steel fibers." *Materials and Structures*, 1989: 357-363.

Khaloo, A.R. and Kim, N. "Mechanical Properties of Normal to High-Strength Steel Fiber-Reinforecd Concrete." *Cement, Concrete and Aggregates*, 1996: Vol 18 (2), Pages 92-97.

Ladkany, S. et al. "Mixing performance and strength of steel fiber-reinforced SCC with varing cementitious materials." *SCC 2005 Proceedings.* Center for advanced cement-based materials, Illinois, Chicago, 2005. 387-391.

Laranjeira, F. et al. "Characterization of the orientation profile of steel fiber reinforced concrete." *Materials and Structures*, 2010: 1-19.

Meda, A. and Rosati, G. "Design and Construction of a Bridge in Very High Performance Fiber-Reinforced Concrete." *ASTM*, 2003: Vol. 8 (5); Page281-287.

www.manaraa.com

Micro-Measurements. *Strain Gage Rosettes: Selection, Application and Data Reduction.* Tech Note TN-515, Vishay Precision Group, 2010.

Mindess, S., Young, J. Francis, and Darwin, D. *Concrete.* 2nd. Prentice Hall, 2003.

Nawy, Edward G. *Fundamentals of High-Performance Concrete.* 2nd. John Wiley, 2001.

Pons, G. et al. "Mechanical behaviour of self-compacting concrete with hybrid fibre reinforcement." *Materials and structures (40),* 2007: 201-210.

Riaz, B. De. "Steel fiber reinforced concrete (SFRC): the use of SFRC in precast segment for tunneling." *World Tunnel Congress*, 2008: Vol. 65(3), Pages 47-56.

Sahin, Y. and Koksal, F. "The influence of matrix and steel fibre tensile strengths on the fracture energy of high-strength concrete." *Construction and Building Materials 25*, 2011: Pages 1801-1806.

Serna, P. et al. "Structural cast-in-place SFRC: technology, control criteria and recent applications in Spain 42." *Materials and Structures.* 2009. 1233-1246.

Shah, A.A and Ribakov, Y. "Recent trends in steel fibered high-strength concrete." *Materials and Design 32,* 2011: Pages 4122-4151.

Steven H. Kosmatka, Beatrix Kerkhoff, and William C. Panarese. *Design and Control of Concrete Mixtures.* PCA, 2002.

Timoshenko, S. *Theory of Plates and Shells, 2nd Edition.* U.S.A.: McGraw-Hill, Inc., 1987.

Torrijos, M. C., Barragan, B. E., and Zerbino, R. L. "Placing conditions, mesosturctural characteristics and post-cracking response of fibre reinforced self-compacting concretes." *Construction and Building Materials 24*, 2010: Pages 1078-1085.

www.manaraa.com

Ugural, Ansel C. *Stresses in Beams, Plates, and Shells, 3rd Edition.* Boca Raton, Fl, USA: CRC Press, 2009.

Xu, B.W.and Shi, H.S. "Correlations among mechanical properties of steel fiber reinforced concrete." *Construction and Building Materials 23*, 2009: Pages 3468-3474.

www.manaraa.com

VITA

Graduate College
University of Nevada, Las Vegas

Abebe Tadesse Berhe

Degrees:

Bachelor of Science, Civil Engineering, 1990
Addis Ababa University, Addis Ababa, Ethiopia

Master of Engineering, Structural Engineering, 1994
McGill University, Montreal, Canada

Special Honors and Awards: Certificate for outstanding academic achievement,
Alliance of Professionals of African Heritage, University of Nevada, Las Vegas.

Conference Publications:

Berhe A. and Ladkany S.G. (2011). Characterization of High Strength Steel Fiber Reinforced Concrete and Self-Consolidating Concrete Mixtures with Various Steel Volume Fractions for Infrastructures, SEI 2011 Structures congress, April, Las Vegas, Nevada.

Berhe A. and Ladkany, S.G. (2013). Characterization and Applications of High Strength Steel Fiber SCC and Flowable Concrete, SCC 2013: Fifth North American Conference, May, Chicago, Illinois.

Berhe A. and Ladkany, S.G. (2013). Structural behavior of high performance fiber-reinforced flowable concrete beams and plates. SEMC 2013: The Fifth International Conference on Structural Engineering, Mechanics and Computation, September 2013, Cape Town, South Africa.

Dissertation Title:

High Strength Steel Fiber Reinforced Flow-Able or SCC Concrete with Variable Fiber by Volume Fractions for Thin Plate and Shell Structures

Dissertation Examination Committee:

Chairperson, Samaan G. Ladkany, Ph. D.
Committee Member, Nader Ghafoori, Ph. D.
Committee Member, Mohamed Kaseko, Ph. D.
Committee Member, Ying Tian, Ph. D.
Graduate Faculty representative, Brendan O'Toole, Ph. D.

www.manaraa.com